Intrinsic and Visually-Evoked Properties of Layer 2/3 Neurons in Mouse Primary Visual Cortex and Their Dependence on Sensory Experience

Alexander P Y Brown

Thesis presented for the degree of

Doctor of Philosophy

The Francis Crick Institute, Mill Hill Laboratory

University College London

August 2015

I, Alexander Brown, confirm that the work presented in this thesis is my own. Where information has been derived either from published sources or the work of others, I confirm that this has been acknowledged in the text.

Alexander Brown, 25 August 2015

Acknowledgements

I would firstly like to thank my supervisor, Troy Margrie, for his support and advice at all stages of my research and in particular for his guidance and patience during the writing of this thesis. I would also like to thank Bruno Pichler for teaching me the basics of *in vivo* work, and particularly the imaging techniques used early in my research, and Ede Rancz and Mateo Velez-Fort for sharing their experience with and advice on whole-cell electrophysiology.

Molly Strom produced all the plasmids and many of the viruses used, and in addition established and maintained the transgenic animal lines. Charly Rousseau created the pipeline for automated serial-section two photon imaging, and his advice along with that of Christian Niedworok with regard to programming and analysis of data has been invaluable.

I would also like to thank all the members of the Margrie Lab, and the wider former Division of Neurophysiology at the National Institute for Medical Research (now part of the Francis Crick Institute) for their valued feedback and insight.

I am indebted to UCL Medical School for accepting me on to the MB/PhD programme and, in particular, to Gordon Stewart for his genial support and encouragement at all stages of the programme, as well as the MRC and the Wellcome Trust for funding.

Finally I am overwhelmingly grateful to my friends and family for their consistent, unwavering support.

Abstract

Neurons in Primary Visual Cortex (V1) are known to respond strongly to visual stimuli. Studies of neuronal responses in V1, carried out first in cats, but later primates and other mammals, have demonstrated that bars of light at particular orientations evoke strong, reliable responses in terms of increased firing rate of action potentials. Tuning of neuronal responses to certain stimulus parameters, such as orientation but also spatial and temporal frequencies, as well as the apparent dichotomy between simple and complex responses, have given rise to a number of influential models not just of V1 function, but more generally in the field of cortical physiology and computer vision.

Owing to its small size and the plethora of available molecular and genetic tools, the visual cortex of the mouse may be a more tractable model system than that of much larger animals. Recent studies of neuronal responses in mouse V1 have shown that these are broadly similar to those of primates and carnivores, although not identical in all aspects.

My thesis aims firstly to characterise intrinsic and sensory-evoked properties in regular-spiking, putative pyramidal neurons in L2/3 of the mouse visual cortex using whole-cell patch clamp recording *in vivo* . In addition, the anatomical connectivity of individual neurons is characterised using virus-assisted circuit mapping. The majority of these neurons are found to be simple cells. Orientation tuning (the degree to which neuronal responses are selective to stimuli of a preferred orientation) is found to be quite variable, even within this singular group of neurons. The potential roles of intrinsic diversity, functional connectivity, and sensory experience in setting the orientation tuning of a particular neuron are investigated. These findings provide an insight in to how diverse responses to sensory stimuli can be generated in an apparently homogenous group of neurons.

Contents

List of Figures

List of Tables

Chapter 1

Introduction

The cortex is the seat of a diverse set of higher brain functions, including sensation, planning, voluntary motor action and cognition. These diverse functions are carried out in cortical areas which share a considerable degree of similarity in terms of their cellular components and gross histological structure, suggesting the possibility of a canonical circuit adapted to a variety of functional roles (Douglas and Martin, 1991; Braitenberg and Schuz, 1998; Silberberg et al., 2002; Harris and Shepherd, 2015) . Despite over a hundred years of study, the definition and function of the cortical circuit remains one of the greatest unsolved challenges of biology.

The primary visual cortex (V1) is perhaps the most widely studied cortical region. In concert with other visual structures, it is involved in processing information derived ultimately from the retina, making a visual percept available to the conscious brain. The main subject of this thesis is the characterisation of a single group of neurons within V1, the layer 2/3 regular-spiking pyramidal neurons, with a view to elucidating the roles of intrinsic, synaptic and connectomic diversity in cortical information processing. However, to begin at the beginning, I first introduce the context in which V1 operates: the mammalian visual system.

1.1 The Mammalian Visual Pathway

1.1.1 Retina and Thalamus

Sensory processing in all systems begins with transduction, the conversion of stimuli external to the organism in to electrical signals. In the mammalian visual system, phototransduction is carried out by rods and cones in the outer nuclear layer of the retina (Wässle, 2004; Masland, 2012, see also fig. 1.1). These cells convert light energy in to a membrane

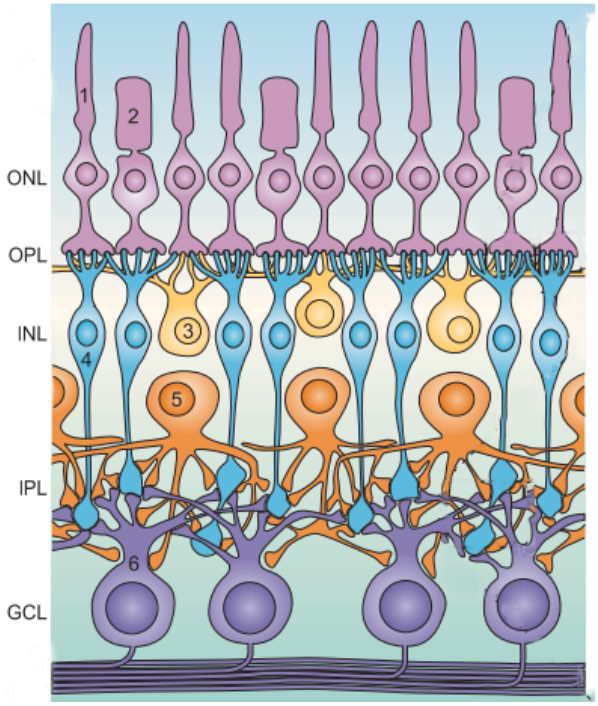

Figure 1.1: Cellular organisation of the retina.
The neuronal components of the retina are organised in a laminar structure, with phototransduction being carried out in the cones (1) and rods (2) of the outer nuclear layer (ONL). These photoreceptor cells synapse in the outer plexifom layer (OPL) on to horizontal (3) and bipolar neurons (4) of the inner nuclear layer (INL). Horizontal neurons mediate lateral inhibition among rods and cones; bipolar cells in turn synapse in the inner plexiform layer (IPL) on to amacrine cells of the INL (5), which carry out a variety of intraretinal processing functions, as well as the output cell of the retina, the retinal ganglion cell (6), located in the ganglion cell layer (GCL). Adapted from Wässle (2004)

potential hyperpolarisation by the use of photoreceptor proteins, including the rod receptor, rhodopsin, and the various cone photopsins. Rhodopsin is the most sensitive of these to low light levels, and rod responses dominate under scotopic conditions. At greater levels of light intensity, the differing spectral response profiles of the photopsins allow for colour vision, mediated by the cone receptors. Primates are trichromats, possessing three types of cone receptor - maximally responsive to long wavelength red light (L-cones), medium wavelength green light (M-cones) and short wavelength blue light (S-cones). Most other mammals are thought to be dichromats, including the mouse, which possess only S- and M- cones (Huberman and Niell, 2011). Rodent vision, like that of cats, is adapted for scotopic conditions, with few cones; in the mouse, around 3% of all photoreceptors are cones (Jeon et al., 1998), somewhat lower the the fraction in humans (Curcio et al., 1990). In both cats and primates, a central region of the retina is enriched with a considerably higher (around one order of magnitude) density of cone receptors, providing a focal region of high-acuity colour vision (Rapaport and Stone, 1984). Rodents do not possess such an area (termed the area centralis in the cat, and the fovea centralis in the primate), and as such their vision may be described as 'unfoveated'.

In addition to the rods and cones, so-called intrinsically photosensitive retinal ganglion cells (ipRGCs) have been described in the retina. These cells contain the photopigment melanopsin, and were originally thought to play a role in the maintenance of the circadian rhythm, by tuning the pacemaker circuit of the suprachiasmatic nucleus of the thalamus

(Ruby et al., 2002; Berson, 2003). However, the distinction between the classical photoreceptor pathway and the ipRGC pathway is one of degree, rather than kind, since rods and cones do play a role in circadian rhythm adjustment in normally sighted animals (Ruby et al., 2002; Panda et al., 2002, 2003). Furthermore, ipRGC axons have been shown to project to other subcortical targets, including the olivary pretectal nucleus, the posterior pretectal nucleus, the superior colliculus, and both the ventral and dorsal lateral geniculate nuclei (Ecker et al., 2010), suggesting that they may play some role in vision.

Once transduction has occurred, signals are transferred on to horizontal and bipolar cells at the junction of the outer plexiform layer (Wässle, 2004). The processes of the inhibitory horizontal cells spread across the inner plexiform layer, receiving and integrating glutamatergic inputs from many rods or cones and, in turn, providing a feedback inhibitory signal that results in centre-surround enhancement of the photoreceptor responses. Bipolar cells then pass information via graded potentials to amacrine cells of the inner nuclear layer, and retinal ganglion cells, which constitute the output layer of the retina. Considerable processing occurs at this stage, with approximately 40-50 morphological forms of amacrine cell, and 10-15 forms of the retinal ganglion cell having been described (Wässle, 2004; Sterling and Demb, 2005).

The functional responses of the retinal ganglion cell were first described in a seminal paper by Stephen Kuffler (Kuffler, 1953), developing on the concept of the receptive field described in earlier work on the optic nerve by Hartline (Hartline, 1938). Retinal ganglion cells were found to have a centre-surround receptive field, comprised of concentric subfields. In so-called on-centre cells, light stimuli restricted to the central region enhanced the spiking activity of the cell, whereas broader stimuli, including the surrounding 'off' subfield, reduced this response. In contrast, off-centre cells have a central off subfield, surrounded by an on subfield. This functional distinction is reflected in a remarkable (at least, to the cortical physiologist) anatomical compartmentalisation, with on-centre and off-centre neurons ramifying their dendrites in separate strata of the inner plexiform layer (Famiglietti and Kolb, 1976; Nelson et al., 1978). It is also complemented by the finding of Enroth-Cugell and Robson (1966) in the cat retina that some ganglion cells, of both on- and off- centre types, respond linearly to visual stimuli, with phasic responses to illumination matching the receptive field arrangement of the cell (so-called X responses). In contrast, other ganglion cells exhibit a nonlinear response to visual stimuli, responding preferentially to changes in illumination (Y responses).

A smaller group of ganglion cells are known to be selective for the direction of stimulus

motion - a form of orientation selectivity (strictly, sensitivity to motion direction). This selectivity has been shown to arise from dendritic processing within cholinergic starburst amacrine cells (Euler et al., 2002; Briggman et al., 2011). The functional relevance of these cells to cortical orientation tuning has remains largely unexplored. Whilst it is possible to integrate such motion signals to produce orientation selective responses, selectivity for stimulus orientation is conventionally regarded as a feature emergent at the level of the projection from the lateral geniculate nucleus to layer IV of V1 (Hubel and Wiesel, 1977). One suggestion is that motion information computed in the retina remains restricted to subcortical regions, and may be involved in pathways such as the control of reflex eye movements (Cheong et al., 2013). However, a recent finding in the mouse suggests that neurons in the shell region of the dorsolateral geniculate nucleus of the thalamus (dLGN) receive direct input from these directionally selective ganglion cells. These shell zone geniculate neurons are highly tuned for stimulus orientation and direction, and they project in turn to superficial layers of V1 (Cruz-Martín et al., 2014). The functional importance of this circuit in V1 orientation and directional tuning remains unknown, although reports of highly tuned responses in koniocellular pathway neurons have also been reported in primates (Cheong et al., 2013).

The majority of retinal ganglion cells send axonal projections along the optic nerve primarily to the lateral geniculate nucleus. In humans, great apes, and most old world primates the lateral geniculate nuclei have a six-layered laminar structure, separated by layers of cells with relatively small nuclei (Jones, 2007). The innermost (ventral) two layers of the LGN are comprised of large, so-called magnocellular neurons, whereas the four dorsal laminae contain smaller parvocellular neurons, with receptive field structures of both these classes of neurons qualitatively resembling those of retinal ganglion cells. This laminar structure varies in other species, such as the new world primates and the cat, in which typically three laminae are recognised (Jones, 2007).

Connectivity from retina to thalamus is thought to be relatively simple, with a typical LGN neuron receiving input from a small number of retinal ganglion cells (Alonso et al., 2006; Guido, 2008), although a single RGC axon can make as many as 100 individual synaptic contacts on to a single geniculate neurons (Hamos et al., 1987). For these reasons, neurons in the LGN are typically described as 'relay' neurons, passing retinal signals on to the cortex without further processing.

The responses of parvocellular and magnocellular neurons were, at first, described as being exclusively of the X- and Y- type, respectively (Dreher et al., 1976; Sherman

et al., 1976). However, later studies reported X-like responses across all geniculate layers, including the magnocellular (Shapley et al., 1981). Anatomically, the magnocellular and parvocellular layers are distinguished by receiving input from distinct classes of retinal ganglion cells, the parasol and midget cells respectively. These parallel pathways are thought to provide distinct streams of information, with M-cells having large, achromatic receptive fields with high contrast sensitivity. P-cells, in contrast, typically have smaller receptive fields, with poorer contrast sensitivity, but strong chromatic tuning (Callaway, 2005). In turn, these cells have distinct projection targets, with M cells projecting to layer 4Cα, and P-cells projecting to layer 4Cβ. These streams are thought to subserve different functional roles, with the magnocellular stream conveying primarily motion information, whereas the parvocellular stream provides finer detail chromatic information involved in object recognition.

In primates, a third pathway, the koniocellular pathway, has also been described (Casagrande, 1994; Hendry and Reid, 2000; White et al., 2001a). The cell bodies of koniocellular neurons in the lateral geniculate nucleus are located between the M- and P-cell layers, and are neurochemically distinct from both parvocellular and magnocellular neurons (Hendry and Yoshioka, 1994). Ganglion cell input to koniocellular neurons arises from non-midget, non-parasol cells with relatively wide receptive fields (Hendry and Reid, 2000). The koniocellular pathway is typically associated with input from short-wavelength photoreceptors ('S-cones'), most particularly a specific class of retinal ganglion cell, the bistratified blue-ON yellow-OFF ganglion cell (Dacey and Lee, 1994) which, unusually, stratify their dendrites in both the inner (on) and outer (off) sub-layers of the inner plexiform layer. Koniocellular neurons also receive input from blue-OFF yellow-ON opponent cells whose precise identity is less clear but which may include a number of other ganglion cells classes (Dacey and Packer, 2003; Szmajda et al., 2008). The koniocellular pathway is thought to be roughly homologous to the W-cell pathway in the cat, and it projects to superficial V1,including layer 1 and cytochrome oxidase patches in layer II/III (L2/3), as well as the superior colliculus (Hendry and Reid, 2000; Solomon, 2002).

The strict three streams hypothesis, under which pathways from retina to cortex via thalamus are homogenous, independent and functionally distinct has come under attack in recent years (Kaplan, 2012), with increasing focus on divergent and convergent information flow. As the number of distinct retinal ganglion cell classes proliferates, and evidence of non-classical projection pathways accumulates, some authors have suggested a solution is to increase the number of described pathways, or to subdivide existing ones (Masland and

Martin, 2007; Masland, 2012). However, others have advocated the softening of the sharp definition of each visual pathway, with a more network-centric approach recognising that different RGCs may encode different aspects of sensory information. This information is then broadly split in to differing channels, but the assignment is a matter of degree, rather than kind (Kaplan, 2012).

1.1.2 Subcortical Visual Nuclei

In addition to the retino-geniculo-cortical pathway, retinal afferents project to a number of subcortical regions, either directly or via the lateral geniculate nucleus. These include the suprachiasmatic nucleus (SCN) of the hypothalamus, involved in setting the circadian rhythm of physiological processes, including arousal state (Moore, 2013); the superior colliculus, involved in eye-movements including saccades, as well as head, limb and whole body motions associated with aligning the animal to an external stimulus (Gandhi and Katnani, 2011); and the pulvinar nuclei of the thalamus, thought to play a role signalling attention/salience of a particular stimulus, by co-ordinating multiple visual and associative cortical areas (Grieve et al., 2000).

1.1.3 Primary Visual Cortex

The dominant cortical target for geniculate neurons is the primary visual cortex (V1). This area corresponds to Brodmann's cortical area 17 (Brodmann, 1909), located in the occipital lobe of higher mammals and in a similar caudal location in rodents, in which the lobar structure of the cerebrum is less apparent. The cytoarchitectonic structure of V1 is quite distinct from that of surrounding cortical regions, with a greatly enlarged thalamorecipient layer IV (L4), subdivided in to distinct sublaminae by the Line of Gennari, an anatomical feature arising from the dense axonal projection of myelinated geniculate neurons in this layer (Gennari, 1782; Braitenberg and Schuz, 1998).

The functional properties of V1 neurons were first described by Hubel and Wiesel in a classic pair of papers (Hubel and Wiesel, 1959, 1962) which still form the basis of many theories relating to visual cortical function today. Recording single units using tungsten electrodes in the anaesthetised visual cortex of the cat, they described responses of individual cells as being maximal not to single spots of contrast (as is the case for RGCs or geniculate neurons). Rather, V1 neurons were found to fire evoked action potentials to elongated, oriented bars of contrast. This response was dependent upon the angle of orientation of the bar, as well as its position in space. By sweeping bars of varying

orientations across the visual field of the animal, a receptive field map of orientation tuning could this be built up. This receptive field consisted of multiple, parallel, non-overlapping subregions in which a light stimulus would increase or decrease the spontaneous firing rate of the neuron, initially termed 'excitatory' and 'inhibitory' (later referred to as ON or OFF regions so as to avoid attaching mechanistic labels to the response).

Neuronal responses in V1 were initially divided by Hubel and Wiesel in to two classes, the simple cell, and the complex cell (Hubel and Wiesel, 1962), and although they conceded that there may exist other classes of functional response, this dichotomy became reified in the literature throughout the latter half of the 20th century, and persists, if slightly modified, to this day. In the light of later schemes that define simple and complex responses, it is worth reiterating, verbatim, the original criteria by which receptive fields were defined as being of the simple class:

1. *they were subdivided into distinct excitatory and inhibitory regions;*
2. *there was summation within the separate excitatory and inhibitory parts;*
3. *there was antagonism between excitatory and inhibitory regions;*
4. *it was possible to predict responses to stationary or moving spots of various shapes from a map of the excitatory and inhibitory areas.*

(Hubel and Wiesel, 1962)

In contrast, complex receptive fields were defined as those which significantly failed on one or more of these criteria. Complex receptive fields included those in which there was considerable overlap between excitatory and inhibitory regions; those containing only a single subregion (either ON or OFF); or those responding phasically to a local change in contrast. Such cells were commonly found to respond to oriented bars, of the preferred orientation, regardless of the precise position of the stimulus within the visual field.

This finding suggested to Hubel and Wiesel a feedforward hierarchy, with connectivity and information flow being ordered as LGN→Simple Cell→Complex Cell (Hubel and Wiesel, 1962). In this view, each layer of the cortical computation derives increasingly abstracted information from the input of those which precede: at first, the detection of edges by simple cells from geniculate input, and higher order features such as motion by complex neurons from simple cell input. Such an arrangement could be achieved by the innervation of a simple cell by geniculate neurons with multiple, overlapping centre-surround receptive fields, aligned along a common axis. In turn, multiple simple cells with

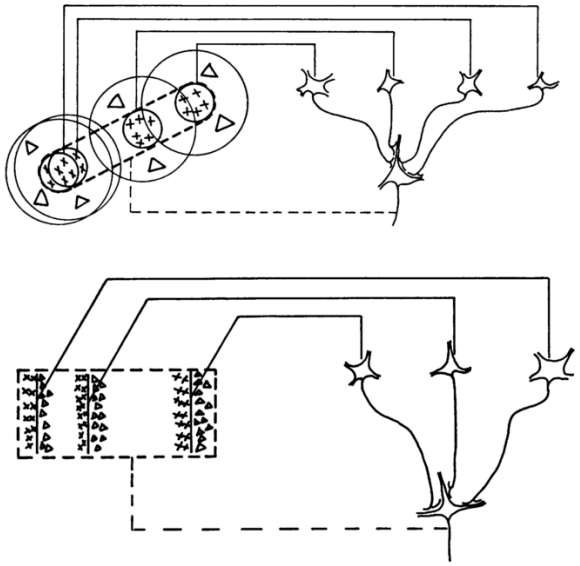

Figure 1.2: The Serial Feedforward Model Under the model originally proposed by Hubel & Wiesel, elongated ON/OFF receptive field subregions in cortical simple cells (above) are created by input from centre-surround dLGN neurons whose receptive fields are aligned in space. In turn, multiple cortical simple cells with similar receptive field orienation but spatially offset receptive fields project on to complex cells (below), creating a response sensitive to stimulus orientation but not phase.

similar preferred orientations, but diverse receptive field phases, could combine to create a complex receptive field (fig. 1.2).

This model has remained highly influential to this day, with several lines of evidence to support it. Firstly, neurons in the thalamorecipient layer 4 are, indeed, overwhelmingly simple (Gilbert, 1977; Ringach et al., 2002), to a far greater extent than those of other cortical layers. Secondly, with the exception of layer 6, other layers were thought not to receive direct thalamic input, with axonal projection of geniculate neurons terminating in layer 4 (Bullier and Henry, 1979). Functionally, the latencies of post-synaptic potentials evoked in response to electrical stimulation in the thalamus have been shown to be consistent with monosynaptic transmission only in layers 4 and 6, although neurons in the lower regions of layer 3 did also display short latency responses (Ferster and Lindström, 1983). Furthermore, inhibitory post-synaptic potentials were found to be exclusively di- or tri- synaptic in all layers, supporting the conclusion that thalamic input is solely excitatory. In support of these conclusions, anatomical observations of the distribution of axonal projections and dendritic arborisations within the cortex supported the general model of information flow as Thal→L4→L2/3→L5→L6→Thal (Gilbert, 1983). Cross correlation analyses have demonstrated that LGN neurons and V1 neurons likely to be monosynaptically connected share receptive field subregions (Tanaka, 1983; Reid and Alonso, 1995), and silencing of intracortical activity by optogenetic stimulation of parvalbumin-expressing interneurons in order to isolate feedforward thalamic afferent drive supports this view (Lien and Scanziani, 2013). The basic feedforward structure, and its link to neuronal function, remains the basis upon which later revisions have been made. Developments in the study

of functional responses and anatomical connectivity of V1 neurons that challenge this model are discussed below (section 1.2).

In addition to this laminar structure, in the primary visual cortices of the cat and the primate, certain functional properties of neurons - orientation preference, ocular dominance and spatial frequency tuning - are distributed in an ordered topographical distribution. The first description of what would later be termed orientation columns was embedded in the early work of Hubel & Wiesel, who described the finding that penetrations made at an angle close to parallel to the cortical surface recorded neurons whose orientation preference changed gradually (Hubel and Wiesel, 1974b). Combined with the earlier work of Mountcastle (Mountcastle, 1957), orientation selectivity was proposed to be organised in a columnar structure, with neurons located in a similar horizontal location, relative to the cortical surface, sharing an orientation preference, and the preference of adjacent columns varying smoothly. The presence of orientation columns was directly demonstrated by 2-deoxyglucose radiography (Hubel et al., 1978; Löwel et al., 1987); however the use of intrinsic signal imaging allowed for V1 responses to all orientations to be mapped in the same animal for the first time, revealing the now-classic 'pinwheel' structure (Bonhoeffer and Grinvald, 1991), in which patches of cortex that respond preferentially to a given orientation are arranged in an orderly fashion around a central discontinuity. With the addition of ocular dominance columns, and later spatial frequency columns, the notion of a cortical 'hypercolumn' was born (Hubel and Wiesel, 1974a), in which the distribution of each functional property varies independently, and therefore a patch of cortex 1-2mm in diameter contains all combinations of functional properties. This was then suggested to represent a functional unit, processing information within a given region of visual space.

Later technical developments have revealed preferential connectivity between columns sharing functional properties (Gilbert and Wiesel, 1989), and the cortical column has been proposed to arise as a result of the radial inside-out development of the cerebral cortex, with clonally-related neurons migrating to the ventral surface in parallel, creating 'ontogenetic columns' (Rakic, 1988). This columnar arrangement is, however, entirely absent in the rodent (Ohki et al., 2005), even in highly visual rodents such as the gray squirrel (Van Hooser et al., 2005). Furthermore, even in primates and carnivores, the functional relevance of cortical columnar structure remains elusive, with some suggestion that it may be an epiphenomenon rather than a core organising principle (Horton and Adams, 2005, see also discussion below section 1.1.5).

1.1.4 Higher Visual Cortical Areas

Outside V1, large regions of the cortex are dedicated to the processing of primarily visual stimuli, particularly in the highly visual primate cortex. In the primate, around 25 areas have been described as being exclusively visual, and an additional 7 as multimodal regions combining visual information with other sensory modalities (Felleman and Van Essen, 1991), although this number does differ between authors and species. The most coarse division of cortical areas differentiates between an occipitotemporal 'ventral' stream, involved in resolving the identity of objects, and the occipitoparietal 'dorsal' stream, crucial for defining the spatial position of these objects, as well as visually guided movements (Ungerleider and Mishkin, 1982; Ungerleider and Haxby, 1994). This notion, that the visual system is not simply one chain of abstraction, but may be composed of two (or more) relatively independent, and evolutionarily distinct pathways was first proposed by Schneider (1969), although the distinction made by Schneider was between retinotectal and retino-geniculo-cortical pathways, a distinction that must be complemented, rather than replaced, by the functional division of dorsal and ventral cortical streams

The ventral stream, also referred to as the 'what' pathway, arises from projections either directly from V1, or via the thin stripes and interstripes of V2, via V4 to the inferior temporal cortex. The dorsal 'where' stream also arises either directly from V1 or via the thick stripes of V2, and projects via areas including the middle temporal area MT to the posterior parietal cortex (Felleman and Van Essen, 1991).Whilst these projection pathways arise, to some degree, from anatomically segregated M and P pathways within V1, some authors have suggested that the differing functional properties of the streams arise not simply as a result of segregated inputs, but from the use of computational schemes tailored to extracting visual information of a certain kind from inputs that are broadly, rather than exclusively, target-specific (Goodale and Milner, 1992).

1.1.5 Model Organisms

Early experiments characterising the response properties of V1 neurons to visual stimuli were carried out mostly in the cortex of the cat (Hubel and Wiesel, 1959, 1962; Wiesel and Hubel, 1963b) or primates such as the macaque (Hubel et al., 1977; Blasdel and Fitzpatrick, 1984; Foster et al., 1985; Ringach et al., 2002). Observations of the nature of these responses have lead directly to several models of cortical processing, most notably the highly influential serial feedforward model (Hubel and Wiesel, 1962). Since these

studies, the repertoire of model species used in visual neuroscience has been expanded greatly. Smaller primate species, including the new world monkeys such as the marmoset, offer a several advantages including a smooth cortical surface, reduced size and shorter lifespan (and thus quicker development) (Solomon and Rosa, 2014), factors which may also motivate, in part, the use of non-primate species such as the ferret (Chapman et al., 1996; Coppola et al., 1998; White et al., 2001b) and tree shrew (Rockland and Lund, 1982; Fitzpatrick, 1996; Bosking et al., 1997). The apparent advantage of rodent species are similar in nature but even more acute. Rodents may be bred and housed cheaply and on a scale that makes larger scale population studies feasible. Like the marmoset, the cortex of the rodent is smooth, allowing the entire cortical surface to be exposed to the experimenter. Rodent cortices are small, and therefore perhaps more tractable - cellular-level calcium imaging techniques are already approaching the ability to record the spiking activity and spatial distribution of thousands of neurons simultaneously in multiple cortical areas (Stirman et al., 2014).

However, the most prominent reason for the explosive rise of the mouse in the past decade in all fields of life science in general, and the neurosciences in particular, has been the advent of genetic manipulation. Genetically modified animals offer a seemingly bottomless cornucopia of tools (Luo et al., 2008), including labelling of genetically identified neuronal subtypes (Tamamaki et al., 2003); stochastic labelling techniques for neuronal identification and tracing (Livet et al., 2007); the targeting of neuronal subtypes for studying function (Zariwala et al., 2011), optogenetic manipulation (Wilson et al., 2012; Atallah et al., 2012) and tracing connectivity (Sun et al., 2014; Vélez-Fort et al., 2014), highly selective pharmacological manipulation of neuronal populations (Urban and Roth, 2015), and expression of genetically encoded calcium indicators (Chen et al., 2012; Dana et al., 2014). The obvious drawback to the use of the mouse is the question of whether the visual system of a small crepuscular/nocturnal prey animal can be of value in understanding the visual system of a much larger animal with good visual acuity and a highly visual brain - namely, *homo sapiens*.

The first report of visual responses in mouse visual cortex (at least in response to classical grating stimuli) was made in Dräger (1975), in which units were shown to display responses to oriented gratings of a qualitatively similar nature to those in the V1 of the cat or macaque, leading Ursula Drager to conclude:

'Receptive field organization of cortical neurons in the mouse does not seem to be basically different from that of other mammals. The way receptive fields are built up in

mammalian visual cortex may indeed be universal.' (Dräger, 1975)

Mangini and Pearlman (1980) reported oriented responses, both simple and complex, in most cortical layers of the mouse, with the exception of L4, which was found to contain predominantly centre-surround units similar to those of the LGN, although this finding has not been supported by more recent recordings in mouse layer 4 (Niell and Stryker, 2008; Li et al., 2012b; Lien and Scanziani, 2013). However results such as this, and reports that other features of higher mammalian vision, such as orientation maps, were absent from rodent V1 (Girman et al., 1999) may explain, in part, the reasons that the mouse remained a relatively marginal model organism in the study of visual cortical processing throughout the 1980s and 1990s (Hübener, 2003).

Using in vivo calcium imaging, Ohki et al. (2005) mapped the orientation preferences of hundreds of individual neurons simultaneously. This technical breakthrough confirmed earlier reports of a lack of orientation columns in the rodent. However, it also reported that up to 75% of neurons in rat visual cortex were responsive to drifting grating stimuli, higher than previous estimates. Using multiunit extracellular recordings, Niell and Stryker (2008) reported the tuning properties of mouse V1 neurons, across all cortical layers, to be far more similar to those of neurons in the cat or primate than previously thought, with the majority of neurons in all cortical layers being classified as orientation selective. The most apparent difference between the responses of *individual* neurons in mouse V1, as compared to those of the primate or cat, is the relatively low spatial preferred frequency (0.04 cycles per degree in the mouse, as compared to around 0.9cpd in the cat, and up to 4cpd in primates) (Niell and Stryker, 2008).

In addition to the absence of orientation columns, rodents lack other mesoscopic local topographies, such as precise retinotopic position (Smith and Häusser, 2010), or ocular dominance within the binocular area (Hofer et al., 2006). Whilst this absence has been proposed as a correlate of the generally less acute visual system of the mouse or rat, orientation columns are also absent in the visual cortex of the gray squirrel, a highly visual animal (Van Hooser et al., 2005). It has been suggested that these topographies may exist in order to reduce the wiring length in the visual cortices of larger animals, and so may be a product of physical necessity rather than functional difference (Koulakov and Chklovskii, 2001), and this explanation seems satisfactory to most rodent visual physiologists. It should be noted that the presence or absence of orientation preference maps is not, however, strictly related to either brain volume or body weight (Kaschube, 2014), and the question of the functional relevance of orientation columns, or their absence, has

still not fully been settled.

As the weight of studies demonstrating the remarkable degree of similarity in numerous qualitative aspects of visual information processing in the mouse, as compared to 'higher' mammals grows (Huberman and Niell, 2011), the justification against using mice in studies of general mechanisms of visual processing diminishes. This is not to say that all concerns regarding the use of mice in visual neuroscience have been vanquished, or even that this is possible. Mice certainly do differ quite considerably from primates - for example, in the complete absence of a fovea or any form of a central area of increased photoreceptor density. Mice, like cats, are dichromats, with vision adapted primarily for low-light conditions. Whilst an increasing number of studies have greatly expanded the suggested number of extrastriate areas in the mouse (Wang et al., 2007, 2011; Andermann et al., 2011; Marshel et al., 2011) - up to between 7-10, from the previous description of just two (Paxinos and Franklin, 2008) - it is difficult to imagine there being analogs of regions involved in higher human visual processing such as the Fusiform Face Area (Kanwisher et al., 1997) in the mouse. As the limitations of the use of rodents in studying particular features of primate vision must be accepted, so too their usefulness in studying more general features of visual and cortical processing are manifold. In particular, the availability of genetic and molecular tools for circuit dissection have allowed for a far more targeted approach to the study of cortical circuitry.

1.2 Neuronal Responses to Visual Stimuli in V1

1.2.1 Orientation Tuning

The findings by Hubel and Wiesel that simple cells possessed a receptive field consisting of mutually antagonistic subregions when mapped with small spots of light, and orientation tuned responses to moving bars of contrast (Hubel and Wiesel, 1959) were used to generate mechanistic anatomical explanations such as the serial feedforward model (Hubel and Wiesel, 1962). However, in a more general manner these experiments, following on from earlier studies of retina and thalamus by Kuffler, Barlow, and others, were critical in ushering in the modern era of cellular visual psychophysics. The driving force behind this approach is that the responses of groups of neurons to carefully designed artificial stimuli may elucidate the computations underlying.

By displaying drifting gratings on a CRT screen, and recording the frequency of evoked action potentials as a function of the angle of rotation of the screen, Campbell et al. (1968)

reported tuning of the 'angular response' of neurons in cat visual cortex. This was the first modern description of orientation (peak response to gratings of a particular direction, and minimal response to gratings orthogonal to this orientation) and directional (uneven responses to gratings drifting in opposite directions i.e. separated by 180°) tuning in single cells. Orientation tuning was found to be roughly evenly distributed, with directional tuning being quite common. On the basis of a wide distribution of sizes of the centre of retinal and geniculate receptive fields, and reports of varying receptive field size in cortical neurons, (Hubel and Wiesel, 1962), the spatial frequency tuning of neurons was investigated by Campbel et al. (1969), demonstrating that neurons in V1 exhibited a broad range of preferred spatial frequency. These two observations - of orientation and spatial frequency tuning - suggested that the incoming visual information may be divided in to multiple parallel channels, like the X/parvocellular and Y/magnocellular streams. Combined with emerging theories of linear systems analysis, this suggested that V1 may be performing a Fourier-like transformation, decomposing the visual scene by two-dimensional frequency. This view persisted throughout the 1970s and 1980s, and still forms the basis of much of the thinking regarding the computational goals of V1.

The Fourier analysis approach clearly overlooks one of the defining features of V1 receptive fields: restriction to a small portion of visual space. This dichotomy, between the receptive field view of the visual system as a feature detector, and the systems analysis view of spatial frequency decomposition, was united by the use of wavelet analyses. A wavelet is defined as a function which integrates to zero in the same manner as a wave; however, unlike Fourier analysis, wavelet functions are restricted to a portion of space (or time, depending on the analysis). The most popular such model uses Gabor functions (Marcelja, 1980), obtained by convolving the Fourier field with a two-dimensional gaussian, which was shown by Jones and Palmer (1987) qualitatively to fit well with observed responses. However, the receptive field map systematically underestimates the observed tuning width measured in response to drifting gratings quite considerably. Two mechanisms have been proposed as the source of this discrepancy. Firstly, cross-orientation inhibition could sharpen excitatory responses to drifting gratings. The role of inhibition in orientation tuning is discussed in the next section. The second possible mechanism is the non-linearity created by the spike threshold sharpens the orientation tuning of the membrane potential response (Carandini and Ferster, 2000; Anderson et al., 2000). In support of this view, Priebe and Ferster (2012) argue based upon findings by Mohanty et al. (2012) that receptive field maps do not become sharpened by inhibition, since mapping

is typically performed by simultaneous illumination of several subfields simultaneously, raising the mean membrane potential of the cell. The relationship between the view of the neuron as a feature detector, and as a frequency analyser, is still yet to be fully reconciled.

In addition to controversies regarding the intracortical mechanisms of orientation tuning, recent findings question whether orientation tuning really does arise only at the level of the thalamocortical projection. Whilst some level of orientation bias has been reported in LGN responses as a result of elongated centre-surround receptive fields in the cat (Shou and Leventhal, 1989) and in primates (White et al., 2001a; Xu et al., 2002), this bias results in weakly selective neurons whose tuning for orientation does not approach that described for cortical neurons.

In the mouse, a significant proportion of neurons in the dLGN are tuned to stimulus orientation to a degree comparable to that of cortical neurons (Marshel et al., 2012; Piscopo et al., 2013), particularly in the superficial shell layer. Directionally selective neurons in the dLGN have been shown to receive receive synaptic input from directionally selective retinal ganglion neurons (Cruz-Martín et al., 2014), and project to superficial layers of the visual cortex, suggested a 'dedicated circuit' transmitting directional information from retina to cortex, without the need for reconstruction of orientation information by cortical simple cells from untuned centre-surround LGN neurons. Furthermore, this may not be a quirk of the rodent visual system, as orientation tuned responses in geniculate neurons of the koniocellular pathway have also been reported in the marmoset (Cheong et al., 2013).

1.2.1.1 Nonlinear Responses and Inhibition

One of the major outstanding questions regarding processing of visual stimuli in V1 is the role of inhibition. Hubel and Wiesel initially labelled what are now termed OFF subregions as 'inhibitory' (Hubel and Wiesel, 1959), however this terminology was eschewed in favour of the more mechanistically ambiguous terms used by later authors. Since feedforward connections from geniculate neurons are exclusively excitatory, OFF responses must arise from either the withdrawal of tonic excitatory input from the LGN, or intracortical inhibition, in the form of either feedforward inhibition in which cortical inhibitory neurons are directly activated by thalamic afferents, or by feedback / lateral inhibition, in which inhibition is recruited by spiking activity of the population of cortical neurons themselves. Early intracellular recordings by Creutzfeldt and Ito (1968) suggested that inhibition did play a role in creating OFF responses, and the finding that the application of bicuculline (a GABA antagonist) disrupted the pattern of ON/OFF subregions (Sillito, 1975) seemed

to confirm the role of inhibition in the creation of the receptive field.

A refinement of the ON/OFF receptive field model, the push-pull model (Glezer et al., 1982; Troyer et al., 1998) predicts that stimuli that match the sign of the subregion (i.e. bright stimuli in an ON subregion, or dark stimuli in an OFF subregion) should result in an excitatory response, whereas stimuli of the opposite sign result in either an inhibitory response, or a withdrawal of tonic geniculate input. It was not until technical refinements in intracellular recordings *in vivo* in the late 1980s that the possibility of a push-pull mechanism could be addressed directly. Receptive field subregions were shown by Hirsch et al. (1998) to match the predictions of the push-pull model, and that the pull elicited by stimuli of the opposite sign to the subfield was caused by active inhibition, rather than passive withdrawal of geniculate input. Furthermore, excitatory conductance does not fall below baseline levels during drifting grating stimulation at non-preferred orientations (Anderson et al., 2000).

Whilst inhibition does clearly play a role in the creation of the push-pull receptive field, the wider role of inhibition is hotly debated. Divisive normalisation has been proposed as a 'canonical' operation normalising the activity of neurons in a variety of circuits, including the visual cortex (Carandini and Heeger, 2012). This view is based upon the observation of a number of phenomena which appear to contradict the linear feedforward model, such as contrast invariance of orientation tuning (Sclar and Freeman, 1982; Skottun et al., 1987), cross-orientation suppression (Morrone et al., 1982; Carandini et al., 1997; DeAngelis et al., 1992), surround suppression (Cavanaugh et al., 2002a,b) or the sharpening of orientation tuning responses as compared to responses predicted by receptive field maps. One model of intracortical suppression, the energy model (Heeger, 1992) sums the squared activity of neurons with varying preferred orientations and receptive field phases. These cells, with a complex-like receptive field, then provide a divisive feedback signal, normalising the responses of simple cells by a form of gain control.

The most parsimonious explanation of such gain control is GABAergic shunting inhibition (Carandini et al., 1997), in which the conductance of the neuron is dramatically increased, effectively short circuiting excitatory currents without necessarily actively hyperpolarising the cell membrane. However, even within the contested realm of intracortical inhibition, shunting inhibition is particularly controversial, with some evidence suggested that inhibition could increase membrane conductance by up to 200-300% (Borg-Graham et al., 1996; Hirsch et al., 1998), and other authors finding little evidence of shunting (Douglas et al., 1988), or even that EPSP responses to electrical stimulation of the geniculate

were actually facilitated by inhibition (Ferster and Jagadeesh, 1992), indicating a *fall* in membrane conductance. Furthermore, based upon theoretical (Holt and Koch, 1997) and experimental (Chance et al., 2002) work, it has been argued that even if shunting inhibition were to be a feature of inhibitory responses in the cortex, that the major effect would be to uniformly reduce responses in a subtractive, rather than divisive manner (reviewed in Abbott and Chance, 2005).

Whilst inhibition clearly occurs within the cortex - where roughly 20% of neurons are GABAergic (Gentet, 2012), and connect promiscuously to excitatory neurons (Fino and Yuste, 2011), the need for a lateral inhibition scheme to sculpt excitatory responses is not well proven. Priebe and Ferster (2012) argue for a more modest role for inhibition based upon a number of observations. Lateral inhibition schemes would require that the tuning of inhibition be broader than the tuning of excitation, in order to sharpen tuned responses. However, inhibitory tuning is generally found closely to match excitatory tuning both in V1 (Anderson et al. (2000); Tan et al. (2011), although see also Monier et al. (2003); Liu et al. (2011); Li et al. (2012b)) and across modalities in a variety of cortical regions(reviewed in Isaacson and Scanziani, 2011). Furthermore, effects such as contrast invariance may be explained without the need for inhibitory normalisation, by mechanisms including threshold nonlinearity (Carandini and Ferster, 2000), depression at the thalamocortical synapse (Carandini et al., 2002; Freeman et al., 2002) and trial-to-trial variability (Churchland et al., 2010). Inhibition then acts more specifically, with similar tuning and temporal profile as excitation, in order to allow for strong feedforward and recurrent excitatory signalling whilst preventing runaway feedback loops generating epileptiform activity (Douglas and Martin, 1991), as well as in certain specific cases such as surround suppression (Priebe et al., 2004).

1.2.2 Response Linearity

Much of the theoretical and experimental work described in the previous sections focuses solely upon the simple cell, for a number of reasons. According to serial feedforward models, the simple cell represents the first stage of cortical processing; therefore, under such an understanding, it may make sense to focus attention on the physiology of these before moving on to the next layer, complex cells. Secondly, simple cells are, at the very least, *closer* to being linear than complex cells, making them an attractive target to theoreticians seeking to propose computationally elegant theories of visual information processing, or cortical function more generally.

Lastly, unlike complex responses, simple responses are defined by their commonality. The original definition of a simple cell was a cell whose responses to gratings satisfied four criteria (Hubel and Wiesel, 1962). In contrast, the classification of complexity, according to this scheme is really nothing of the sort, but rather a classification of non-simplicity. Complex neurons are therefore defined as such by *failing* to conform to one or more criteria that define a simple cell. Therefore, complex cells may well encompass a more heterogenous group; some models explicitly reference multiple tiers of complex neurons (Martinez and Alonso, 2003).

The challenge of defining complex cells in a reliable manner, consistent between experimenters, was addressed by De Valois et al. (1982), who suggested the use of the spiking modulation ratio (F1/F0) ratio. This value was found to be bimodally distributed, suggested a robust classification. By comparing the F1/F0 to definitions of simple/complex responses based upon other criteria, (Skottun et al., 1991) demonstrated that this simple, unitary, measure was well-related to more arbitrary combinations of decision rules. As a result, F1/F0 has become one of the most well-used metrics in visual neurophysiology, and the observed bimodality has been taken to be a demonstration of two distinct populations. This assumption has, in turn, been questioned from both a theoretical (Mechler and Ringach, 2002) and an experimental (Priebe et al., 2004) perspective, showing that a unimodal input distribution may give rise to a bimodal output distribution, given a sufficiently non-linear transformation function. Furthermore, the membrane potential modulation ratio (Vm1/Vm0) has been shown to be unimodally distributed (Priebe et al., 2004). However, the observation of a unimodal input distribution does not, in itself, rule out the possibility of distinct populations:

'Neuroscientists do not discuss whether pyramidal cells and spiny stellate cells are different classes, and to our knowledge, nobody has shown that soma shapes are bimodally distributed.' (Martinez and Alonso, 2003)

1.2.3 Information Processing within Cortical Neurons

Whilst visual psychophysics has generated voluminous datasets and computationally elegant models, the relative paucity of empirical, mechanistic explanations for observed phenomena has stymied the development of biologically plausible descriptions of cortical function. Such empirical information consists of intracellular recordings of neuronal membrane potentials *in vivo* during visual stimulation, as well as careful characterisation of the rules of neuronal arithmetic (Silver, 2010) derived from work *in vivo* , *in vitro* and *in*

silico.

For much of the history of neuroscience, the neuron has been modelled as a computationally simple unit - most notably in the influential Perceptron model (Rosenblatt, 1958), in which the output of a neuron is related solely to the sum of its synaptic inputs. Whilst the output function itself may be elaborated in order to take account of biological realities such as spike threshold or the refractory period, this has typically been 'bolted-on' to a linear model (as in the Linear-Nonlinear-Poisson Model e.g. Carandini et al. (2005)). In this approach, the complexity of neuronal computations has been ascribed to the specificity of synaptic connectivity. Simple cells are simple because they receive patterned input from geniculate projection neurons; complex cells are complex because they receive inputs from diversely tuned simple cells.

Two principal objections may be raised to this view of the nervous system. Firstly, the implicit assumption behind many such models is that there is such an object as the platonic neuron (Llinás, 1988); that neurons are, essentially, of one form and that differences in neuronal activity arise solely from differential connectivity. However, intrinsic neuronal properties vary between brain regions (Llinás, 1988; Amatrudo et al., 2012) , between cell types within a region (Cauli et al., 1997; Kawaguchi and Kubota, 1997), and between cells of different cortical layers (McCormick et al., 1985). In order to understand the neuronal arithmetic involved in sensory circuits, it is therefore necessary to characterise the individual neurons that make up any such circuit.

Secondly, Perceptron-like models simply ignore the complex and dynamic synaptic properties and dendritic processing that underlie often highly nonlinear computations within a single neuron (London et al., 2005). These can occur at the level of the individual synapse (Thomson et al., 1993; Abbott et al., 1997) and in the interaction between multiple synapses activated in precise spatiotemporal patterns (Branco et al., 2010; Branco and Häusser, 2011).

Rather than being uniformly distributed on an idealised spherical neuron, synapses are located in a variety of positions along the basal and apical dendrites, as well as the soma itself (Gray, 1959) and the axon initial segment (Somogyi et al., 1982; Szabadics et al., 2006). Excitatory post-synaptic potentials in the distal dendrite are passively filtered, becoming smaller and broader at the soma than an EPSP of similar magnitude and duration occurring more proximally. Furthermore, the non-instantaneous conduction along the dendrite may have functional significance by the creation of 'delay lines' (Rall, 1964). Coincident activity of two or more synapses located in close proximity is also

likely to be highly nonlinear, as the activation of a synapse does not simply cause a depolarisation or hyperpolarisation, but increases membrane conductance, reducing the effect of additional synaptic activation of the same conductances (London et al., 2005). Synaptic depolarisation has been shown to depend not only upon the number and position of activated synapses, but also the temporal structure of activation (Branco et al., 2010; Branco and Häusser, 2011) - synapses activated from the outside-in (distal to proximal) result in far greater somatic depolarisation and probability of spike generation, in line with Rall's predictions.

Whilst limited reports suggested that dendrites might support active propagation of action potentials (Llinas and Nicholson, 1971), the systematic investigation of active properties of dendrites was only made possible by technical advances in patch-clamp techniques and DIC optics in the early 1990s (Stuart et al., 1993). One of the first major findings using this technique was that, rather than acting simply as passive cables, dendrites are able to actively propagate action potentials (Stuart and Sakmann, 1994). These back-propagating action potentials (bAPs, reviewed in Stuart et al., 1997) are critical both for induction of synaptic plasticity (Magee and Johnston, 1997; Linden, 1999) as well as triggering bursts of somatic action potentials (Magee and Carruth, 1999; Williams and Stuart, 1999).

In addition to back-propagating action potentials, local dendritic spikes have been described in a number of cell types, including CA1 pyramidal neurons and layer 5 neurons (Golding and Spruston, 1998; Schiller et al., 2000; Gasparini et al., 2004), and layer 2/3 neurons (Larkum et al., 2007; Smith et al., 2013). These events are distinct from somatic action potentials, which propagate anterogradely down the axon, and may additionally result in a bAP. In contrast, dendritic spikes generally remain localised to a region of the dendrite, and may arise as a result of feedback excitation involving voltage gated sodium or calcium, or NMDA receptors, which are present in the dendritic membrane (reviewed in Migliore and Shepherd, 2002; Johnston and Narayanan, 2008). Dendritic spikes are classically defined as all-or-none threshold events, caused by one of these three conductances, with NMDA spikes being present in fine distal dendrites such as the tuft of the layer 5 apical dendrite and the outer basal dendrites; calcium spikes occurring at the base of the tuft, near the top of the apical dendrite, and sodium spikes occurring in the apical shaft and soma (Major et al., 2013). Dendritic spikes may also interact with bAPs, with a single bAP coincident with a synaptic depolarisation in the distal dendrite triggering a large calcium spike (so-called back-propagating action potential elicited Ca^{2+}

spike, BAC) (Larkum et al., 1999) which in turn trigers a burst of action potentials at the soma. This has been proposed as general mechanism of coincidence detection across the cortex (Larkum, 2012), with the timing of feedforward sensory inputs to basal dendrites being compared to feedback information, representing internal models or predictions, at the distal tuft.

Whilst extensively characterised *in vitro* , the role of dendritic spikes *in vivo* has remained controversial, with scant evidence even of their existence (Major et al., 2013). However, dendritic spikes likely distinct from bAPs have been shown to be triggered during visual stimulation in layer 2/3 neurons, and may act to sharpen orientation selectivity (Smith et al., 2013).

Non-linear dendritic integration has also been shown to play an important role in binocular integration (Longordo et al., 2013; Zhao et al., 2013). Membrane potential responses to visual stimulation of both eyes together, in neurons of the binocular region of V1, is markedly less than the linear sum of the monocular responses, preserving orientation selectivity tuning.

In light of these mechanisms, the notion that visual information processing is a function of linear integration followed by nonlinear transformation in to an action potential train becomes rather unconvincing. Single neurons are highly complex computational machines, whose synaptic input defines only the starting point for a range of nonlinear operations.

1.3 Presynaptic Connectivity

This focus on the neuron as an elaborate computational unit complements, rather than replaces, the need to define the patterns of synaptic connectivity within a neural circuit. More so than any other organ, the function of the brain can not be understood without a detailed account of its microscopic structure. Indeed, a great deal of information can be deduced about the nature of neuronal circuitry from anatomy alone, as evidenced by Cajal's pioneering description of diverse regions of the nervous system using Golgi's black reaction (Ramón Y Cajal, 1995). By painstakingly detailing the morphology of the neuronal components of various circuits, Ramón Y Cajal was able to deduce the likely path of information flow, long before the electrochemical mechanisms of action potential singalling and synaptic transmission were described. These proposed schemes have proven to be remarkably prescient, including the general deduction that conduction was unidirectional, from the dendrites to the soma to the axon (Ramón Y Cajal's Law of

Dynamic Polarisation), as well as specific predictions regarding the circuit structure of the retina (Piccolino, 1988), hippocampus (Freund, 2002), and olfactory bulb (Figueres-Onate et al., 2014) that remain broadly accepted over one hundred years later. However, the cortex remained enigmatic, even when subjected to Ramón Y Cajal's keen eye and sharp intellect, remaining a tangled thicket in which no clear pattern of connectivity could be deduced. To this day, one of the most outstandingly difficult endeavours in neuroscience has remained the quest to 'solve the cortex'; to provide a detailed account of cortical structure and function that explains existing observations and predicts novel ones. A discussion of modern models of cortical connectivity and function follows in section 1.4, however first I outline the techniques that have been used in creating such models.

1.3.1 Lesioning, Degeneration, and Axonal Transport

Following Waller's description of the 'degeneration' of axons following the sectioning of the hypoglossal and glossopharyngeal nerves in the frog (Waller, 1850), the lesioning of a nerve or small portion of the brain, and observation of the attendant pattern of anterograde degradation, could be used to determine projection patterns. This was the first target-specific, long range connectivity mapping approach, with two distinct advantages over dense neuronal labelling such as the Golgi stain, particularly when combined with similar silver-based stains that enhanced the observable degeneration (Glees, 1946). Firstly, only areas of connectivity (anterograde, in this case) germane to the cell or region in question are labelled. This feature makes possible the detection of connectivity which might otherwise be lost in a forest of dendrites. This signal selectivity underpins the second advantage of target-specific tracing: easy identification of long-range connectivity. Even when single processes may be traced in densely labelled stained tissue, visualisation of such tissue has historically been carried out in thinly sliced histological sections, making the task of reconstructing axons over distances of tens of millimetres (or tens of centimetres, in the case of spinal projection neurons) impossible. In contrast, a targeted approach stains only the tract in question, allowing for unambiguous identification of connectivity by visualisation of distal labelling alone. It is these twin properties of targeted and specific labelling that are key to any useful tracing system.

However, dense labelling and tract degeneration remained essentially the only techniques available in the biologist's arsenal until around the 1970s, with the finding that axons could actively transport proteins in a retrograde (i.e. towards the soma) direction. All that was needed to hijack this system for the purposes of tracing connectivity was a

suitable stain. Fluorescent stains of the time, such as Evans Blue, were weak and easily dissociated from the conjugated protein; however enzymes such as horseradish peroxidase are readily transported by the axon (Kristensson and Olsson, 1971; Kuypers and Maisky, 1975). HRP is a potent oxidising agent not found in mammalian cells, and thus its presence may be deemed to be a specific result of the experimental treatment. Alone, HRP is not visible, however, when incubated with hydrogen peroxide and a suitable reduced chromogenic substrate such as 3'3-diaminobezidine, a very high contrast, stable staining is obtained.

When used alone, HRP tracing is relatively inefficient, weakly labelling only a few neurons. Conjugation to wheatgerm agglutinin (Gonatas et al., 1979) or other lectins greatly increases the efficiency of uptake and transport of the label. Other tracing systems leverage the active transport of bacterial toxins, such as tetanus or cholera toxin (subunit b) (Stoeckel et al., 1977) or dextrans (Glover et al., 1986; Nance and Burns, 1990) to achieve a broadly similar outcome.

Four key disadvantages limit the scope of HRP anatomical tracing techniques. Firstly, as noted above, contrast is not inherent in the enzyme itself, but must be introduced by chemical processing. This laborious process greatly reduces the potential throughput of the technique. Secondly, the monochromicity of such contrast precludes combinatorial studies, examining features such as convergent connectivity from multiple brain regions. Thirdly, although certain conjugates show broad specificities for retrograde (lectins, toxins) or anterograde (dextrans) transport, an ideal tracing tool should be exquisitely specific to neurons of interest, spread in a predictable and unidirectional manner, and not label local axons of passage. Lastly, these techniques stain only the cell itself. Whilst axonal transport can label somata distant to the injection site or, conversely, somatic labelling can stain axonal processes over long distances, particularly with the use of biocytin filling (Marx et al., 2012), the ability to label presynaptic connectivity or postsynaptic targets of the neuron is necessary in order to investigate the functional relevance of axonal projections.

1.3.2 Fluorescent Labelling

Fluorescent latex beads (Katz et al., 1984) address some of the issues with chemical stains as outlined above. Small latex microspheres are taken up by neurons by largely unknown mechanisms, and are transported exclusively in a retrograde fashion by axons. Beads of multiple colours can be combined in order to investigate anatomical convergence or divergence, and labelling is bright and stable without the requirement of additional chemical

process. Fluorescent lipophilic dyes such as DiI (Honig and Hume, 1986) may also be used to stably label the cell membrane of neurons over days or weeks; a number of chemical variants (DiO, DiD) of this class provide for a palette of colours. However, just like HRP labelling, bead and DiI/DiO labelling are restricted to the neuron itself, rather than its synaptic partners, and are non-specific with regard to neuronal class.

The development of stable, bright, organic fluorescent dyes such as green fluorescent protein (Tsien, 1998) and an extended palette of colours distinguishable by conventional and advanced microscopic techniques (Matz et al., 1999; Shaner et al., 2004) has been rightly heralded as one of the triumphs of modern molecular genetics, finding application across the entirety of biological science. A promising, novel technique involving the stochastic and combinatorial (on a cell-to-cell level) expression of several of these proteins, the 'Brainbow' (Livet et al., 2007), offered the possibility of combining dense labelling with identifiability of individual neurons. However, the fine diameter of axons in the central nervous system of the mammal, combined with limited numbers of identifiably distinct combinations of fluorophores, has prevented the promise of the Brainbow, to untangle the cortical thicket, from being realised.

1.3.3 Viral Techniques

Rather than engineering the ideal tracing tool *de novo*, biologists have adapted existing agents uniquely designed by natural selection to enter neurons and spread in a predictable, unidirectional manner - the viruses. One approach involves the use of lentiviruses (Grinevich et al., 2005) or adeno-associated viruses (Chamberlin et al., 1998; Harris et al., 2012) to label groups of neurons with fluorophores, such as eGFP. This label is expressed throughout the neuron, including the axon, and by detecting fluorescence in distal regions the presence of an axonal projection may be inferred. Expression of the fluorophore may be restricted to a group of neurons by simply targeting the location and size of the virus injection, by linking expression to a cell-specific promoter, or by the use of the Cre-lox system (or similar) to allow for viral expression only in neurons expressing the Cre enzyme (Hardy et al., 1997). This approach has been used to define a 'mesoscale connectome' (Oh et al., 2014) based upon brainwide mapping of labelled axons from around 80 injection sites. However, the distribution of axons is not the same as the distribution of synaptic connections; axons of passage, which do not form synaptic connections within a particular region, can not be readily distinguished from axon terminals. A more refined approach is the use of trans-synaptic tracing, in which connectivity is detected by the labelling of

either pre- or post- synaptic neurons - retrograde or anterograde trans-synaptic tracing.

A number of viruses are of particular interest in the context of trans-synaptic tracing. The most notable classes are the Herpesviridiae (HSV-1 and Pseudorabies Virus) and the Rhabdoviridiae (Rabies Virus and Vesicular Stomatitis Virus) (Ugolini, 2010). Each viral *vector* - a term referring not just to the class and strain of the virus, but also the particular engineered variant - has a distinct profile of properties (Nassi et al., 2015) that must be considered for the particular experiment. These properties include genome size, genetic payload, expression level and duration, titer, nucleic acid (RNA or DNA), direction of trans-synaptic spread (anterograde or retrograde), kinetics of expression and trans-synaptic spread, the presence or absence of an envelope, toxicity, and safety (to the experimenter, the subject, or to the environment). This last is of particular importance to the experimenter, as all the viruses listed here cause disease in either man or livestock, with rabies virus infection being particularly lethal in most animals, including humans.

Early trans-synaptic tracing using HSV-1 or pseudorabies was a fickle process, with a fine balance needing to be stuck between the invasiveness of the virus and host viability (Aston-Jones and Card, 2000; Ugolini, 2010). Herpesviridiae are quite toxic to the cells in which they replicate, causing degradation of the host neurons within a similar timeframe to the labelling of presynaptic neurons, with extensive lysis typically occurring at around 2-3 days post-infection (Ugolini et al., 1987). Furthermore, both HSV-1 and PrV cause non-specific labelling of neighbouring neurons and glia, most probably as a result of this lysis (Ugolini, 1995b).

In contrast, the rabies virus - whose gross clinical course is by far the most deadly of the viruses listed here - does not cause the rapid neuronal degeneration and attendant inflammation typical of the α-herpesviruses (it is this fact, in part, which allows the virus to spread unchecked throughout the nervous system of an infected host animal), nor the resulting spurious labelling of neighbouring cellular populations (Ugolini, 1995a). In addition, unlike the herpesviruses, rabies virus spreads exclusively in a unidirectional (retrograde) manner, allowing for unequivocal interpretation of the experimental result (Kelly and Strick, 2000; Ugolini, 2010).

1.3.3.1 The Rabies Virus

The rabies virus itself is a single-stranded negative sense (complementary to mRNA) virus of the genus *Lyssavrius*, with a characteristic morphology typically described as 'bullet-shaped'. The viral genome is relatively compact, approximately 12kb in length

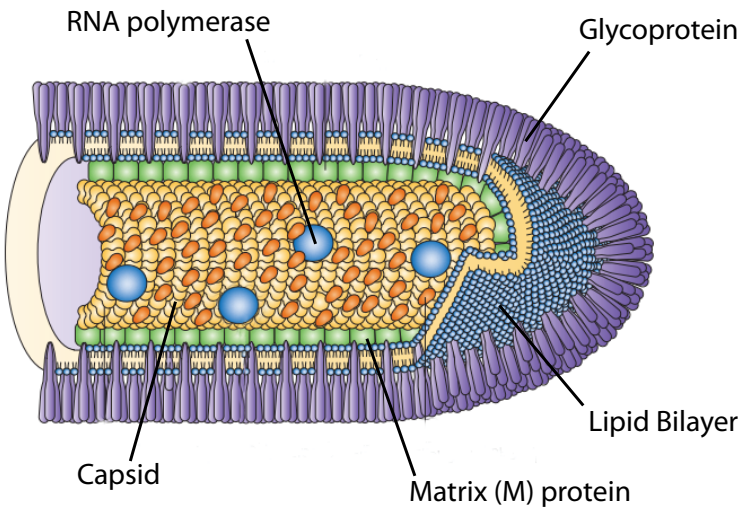

Figure 1.3: The Structure of the Rabies Virus
A complete, bullet-shaped rabies virion comprises a helical core of single-stranded negative sense RNA, tightly associated with the nucleoprotein (yellow). The capsid consists of the ribonucleoprotein in association with phosphoproteins (orange) and RNA polymerase (blue). The capsid is surrounded by a mesh of matrix protein (green), and a phospholipid bilayer derived from the host cell membrane, densely studded with the trimeric transmembrane glycoprotein, which mediates the binding of the virus to presynaptic receptors. Adapted from Schnell et al. (2010).

(Conzelmann et al., 1990), and it encodes only 5 distinct proteins: the nucleoprotein (N), the matrix protein (M), the RNA polymerase (L), a polymerase cofactor (P), and an external glycoprotein (G), in the order 3'-N-P-M-G-L-5' (Ugolini, 2010). The complete virion (fig. 1.3) consists of a central core, containing the helical nucleic acid and the N, L, and P proteins, surrounded by a M protein mesh (Knipe and Howley, 2007). Rabies is an enveloped virus, with the virion being surrounded by a lipid bilayer derived from budding from the host cell. This membrane is modified with the addition of the G protein, which defines the specificity of the virion to target receptors.

The G gene encodes for a 505 amino acid transmembrane protein. The majority of the protein forms a 439 amino acid ectodomain (projected from the cell membrane in to the extracellular space), with a 22 amino acid transmembrane anchor, and a 44 amino acid cytoplasmic domain (Conzelmann et al., 1990; Ghanem and Conzelmann, 2015). Mature G protein, produced in the endoplasmic reticulum by the host cell, is trafficked to the cell membrane where it forms a homotrimer (Gaudin et al., 1992). The intracellular domain of these G protein trimers then guides the incorporation of the virion (Ghanem and Conzelmann, 2015). However, deletion of the G protein reduces budding by only around 30-fold (Mebatsion et al., 1996). Rabies virus budding is primarily driven by the

M protein; complete deletion of the M gene results in reduction of budding rates by around 500,000 times (Mebatsion et al., 1999).

The primary function of the G protein spike is to bind the released virion to receptors on target cells, and to trigger actin-dependent endocytosis (Piccinotti et al., 2013). The identity of the receptor is still somewhat debated (reviewed in Lafon, 2005). In vitro studies have demonstrated binding of G protein to nictonic acetylcholine receptors (nAChR), cell adhesion molecules such as NCAM, and the low-affinity neurotrophin receptor p75NTR. The role of nAChR in virus spread is likely to be indirect, since at the neuromuscular junction it is exclusively located on the (postsynaptic) muscle cell. One suggestion is that nAChR acts to concentrate the virus, making terminal uptake more likely (Lafon, 2005). Therefore, NCAM and p75NTR are considered the most likely general candidates. However, animal models in which these molecules are deleted or not expressed delay rather than prevent rabies virus infection (Ghanem and Conzelmann, 2015). The role of other molecules, including carbohydrates, gangliosides and lipids, in rabies virus spread is still a matter of active research (Schnell et al., 2010; Ghanem and Conzelmann, 2015), and it seems likely a number of separate molecules mediate G-protein binding during infection. In principle, such mechanisms could allow for spread of the virus from an infected cell to any neighbouring cell - neuron or otherwise. However, rabies virus displays two key properties that make it useful for neuronal tracing - neurotropism, and unidirectional (retrograde) spread, across synapses.

The mechanism restricting rabies virus spread to trans-synaptic retrograde transmission is not well understood. It seems likely that the distribution of receptor proteins is not a sufficient explanation (Lafon, 2005); active trafficking of the G protein to postsynaptic domains may contribute, however *in vitro* studies have not demonstrated preferential budding at any cellular location (Ghanem and Conzelmann, 2015). However, the *direction* of trans-synaptic spread is primarily determined by the G protein. VSV whose G protein is replaced by the rabies G spreads exclusively in a retrograde fashion; in contrast VSV carrying the lymphocytic choriomeningitis virus G protein spreads in an exclusively anterograde fashion (Beier et al., 2012).

1.3.3.2 Polysynaptic and monosynaptic tracing

The unidirectional, neurotrophic infection caused by RV makes it highly suitable for the study of projection pathways (Ugolini, 1995a; Kelly and Strick, 2000). However, even attenuated strains such as the commonly used Street Alabama Dufferin (SAD), which

can not reach the central nervous system following peripheral infection in most mammals, spread unchecked within the central nervous system. The study of connectivity of a defined synaptic order using intact rabies virus is therefore made difficult; careful timing may allow mono, di- or tri- synaptic connections to be identified, but this is highly dependent upon the region, animal and viral strains, as well as the titre of the particular viral preparation. Furthermore, in some cases, the rate of viral spread has been shown to be dependent upon the strength of the connectivity, with spread occurring to second-order neurons from some first-order neurons before more weakly connected first-order neurons are labelled (Ugolini et al., 1987; Ugolini, 1995a). An ideal viral tracer should be restricted not just in direction of spread, but in the order of spread, such that experimental findings are robust.

The first step in the development of modern RV tracing was the creation of the RV-ΔG, genetically engineered to be lacking the rabies glycoprotein (Mebatsion et al., 1996). As noted above, the deletion of the G protein only attenuates, rather than prevents, budding of the virus. However, the 'bald' virions produced in the absence of the G-protein are unable to bind to and/or triger endocytosis in an uninfected cell, effectively preventing the spread of the virus (Etessami et al., 2000). Therefore, an engineered virus strain in which the G protein is replaced with a fluorescent marker, such as the SAD ΔG-eGFP(Wickersham et al., 2007a) will label only the infected neuron, unable to spread. Used alone, fluorescent ΔG rabies viruses brightly label neurons whose somata or processes are close to the site of injection, since the virus may replicate within the neuron, amplifying the signal such that dendritic or even axonal morphology may be visualised (Wickersham et al., 2007a).

The true power of the ΔG system is that the starter neuron (or neurons) can be provided with the deleted G gene (transcomplementation) restoring the infectivity of the rabies virus within the transfected cell or cells (Etessami et al., 2000; Wickersham et al., 2007a). However, when the virions reach the first-order neurons, which are not transfected with the G protein, further trans-synaptic transmission on to higher-order connections is prevented.

In order to complete this molecular targeting approach, Wickersham et al. (2007b) took advantage of the specificity of the avian sarcoma and leukosis virus envelope protein (EnvA) for the avian TVA receptor. This receptor protein, related to the low-density lipoprotein receptor (Bates et al., 1993) is constitutively expressed in birds including the chicken and quail, but not in mammals. Blockade of the receptor using antibodies in cell culture prevents ASLV infection (Bates et al., 1993), whereas transfection of primate cells with the TVA gene confers susceptibility to ASLV infection (Young et al., 1993). TVA is

therefore both necessary and specific for infection by ASLV, and may therefore be used to target infection in mammlian tissue (Federspiel et al., 1994). By pseudotyping the rabies virus with the EnvA protein, (Wickersham et al., 2007b) demonstrated that RV infection could be restricted to target neurons.

The complete modified rabies virus tracing system therefore consists of two stages. First, starter cells are transfected with plasmids containing three genes: the rabies glycoprotein, the TVA receptor, and a fluorophore distinct from that carried on the RVΔG. This last is not strictly necessary, but it aids in confirming the identity of the transfected cells. Following transfection, RVΔG pseudotyped with an EnvA membrane is injected close to the transfected cells. The virus is then specifically taken up by the transfected neurons (fig. 1.4), but not other cells, and from these neurons it spreads to monosynaptically connected neurons only. Viral spread is thought to be highly sensitive and specific (Wickersham et al., 2007b). In experiments which directly assessed functional connectivity, 9/11 virally labelled putative presynaptic neurons were found to be functionally connected to a single nearby starter cell (Wickersham et al., 2007b), indicating a good correlation between transsynaptic spread and connectivity. This is likely to be an underestimate, since in these experiments multiple starter cells were transfected in the same slice, and so the 2/11 neurons not found to be connected to the single chosen starter may have been labelled as a result of connections from other starter cells. The sensitivity of the system, however, is largely unknown.

Targeting of starter cells may be accomplished in a number of ways. Marshel et al. (2010) and Wertz et al. (2015) used single electroporation to transfect a single starter neuron in visual cortex; Rancz et al. (2011) and Vélez-Fort et al. (2014) used dialysis of plasmids within the intracellular solution during whole-cell patch clamp recordings. Multiple starter cells may also be transfected using a second helper virus such as the adeno-associated virus (AAV). By restricted expression to genetically identified cell types using the Cre-lox system (Hardy et al., 1997) in genetically modified mice, the presynaptic connectivity of distinct molecular classes of neurons may be examined (Watabe-Uchida et al., 2012; Miyamichi et al., 2013; Sun et al., 2014; Vélez-Fort et al., 2014). However, whole-cell transfection allows for simultaneous functional characterisation of the targeted neuron. RVΔG-GCaMP6s has been used to characterise spiking-related activity in response to sensory stimulation in both the presynaptic and starter cells (Wertz et al., 2015). Whilst rabies virus infection does not cause the acute degeneration typical of the α-herpesviruses (Ugolini, 1995a, 2010), nor does it grossly alter the electrophysiological

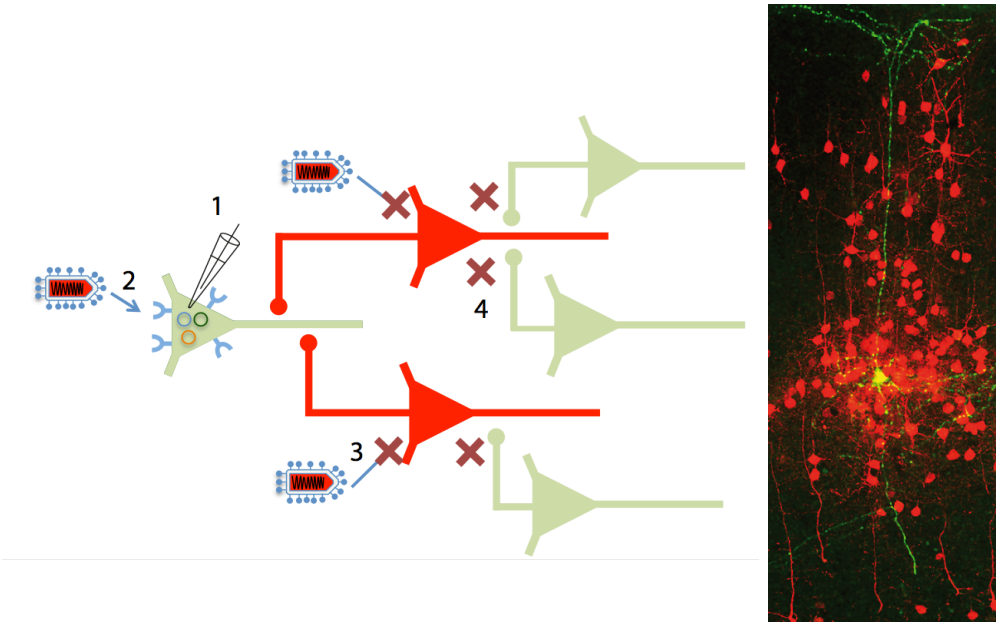

Figure 1.4: Single Cell Monosynaptic Rabies Virus Tracing.
Left: Schematic of the technique. Labelling of the first-order presynaptic neurons (red) of a single cell (left) is achieved using an engineered, pseudotyped fluorescent rabies virus. First, a single neuron is transfected with plasmids encoding the deleted G-protein, the TVA receptor, and a fluorophore distinct from that carried by the virus. In this example, transfection is carried out using dialysis of nucleic acids during whole-cell recordings (1). Pseudotyped RV, with an envelope containing the EnvA protein (blue), is injected close by, and is able to enter the host neuron, which expresses the TVA receptor on its surface (2), but not any other cell (3) Once inside the host cell, the virus is able to replicate and spread to presynaptic neurons, in which replication continues and the neuron is brightly labelled. However, further transmission to higher order presynaptic connections is prevented by the lack of G protein either on the virus itself, or in the first-order cells (4).
Right: Single-cell presynaptic tracing of a layer 5 neuron (yellow), surrounded by local presynaptic neurons (red) (Rancz et al., 2011, from).

properties of infected neurons, up to 12 days post-infection (Wickersham et al., 2007a), it does cause some cell death, beginning at around 16 days. The precise effect, if any, of rabies virus infection on neuronal function is not yet known.

1.4 Cortical Connectivity and Function

1.4.1 The Cortical Microcircuit

Despite its involvement in a great variety of sensory, motor, and cognitive processes, one of the defining feature of the cortex is its conserved six-layered structure. Cortical laminae contain distinct morphological classes of cells, such as the large pyramidal neurons of layer 5, smaller pyramidal neurons of layer 2/3, spiny stellate cells found only in layer 4, or the predominantly acellular layer 1 (Oberlaender et al., 2012). This basic structure, as well as patterns of connectivity between layers within a cortical area (Thomson and Lamy, 2007; Douglas and Martin, 2004), as well as subcortical and interareal connecitivity (Thomson and Lamy, 2007; Harris and Mrsic-Flogel, 2013) are generally found to be similar not just in different cortical areas, but across mammalian species (Defelipe, 2011).

This basic, conserved structure has lead many to conclude that the cortex may perform diverse computational tasks by similar mechanisms, as a result of a 'canonical' (Douglas and Martin, 1991; Bastos et al., 2012) microcircuit. Early models (Gilbert, 1983) focussed upon the excitatory components of the circuit, using horseradish peroxidase reconstructions of neuronal morphology and axonal projections. These models largely conform to the predictions of the serial feedforward model of V1 function, with geniculate neurons projecting to the largely simple cells of layers 4 and 6 directly, layer 2/3 receiving inputs from layer 4 and, in turn, sending projections to layer 5. This basic structure remains at the core of all models of cortical connectivity, including those modified to include the connectivity of inhibitory interneurons (Douglas and Martin, 1991; Packer and Yuste, 2011), as well as neuronal subclasses within cortical layers.

However, connectivity is not structured by cell class or laminar location alone. Bidirectional connectivity between pairs of neurons located in close proximity to one another is around four times more common than would be expected by chance (Song et al., 2005), and more complex connectional motifs among larger groups of neurons are also overrepresented in reality. Neurons in layer 2/3 that are functionally connected are more likely to receive common input from layer 4 and from other layer 2/3 neurons (Yoshimura et al., 2005). Clonally related neurons are more likely to be electrically coupled than nearby neurons descended from different lineages of the same cell class (Yu et al., 2012); this finding may partially explain the greater degree to which sister neurons share tuning properties to visual stimulation (Ohtsuki et al., 2012; Li et al., 2012a). Regardless of lineage, neurons sharing response properties to both artificial and naturalistic visual stimuli

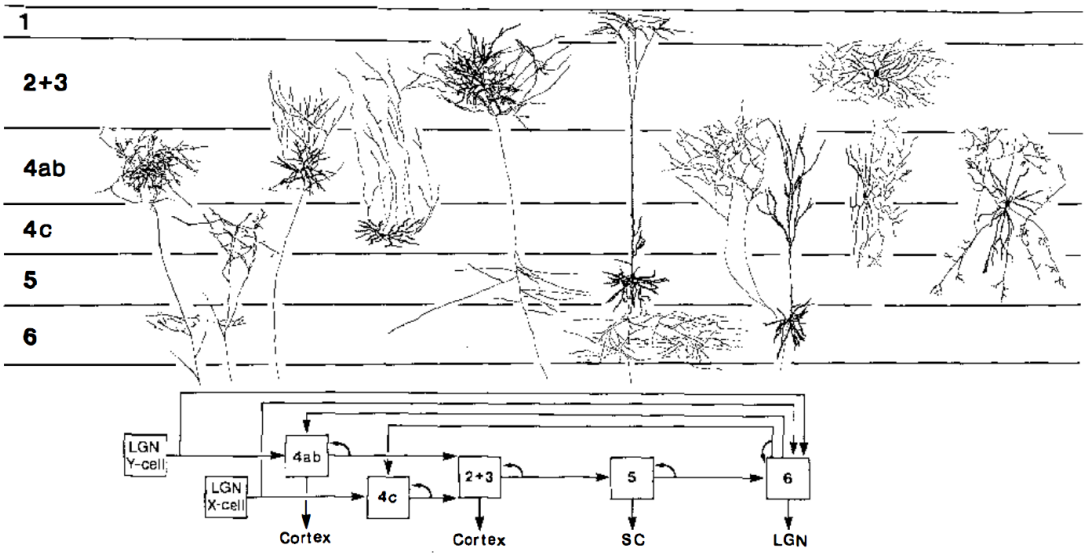

Figure 1.5: Neuronal morphology and connectivity in the visual cortex. Above: Examples of the distinct morphologies of principal cells of different cortical layers, visualised by HRP fills of individual neurons.
Below: A general model of information flow in the cortex, derived from patterns of axonal projection. In addition to some recurrent connectivity, information flows broadly from thalamus→L4→L2/3→L5→L6. In addition, L/3 neurons project to other cortical areas, L5 neurons to subcortical targets (in addition to other cortical areas), and L6 projects back to the dLGN (although more recent studies restrict this projection to a particular class of L6 excitatory neuron). This general schema remains highly influential in models of the cortical circuit. Adapted from Gilbert (1983)

are more likely to be connected (Ko et al., 2011; Bock et al., 2011). This nonrandom connectivity suggests that the cortical population may contain interdigitating subnetworks, not wholly separated one from another, but yet sharing a greater proportion of connectivity within the network than to other nearby neurons in general (Harris and Mrsic-Flogel, 2013).

In contrast to the specific connection patterns observed for pyramidal neurons, local presynaptic connectivity of cortical interneurons is thought to be largely non-specific, approaching 100% for some classes of interneuron (Fino and Yuste, 2011; Packer and Yuste, 2011; Scholl et al., 2015). This finding has been proposed by Kerlin et al. (2010) and others as an explanation for the greater evidence of the role of lateral inhibition in orientation tuning in rodents (Liu et al., 2011) than in the cat (Anderson et al., 2000). Since interneurons integrate the population activity of almost all neurons in the local area (within approximately 100µm of their soma, Scholl et al., 2015), in rodents, which lack a topographical arrangement of excitatory neurons by orientation preference, the summed activity of the local network is not well tuned for orientation; therefore, the orientation selectivity of interneurons is low (Sohya et al., 2007; Hofer et al., 2011). In contrast, in the cat, the orientation tuning properties of neurons within the local cortical region are far

more homogenous, resulting in inhibitory neurons that are more narrowly tuned (Cardin et al., 2007). Therefore, the tuning of feedback inhibition on to a given pyramidal neuron is likely to be much more similar to the excitatory feedforward input on to that same neuron than in species lacking orientation columns, resulting in a potentially reduced role for lateral inhibition in cats or primates.

1.4.2 Recurrent and Feedback Connectivity

Perhaps the most severe blow to a classical feedforward model is that the observed connectivity of cortical neural circuits is dominated by recurrent connectivity (Douglas et al., 1995). As noted above, lateral connectivity within a cortical area and layer is extensive, particularly in L2/3 (Binzegger et al., 2004). Furthermore, even within layer 4, only a small minority of synapses are formed by geniculate afferents. Estimates of the precise fraction vary (reviewed in Douglas and Martin, 2007), but the general consensus is around 5% for a layer 4 spiny stellate neuron, with the remainder of the connections originating predominantly from other spiny stellate neurons, and cells in layer 6 (Ahmed et al., 1997). However, the thalamocortical synapse is particularly efficient, containing a greater number of release sites, and having a higher release probability such that, overall, synaptic transmission is around 5 times more effective than a corticocortical excitatory synapse (Ziv et al., 1999). Despite this, geniculate afferents still contribute only a minority of the synaptic drive on to a layer 4 neuron. Similarly, layer 4 axons do project on to L2/3 neurons, but recurrent L2/3 connectivity is thought to be far more prominent (Binzegger et al., 2004), although this figure is more difficult to derive precisely. Douglas and Martin (2007) suggest that rather than being solely driven by feedforward excitation, layer 4 neurons are largely driven by recurrent cortical activity, with thalamic input being 'just enough' to drive spiking activity when sufficiently synchronised. Moreover, recent experimental work in L4 neurons has demonstrated directly that optogenetically silencing the surrounding cortex greatly reduces synaptic input evoked by visual stimuli as, and almost totally eliminated spiking activity, thereby elegantly demonstrating the necessity of recurrent connectivity in amplifying thalamic input to the cortex (Lien and Scanziani, 2013). The precise role of recurrent activity is not fully characterised. However, under the just-in-time/just-enough model, it may serve to amplify weak feedforward connections, providing a form of gain control or context-dependent modulation.

In addition to recurrent connectivity, interareal connectivity is a prominent feature of all cortical areas, including primary sensory cortex (Harris and Mrsic-Flogel, 2013).

Neurons in V1 have been shown to integrate non-visual sensory information (Iurilli et al., 2011), respond to reward (Shuler and Bear, 2006), sensorimotor mismatch (Keller et al., 2012), motion information (Saleem et al., 2013) and reward-related salience of visual stimuli (Poort et al., 2015). Furthermore, V1 receives feedback / top down information from higher cortical areas that may modify even classical receptive field properties either by direct, long-range corticocortical connections or via subcortical structures such as the pulvinar (reviewed in Gilbert and Li, 2013). These findings are greatly at odds with a mechanistic view of a feedforward model, in which V1 performs a context-invariant piecewise Fourier transform, and then passes information up the cortical hierarchy, with each level of computation adding to the abstraction.

1.4.3 Neuronal Diversity

In creating a general model of cortical function, even one restricted to the specifics of a given area and species, neurons must be grouped in to classes. There are a number of criteria by which this classification may be carried out, including morphology (Oberlaender et al., 2012; Marx and Feldmeyer, 2013), electrophysiological properties (Cauli et al., 2000; Nowak et al., 2003; Marx and Feldmeyer, 2013) and molecular or genetic identity (Gonchar et al., 2007; Sohya et al., 2007; Zariwala et al., 2011; Pinto and Dan, 2015). Such classifications may be used to investigate the differences in intrinsic and synaptically evoked properties, as well as connectivity, between neuronal classes, in order to dissect the neural circuit.

However, this grouping process may overlook variation *within* a neuronal class. For example, although the orientation selectivity of L2/3 parvalbumin positive neurons is, on average, less than the orientation selectivity of excitatory neurons (Hofer et al., 2011), the OSI variability within each group is still large. This finding, and others like it, can be explained in a number of ways. Firstly, it is possible that a particular group actually contains multiple subgroups with distinct properties (see e.g. Helm et al., 2013). However, assuming that variability within a proposed subgroup is small, this should result in a multimodal distribution, with discrete peaks arising from each subgroup. This pattern is not generally observed in distributions of intrinsic, or synaptically-evoked properties. Whilst it is possible that the subgroups themselves are broadly distributed, this would then beg the original question: why are distinct neuronal classes seemingly so variable?

A second possibility is that variability represents either biological noise or measurement of a property unimportant to the underlying function of the circuit. Excitatory cell OSI

could vary widely simply because it is not a realistic measure of the function of visual system neurons under more naturalistic conditions, or because stochastic developmental processes are unreliable. Whilst both of these postulates are possible, and indeed likely, causes of some variation, serious objections must be raised to the explaining away of within-class variation as artefact. Might there be positive reasons for a sensory neural circuit to include neurons with diverse properties?

The role of within class diversity has been explored in a number of contexts. In the crustacean somatogastic ganglion, Prinz et al. (2004) demonstrated that differing the properties of a simple triad of neurons generating rhythmic output could result in hundreds of thousands of model networks with spiking behaviours indistinguishable from that observed experimentally - in other words, that the same computational goal may be achieved by a diverse array of actual network implementations. Furthermore, the expression profiles of ion channels in these neurons do vary extensively from animal to animal, but in a constrained manner such that the broad response property of a given, identified neuron, remains relatively constant (Schulz et al., 2007). These findings indicate that even in the stereotyped crustacean nervous system, a single model may not suffice to explain the function of a neural circuit. Furthermore, it has been argued that the analysis of mean properties of neurons may not simply obscure the role of variability, but create a model neuron whose particular combination of properties is never seen in the population (Marder and Taylor, 2011).

In the mammalian olfactory bulb, variability in the intrinsic properties of mitral cells has been shown to decorrelate sensory input, doubling the information capacity of the system (Padmanabhan and Urban, 2010). Physiological levels of intrinsic diversity create populations whose decoding ability of heterogenous stimuli is increased, relative to simulations consisting of homogenous or wildly diverse populations (Tripathy et al., 2013). This may explain the finding that differences in the I_h current of pairs of mitral cells which connect to the same glomerulus, and therefore receive similar sensory input, are significantly less than the differences between mitral cell pairs of different glomeruli (Angelo et al., 2012).

In contrast to the olfactory bulb, investigation of the functional impact of within-class diversity of cortical neurons is limited. Dendritic length of parvalbumin positive inhibitory interneurons has been shown to correlate inversely with orientation tuning (Runyan and Sur, 2013), but most studies of cortical neuronal function focus on the general rules governing information processing, often combining data from multiple cortical layers and species

(Priebe et al., 2004; Tan et al., 2011). The question of the role of variation within a single cortical layer, in the mouse (or otherwise), remains ripe for exploration.

1.5 Recording Neuronal Activity In Vivo

1.5.1 Single-Unit Extracellular Recording Techniques

The first experiments recording neuronal activity in primary visual cortex (Hubel and Wiesel, 1959, 1962) were carried out using tungsten microelectrodes. These consist, essentially, of a long, thin wire, coated with an insulating layer of laquer, epoxy, or glass for its entire length, save the tip. Similar recordings may also be obtained using glass (typically borosilicate) micropipettes pulled to a tip diameter of approximately 0.5-1.0µm, filled with a conducting electrolyte (typically 2M NaCl solution). In either case, the electrode is advanced in to the brain, whilst monitoring the potential at the tip, with the aim of detecting action potentials from a single, isolated unit. One common technique is to stimulate the system under investigation, in order to evoke spiking activity - in the case of the visual system, using classical grating or bar stimuli (Gao et al., 2010). Once recordings have been made from a single neuron, additional units can be sampled by simply advancing the electrode until another neuron is encountered. Single unit recordings have been extensively in the study of visual cortex physiology, inter alia to describe properties of neuronal receptive fields (Hubel and Wiesel, 1959, 1962; Dräger, 1975; Movshon et al., 1978a; Emerson et al., 1987), spatial summation in simple cells (Movshon et al., 1978b), to map cortical representation of retinotopic position (Blasdel and Fitzpatrick, 1984), as well as to study effects such as non-classical contextual stimuli on orientation tuning (Gilbert and Wiesel, 1990). However, single-unit recordings remain limited by their being relatively low-yield, as sampling is limited to one neuron.

1.5.2 Multi-Unit Extracellular Recordings

Recording the activity of multiple neurons simultaneously is advantageous for two distinct reasons. The first, as already alluded to, is throughput: obtaining single-cell recordings of large numbers of neurons is laborious and time-consuming, as well as (typically) requiring larger numbers of animals. The second principal advantage of recording large numbers of neurons simultaneously is that the neuronal responses may be related one to another, allowing for cross-correlational network analyses to generate and test models of information flow within and between brain regions, such as feature binding by temporal integration

(Gray et al., 1989; Singer and Gray, 1995).

The individual activity of several tens to hundreds of neurons may be recorded using multisite electrodes, with spiking activity assigned to individual units by statistical techniques ('spike sorting'). This approach as enabled population-level studies of visual cortical responses (Niell and Stryker, 2008). As the density of recording sites increases, so does the potential yield of multisite recordings - up to thousands of neurons simultaneously (Einevoll et al., 2011), although more typically recordings are limited to several hundreds of units (Marblestone et al., 2013). The technological increase in recording capacity has been described as following an exponential law similar to that described by Moore for microprocessors, although at a slower pace, with the number of neurons that may be sampled simulataneously doubling roughly every 7 years (Stevenson and Kording, 2011).

Whilst allowing for high-throughput recordings of large numbers of neurons simultaneously, multisite electrode recordings are limited by a number of factors. Firstly, spike sorting remains a non-trivial statistical exercise, with different groups employing a range of approaches that may affect experimental results (Einevoll et al., 2011). Secondly, very sparsely firing neurons may be underrepresented by both single-unit and multi-unit recordings, as spiking activity is used to detect the presence of a neuron. Olshausen and Field (2005) argue that this bias is likely present in many extracellular recordings in V1, based upon a comparison of reported firing rates to theoretical modelling of spike rate distributions, although this effect is likely to be highly dependent upon the particular experimental paradigm employed. Lastly, multiunit recordings provide very indirect data on the spatial position of recorded units, although current source density information (Mitzdorf, 1985), obtained by comparing the potentials at multiple electrodes, may provide information on features such as the laminar flow of visual information (Niell and Stryker, 2008).

1.5.3 Imaging Neuronal Activity

Whilst neuronal action potential activity is, by definition, an electrical phenomenon, a variety of methods have been employed to image signals evoked by, or correlated to, neuronal activity. One more direct method is the use of voltage sensitive dyes. This approach is currently restricted to single cells in cell culture or slices (Djurisic et al., 2004; Stuart and Palmer, 2006; Bradley et al., 2009) or wide-field imaging in vivo (Petersen et al., 2003; Benucci et al., 2007; Katzner et al., 2009). Alternative imaging methodologies have been used to detect correlates of neuronal activity, such as by intrinsic signal imaging (Grinvald

et al., 1986; Toth et al., 1996; Van Hooser et al., 2005; Garrett et al., 2014), thought to reflect metabolic changes in haemodynamic activity. However, the signal-to-noise of this methodology is very low, with responses typically only detectable following averaging of responses to many stimulus presentations or by analysing higher-order statistical features (Kalatsky and Stryker, 2003). Furthermore, the spatial resolution of intrinsic signal imaging is limited to around 100µm, as the signal arises from haemodynamic changes in response to bulk population activity. The BOLD signal change detected by functional magnetic imaging (fMRI) is thought to derive from a similar mechanism to that of intrinsic signal imaging, and is therefore limited to similar spatial resolutions, and low temporal resolution (Goense and Logothetis, 2006)

Fluorescent dyes able to report changes in intracellular calcium associated with electrical activity have been in use since the 1980s (Grynkiewicz et al., 1985). A key step forward was the ability to label populations of cells with calcium-sensitive fluorescent dyes by pressure ejection of acetoxymethl dye esters *in vivo* (Stosiek et al., 2003), labelling all cells within approximately 200µm of the ejection site. These dyes report changes in intracellular calcium concentrations, which reflect well the spiking activity of the cell (Kerr et al., 2005; Garaschuk et al., 2006; Rochefort et al., 2009). Furthermore, unlike electrophysiological techniques, spatial information is obtained alongside action potential activity.

Since living cells break down synthetic dyes relatively quickly (typically over approximately 24-48 hours), in recent years, much attention has been placed on the development of genetically encoded calcium indicators (GECIs), which would allow chronic experiments over days or weeks. Although much progress has been made, GECIs were traditionally unable to match the traditional synthetic dyes in terms of brightness, calcium affinity, stability or detection of small numbers of action potentials (Looger and Griesbeck, 2012). However, recent developments such as the GECO family (Zhao et al., 2011), and the GCaMP6 family (Chen et al., 2013; Dana et al., 2014) report much improved responsiveness and signal-to-noise ratios.

Two-photon microscopy (Denk et al., 1990) relies on nonlinear excitation of fluorophores by the absorption of two photons near-simultaneously, resulting in the emission of one photon of shorter wavelength. This technique allows for imaging of fluorescent signals deep within living tissue, with good optical sectioning properties, and little photodamage (Helmchen and Denk, 2005; Svoboda and Yasuda, 2006). However, despite technical advances allowing for functional imaging almost a millimetre deep within living cortical tissue (Mittmann et al., 2011), no current system based on two-photon imaging can image

the entire cortical thickness. One other drawback of two-photon calcium imaging is limited temporal resolution. Typically, frame rates in the region of 10-30 frames per second are achievable by raster scanning (though AOD-based devices allow for much faster imaging e.g. Grewe et al. (2010); Kirkby et al. (2010); Botcherby et al. (2011)).

Calcium imaging remains the only imaging-based technique able to record the individual activity of hundreds of neurons *in vivo* , with sufficient temporal resolution to detect individual spikes, and thus has become an extremely popular technique in neurophysiology. However, translating fluorescence changes into spike trains remains a matter of statistical inference (Vogelstein et al., 2010; Oñativia et al., 2013). Furthermore, improvements in action-potential evoked fluorescence changes have been made at the cost of baseline fluorescence levels, making unambiguous detection of silent neurons difficult. Transfection of neurons by genetically encoded dyes, either by in-utero electroporation or viral delivery typically labels only a fraction of neurons, often in a layer-specific manner. The production of genetically modified lines of animals, which constitutively express a calcium indicator, has proven to be difficult, and although recent advances in this field have finally been made (Dana et al., 2014) these lines still only express the indicator in around 50% of neurons. Despite such limitations, two-photon calcium imaging has allowed the functional properties of dozens to hundreds of cells to be interrogated in vivo and even in awake, behaving animals (Dombeck et al., 2007; Greenberg and Kerr, 2009; Andermann et al., 2011; Keller et al., 2012; Poort et al., 2015), greatly enhancing the understanding of neuronal responses in V1.

1.5.4 Intracellular Recordings

All the recording methodologies described thus far report patterns of spiking activity in individual neurons, or groups of neurons, either directly or indirectly. However, this activity represents only the output of a complex series of intracellular processes responsible for integrating synaptic input (Hirsch et al., 1998; Silver, 2010) and converting this in to a train of action potentials (Carandini and Ferster, 2000; Azouz and Gray, 2000; Ferguson and Stone, 2010). Direct recording of intracellular potential responses to sensory stimuli is therefore necessary in order to investigate the mechanisms of sensory integration *in vivo* (Chadderton et al., 2014).

Intracellular recording of action potentials was initially performed in the specialised giant axon of the *Loligo* (Hodgkin and Huxley, 1939). This technique allowed for a detailed investigation of the ionic conductances which underlie the generation of the action potential

(Hodgkin and Huxley, 1952). However, intracellular recordings were initially limited to specialised preparations, such as the giant axon, and the cardiac Purkinje fibre (Draper and Weidmann, 1951). Intracellular recordings of electrical activity in the living brain was first reported in the 1950s (Buser and Albe-Fessard, 1953; Tasaki et al., 1953), using sharp microelectrodes. In the visual cortex, sharp microelectrode recordings have been used to characterise the relative tuning of excitatory and inhibitory conductances (Ferster, 1986), to investigate inhibitory conductance changes (Douglas et al., 1988) and to investigate differential information processing in multiple cell classes (Nowak et al., 2008). However, impalement of the neuron by sharp electrodes introduces a leak conductance that may significantly affect both the viability of the neuron, and measured intrinsic and synpatic properties (Staley et al., 1992; Hirsch et al., 1998; Li et al., 2004).

An alternative technique, whole cell patch clamp, is based upon the patch clamp technique originally developed for the study of single-channel currents (Hammill et al., 1981). This approach relies upon the formation of a tight physico-chemical 'gigaseal' (so-called, in reference to the high resistance of the seal, typically reaching several gigaohms). In the whole-cell variant, the membrane at the tip of the pipette is ruptured by application of negative pressure, allowing electrical access to the interior of the cell. This approach has been used extensively to characterise neuronal properties in acute brain slices (Blanton et al., 1989; Stuart et al., 1993). In vivo whole-cell recordings (Pei et al., 1991; Margrie et al., 2002) have been used to characterise synaptic integration of receptive field subregions (Ferster and Jagadeesh, 1992; Hirsch et al., 1998; Martinez et al., 2005), the orientation tuning of membrane potential responses (Carandini and Ferster, 2000), the effect of spike threshold on response linearity (Priebe et al., 2004) and orientation tuning (Tan et al., 2011), the tuning of inhibitory and excitatory conductances (Anderson et al., 2000; Liu et al., 2011; Li et al., 2012b), the linearity of binocular integration (Longordo et al., 2013; Zhao et al., 2013), and multimodal synaptic integration (Olcese et al., 2013).

Standard intracellular recording methods, just like single-unit extracellular methods, suffer from low throughput, since only a single neuron can be recorded by a single electrode. Furthermore, unlike single-unit recordings in which further recordings may be obtained by advancing the electrode, whole-cell recordings permit only one recording per electrode, since contamination of the pipette tip prevents more than one attempt at formation of a gigaseal. Lastly, although great care is taken to produce an electrolyte solution that mimicks the internal milieu of the neuron, dialysis of the cytoplasm by whole-cell recordings practically limits recording time to around 30-60 minutes, depending upon the cell type

and experimental paradigm.

The silver lining of dialysis is that it allows for the introduction of substances in to the neuron, such as biocytin for post-hoc neuronal reconstruction (Horikawa and Armstrong, 1988; Marx et al., 2012), calcium indicators (Jia et al., 2010; Hill et al., 2013) or nucleic acids for transfection and presynaptic tracing (Rancz et al., 2011; Vélez-Fort et al., 2014). Whilst other methods of single-cell staining and tracing exist, for example electroporation (Haas et al., 2001; Marshel et al., 2010), only whole-cell recordings combine electrophysiological characterisation of membrane potential and spiking responses, along with dye loading or transfection, making *in vivo* whole cell patch clamp a uniquely powerful tool.

1.6 Motivation of This Work

With new model species gaining traction, established experimental results must be revalidated to determine whether species difference are significant to the question at hand; properties determined in the macaque, cat or ferret can not simply be assumed to be true in the rodent

Early experiments characterising the response properties of V1 neurons to visual stimuli were carried out mostly in the cortex of the cat (Hubel and Wiesel, 1959, 1962; Wiesel and Hubel, 1963b) or primates such as the macaque (Hubel et al., 1977; Blasdel and Fitzpatrick, 1984; Foster et al., 1985; Ringach et al., 2002). Observations of the nature of these responses have lead directly to several models of cortical processing, most notably the highly influential serial feedforward model (Hubel and Wiesel, 1962). Since these studies, the repertoire of model species used in visual neuroscience has been expanded greatly, with the availability of genetic manipulations and comparative ease of housing large numbers of animals leading to the mouse becoming one of the most popular. New types of experiments have suggested entirely new forms of model, including those that focus on the effects of different classes of inhibitory interneurons on neuronal computations (Atallah et al., 2012; Wilson et al., 2012), the effect of locomotion (Keller et al., 2012; Saleem et al., 2013) and of cortical state more generally (Harris and Thiele, 2011; Kimura et al., 2014; Scholvinck et al., 2015). Most of these studies, however, still rely upon decades-old metrics of neuronal tuning, in particular to drifting grating stimuli.

A large number of papers have been published describing, inter alia, several of the classical tuning statistics for neurons in rodent V1. A brief summary of the major studies in recent years is presented in table 1.1.

Whilst this summary is not exhaustive, it demonstrates two key features. Firstly, there have been only a few studies (Dräger, 1975; Van den Bergh et al., 2010; Medini, 2011a; Marshel et al., 2011; Roth et al., 2012) which were explicitly set out with the aim to characterise neuronal responses in V1 in the rodent. Other studies have used population parameters, and the change in these statistics, to probe the effect of neuronal subtypes (mostly inhibitory subtypes) on network function (Atallah et al., 2012), as comparators to other visual areas (Scholl et al., 2013) or to investigate the effects of altered visual experience (Ko et al., 2014).

Paper	Parameters Examined	Recording Method	Study aim
Dräger (1975)	Tuning width, simple/complex	Extracellular (mostly single unit)	Demonstration of response properties in mouse V1; topography of V1
Sohya et al. (2007)	mean firing rate OSI (OSI_{F0})	Calcium Imaging	Comparison of OSI of GABA+ and GABA- neurons
Niell and Stryker (2008)	OSI_{F0}, DSI, SF, TF, F1/F0	Extracellular (16-site linear probe)	Tuning properties of neurons in mouse V1
Kerlin et al. (2010)	OSI_{F0}, SF	Calcium Imaging	Tuning properties of GABAergic subtypes (and pyramidal)
Van den Bergh et al. (2010)	F1/F0, SF, TF, OSI_{F0}, DSI	Extracellular (single unit)	Tuning properties in V1 and V2; comparison to macaque and to multi-unit recordings
Gao et al. (2010)	SF, TF, Speed, RF size, latency, motion coherence, F1/F0	Extracellular (single unit)	Investigation of neuronal responses and parallel information channels in V1
Rochefort et al. (2011)	OSI_{F0}, DSI, responsiveness	Calcium Imaging	Effect of dark-rearing on development of tuning properties
Medini (2011a)	OSI_{F0}, DSI, F1	Whole-cell patch	Tuning properties and morphologies of L2/3 and L4 neurons
Tan et al. (2011)	OSI_{Vm0}, OSI_{F0}	Whole-cell patch	Orientation Selectivity computation
Bonin et al. (2011)	OSI_{F0}, F1/F0, RF mapping	Calcium Imaging	Cortical topology of receptive fields
Marshel et al. (2011)	OSI_{F0}, DSI, SF, TF	Calcium Imaging	Tuning properties of V1 and other visual cortical areas
Zariwala et al. (2011)	OSI_{F0}, SF	Calcium Imaging	Tuning properties of Parvalbumin and *Wfs1+* (putative excitatory) neurons
Roth et al. (2012)	OSI_{F0}, SF, TF, speed	Calcium Imaging	Tuning properties of V1 and other visual cortical areas
Atallah et al. (2012)	OSI_{F0}, Contrast	Loose-cell patch	Tuning properties of PV+ and effect of photostimulation of these neurons
Scholl et al. (2013)	OSI_{Vm0}, OSI_{F0}	Whole-cell patch	Demonstration of orientation tuning in dLGN neurons in the mouse; comparison to V1 tuning
Ko et al. (2014)	OSI_{F0}	Calcium Imaging	The effect of visually deprived (VD) on development of orientation tuning

Table 1.1: A summary of studies of classic tuning parameters in rodent visual cortex. $F0$: mean firing rate; $F1$: firing rate modulation at the stimulus fundamental frequency; $Vm0$: mean membrane potential depolarisation. All studies were carried out in the mouse, with the exception of Medini (2011a), which was carried out in the rat. All calcium imaging studies listed here used the Oregon Green BAPTA-1 indicator, bulk loaded in to neurons *in vivo* (Stosiek et al., 2003)

Secondly, few studies have been conducted in the mouse specifically using in-vivo whole cell patch clamp. Whilst this method does have some specific drawbacks, it has several advantages. Firstly, unlike extracellular methods, there is no activity bias to neuron selection; since formation and detection of a seal on to a neuron does not require spiking activity, and current injections can confirm the identity of a neuron even in the absence of spontaneous and sensory-evoked spiking activity. It may, therefore, be the case that whole-cell recordings can therefore give a better estimate of population parameters than other methods, including calcium imaging. It is true, however, that blind patch clamp is, most likely, biased to neuronal morphology, in particular soma size (Wu et al., 2008; Liu et al., 2009). Estimates of proportions of neurons based upon features which likely cluster to subtype identity are therefore to be treated with caution. Additionally, whole-cell recording (in common with sharp microelectrode recordings) can give detailed information on spontaneous and evoked changes in membrane potential (at least at the soma, unless dendritic recordings are performed), allowing for study of the mechanisms underlying the transformation of synaptic input in to a spiking output. Lastly, whole-cell recording allows for simultaneous filling of the neuron with markers such as biocytin, for morphological reconstruction (Marx et al., 2012) , and transfection by engineered plasmids, allowing for single-cell synaptic tracing (Rancz et al., 2011). Whilst such tracing is also possible using single-cell electroporation techniques (Haas et al., 2001; Marshel et al., 2010), only whole-cell recordings give access to the full picture for a given neuron - synaptic input, spiking output and presynaptic connectivity.

Lastly, no studies have been carried out, in any species, which characterise the intrinsic and evoked properties of V1 neurons of a single class, with the goal of exploring the role of biophysical diversity in cortical information processing. It is these questions which I attempt, at least in part, to address here.

Chapter 2

Materials & Methods

All physiological data presented in this thesis were acquired using methods in accordance with the Animals (Scientific Procedures) Act 1986, Home Office and local guidelines.

2.1 Surgical Procedures

C57Bl/6 (ages P34-65) mice were used in all experiments. Where transgenic lines were used, these were bred on to the C57Bl/6 background to minimise strain difference.

Animals were anaesthetised by an intraperitoneal injection of a mix of fentanyl (50µg/kg) / midazolam (5mg/kg) / meloxicam (500µg/kg). Animals were placed in a warm (30°C) incubator and monitored until cessation of all spontaneous locomotor activity (approximately 5 minutes), and were then placed on a homothermic surgical pad maintained at 37.5 ± 0.5°C by a DC feedback thermostat (FHC Inc.).

Animals to be recovered post-surgery were additionally given 1-2mg/kg meloxicam (for post-operative analgesia and reduction of inflammation) and 2-4mg/kg (for reduction of inflammation, prevention of intracranial oedema and to reduce lung secretions) along with the anaesthesia.

During all surgical procedures both eyes were protected by the application of ointment (Maxitrol®, Alcon), which was then carefully removed from the right eye using a cotton bud and suction before visual stimulation. All mice were checked for any discolouration/opacity around the pupil; any such animals were not used in experiments.

The scalp was shaved and prepared by the application of a skin disinfectant, chlorhexidine gluconate (Hibitane®, 0.5% in 70% ethanol). Scalp overlying the left primary visual cortex (V1) was removed and the exposed bone was carefully cleaned and roughened using a 10A scalpel blade, and then allowed to dry fully in the air.

Figure 2.1: Surgical implant used for head fixation in acute and chronic experiments. Markings show length in centimetres.

A custom-designed combined imaging arena/head fixation implant (see fig. 2.1) was affixed to the cranium using first a cyanoacrylate-based adhesive (Histoacryl®, Braun) then a dental cement mixture (Simplex Rapid®, Kemdent), blackened using 2% carbon powder. The implant and dental cement combined typically weighed 0.9 ± 0.1g. The implant was then fixed in a custom clamp, giving excellent stability for subsequent surgical procedures and recordings, when necessary.

A craniotomy, typically ∼1mm x 1mm was drilled over V1 using a dental drill (Osada) with a 300µm burr (Cookson). Following removal of the bone, the exposed dura was carefully washed with cortex buffer (see table 2.1 for composition) until any bleeding had ceased, to ensure that the surface remained clear of erythrocytes. Bleeding was typically very minor and represented no danger to the animals circulating volume, however any blood on the surface dramatically reduced the chance of obtaining a successful gigaseal. In some animals, a small durectomy was performed before experimentation began.

During experiments, depth of anaesthesia was monitored every 10-15 minutes, and where any toe pinch reflex was observed, animals were injected with one-sixth the original dose of anaesthesia. Typically, the initial dose provided 90-120 minutes of light anaesthesia, with subsequent doses lasting around 60 minutes until another dose was required.

2.1.1 Recovery Procedure

For chronic or recovery experiments, the craniotomy was closed either by first filling the craniotomy with a small amount of a silicon polymer (Kwik-Cast®, WPI). This was then covered with a 3mm, #1 cover glass (Warner). The cover glass was gently pressed down

Ion Species	Concentration (mM)
Na^+	125
K^+	5
Mg^+	2
Ca^{2+}	2
Cl^-	134
$S0_4^{2-}$	2
HEPES	10
Glucose	10

Table 2.1: Cortex Buffer (HEPES-buffered ACSF) composition. pH was adjusted to 7.4 using NaOH

flush with the margin of the craniotomy whilst the polymer was still liquid. More polymer was then placed over the coverglass so as to fill the implant chamber, and once set a thin layer of dental cement was placed over the top of the entire implant to prevent the animal from removing the polymer. This arrangement seemed to minimise regrowth of connective tissue within the craniotomy (owing to the mass effect of the polymer under the glass), as well as any physical damage to the underlying cortex - which occurred far less often than when the coverglass was not used (presumably because the glass would shield the cortex from any mechanical forces).

The animal was then brought out of anaesthesia by an intraperitoneal injection of antagonists naloxone (0.6-1.2mg/kg), flumazenil (0.25-0.5mg/kg), and atipamezol (1.25-2.5mg/kg). This dose was varied according to how recently an anaesthetic dose had been administered. After regaining consciousness and the onset of spontaneous locomotion the animal was placed in an incubation chamber for one hour, with wet chow and water provided. Following this period the animal was returned to the home cage.

2.2 Electrophysiological Recording

Patch pipettes for blind in vivo whole-cell recordings were fashioned from borosilicate glass (outer diameter: 1.5mm, inner diameter 0.86mm, Harvard Apparatus) using a two-stage filament puller (PC10, Narashige). The resistance at the tip was 5-7MΩ; any pipettes outside this range were discarded. The tip size of such pipettes was approximately 1.5µm.

Once filled with 4µL intracellular solution (see below, section 2.2.1), the pipettes were placed in a holder attached to a preamplifier (HS-2A, Axon), mounted on a manipulator (4-axis Junior, Luigs & Neumann) and connected to an Axoclamp 2B amplifier (Axon). After applying high pressure to the pipette, it was lowered to the brain surface under a 10x

water dipping objective (Olympus), and then rapidly advanced to ∼200μm penetration, corresponding approximately to the top of layer II/III (L2/3) in the mouse.

After reaching this depth, the positive pressure was reduced to a more moderate level (approximately 30 mbar). Searching for cells was carried out in voltage-clamp mode as described in (Margrie et al., 2002). The amplifier was set to 0mV holding potential with a +12mV square-wave pulse at 80Hz. The pipette was advanced in steps of 3µm whilst monitoring the evoked current. A drop in current over three or more consecutive steps, along with modulation at the heartbeat frequency of the mouse (several hundred hertz) were indicative of a hit on a cell membrane, following which pressure was rapidly released. Under optimal conditions this result in the near-instantaneous formation of a gigaseal (typically $> 5G\Omega$), although in roughly 50% of cases a slower seal formation occurred. This could be encouraged by the use of very mild negative pressure and by hyperpolarising the command potential.

Following successful formation of a gigaseal the pipette was withdrawn slowly by 3µm, which was found to result in an easier break-in. The holding potential was set to -70mV, and the step size increased to 40mV to better visualise the breakin. The cell membrane at the tip of the pipette was carefully ruptured using a ramp of negative pressure until a large capacitive transient was observed.

Once whole-cell access was obtained, the amplifier was switched to current-clamp mode and the series resistance was compensated for manually using a bridge circuit. Access resistance was in the range of 15-55MΩ (mean 30.3 ± 9.4 MΩ for regular spiking neurons, n=150; 35.0 ± 10.8 MΩ for non-regular spiking neurons, n=10) and no statistical difference was observed between regular and non-regular spiking neurons (p=0.7078, Wilcoxon rank-sum test). Compensation for electrode capacitance was not used, as the nature of these experiments did not require highly accurate temporal resolution of fast events. All the experiments described here were carried out in current-clamp mode, with no holding current unless otherwise noted. Junction potential was not corrected for.

Data were low-pass filtered by the amplifier at 10kHz and acquired at 25kHz using an ITC-18 interface (Instrutech) using IGOR Pro software (Wavemetrics) running the Neuromatic package (available at http://www.neuromatic.thinkrandom.com/). Electrical (50Hz) noise was minimised by passive electromagnetic shielding of the sample and preamplifier. Additionally, a HumBug device (Quest Scientific) was used to further reduce any residual 50Hz electrical noise.

2.2.1 Intracellular solution composition

Intracellular solution was prepared in batches of 2x concentration and adjusted to pH 7.28±0.1 using KOH and/or HCl. It was then frozen in single-use aliquots at -20°C for one month or less, or -80°C for longer periods. On the morning of an experiment, this stock was diluted to 1x, and measured for osmolality (mean 289mOsm ± 3.64, range 281-295mOsm) using a vapour osmometer (Vapro 5520, Wecor). Once prepared the solution was kept on ice for the duration of the experiment. Composition of the final 1x solution is shown in table 2.2.

Ion Species	Concentration (mM)
K^+	110
Na^+	8.5
Mg^+	5
Ca^{2+}	0.04
HEPES	40
EGTA	0.05
Cl^-	12.04
$MeSO_3^-$	110
ATP	4
GTP	0.5

Table 2.2: Final composition of intracellular solution

2.2.2 Transfection and transsynaptic tracing

In some experiments, the intracellular solution was prepared with the addition of two plasmids: 200ng/µL RG-eGFP and 40ng/µL TVA. These plasmids allow the entry, replication, and spread of pseudotyped replication-deficient rabies virus. The whole cell patch technique was identical to using regular intracellular solution in all other respects, including osmolality.

Following completion of recording, the pipette was slowly withdrawn under very mild positive pressure, whilst monitoring access resistance in voltage clamp mode, until the seal was re-established. This typically occurred after ∼100µm of retraction, at which point the outside-in patch was ruptured by a large negative pressure and the pipette rapidly withdrawn.

Following removal of the patch pipette, 100-150nL of the rabies virus, RVG-tagRFP.EnvA was injected slowly from an injection pipette (with a long, narrow shank) broken to a tip diameter of 20-30µm. The tip of the pipette was placed 50-100µm away from the estimated

location of the transfected cell. The craniotomy was then closed as described above; the animal was recovered and returned to the home cage for 10-14 days before being sacrificed and the brain removed.

2.3 Response to Current Injection

Once stable access to the cell was obtained and bridge compensation set, an IV protocol was carried out. Square wave current pulses of 1000ms duration were applied, beginning with a hyperpolarising step of -400pA. Further steps decreased this by 50pA, until the 9th step in which no current was injected. Depolarising steps increased by 25pA on each step to better resolve the rheobase. Supra-threshold current steps were carried out up to at least 1.5x rheobase. Whilst it is conventional to use a value of 2x rheobase to characterise spiking response to depolarising input, the low input resistance of L2/3 neurons *in vivo* would necessitate very large current injections, up to over 1nA in some cases. The lower value of 1.5x rheobase was therefore chosen as the value at which to analyse spiking properties of these neurons.

2.4 Visual Stimulation

Visual stimulation was carried out using a 8" monitor (ADP-1081AT, DataSound Laboratories) positioned 9cm from the animals left eye, subtending approximately $\pm 42^\circ$ in azimuth and $\pm 34^\circ$ in elevation, positioned at $\sim 45^\circ$ to the long body axis. A photodiode was positioned over the lower-left corner of the monitor and data were acquired in parallel with imaging or electrophysiological recordings to provide an accurate stimulus timestamp.

Stimuli were generated using scripts written in MATLAB (Mathworks) using the Psychophysics Toolbox (version 3, http://psychtoolbox.org/). Stimuli were generated on a dedicated computer to ensure reliable performance.

Stimuli included both a full field flicker ('flip') visual stimulus and various drifting grating stimuli. The flip stimulus consisted of 10 repeats of a full-field maximal contrast reversal (0-100% illumination) at a stimulus rate of 1Hz (i.e. 500ms black screen followed by 500ms white screen at full illumination).

Drifting grating stimuli consisted of square-wave or sine-wave full contrast gratings, as detailed in table 2.3. Grating stimuli consisted of a stationary oriented grating (hold), with drift onset occurring after a predetermined period, followed by a sustained period

Stimulus Mode	Abbreviation	Duration (s)		Directions	SF (cpd)	TF (Hz)	Repetitions
		Hold	Drift				
Drifting Gratings	'HD'	2	2.5	12	0.0283	2	3-15
Spatial Frequency	'SF'	2	3	1	0.01, 0.0141, 0.02, 0.283, 0.04, 0.0566	2	5-15
Temporal Frequency	'TF'	2	3	1	0.0283	1, 1.41, 2, 2.83, 4	5-15
Combined	'F'	2	3	1	0.01, 0.0141, 0.02, 0.283, 0.04, 0.0566	1, 1.41, 2, 2.83, 4	3
Retinotopy	'Ret'	-	0.4	8	0.283	2	3

Table 2.3: Drifting Grating stimulus parameters.

of drifting grating, followed directly by the next stationary grating. Retinotopy experiments consisted of a rapid sequence of drifting gratings in multiple directions restricted to a portion of visual space, with no stationary gratings. Spatial, temporal and combined frequency tuning experiments were carried out at the cell's preferred orientation and direction, as determined by online analysis (see eq. (2.6)).

Following break in and the current injection protocol, a period of progressive membrane depolarisation was observed, accompanied by increasing magnitude and frequency of spontaneous synaptic events, and increased response to flicker stimulation. Neither visual nor other stimulation protocols were carried out in until these settled at a stable level. This period typically lasted around 8 minutes. The finding that neurons are hyperpolarised with little spontaneous activity shortly after breakin (relative to a stable state some minutes aftward) is common. The usual interpretation of this effect it that it arises from network suppression caused by high levels of K^+ ions in the extracellular space from intracellular solution ejected from the patch pipette, which gradually diffuses away. For this reason, no stimulation protocols were carried out during this period. For visually deprived animals, flicker stimuli were not carried out during the baseline period, so as to avoid exposing the animal to light before stimulation.

Baseline membrane potential relative to spike threshold ($Vm_{dist-thresh}$), a measure of neuronal excitability, was defined from drifting grating recordings. It was calculated as the average difference between spike threshold and mean membrane potential during baseline (the final 500ms of stationary grating preceding drift onset). Whilst related to resting membrane potential (RMP), $Vm_{dist-thresh}$ also captures the effect of spontaneous activity. Calculation of the $Vm_{dist-thresh}$ by this method is not susceptible to the effects of any tuning of the baseline measure, since it is a singular metric computed across the average of all stimuli, to all directions. Furthermore, the baseline measure used in this thesis was not found to be significantly tuned across the population (see below, section 2.7.4)

2.5 Auditory Stimulation

Auditory white noise stimuli were delivered by a 10W speaker connected to a custom-built amplifier. Stimuli consisted of a 100ms burst of white noise at approximately 90dB SPL.

2.6 Visual Deprivation

For experiments involving visual deprivation, animals were transferred to cages with fully blackened walls at P19, immediately after weaning (but after eye opening). The cages were blackened with several layers of matt black emulsion, and covered with blackout curtain (Thorlabs) to ensure no light could enter around the edges. The blackening of the cages was tested using a light meter (X-Cite XR2100), revealing that minimal light was transmitted through the cage walls even in strong sunlight ($<0.005\mu W/m^2$). Animals were kept in full darkness until the experiment day, with the exception of brief daily checks for health which were carried out under low intensity red light.

On the day of the experiment, animals were anaesthetised under red lights and placed in a blacked out box until the anaesthetic had taken full effect. The eyes were then covered with cream in a similar fashion to usual, but then were further covered in with blackout material to avoid exposure to surgical lighting. This material was not removed until immediately prior to the experiment, following which the animal was kept in the dark as much as possible.

Experiments on visually deprived (VD) animals were performed after at least 18 days of visual deprivation, (P37), up to P53. As the age profile of the VD animal cohort did not precisely match that of the control dataset, all variables described in chapter 6 were tested for correlation with age; none were significantly correlated.

The experiments described here differ from classical dark rearing protocols in which the animal is totally deprived of all visual stimuli from birth by elimination of light from birth, lid suturing, or enucleation. Therefore, I favour the term 'visual deprivation' rather than 'dark rearing'.

2.7 Data Analysis

All experiments were logged in a central database (FileMaker Pro, FileMaker) and were analysed using MATLAB (Mathworks).

Electrophysiological data were imported from Igro PXP format and read in to MATLAB using a package written by the author, based on a similar R package provided by the laboratory of Greg Jefferis (available at: https://github.com/jefferis/IgorR).

Action potentials (APs, 'spikes') were detected using a two-step algorithm. First, spikes were detected by finding peaks of dV/dt greater than a threshold of 8x the standard deviation of a 100ms baseline period at the start of the trace. Spike threshold was defined

as the membrane potential (V_m) at maximal d^2V/dt^2 up to 4ms before this point. Results of the spike detection procedure were manually verified in all cases. Before any analysis of intrinsic or evoked membrane potential properties, spikes were clipped by removing data points from 1ms before spike threshold till 10ms after and linearly interpolating. All references to V_m values/changes in this text refer to spike-clipped data.

2.7.1 Spike Waveform Analysis

Classification of neurons was carried out by analysis of the waveform of the first evoked AP at rheobase. The only parameters used in classification were the amplitude and time-to-peak of the after-hyperpolarisation (AHP). AHP amplitude was defined as the peak hyperpolarisation within 10ms of the peak of the spike, relative to the steady-state membrane potential (Vm_{ss}) of the neuron at rheobase. By this definition, AHPs take positive values, whereas after-depolarisations (ADPs) take negative values. Vm_{ss} was used as the baseline measure for calculating AHP amplitude rather than spike threshold, as some neurons displayed a prominent, long-lasting ramp potential before reaching spike threshold, which then artificially increased the estimate of AHP amplitude.

Neurons were classed as regular spiking (RS), fast spiking (FS), or broad after-hyperpolarisation (BAH) based upon peak amplitude and time-to-peak of the fast/medium AHPs as follows. Neurons with an AHP amplitude < 5mV in the 10ms following the peak spike depolarisation were classed as regular spiking. Of the remaining neurons, those with a fast ($<$5ms) time-to-peak AHP were classed as fast spiking. The remaining neurons were classed as BAH neurons, based upon their prominent but slower after-hyperpolarisations.

2.7.2 Analysis of spontaneous activity

Spontaneous activity was assessed by analysing recordings taken during the period before the first stimulus (the flip stimulus). Many neurons did not fire any action potentials during the short period of recording before stimulation began. When considering the estimation of firing rate for sparse or silent cells, the duration of recording is an important factor. Whilst the absence of action potentials during any finite duration recording can not categorically demonstrate a spontaneous rate of 0Hz intuitively, as recording length increases, the upper bound of the estimated firing rate decreases.

Assuming a homogenous Poisson process, the probability of observing n spikes depends upton both the time period, t and the true mean firing rate r:

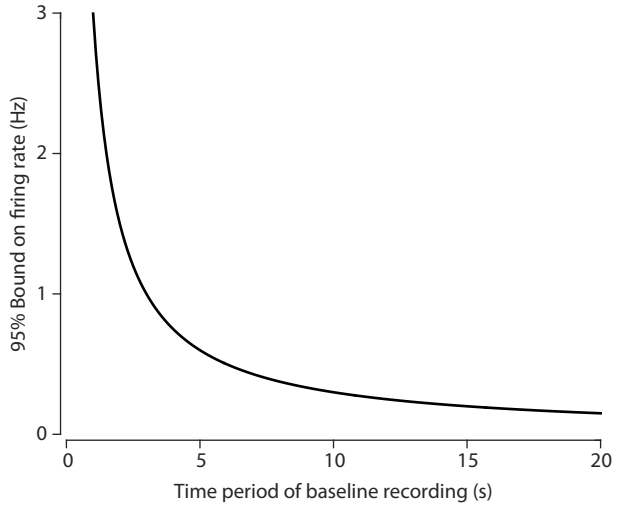

Figure 2.2: 95% confidence upper bound of mean firing rate (r), as a function of recording length t, assuming a homogenous poisson process

$$P(n) = e^{rt}\frac{(rt)^n}{n!} \tag{2.1}$$

For 0 spikes, this simplifies to $P(0) = e^{-rt}$, giving an upper bound of r at the 95% confidence level as:

$$\frac{-log(0.05)}{t} \tag{2.2}$$

In other words, the confidence with with a neuron can be described as having a spontaneous firing rate of 0Hz varies with $1/t$, as shown in fig. 2.2. Recording length in all cases was at least 5 seconds, giving an upper bound of 0.60Hz for 'silent' neurons. Including only those neurons with at least 10 seconds baseline recording (giving an upper bound of 0.30Hz) did not affect the results presented in section 6.2.4.

2.7.3 Analysis of Responses to Ballistic Stimuli

Before recording responses to drifting grating stimuli, neuronal responses were recorded to flip visual stimulation and auditory white noise. Flip stimuli consisted of a period of baseline recording at 0% illumination, followed by 10 repetitions of a full-contrast reversal to 100% illumination, and back to 0%, at a frequency of 1Hz (500ms 100% illumination, 500ms 0%). The first repetition was excluded from further analysis.

Membrane potential depolarisations in response to dark-to-light ('up') and light-to-dark ('down') transitions were defined relative to the mean membrane potential during baseline. Stimulus evoked spike rate was similarly defined relative the the spontaneous

firing rate during baseline (although for most neurons this rate was 0Hz).

For neurons which did fire at least one action potential, an up/down (UD) ratio was defined as:

$$UD = \frac{n_{up} - n_{down}}{n_{up} + n_{down}} \tag{2.3}$$

where n_{up} and n_{down} represent the number of spikes fired in response after dark-to-light and light-to-dark transitions respectively.

Auditory stimuli consisted of a period of 2000ms baseline recording, 100ms white noise stimulus and 2000ms post-stimulus recording.

2.7.4 Analysis of grating-evoked responses

Mean V_m response to stimulation (Vm0) was defined as follows. For each trial of each stimulus condition, Vm0 was calculated as:

$$Vm0 = Vm_{evoked} - Vm_{baseline} \tag{2.4}$$

where $\mathrm{Vm}_{baseline}$ was defined as the mean membrane potential of the final 500ms before stimulus drift onset. Vm_{evoked} was defined as mean membrane potential from 500ms after drift onset until the termination of the particular drifting grating stimulus. This provided a convenient, if a little one-dimensional, scalar measure of mean response to a given stimulus, compared to baseline activity.

One concern in defining the baseline in this way is that it may differ in an orientation selective manner - in other words, that the neuron is tuned for stationary stimuli. In turn, an orientation-dependent baseline measure may introduce an apparent tuning in a cell not otherwise tuned for drift orientation, or mask the orientation tuning of a cell which is tuned. Whilst this seems unlikely, as the baseline analysis window was chosen so as to include only the membrane potential following adaptation of the response to a stationary grating, it should not be discounted out of hand. Therefore, in order to investigate this possibility, the probability of the baseline of each neuron being tuned was calculated using a one-way ANOVA, testing the hypothesis that the baseline differed across orientation conditions. At the 0.05 significance level only 3/139 neurons were found to have a baseline which varied across conditions, fewer than the predicted number of type I errors (7). Indeed, fewer cells were found to have a stimulus-responsive baseline than would be predicted by the type I error rate at *all* significance levels. Therefore, the possibility that the measure of baseline

used here is in fact tuned should be discounted.

In defining a spiking response to a stimulus, many authors subtract the spontaneous or prestimulus activity (Van Hooser et al., 2005; Niell and Stryker, 2008; Li et al., 2012b), particularly when using calcium indicators to image action potential activity *in vivo* (Roth et al., 2012; Runyan and Sur, 2013). Some, however, do not (Ringach et al., 2002), arguing that orientation tuning should be measure of preference for one stimulus over another, and therefore that baseline activity is not directly relevant.

When considering what is the response of a system to a stimulus, it is important to consider the activity of a cell absent that stimulus. For example, consider a hypothetical pair of neurons, A and B. Neuron A fires spontaneously at 2Hz, and indeed fires at 2Hz during visual stimulation, perhaps because it does not receive any visual input. Neuron B also fires at 2Hz to all visual stimuli. However, it only fires at a spontaneous rate of 1Hz. Naively, one might consider that both neurons are perfectly untuned cells that respond to all visual stimuli, at 2Hz. However, if spontaneous rates are subtracted it becomes clear that neuron A does not respond to a visual stimulus at all.

Furthermore, the membrane potential response can only be defined relative to some reference value (since V_m is always negative, except during an action potential). Since evoked depolarisations were defined relative to mean membrane potential at baseline, measuring evoked firing rate relative to baseline firing rates means that Vm0 and F0 are defined similarly. For these reasons, mean pre-stimulus firing rate *was* subtracted before further analysis.

Since spontaneous firing in these neurons was low (see section 6.2.4), baseline firing rates were first averaged across all trials, to give:

$$F_0 = F_{evoked} - \overline{F}_{baseline} \tag{2.5}$$

2.7.4.1 Responsiveness to Drifting Gratings

Neurons were classified as responsive to drifting gratings based upon whether changes in mean firing rate during the drifting gratings (F_0) where statistically significant. Responses to all trials of all directions were converted into an absolute change in firing rates ($|F_0|$), which was then tested for significance using a Wilcoxon Sign Rank test:

$$H_0 : \mu_{|F_0|} = 0$$

$$H_1 : \mu_{|F_0|} \neq 0$$

2.7.4.2 Preferred Orientation and Orientation Selectivity

Preferred orientation and Orientation Selectivity Index (OSI) were both calculated using vector methods.

$$PO = \frac{1}{2} arg(S) \tag{2.6}$$

$$OSI = |S| \tag{2.7}$$

where S is the *normalised vector average* of the responses, over orientation space:

$$S = \frac{\Sigma R(\theta) e^{2i\theta}}{\Sigma R(\theta)} \tag{2.8}$$

Preferred direction was defined as either the preferred orientation or the preferred orientation + 180°, by comparing responses to the closest stimulus conditions to these two directions. For example, a neuron with a preferred orientation of 20° would have a preferred direction of 200° if the response to drifting gratings at 210° exceeded the response to gratings at 30°; otherwise the preferred direction would be defined as 20°.

The definition of OSI given in eq. (2.7) is closely related to the Circular Variance (CV) - indeed, CV is simply $1 - OSI$. This method of defining OSI is commonly used (see e.g. Ringach et al., 2002; Sohya et al., 2007; Li et al., 2012b; Lien and Scanziani, 2013) and may be most favoured definition (Grabska-Barwiska et al., 2012). However, a variety of alternative methods are also commonly used to calculated measures of tuning width. Some authors measure a peak-to-trough ratio, comparing the ratio of the maximal response to those at the orthogonal direction. This can be done by simply defining θ_{pref} as the orientation at which the response is maximal, and $\theta_{orth} = \theta_{pref} + 90°$. A measure of orientation selectivity is then given by:

$$OSI_m = \frac{R_{pref} - R_{orth}}{R_{pref} + R_{orth}}$$

Some authors (Van Hooser et al., 2005) use only only R_{pref} as the denominator, a measure commonly referred to as the Orientation Index (OI) Here I use orientation selectivity, peak-trough method (OSI_{pt}) to refer to this specific method of calculating OSI, to differentiate it from the vector method.

Whilst OSI_{pt} is easy to calculate, it is not a robust measure as it does not use any

information from responses other the 'preferred' and 'orthogonal'. Furthermore, whilst providing a good measure of the tuning of a responsive neurons with moderate to high tuning, the OSI_{pt} tends to drastically overestimate the tuning of weakly responsive or non-selective neurons (Mazurek et al., 2014). This occurs since, in this approach, R_{pref} is chosen as the empirical maximum response. It is therefore axiomatic that the other responses will be less than this value, giving an impression of tuning that arises solely from the effect of reversion to the mean.

An improvement on this general approach is to first fit the data with an appropriate model function - most commonly a wrapped gaussian in orientation space, or a wrapped double gaussian in direction space (see Swindale, 1998, for a review of commonly used models). R_{pref} and R_{ortho} can then be read from the fitted curve. This method is used quite extensively (Carandini and Ferster, 2000; Niell and Stryker, 2008; Ko et al., 2011; Liu et al., 2011) in the literature, and is certainly a useful metric. However, (Mazurek et al., 2014) argue persuasively that even using curve fitting, OSI_{pt} is both susceptible to overestimating the selectivity of weakly responsive or weakly selective neurons, and less useful in estimating the 'true' orientation tuning of a neuron in the presence of moderate noise conditions. Furthermore, the curve fitting approach requires making *a priori* assumptions about the shape of the distribution. Here, I use the vector method in order to avoid these issues.

Nominally, OSI takes a value in the range [0,1]. However, it *can* exceed 1 in circumstances where the response to one or more conditions is negative Mazurek et al. (2014), which typically occurs at directions close to the orthogonal Carandini and Ferster (2000). Indeed, this was the case in a small number (3/134) of cells. OSIs from such cells are plotted with a value of 1 for readability, but the values are unchanged in underlying statistical calculations.

Response reliability was calculated using a vector-method related to the calculation of OSI, outlined in Grabska-Barwiska et al. (2012). Briefly, individual estimates of preferred orientation, are obtained for each individual trial 1,2, ..., k and plotted as vectors of unit length. The length of the normalised vector average of these estimates is then used as a measure of the spread of individual estimates. This test statistic, preferred orientation reproducibility (R_{PO}) can then be compared to empirical distributions obtained by Monte Carlo methods, since the shape of the distribution is not analytically soluble and is highly dependent on the number of trials. This was done using the software package and lookup tables developed by Grabska-Barwiska et al. (2012) to give a p-scored value preferred

orientation reproducibility probability ($p(R_{PO})$), allowing for a statistical test of tuning reliability not directly based upon tuning width.

Spiking modulation ratio (F1/F0) was calculated by dividing the firing rate modulation at the stimulus fundamental frequency (F1), at the preferred direction, by the F0 at the same direction. F0 was defined simply as the mean evoked spike rate, as used in calculating OSI. To obtain F1, a single-sided amplitude spectrum was calculated based upon the binned spike rate (bin size 20ms, spikes pooled across repetitions) during the stimulus analysis window. The value of this function at the first fundamental frequency the stimulus temporal frequency was then used as the F1. Membrane potential modulation ratio (Vm1/Vm0) was defined similarly, based upon the ratio of the membrane potential modulation at the stimulus fundamental frequency (Vm1) and the mean membrane potential response to stimulation (Vm0).

2.7.4.3 Total Evoked Depolarisation

In order to obtain a measure of the total Vm0 a cell receives to all stimuli, the total mean evoked depolarisation (Σ_{Vm0}) was calculated as the area within the polar plot of Vm0 responses. This metric is not directly related to OSI - a broad response (low OSI) with a small amplitude to all directions will still have a low Σ_{Vm0}. However, for a given maximum response amplitude, responses with a higher OSI will have a lower Σ_{Vm0}.

2.7.5 Response Model

In order to predict the mean evoked spiking response (F0) of a neuron to an arbitrary combination of mean membrane depolarisation (Vm0) and membrane potential modulation (Vm1), a double power-law response model was fitted to the data. For each neuron, responses to all trials of all orientations were pooled and fitted with a power-law model with a threshold nonlinearity (Priebe et al., 2004; Tan et al., 2011):

$$F0 = k_0[Vm0]_+^{p0} + k_1[Vm1]_+^{p1} \tag{2.9}$$

Fits were calculated using a nonlinear curve-fitting algorithm (lsqcurvefit, MATLAB), with all parameters constrained to positive values. The addition of a nonlinear component (either the quotient or the product of the Vm0 and the Vm1) did not improve the overall quality of the curve fitting (assessed using the adjusted R-squared).

2.8 Ex vivo imaging

In order to quantify the number and location of presynaptic neurons projecting on to single L2/3 neurons, animals were perfused transcardially under deep ketamine/xylazine anaesthesia with 4% paraformaldehyde (PFA). The brains were removed and further fixed in 4% PFA overnight, then stored at 4°C in phosphate-buffered saline (100mM) with 0.01% sodium azide (NaN_3) to prevent bacterial or other contamination.

Following this, most brains were imaged using Serial Two Photon Tomography (STPT) (TissueCyte, TissueVision) as described in Ragan et al. (2012). Briefly, the whole brain was embedded in 4% type 1 agarose (Sigma) and placed in to an automated two-photon microscope with integrated vibratome. Imaging was carried out using a 10x 0.6NA objective (Olympus) at 800nm illumination.

The brain was scanned coronally in a mosaic pattern of 9x6 image tiles, each 1500x1500µm with an xy pixel spacing of approximately 1µm. At each tile position 10 optical sections were acquired 5µm apart to give a voxel size of 1x1x5µm. Following acquisition of all 10 optical layers of all tiles in a single physical section, the sample was transferred to a vibratome, which removed the top layer of the tissue, and the process repeated 50µm deeper. Importantly, the imaging plane is set *below* the cut brain surface, ensuring that at the time of acquisition the sample is entirely undamaged. Thus the entire brain can be imaged at cellular resolution, with minimal damage artefacts.

The STPT system used was based around a two-photon microscope with a single excitation wavelength and simultaneous collection of emitted fluorescence in three channels. Therefore, excitation of all fluorophores occurred simultaneously (unlike in most modern confocal microscopes, in which sequential illumination of different lasers can be used in order better to separate signals arising from different fluorophores). Optical bleed-through of eGFP signal in to the red emission channel (and vice-versa, of the red tagRFP or mCherry carried by the virus, in to the green channel) was substantial, making identification of the host neuron difficult (fig. 2.3, top row).

In order to separate the green and red signals, a linear unmixing algorithm was applied to the data (Dickinson et al., 2001; Garini et al., 2006). First, specimens containing only one fluorophore were imaged (slices of GAD67-GFP transgenic mice, and distal presynaptic neurons in wild type mice infected with RV-tagRFP or RV-mCherry). The emission of the pure fluorophore was measured across all three (red, green, blue) channels in order to create an emission profile.

This algorithm relies on assumptions that fluorescent emission is linear according to concentration of different fluorophores. Firstly, this means that an fractional change in concentration of one fluorophore should result in a proportional change in emission. This assumption therefore relies on the absence of processes such as photobleaching or saturation. Furthermore, the emission of two or more different fluorophores should summate linearly. The presence of a pair of fluorophores that constitute a fluorescence resonance energy transfer (FRET) system will, therefore, prevent the use of a simple linear unmixing approach. Most well-configured fluorescence-based imaging systems should conform to all of these assumptions, including the STPT system used here. Indeed, using a simple linear unmixing algorithm was very effective in separating out tagRFP or mCherry emission from eGFP emission (fig. 2.3, bottom row). Comparison of the results of this algorithm with confocal images taken using sequential illumination and narrower filters demonstrated that validity of the approach (fig. 2.3, right). Quantitative analysis (fig. 2.4) of the red and green intensity in host (ROI 1, containing eGFP and tagRFP), presynaptic (ROIs 2-4, containing only tagRFP), and background (ROIs 5-7, containing neither fluorophore) regions of interest demonstrated a selective reduction in the green, but not red, intensity in presynaptic ROIs, whilst preserving the signal in both channels in the host ROI (fig. 2.4a). The intensity of presynaptic ROIs in the green channel was reduced to a level comaparable to background (fig. 2.4c, cf. fig. 2.3), making unambiguous identification of the host neuron trivial.

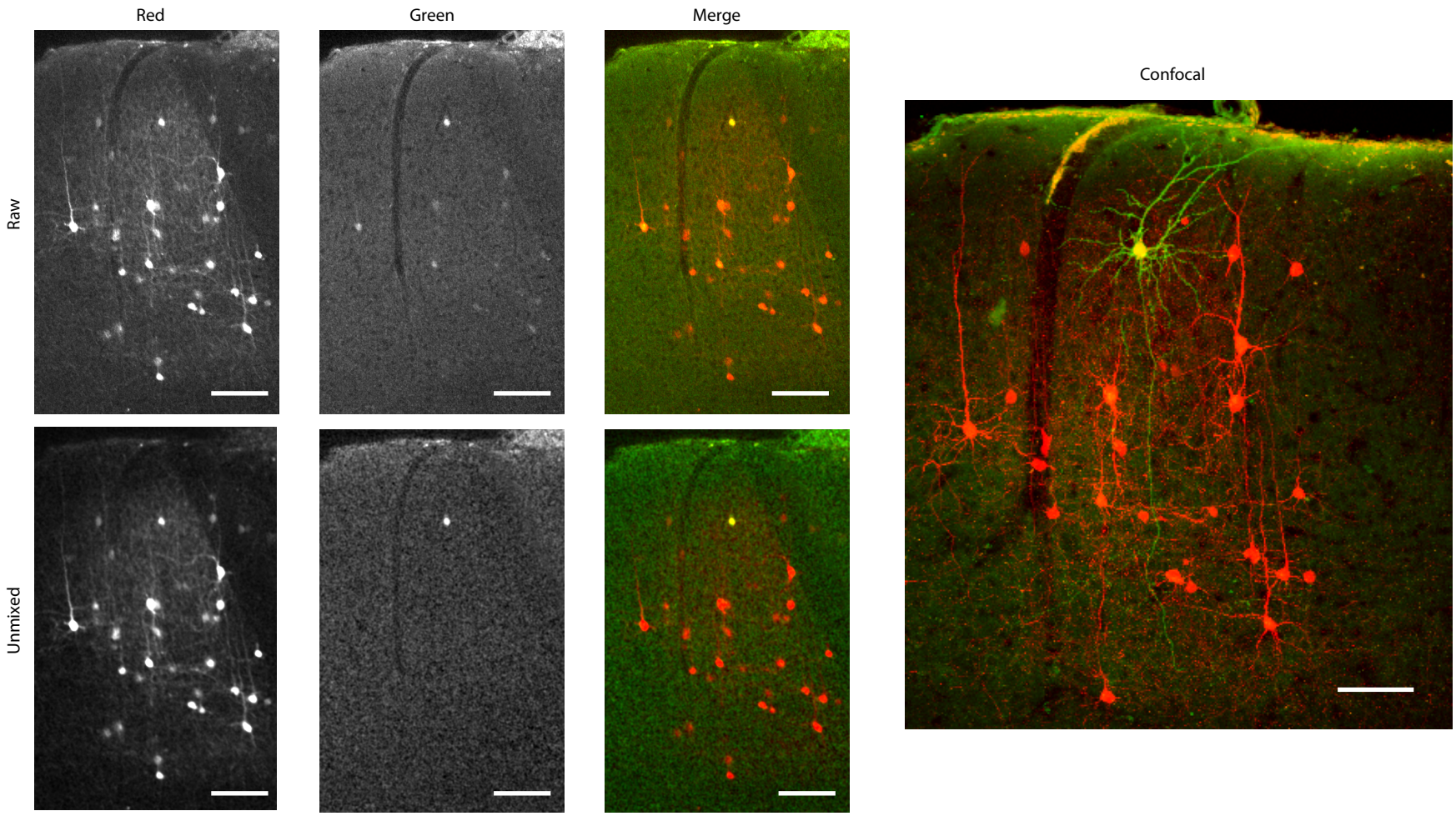

Figure 2.3: (Caption on the following page)

Figure 2.3: (Previous page.) Host cell identification Raw STPT data show a group of presynaptic neurons in red (top left), but several of these have significant signal in the green channel (top middle), a result of optical bleed-through. This prevents unambiguous identification of the host neuron, which expresses eGFP and, as such, should be the only green signal in the image, shown with both channels overlayed on the right.
By unmixing the images using a linear deconvolution approach, a single genuine green cell body is revealed unambiguously (bottom, middle), without affecting negatively the signal in the red channel (bottom left, overlay shown bottom right).
Following STPT imaging, the 50µm slices were manually sorted and re-imaged using conventional epifluorescence and confocal microscopy, enhanced using anti-RFP (red) and anti-eGFP (green) immunohistochemistry. The host neuron can be seen clearly labelled in the enlarged confocal image on the right, taken on a Leica SP5 using sequential illumination.
This particular host neuron (from the experiment shown in fig. 4.1) is a superficial pyramidal neuron near the border of layer 1, with an unusual second apical dendrite, along with multiple basal dendrites. The axon can be seen clearly descending from the ventral surface of the neuron. All scale bars 100µm.

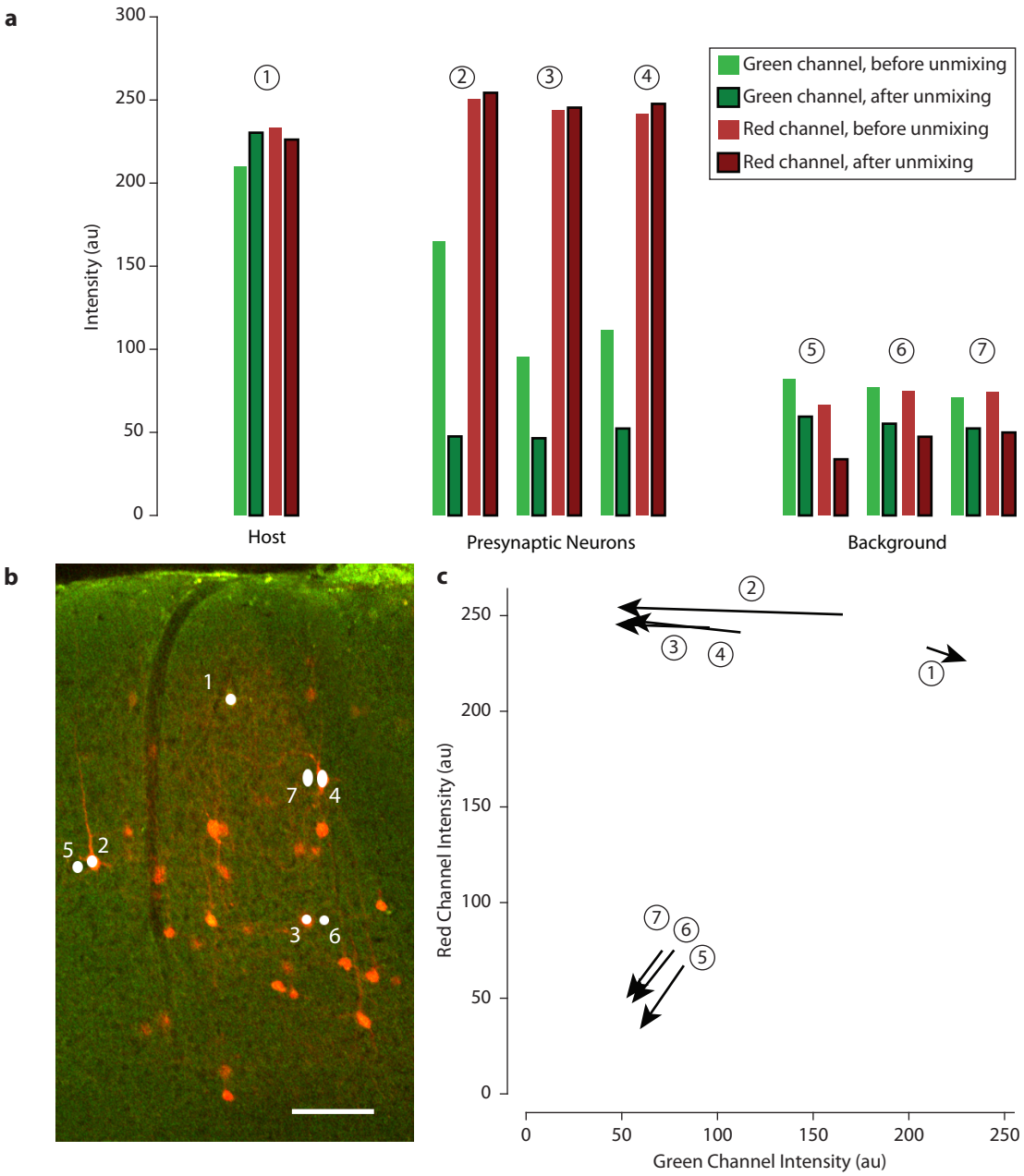

Figure 2.4: Verification of Unmixing Procedure on data acquired by STPT
(a) Red and green channel intensity of seven example regions of interest (ROIs) before and after unmixing, from the same image as in fig. 2.3. ROI 1 was chosen as the host neuron, as identified by confocal imaging (fig. 2.3). ROIs 2-4 were taken from presynaptic neurons spaced across the field of view; ROIs 5-7 were taken from ROIs of identical size to those of 2-4, offset slightly from the soma in order to sample the background. Unmixing did not greatly affect the intensity of either channel in the host neuron (ROI 1), in which both eGFP and tagRFP are present. However, it greatly reduced the green channel intensity in presynaptic neurons (ROIs 2-4), without affecting the red channel intensity arising from the tagRFP labelling. Unmixing also reduced the intensity of the background in all ROIs (5-7), further increasing the signal-to-noise ratio of the images.
(b) Red/Green overlay (before unmixing) of STPT image, showing the position of ROIs 1-7.
(c) Vector plot of Green (x axis) and Red (y-axis) intensities of ROIs 1-7. Vectors denote the change in intensity resulting from unmixing. The reduction in green intensity, but not red intensity, of presynaptic neuron ROIs (2-4) aids separation from the host ROI (1), in which little change in either channel occurs. Background ROI intensity is reduced in both channels (5-7)

Following completion of the scan, slices were manually collected and sorted. In some cases, immunohistochemistry was performed including a DAPI stain to better visualise the precise location of the layer 4 striation in primary visual cortex. The slices were then mounted on glass slides and imaged using an automated slide scanning fluorescence microscope (VS-120, Olympus). Quoted cell counts were obtained from either the STPT or manual (widefield fluorescence) imaging of fixed slices, before immunohistochemistry.

2.9 Statistical Analyses

Statistics were calculated using MATLAB; parametric tests were used where appropriate, and in cases where normality could not be assumed a Lillefors test was used to determine the appropriateness of such measures. Results are presented as mean ± SD or SEM (as appropriate), unless non-parametric tests were used, in which case median and range are quoted. A standard significance value of $p < 0.05$ is used, and denoted by a single asterisk; p-values <0.01 and <0.001 are denoted by double and triple asterisks respectively.

Chapter 3

Intrinsic Properties of Layer 2/3 Neurons

3.1 Introduction

The data presented in this chapter outline the electrophysiological characteristics of neurons in layer II/III (L2/3) of mouse V1, recorded using blind in-vivo whole-cell patch clamp and assessed using analysis of membrane potential responses to current injections. The classification of neurons in to distinct and non-overlapping subtypes based on these electrophysiological characteristics alone is attempted and discussed.

The division of neurons in to discrete groups is not without difficulty or controversy. Pharmacological interventions and precise spike-timing characterisation are much more problematic in the in-vivo preparation, where ongoing network activity obscures subtle differences in response. Therefore, the data and analysis presented here should not be considered as a concrete attempt to validate previous classification schemes, or to apply them without question to the mouse primary visual cortex. Rather these data represent a *dramatis neuronae* to the upcoming chapters, which focus on the responses of these neurons to sensory stimuli, and the presynaptic connectivity which may, in part, underpin these responses.

3.1.1 Electrophysiological Classification of Neuronal Subtypes in the Cortex

Many electrophysiological parameters have been used to classify neurons (Connors and Gutnick, 1990). The shape of the action potential, and parameters relating to spontaneous

or sensory-evoked firing rates (such as spontaneous firing rate, maximum firing rate, and burstiness) are readily quantified using extracellular recordings alone. Whilst the majority of neurons in the cortex are regular spiking (RS) neurons, some have a characteristically 'thin' (narrow) AP waveform as described by (Mountcastle et al., 1969) and a higher spontaneous and evoked firing rate (Simons, 1978). Such neurons are typically described as fast spiking (FS).

The use of intracellular recording electrodes to record from neurons in the cortex (Ling and Gerard, 1949; Buser and Albe-Fessard, 1953) allows for the injection of current to depolarise or hyperpolarise the cell, whilst recording the resulting changes in membrane potential. Whilst extracellular recordings did reveal subgroups of RS neurons that fired in bursts, the heterogeneity of such behaviour *in vivo* made rigorous classification difficult. The controlled application of depolarising current steps *in vitro* made the possible the recognition of two subgroups of RS neurons - the intrinsically bursting (IB) neuron, typically found in cortical layer V (L5) (Connors et al., 1982), although not exclusively (Nowak et al., 2003). The chattering (CH) neuron, also known as the fast-rhythmic bursting (FRB) neuron (Cardin et al., 2005). These neurons appear to be found only in L2/3 and occasionally layer IV (L4) in V1 (Gray and McCormick, 1996), particularly in or near the border between these two layers (Nowak et al., 2003). However, they are seen throughout the cortical depth in motor and association cortex (Steriade et al., 1998).

The direct recording of membrane potential (V_m) permitted by the use of intracellular recording techniques also allows for the measurement of a wide range of bio[physical properties beyond AP shape and pattern. These include input resistance (R_i), membrane capacitance, rheobase and frequency-current slope (f-I). Such measures provide an insight in manner by which individual neurons of similar or different classes may process their inputs to produce the observed spiking outputs.

3.1.2 Morphological and Laminar Classification

The history of morphological classification of cortical neurons stretches back to the pioneering work of Ramon y Cajal using Golgi staining. Cajal distinguished between neurons with a long axon (projection neurons) and those with a shorter, more localised axon (intrinsic neurons). This distinction has remained to this day; L2/3 projection neurons have a characteristic pyramidal morphology, with a single large apical dendrite which rises towards the pial surface and branches in to a tuft in or near the border of layer 1 (Spruston, 2008). These apical dendrites, as well as any number of smaller basal dendrites, are cov-

ered in dendritic spines of varying density (Larkman, 1991). The single long, often highly branching axon of the pyramidal neuron emerges from the basal (deep) surface of the neuron. It may ramify locally before sending at least one branch to other cortical layers or areas, or to subcortical targets. The numerous synaptic connections made to other neurons are gluatamatergic excitatory connections; in L2/3 and L5 pyramidal neurons are the only excitatory neurons (Oberlaender et al., 2012). L4 excitatory neurons, in contrast, are typically of a spiny stellate morphology, and in layer VI (L6) excitatory neurons are of a variety of morphological types, including pyramids but also inverted pyramids, tangential, horizontal or multipolar neurons (Marx and Feldmeyer, 2013).

In contrast to the pyramidal neuron, which accounts for approximately 80% of neurons in L2/3 and a similar proportion in L5 (Feldman, 1984), aspiny, the term 'interneuron encompasses a great diversity of morphological types. These neurons are united by two factors alone the use of $\gamma-$aminobutyrate (GABA) as a primary, inhibitory, neurotransmitter; and their lack of dendritic spines (leading to their being commonly termed 'aspiny'). Indeed, so varied are the morphologies (defined primarily by dendritic arborisation, but also by somatic morphology and axonal projection) of the inhibitory interneurons that classification schemes used vary widely between groups and publications, making direct comparison difficult:

'...different investigators use their own, mutually inconsistent schemes for classifying neurons based on morphological criteria' (DeFelipe et al., 2013)

Nonetheless, several major grouping are near-universally recognised, including basket, chandelier, bitufted, Marinotti, neurogliaform and bipolar neurons (Markram et al., 2004).

Early studies (Mountcastle et al., 1969) initially suggested that RS units corresponded to pyramidal neurons, with FS recordings deriving from the spiny stellate neurons of L4. Later it was suggested that such L4 neurons produced an intrinsically bursting (IB) phenotype, and that FS recordings rather originated from aspiny interneurons in all cortical layers (Connors and Gutnick, 1990). It is now recognised that it is only the parvalbumin-positive basket and chandelier morphological classes that produce a fast-spiking output (Kawaguchi and Kubota, 1997), with other aspiny neurons generating an RS-like discharge pattern (including so-called low-threshold spiking neurons) (Contreras, 2004; Gentet et al., 2010) that can be difficult to distinguish from that of a pyramidal neuron, at least *in vivo*
.

3.1.3 Molecular Classification

The use of molecular markers adds a third dimension to the classification of interneuron subtypes.

Neurons which express the calcium-binding protein parvalbumin are almost exclusively of a basket or chandelier morphology (DeFelipe et al., 1989), and do not co-express any other molecular markers associated with interneurons except for calbindinin (Gonchar et al., 2007). These PV+, FS (Gentet et al., 2010) neurons make up around 40% of the GABAergic population in the adult mouse. The remaining 60% of neurons expressing a variety of markers including somatostatin (SST), calretinin (CR), cholecystokinin (CCK), vasoactive intestinal peptide (VIP) , neuropeptide Y (NPY), and choline acetyltransferase (ChAT) (Kawaguchi and Kubota, 1997; Tamamaki et al., 2003; Markram et al., 2004; Gonchar et al., 2007; Gentet, 2012). Expression of these particular markers is often highly overlapping, and corresponds to morphological classes including Martinotti, bipolar, and neurogliaform cells.

The precise subdivision of the GABAergic interneurons according to molecular and/or morphological identity is a hotly contested and complex field, and is far beyond the scope of this thesis. Indeed, it has been suggested that interneuron classes may be no more than clumps on a continuum (Markram et al., 2004) . However, the parvalbumin (PV)+ FS basket/chandelier neurons do seem to be distinct enough so as to be easily identifiable as a seperate subgroup (albeit not completely homogenous).

3.2 Results

Blind *in vivo* patch clamp was used to investigate the diversity of intrinsic and sensory-evoked properties (chapter 5) in L2/3 neurons, in conjunction with post-hoc morphological assessment and single-cell transsynaptic tracing (chapter 4). The results presented in this chapter focus on intrinsic biophysical properties of these neurons, assessed using current injections in the current-clamp configuration.

3.2.1 Identification of L2/3 V1 neurons

In order to ensure that recordings were in the correct brain region and layer, a subset of neurons recorded consecutively were filled with biocytin at the time of recording, by inclusion of the biocytin (0.2%) in the intracellular solution (Horikawa and Armstrong, 1988). Following perfusion and slicing, the filled neurons could be visualised post-hoc

using fluorescent streptavidin staining. Counter-staining cell nuclei with 4',6-diamidino-2-phenylindole (DAPI) allowed the cortical layers to identified (fig. 3.1a); area identity was confirmed by reference to a standard brain atlas (Paxinos and Franklin, 2008).

In all cases (7/7), the recorded neurons were indeed found to be within L2/3 of cortical area V1. Furthermore, all these neurons were classed as pyramidal based on soma shape and size, the presence of a distinct apical dendrite (fig. 3.1b), and the presence of dendritic spines (inset).

These these 7 neurons, along with 2 host neurons unambiguously identifed from single-cell Rabies Virus assisted Circuit Mapping (RVCM) experiments (see chapter 4) were used to calibrate the penetration depth (read from the manipulator during the experiment) against true depth perpendicular to the pia (fig. 3.1c). By fitting a line to these data, the relationship between axial penetration and true depth could be approximated. According to this relationship, the lower limit of L2/3 (taken to be 350µm) corresponded to 616µm axial penetration; thus 600µm axial penetration was used as a cut-off for classifying cells as being within L2/3. By this criterion, 6/166 neurons were excluded from the dataset.

3.2.2 Electrophysiological Subtype Classification

Neurons were classified by spike waveform in to distinct groups (fig. 3.2, see also section 2.7.1) by the size and shape of the after-hyperpolarisation (AHP). Whilst pyramidal neuron action potentials can involve both AHPs and after-depolarisations (ADPs), these are much slower than those observed in non-pyramidal neurons (Contreras, 2004). Of the 160 neurons recorded in L2/3, 150 had a regular spiking spike waveform with little or no AHP/ADP (peak AHP magnitude mean -2.48 ± 5.2mV, fig. 3.2a). As such, these were assigned as putative pyramidal neurons / RS; here, I use the terms interchangeably.

10 neurons had a distinct fast AHP, with a peak amplitude of at least 5mV within 10ms of the action potential (AP) peak. Of these, 6 (fig. 3.2b) had a waveform typical of either a basket or chandelier parvalbumin-positive (PV^+) neuron (Gentet, 2012), with a large (peak magnitude 12.6 ± 3.1mV), very fast (time-to-peak 1.64 ± 0.80ms) AHP.

Of the remaining 4 non-fast spiking (NFS) neurons, 3 showed a prominent (peak magnitude 9.68 ± 3.9mV), monophasic, but slower (time-to-peak 9.12 ± 0.93ms) AHP (fig. 3.2c). However, the AHP of two of these neurons had not reached peak amplitude by the end of the 10ms analysis window. When extended to a 25ms window, the time-to-peak of these neurons was found to be of 11.6 ± 3.1ms was obtained. These I term broad after-hyperpolarisation (BAH) neurons.

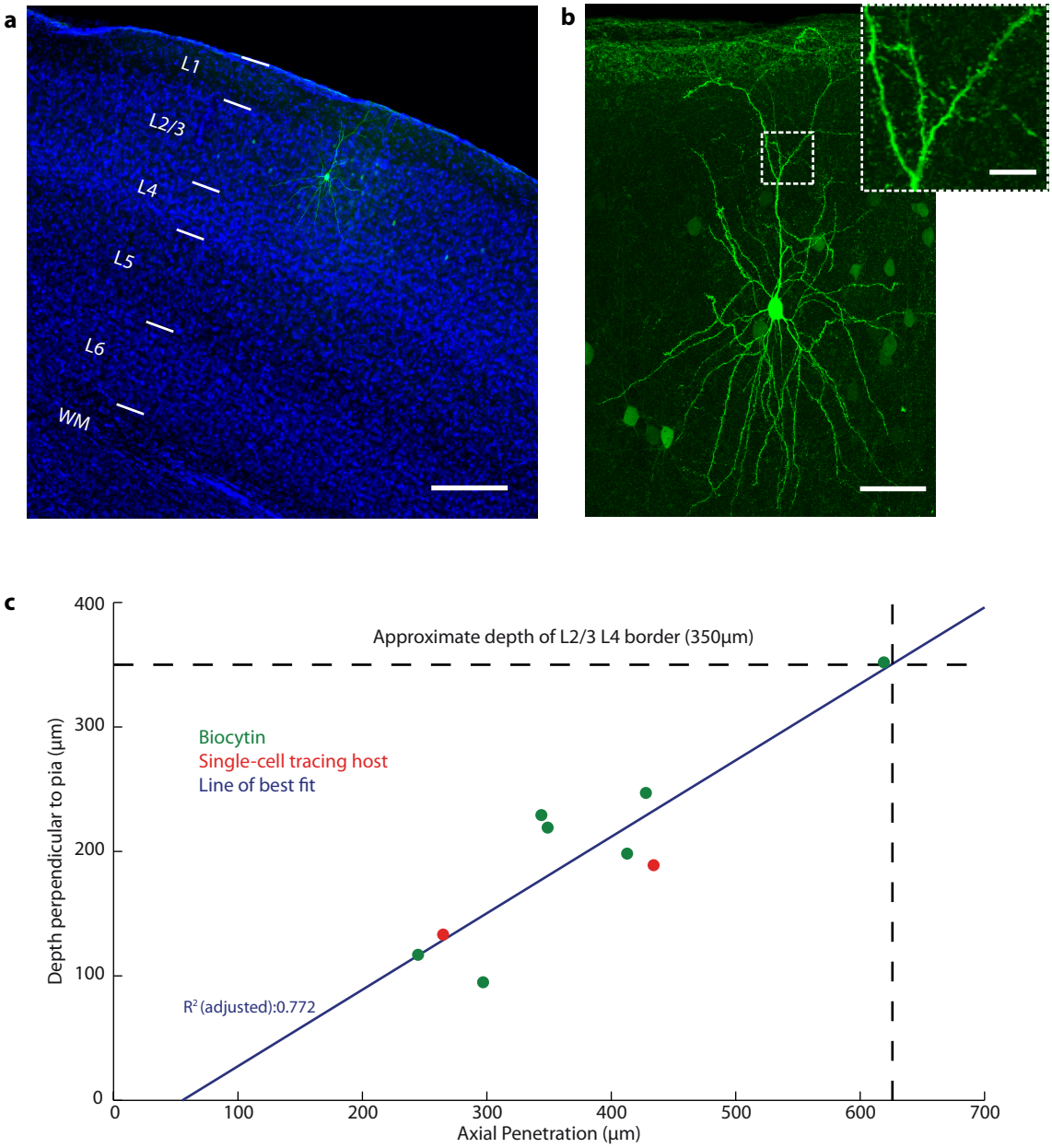

Figure 3.1: Identification of recorded neurons

(a) Overview image of a single neuron, recorded in vivo using whole-cell patch-clamp, with 0.2% biocytin in the intracellular solution for post-hoc visualisation. Blue: DAPI; green: streptavidin-GFP. The pial surface, the borders between cortical layers 1-6, and between layer 6 and the white matter (WM) are indicated by line markers. Scale bar: 200µm

(b) Maximum intensity projection of the neuron shown in **(a)**, from an 80µm-deep confocal stack. Scale bar, 50µm. Note that although some weakly-filled ghost neurons do appear alongside, the filled cell is clearly distinguishable. Inset - an enlarged view of the primary fork point of the apical dendrite, showing clearly the characteristic dendritic spines. Scale bar 10µm.

(c) Scatter plot of electrode axial penetration against cell actual depth from pia. Seven neurons were visualised post-hoc using biocytin-streptavidin labelling (green); two host neurons (red) were unambiguously identified from single-cell tracing experiments (see chapter 4). The border between L2/3 and L4 was determined by the change in density of DAPI staining as apparent in **(a)**.

One neuron showed a combination of both fast- and medium- latency AHP, quite distinct to the others (fig. 3.2d). The time-to-(first) peak of this neuron was 1.40ms, with a magnitude of 8.32mV. A second peak of magnitude 6.14mV was observed at 21.3ms. Since only one example of this neuronal type was observed I am not able to quantitatively assess the intrinsic properties of this cell type, assuming in fact that this is a separate class of cell.

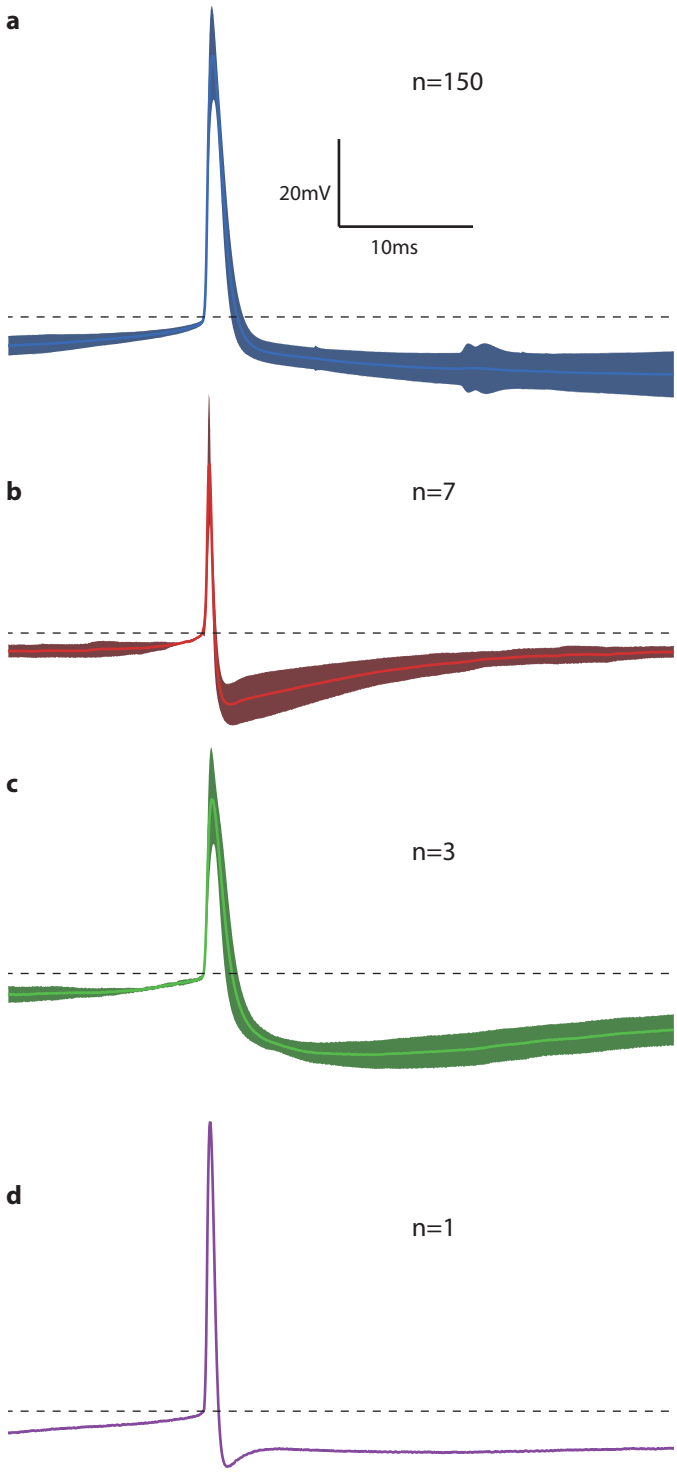

Figure 3.2: Spike waveforms of recorded neurons
(a) Regular spiking (RS) neurons, defined as having a fast AHP with a peak amplitude less than 5mV. Dotted line indicates the spike threshold
(b) Fast spiking (FS) neurons, defined as having a fast AHP with a peak amplitude of at least 5mV, and a time-to-peak of less than 5ms
(c) Neurons with an AHP of at least 5mV but whose timecourse was considerably slower (time-to-peak >5ms)
(d) One neuron displayed an unusual waveform, with both a fast and a prominent slower AHP

All traces show the mean (bold) waveform of the first evoked AP at rheobase. The shaded region in **(a-c)** indicates mean ± SD.

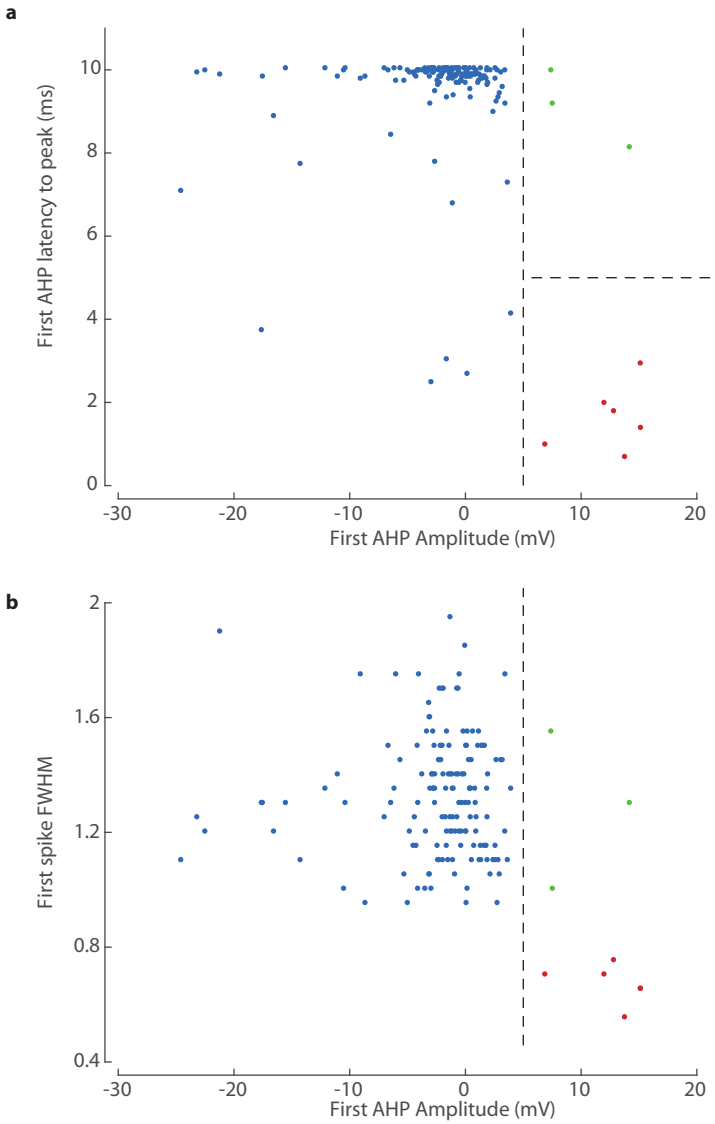

Figure 3.3: Cell classification by Electrophysiological Properties

(a) Classification protocol. Cells were initially classified as regular-spiking (blue) or non regular-spiking by the maximal amplitude of the afterhyperpolarisation (x-axis, cutoff value 5mV denoted by the dotted line).

Non regular-spiking cells were then subdivided in to FS or BAH subsets by the latency to AHP peak, with a cutoff value of 5ms (y-axis, dotted line). This division was clearly bimodal, with FS neurons (red) having a fast time-to-peak of less than 4ms in all cases, whereas BAH neurons had a time-to-peak of at least 8ms.

(b) Verification of classification. The full-width at half maximum is plotted on the y-axis against the amplitude of the AHP. FWHM was not used in the classification procedure; nonetheless the separation between FS and BAH neurons was also seen in the FWHM. Furthermore, RS neurons with a short latency to peak AHP (outliers in the bottom left quadrant of fig. 3.3a) are seen to have a wide spike waveform in all cases, confirming the accuracy of their classification as RS.

3.2.3 Characterisation of Neuronal Subtype Properties

Intrinsic properties were assessed by means of an IV analysis, performed by injecting steps of current into the cell and monitoring the membrane potential (in the current-clamp configuration). This was performed immediately after rupturing the cell membrane (break-in), during which period spontaneous synaptic activity is low. Square-wave current pulses of 1000ms duration were injected in to the cell, starting with a 400pA hyperpolarising step. Subsequent step magnitude decreased by 50pA until the no-current step, after which steps increased by 25pA/step, in order to better estimate rheobase.

Example results for the three types of neurons are shown in (fig. 3.4), with intrinsic and spiking properties summarised in table 3.1 and shown in dotplot format in fig. 3.5.

Of note, putative fast-spiking neurons had a narrow AP, with full-width at half maximum (FWHM) being around half that of either regular-spiking or BAH neurons, a known characteristic of this cell type.

In response to a current injection of 150% rheobase, FS neurons seemed to exhibit much higher mean and maximum firing rates than RS neurons. FS firing rate did not accommodate, with negative accommodation (acceleration) being evident in some cases. In contrast, RS neurons accommodated quickly, on average to around half their initial firing rate. BAH neurons showed a spiking phenotype similar to RS neurons, with low max and mean firing rates. However, there was a tendency for these neurons to accommodate less than regular-spiking neurons.

Property	RS (n=150)	FS (n=6)	BAH (n=3)
AHP Peak Amplitude (mV)	-2.48 ± 5.2	12.6 ± 3.1	9.68 ± 3.9
AP FWHM (ms)	1.28 ± 0.21	0.617 ± 0.068	1.23 ± 0.28
Resting Membrane Potential (RMP) (mV)	-75.6 ± 7.6	-66.7 ± 3.8	-59.8 ± 4.2
Input Resistance (R_i) (MΩ)	57.6 ± 28	53.4 ± 13	107 ± 27
Rheobase (pA)	285 ± 111	475 ± 151	208 ± 63
Mean Firing Rate (Hz)	19.3 ± 7.6	91.0 ± 20	16.0 ± 3.5
Max. Firing Rate (Hz)	50.4 ± 23	152 ± 60	25.4 ± 3.5
Early Accommodation (%)	48.6 ± 17	-6.13 ± 22	17.8 ± 14
Late Accommodation (%)	51.1 ± 49	-51.5 ± 86.8	14.7 ± 1.0

Table 3.1: Intrinsic Spiking Properties of RS, FS and BAH Neurons. Mean Firing Rate, Max. Firing Rate, Early and Late Accommodation are all calculated at 150% rheobase. Since not all neurons were depolarised to this level, these number of neurons included in these measures is slightly lower (RS n=134; FS n=4; BAH n=3). These results are shown as dotplots in (fig. 3.5a-i).

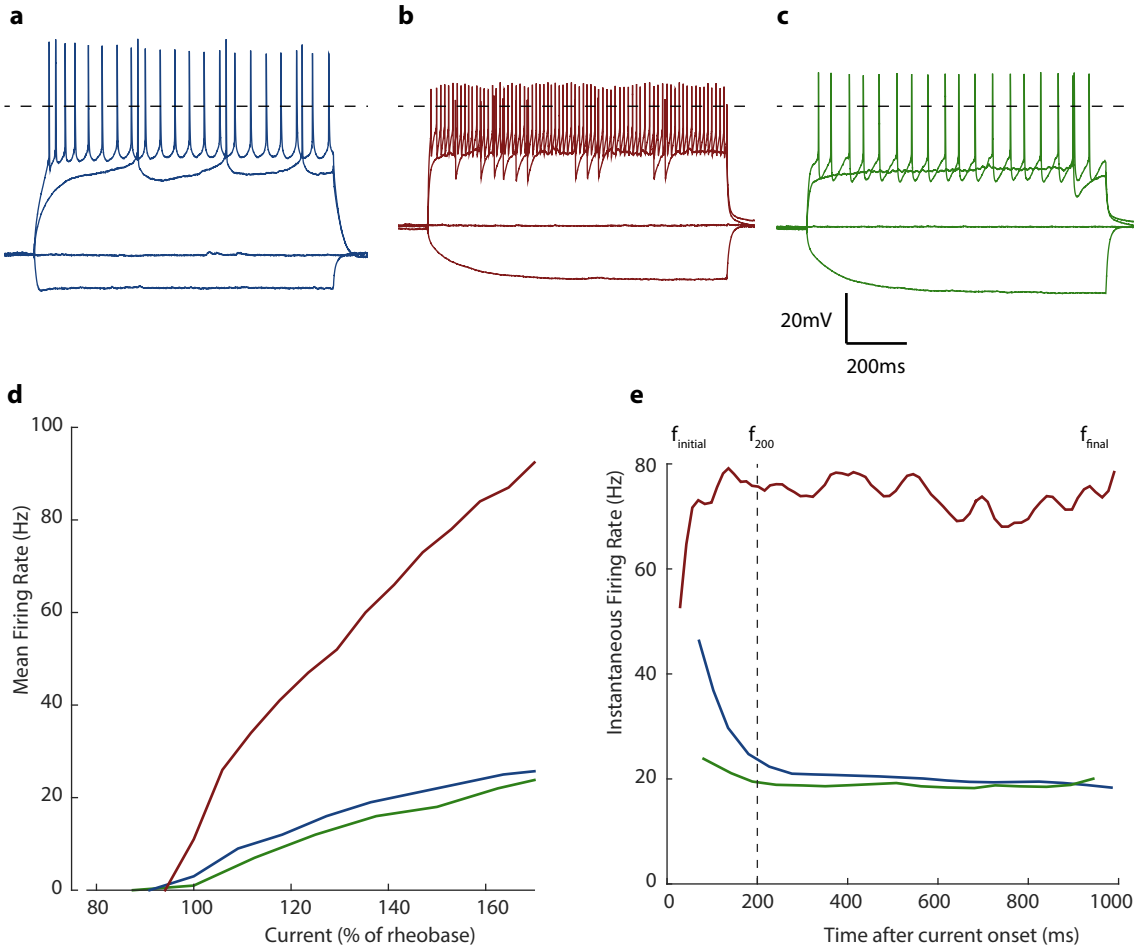

Figure 3.4: Sample Results from Current Injection Experiments.
(a) An example of the membrane potential response of a regular spiking (RS) neuron. Shown are the first hyperpolarising step, the no-current step, the rheobase step and the 150% rheobase step. The dotted line indicates 0mV.
(b) An example of a fast spiking (FS) neuron.
(b) An example of a broad after-hyperpolarisation (BAH) neuron.
(d) Mean firing rate response of the three example neurons to increasing current steps. Current injections have been normalised to rheobase. Note the markedly steeper slope of the FS neuron (red), compared to the RS (blue) and BAH (green) neurons.
(e) Firing rates of the three example neurons over time at 150% rheobase. Instantaneous firing rates (1/interpsike interval) are plotted against time. Firing rates have been averaged using a 3-element running average for presentation purposes only. $f_{initial}$ and f_{final} are defined as the reciprocal of the first and last interspike intervals respectively; f_{200} is defined as the reciprocal of the interspike interval which encompasses the 200ms timepoint.

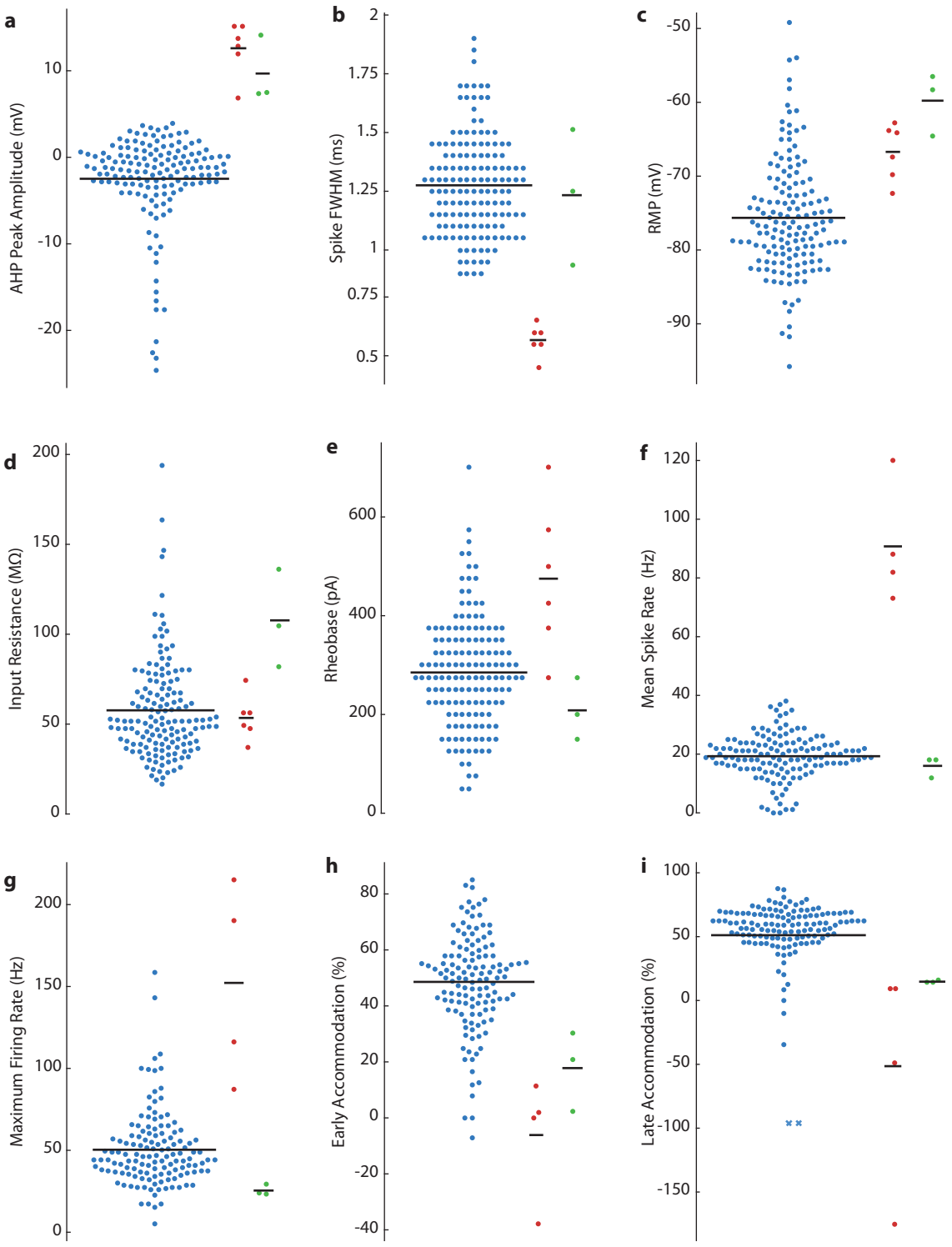

Figure 3.5: Individual electrophysiological properties of all recorded neurons, split by subtype (blue: RS, red: FS, green: BAH).
(a) After-hyperpolarisation peak amplitude
(b) Full-Width at Half-Maximum of the first action potential at rheobase
(c) Resting membrane potential during 0-pA current injection
(d) Input resistance, measured in response to the first hyperpolarising current injection
(e) Rheobase (the current required to elicit at least one action potential)
(f) Mean firing rate at 150% rheobase
(g) Maximum firing rate at 150% rheobase
(h) Early spike rate accommodation at 150% rheobase
(i) Late spike rate accommodation at 150% rheobase.
Means are shown for each group by a black horizontal bar. Summary statistics for these data are found in table 3.1.

3.3 Discussion

3.3.1 Neuronal Subtype Classification

In this chapter, I describe the classification criteria by which recordings were targeted to L2/3 of V1, and how regular spiking (RS) neurons were identified. It is these neurons which make up the basis for the vast majority of the following chapters.

Whilst some authors do not explicitly mention the removal or segregation of non-regular spiking neurons from datasets (Tan et al., 2011), in many electrophysiological studies involving blind electrophysiological recordings (Steriade et al., 2001; Nowak et al., 2003, 2008; Niell and Stryker, 2008) neurons are identified as regular-spiking or fast-spiking (and in some cases as intrinsically bursting or chattering). Non-fast spiking inhibitory interneurons can not be identified by such criteria, as their spike waveforms and firing rates are thought to closely resemble those of regular spiking pyramidal neurons.

Two-photon targeted patch-clamp (Margrie et al., 2003; Komai et al., 2006) has been used to record in the cell-attached configuration from identified regular-spiking GABAergic neurons in V1 neurons (Liu et al., 2009) and in the whole-cell configuration in barrel cortex (Gentet et al., 2010). Other authors have correlated properties recorded *in vivo* with post-hoc anatomical reconstruction (Medini, 2011a; Vélez-Fort et al., 2014), or identified non-fast spiking interneuron classes by optogentic stimulation (Pi et al., 2013). Whilst powerful, such methods are laborious as compared to blind recordings, dramatically reducing the number of neurons that can be sampled.

Every property examined differed significantly between the three subtype groups here identified by AHP magnitude and time-to-peak (RS, FS, BAH), using a Kruskal-Wallis one-way analysis of variance. However, the small numbers of FS and especially BAH neurons made post-hoc analysis impossible. For spiking properties, with 7 data points in total, no significant outcome was possible whatever the rank separation. Whilst parametric t-tests would allow greater statistical power to detect a difference in sample means, with such small groups it is impossible to verify normality, a key assumption in the use of the t-test. Furthermore, for the large RS group, normality was rejected by the Lillefors test for all parameters except for the rheobase, and early accommodation.

Despite these limitations, taken in aggregate, it is clear that the three subtypes, defined by AHP magnitude and time-to-peak alone have quite different sets of properties. The purpose of this chapter is not to quantitatively assess the precise differences between neuronal subtypes, nor to examine the basis of neuronal identification. Such a study

would require a greatly higher number of both FS and BAH neurons, most probably by carrying out targeted *in vivo* patch clamp in transgenic animals. However, this was never the motivation for my project. I only wish to demonstrate that the neurons which make up the datasets that follow have been rigorously classified as being regular-spiking, putative pyramidal neurons. The experiments and results described in the rest of this thesis focus almost entirely on variations within the RS group.

BAH neurons may constitute a subdivision of either regular-spiking or fast-spiking neurons, although their low firing rates would argue against the latter possibility. However, their biophysical signature may suggest that they represent at a group of non-fast spiking interneurons (NFS). Gentet et al. (2010) reported NFS neurons in awake mouse barrel cortex to have a similar cluster of properties as the BAH neurons described here: broad action potential waveforms, high input resistance, a depolarised resting membrane potential and low AP frequency. However, without directly visualising recorded cells, either during the recording or afterwards, it is impossible to make any categorical statement assigning BAH neurons to a particular morphological or molecular class of neuron.

Whether or not BAH neurons are, indeed, NFS neurons, it is striking that regular-spiking neurons accounted for 150 of the 160 neurons recorded in L2/3 (93.8%). This may seem puzzling, since interneurons are thought to comprise roughly 15-20% of all neurons in this layer (Gonchar et al., 2007; Gentet, 2012). However, the large tip size (5-7MΩ) used in these experiments reduces the probability of obtaining a recording from interneurons (Wu et al., 2008; Liu et al., 2009), which have smaller somata.

3.3.2 Absence of Intrinsically Bursting or Chattering Responses

In no case did a recorded neuron in L2/3 of mouse V1 exhibit properties characteristic of intrinsically bursting (IB) or chattering (CH) neurons. Although some RS neurons did exhibit high instantaneous firing frequencies at 150% rheobase (over 100Hz in 4/134 cases), these values are much lower than the reported firing rates during bursts in IB and CH neurons (200-350Hz and 400-700Hz respecitvely) (Nowak et al., 2003; Cardin et al., 2005).

The absence of these neuronal may be explained by their laminar distributions. Connors et al. (1982) reported IB neurons to be located in L4 and superficial L5 in guinea pig cortex. Later reports described IB phenotypes to be confined to L5 (Connors and Gutnick, 1990; Agmon and Connors, 1992), although (Nowak et al., 2003) reported finding a number of IB neurons in L2/3 of cat V1.

CH neurons have been reported to be found in a *'narrow band'* in lower L2/3 and L4 in cat visual cortex by some authors (Nowak et al., 2003). It is possible that restricting recordings by penetration depth means that deeper CH neurons near the L2/3/L4 border are missed. However, in that study, 42% of neurons in L2/3 overall were reported to have a chattering phenotype, and the cutoff of 600µm, whilst being slightly conservative, should not exclude the entirety of deep layer 3. Furthermore, other studies have reported CH responses throughout layers 2-6 (Cardin et al., 2005).

Therefore, it is not clear that one should expect an absence of either IB or CH neurons in mouse L2/3. Their absence from this dataset may indicate that these classes are not found in supragranular mouse V1, but this finding may also arise from reduced probability of being recorded owing to small soma size, or simply as a result of limited sampling. It is also possible that these spiking phenotypes do not represent immutable neuronal classes, but rather may be impacted by anaesthesia or the sleep/wake cycle. (Steriade et al., 2001) found that both IB and CH phenotypes were much more rare in the awake cat cortex than in either deeply anaesthetised animals or acute brain slices, and that most (4/5) individual IB neurons recorded during transition from slow-wave sleep to either REM sleep or to wake converted to a regular spiking phenotype.

Other classes of neuronal response beyond these, such as low threshold spiking (LTS), as well as more precise subdivisions of spiking characteristics (Markram et al., 2004) are commonly used in *in vitro* studies, but are difficult to detect in *in vivo* preparations, in which spontaneous activity may mask subtle differences in properties such as spike delay or spike-width accommodation.

Chapter 4

Monosynaptic Input on to Individual L2/3 Neurons

4.1 Introduction

4.1.1 Identification of Presynaptic Connectivity of Single Cells

The flow of information through neuronal circuits is governed by the connectivity of the circuit components. Whilst intracellular processing of synaptic inputs is complex and dynamic (London et al., 2005), the connectivity of a neuron defines the substrate upon which these computations may be performed. For this reason, characterising the presynaptic connectivity as well as the projection targets of either individual neurons or groups of an identifiable class, remains key in building an understanding of cortical processing.

A number of techniques have been used in this endeavour (see section 1.3 for an outline of developments in this field). One of the most promising is the use of genetically engineered viruses, most particularly the Rabies Virus (RV), targeted to molecularly identified neurons using techniques such as the Cre-Lox system or single-cell transfection (Wickersham et al., 2007b; Marshel et al., 2010; Rancz et al., 2011).

This single-cell approach may be of particular importance in studying the function of real, as opposed to averaged, neuronal circuits, as molecular identity is only part of the story of neuronal heterogeneity. Within the (molecularly homogenous) grouping of layer II/III (L2/3) neurons there remains considerable variability in input and spiking output parameters. Population tracing studies can only give an indication of the average connectivity of a group of presynaptic neurons (although very small injections may restrict this to low tens of hosts, rather than hundreds).

Single cell tracing, therefore, offers the possibility both of characterising presynaptic connectivity, and of examining variability in this parameter. Transfection for tracing has been carried out by other authors using electroporation (Haas et al., 2001; Kitamura et al., 2008; Marshel et al., 2010; Wertz et al., 2015). However, this technique does not offer the possibility of recording the function of the transfected host neuron. Whilst it is possible to combine tracing with calcium imaging (as in Wertz et al. (2015), who use a rabies virus carrying GCaMP6s rather than a conventional fluorophore), it is not known if, and how, the function of the neuron may be affected by infection with rabies virus, and any attendant toxicity that may occur. Therefore, it is preferable to record neuronal function prior to viral infection. Furthermore, only whole-cell patch clamp allows for the recording of intrinsic electrophysiological properties and sensory-evoked depolarisations, as well as transfection.

4.1.2 Classification of Neurons in to Brain Regions, Layers and Classes

Following the detection of presynaptic inputs on to a neuron, or group of neurons, the next logical step is to define the number and class of the presynaptic neurons, and thereafter to examine how this may differ between different host neurons. When considering the classification of neurons, several parameters are of immediate interest. Firstly, and most obviously, is the brain area in which the neuron is located. The specialisation of regions in terms of sensory modality or other function has been recognised since the beginnings of modern neuroscience. Cytoarchitectonic parcellation of the brain in to distinct areas based upon histological consideration was described in detail by (Brodmann, 1909), and indeed this broad scheme of classification remains to this day. Whilst it is certainly true that most brain processes of any complexity involve the concerted activity of many interconnected brain regions (Sporns, 2011; Bullmore and Sporns, 2012; Stafford et al., 2014), regional identity remains a key component in the description of a particular neuron, and the nature of the information processing in which it may be likely to be involved.

However, the definition of brain regions can be difficult and controversial. Whilst some regions, such as primary sensory cortices, are quite easily defined by cytoarchitectonic discontinuities, others are less easily differentiated. Until recently, extrastriate visual areas in the mouse were simply defined by broad homology to primate/carnivore areas (Caviness, 1975; Dräger, 1975), or as medial or lateral as compared to primary visual cortex (V1) (Paxinos and Franklin, 2008) . More recent studies have described a number of individual cortical areas, defined by mapping of retrograde dextran labelling (Wang and Burkhalter,

2007; Wang et al., 2007), immunostaining density changes (Wang et al., 2011), widefield intrinsic (Marshel et al., 2011) or combined intrinsic and calcium imaging (Andermann et al., 2011). These schemes differ not only in the particular nomenclature for individual areas, but in the position of the borders and even in the numbers of extrastriate visual areas. Indeed, the number and position of higher-order visual areas may in fact be quite variable from animal to animal, even using the exact same methodology (Garrett et al., 2014). Therefore, in assessing areal identity of presynaptic connectivity, some caution must be taken in being overly precise.

Laminar identity is far more easy to define, although still not entirely straightforward. Whilst the broad scheme of the six-layered cerebral neocortex is well agreed upon, some borders (such as the border between layers 5 and 6) can be difficult to define precisely without specialist stains. However, gross laminar identity is fairly well agreed upon in the field.

Lastly, the neuron itself can be classified by morphology and molecular identity. Whilst this depends to some degree upon layer and area (for example, pyramidal neurons are only found in layers 2,3,5 and 6 of the cerebral cortex, as well as the hippocampus and amygdala Spruston, 2008), class will still vary within one layer of one region. Most importantly, within L2/3 there are excitatory pyramidal neurons, and a variety of subclasses of GABAergic inhibitory interneurons. The postsynaptic effect of input from excitatory and inhibitory neurons on to a postsynaptic cell is clearly quite different, and so it is important to build an understanding not just of *where* a presynaptic neuron may be located, but *what* that neuron is, and how it may affect the membrane potential and spiking probability of its target.

In this chapter, I outline the results of single-cell monosynaptic tracing in mouse layer II/III. The data described here constitutes one of the first datasets of its kind and, therefore, may represent a useful descriptive dataset for the scientific community. Moreover, I set out to test specific hypotheses with the experiments. Firstly, does the laminar distribution of presynaptic neurons differ between local (V1) neurons and more distant connections, and between individual distant areas? Secondly, is the distribution of local excitatory and inhibitory presynaptic neurons similar, or does it differ? Lastly, can any anatomical correlate of orientation tuning be found?

4.2 Results

A subset of recorded neurons were transfected by the inclusion of two plasmid constructs in the intracellular solution. The first of these encoded for the avian receptor TVA (allowing for entry of pseudotyped rabies virus), and the second for rabies glycoprotein (allowing for replication and spread of the deletion-mutant virus from the host neuron alone), along with eGFP in order to label the host neuron. Following a successful recording and pull-off, rabies virus was injected close to the location of the recorded/transfected neuron (see section 2.2.2), and the animal recovered (section 2.1.1). Animals were then returned to the home cage, and kept for 10-14 days to allow for replication and spread of the virus. Following this period, the brain was fixed using transcardial perfusion of 4% paraformaldehyde (PFA), removed from the cranium, and imaged.

Where possible, Serial Two Photon Tomography (STPT) was used in order to obtain a cellular-level resolution dataset from the whole, intact brain (since physical sectioning only occurs after imaging of a particular layer); in some cases perfused brains were sliced manually (by Danielle Carmignac) and imaged using conventional epifluorescence and confocal microscopy. Where STPT was used, slices were recovered from the imaging chamber, roughly sorted, stained and mounted for further confocal imaging.

Selected images from an experiment imaged using STPT, representative of various regions in which presynaptic neurons were observed, are shown in fig. 4.1a-fig. 4.1c. The particular host neuron in this experiments was a regular spiking (RS) putative pyramidal neuron, with a clear regular-spiking pattern in response to current step injections (fig. 4.1d). In response to visual stimulation, membrane potential (V_m) responses were relatively large (maximum mean evoked depolarisation 9.4mV) and significantly reproducible for preferred orientation ($p=0.024$); however no evoked spikes were observed (fig. 4.1e). This may be partly explained by the orientation-tuning stimulus not being optimal in this case, since a frequency-tuning stimulus set at the preferred membrane potential orientation did evoke some limited firing (fig. 4.1e). However, even at the preferred spatiotemporal frequency, this neuron only fired twice in three trials. A more satisfactory explanation is this neurons very hyperpolarised resting potential, 38.6mV below spike threshold. This is one of the most extreme values observed in any experiment (fig. 5.13c).

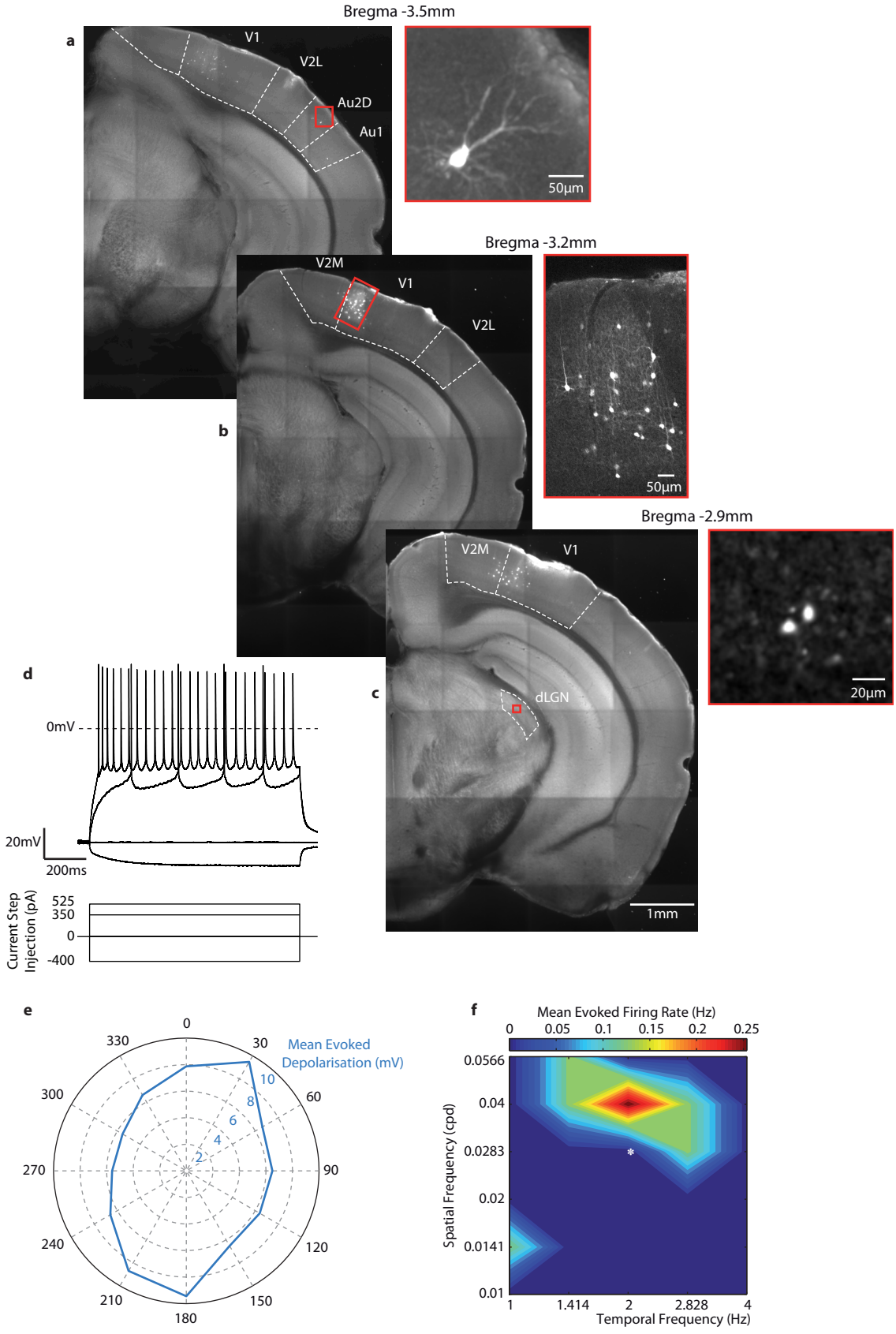

Figure 4.1: (Caption on the following page)

Figure 4.1: (Previous page.) Combined Single-Cell Electrophysiology and Presynaptic Tracing
(a-c) Representative coronal slices from whole-brain serial two-photon tomography of neuronal inputs to a single neuron (RV-tagRFP). Inset (red), expanded views of **(a)** a layer 2/3 pyramidal cell in secondary auditory cortex, dorsal (Au2D); **(b)** the centre of the local cloud of presynaptic cells in primary visual cortex (V1), including the host cell; and **(c)** two neurons in the lateral geniculate nucleus, dorsal region (dLGN).
(d) IV relationship summary plot for the host cell, showing responses to hyperpolarising, no-current, rheobase and 150% rheobase current steps.
(e) Polar plot of responses to drifting grating stimuli. Evoked depolarisations to oriented drifting gratings showed a clear orientation preference (preferred orientation probability 0.0239*, OSI 0.12), although no evoked spikes were observed (n=5 repeats of each orientation at a fixed spatiotemporal frequency).
(f) Spiking activity was elicited by drifting gratings at the preferred direction of the depolarisation, at other spatial/temporal frequencies (frequency pair used for orientation tuning experiments denoted by *).

4.2.1 Host Survival and Identification

Patch clamp recordings were typically performed blind, with no imaging of the host neuron. Therefore, the plasmids used included eGFP, in order to label the host for subsequent identification.

Host neurons were detected in 2/2 experiments carried out in wild-type animals (RS2 and RS6). The other 7 experiments were carried out in GAD67-GFP transgenic animals in order to identify the inhibitory vs. putative excitatory presynaptic connectivity (see section 4.2.4). This made identification of the host neuron difficult, as all inhibitory neurons were also labelled with eGFP. In two cases (RS5 and RS9), the host neuron could be identified as the only green neuron with a clear pyramidal morphology, with a large soma and a prominent apical dendrite. In the remaining 3 experiments imaged using STPT, the identity of the host neuron could not be determined unambiguously. Therefore, from these data it would appear that in at least the majority of cases, the host neuron remains labelled for the 10-14 days of incubation, in contrast to Wertz et al. (2015), who report an almost complete loss of all host neurons by day 11. Whether the physiological function of the neuron remains unaffected by the procedure is, of course, unknown.

4.2.2 Area Distribution of Presynaptic Neurons

Combined whole-cell recordings and presynaptic tracing data were obtained from 10 host neurons in 10 animals, 9 of which were regular-spiking (RS) neurons and one a fast-spiking neuron (FS), with an average of 140 presynaptic neurons (range 54-351). In the first instance, presynaptic neurons were assigned to seven regions, based upon a standard mouse brain atlas (Paxinos and Franklin, 2008). This areas were: V1; medial secondary visual areas (V2M); lateral secondary visual areas (V2L); retrosplenial cortex (RSP); other

ipsilateral cortical areas (IpsiCx), incorporating auditory, somatosensory and association cortices ipsilateral to the host neuron; dorsolateral geniculate nucleus of the thalamus (dLGN); and other brain areas (other), including contralateral cortex and non-dLGN subcortical neurons. The percentage of presynaptic neurons in each of these areas is shown for all neurons individually in fig. 4.2, with polar plots outlining the orientation tuning of the neuron shown below, where available. The experiment outlined in figure fig. 4.1 corresponds to RS6.

For regular spiking neurons, a large majority (mean 90.6 ± 7 %) of presynaptic neurons were found within V1. These neurons typically appeared clustered in a cloud surrounding (but not necessarily wholly centred upon) the host neuron. However, individual neurons and small, distinct clusters not contiguous with the main cloud were observed 7/9 clouds, constituting approximately 5% of neurons within V1 (5.2 ± 5.0 % of V1 neurons averaged across all experiments, 6.6 ± 4.7 % of V1 neurons in the 7 experiments in which any were observed).

Input fractions from other areas were quite variable. 8/9 neurons had at least one presynaptic neuron in V2L, and these constituted 3.3 ± 2.5 % of inputs overall (3.7 ± 2.3 % in inputs in experiments with any neurons in V2L). The second most common extrastriate area was V2M, with 3.2 ± 4.2 % of inputs overall (5.7 ± 4.1 % in the 5/9 experiments in which any neurons were detected in V2M). Smaller numbers of neurons were observed in ipsilateral retrosplenial cortex; other cortical areas including primary and secondary auditory cortices and somatosensory cortex as well as temporal and parietal association areas; contralateral V1 and piriform cortex. Presynaptic neurons were detected in dLGN in 6/9 experiments, with neurons detected in ventral geniculate nucleus of the thalamus (vLGN) and lateral posterior nucleus, mediorostral part (LPMR) in one experiment. Percentages of neurons in these areas, across all experiments and across only experiments in which any neurons were detected, are summarised in table 4.1.

In the one fast spiking (FS) neuron from which presynaptic connectivity data were obtained, results were strikingly different (fig. 4.2 , right). Most notably, 11.2% of input neurons (28/250) were located in the dLGN (dorsolateral core region, close to the border of the shell; examples are shown in fig. 4.3a-b). This contrasts with 1.1 ± 1.0% for regular spiking neurons. A formal hypothesis test is, unfortunately, impossible in this case, since only one example was observed. However, if the data are z-scored according to the observed distribution for RS neurons a value of 9.82σ is obtained. The distribution of RS values for fractional input from the dLGN did not show a significant deviation from normality

Area	% overall	n	% in experiments with > 0 neurons
V2L	3.3 ± 2.5	8/9	3.7 ± 2.3
V2M	3.2 ± 4.2	5/9	5.7 ± 4.1
RSP	0.5 ± 1.2	2/9	2.2 ± 1.7
IpsiCx	1.1 ± 1.8	3/9	3.2 ± 1.9
dLGN	1.1 ± 1.0	6/9	1.6 ± 0.8
other	0.24 ± 0.48	2/9	1.1 ± 0.1

Table 4.1: Distribution of Presynaptic Neurons in Extrastriate Brain Regions. Percentages are given averaged across all experiments, as well as averaged only across experiments in which at least 1 neuron was detected in the particular brain area. The fractions of experiments which constitute this group are also given ('n').

(Lillefors test p=0.19). However, even allowing for some possible small deviation from a normal distribution, masked by low numbers, and allowing for some limited skew in the distribution of z-values, this extreme value is highly provocative.

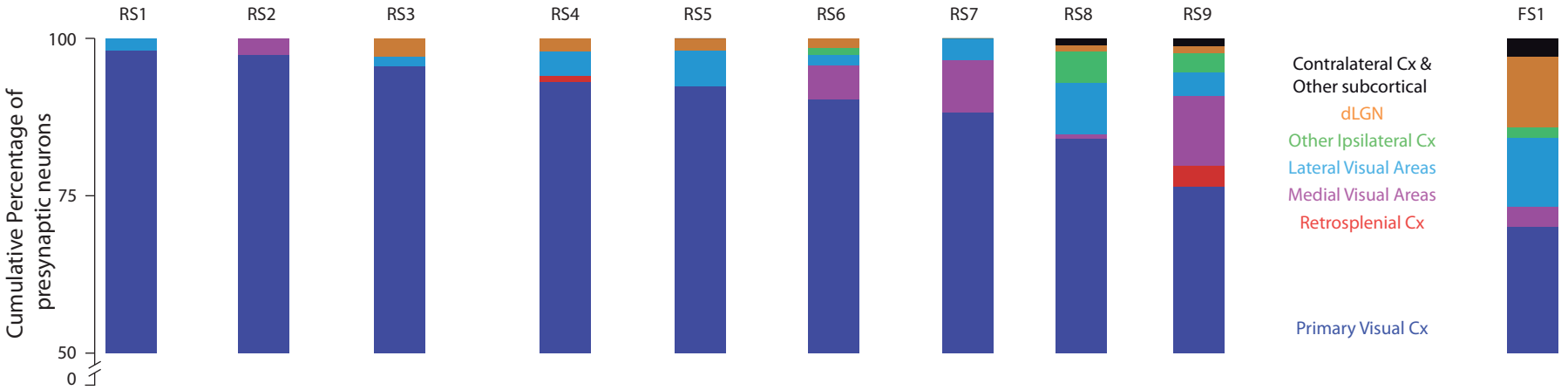

Figure 4.2: Area Distribution of Presynaptic Input
Individual distributions of presynaptic connectivity is shown for all 9 regular spiking, and 1 fast spiking neurons in which Rabies Virus assisted Circuit Mapping (RVCM) was successful. The percentage of neurons in primary visual is shown in blue (truncated), with the percentage in other brain regions displayed as a stacked bar chart.

4.2.3 Laminar Distribution of Presynaptic Neurons

The laminar structure of the cortex arranges with some precision a varied array of neuronal cell types (DeFelipe et al., 2002; Oberlaender et al., 2012), which is reflected by different intrinsic and functional properties (Mangini and Pearlman, 1980; Ringach et al., 2002; Martinez et al., 2005; Niell and Stryker, 2008). Furthermore, synaptic contacts are known to be made on to different regions of the dendritic arbor of an individual neuron in a layer-specific manner (Shepherd and Svoboda, 2005; Kätzel et al., 2011), which is likely to have functional significance and has even been proposed as a fundamental organising principle of cortical processing (Larkum, 2012). Therefore, the laminar distribution of presynaptic inputs to a neuron is a key question in dissecting information flow in cortex.

Presynaptic neurons located in cortical areas were assigned to laminae based upon standard classification criteria. Where possible, this classification was carried out on slides recovered from STPT imaging and mounted on glass slides. Before mounting, slices were incubated with 4',6-diamidino-2-phenylindole (DAPI), a nuclear marker. Layers were then identified based upon variation in cell density, and neurons were counted again, and assigned to layer 1 (L1), L2/3, layer IV (L4), layer V (L5) or layer VI (L6). Such an assignment, even with the use of DAPI as a counterstain, can not be perfect, as some borders (such as the L5/L6 border) are less than stark. Furthermore textbook descriptions of the borders between laminae as being sharp and well-defined prove to be less than binary in reality, with borders being more a matter of relative probability than micrometre resolution watersheds (Oberlaender et al., 2012; Wertz et al., 2015). However, even granting this caveat, laminar identity offers a great improvement over assignation by depth alone.

Laminar identity was investigated for four cortical areas/groupings: V2L, V2M, V1 itself, and all other ipsilateral cortical regions, pooling neurons in retrosplenial, sensori-motor, auditory and association cortices.

In V2M and in non-visual ipsilateral cortical areas, the majority of presynaptic neurons were located in L2/3 (65% and 62% respectively). In V1, the plurality of presynaptic neurons were also in L2/3, falling just short of an absolute majority at 46%. The most distinct difference was, of course, the large fraction (19%) of neurons in L4 of V1. In contrast, no L4 neurons were observed in either V2M or the non-visual cortical areas, and only 1 neuron in V2L. V2L differed from all the other cortical in that the largest fraction of presynaptic inputs in this area were found in L5.

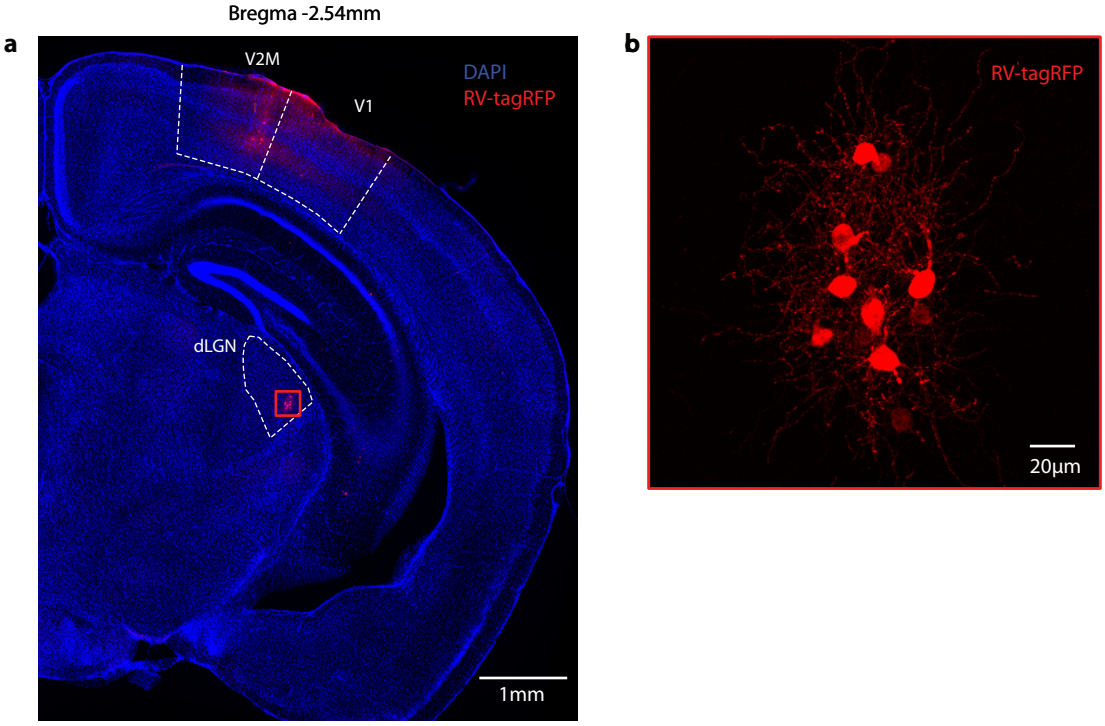

Figure 4.3:
Substantial Presynaptic Input from dLGN in a Single Fast-Spiking Interneuron
(a) Widefield epifluorescence image of a single 100µm coronal slice from FS1, showing presynaptic cortical neurons in V2M and V1, as well as a cluster of neurons in the dLGN. This cluster, outlined in red, is shown enlarged in a confocal maximum-intensity projection in **(b)**, where 8 well-labelled cell bodies can be seen, along with extensive arborisations.

Comparing the fraction of L2/3 and L5 between V2M and V2L indicated that this difference was significant (χ^2 p=0.042*). However, no significant difference was found between V1 and either V2L or V2M in terms of the ratio of L2/3 to L5. The fraction of neurons in non-visual cortical areas was not formally tested, as these came from a highly diverse set of regions such that pooling may make any results difficult to interpret. Furthermore, low numbers would make observation of statistical differences difficult.

4.2.4 Precise Location of Local Excitatory and Inhibitory Presynaptic Neurons

Assignment of a presynaptic neuron to a particular layer and region is a useful exercise, but it is a rather crude method for studying complex patterns of connectivity, particularly for local connections (in this context, referring to intra-areal or recurrent connectivity). Furthermore, no distinction can be made reliably between excitatory and inhibitory presynaptic neurons (although many neurons can be seen to have a clear pyramidal morphology when labelled with RV-tagRFP, a cell without such clear morphology may be a stellate neuron, an interneuron, or simply a poorly labelled / sectioned pyramid).

Therefore, local connectivity was examined in five experiments (RS1,RS3,RS4,RS5,RS9), which had been performed in GAD67-GFP animals, and imaged using STPT. Images were first unmixed (see section 4.2.1) in order to separate true eGFP signal from bleed-through from bright tagRFP or mCherry labelling (fig. 4.5a). Image stacks were then rotated such that the cortical surface was horizontal (fig. 4.5b), and inhibitory and non-inhibitory (putative excitatory) presynaptic neurons were manually identified. In a few instances the interpretation of unmixed data was difficult as very brightly labelled neurons saturated the photomultipliers, causing spurious inferred eGFP signal in the resulting unmixed image. However, this was rare, and most typical in large L5 pyramidal neurons, whose size and morphology made manual classification as excitatory neurons trivial.

Overall, the spread of excitatory neurons was greater than that of inhibitory neurons in all three cardinal directions (medio-lateral (ML), anter-posterior (AP), dorso-ventral / depth (DV), fig. 4.5c). The degree of difference was roughly similar: in the ML axis the median values were 91µm for excitatory neurons and 64µm for inhibitory, a difference of 41%; AP 183µm vs. 121µm (51%); DV 88µm vs. 60µm (47%).

Comparing the distribution of distances within each group revealed that connectivity was highly non-isomorphic. (Kruskal-Wallis test p = $7\text{x}10^{-26}$ for excitatory neurons, p = $7\text{x}10^{-9}$ for inhibitory). Interestingly, this result was driven by the spread of connectivity

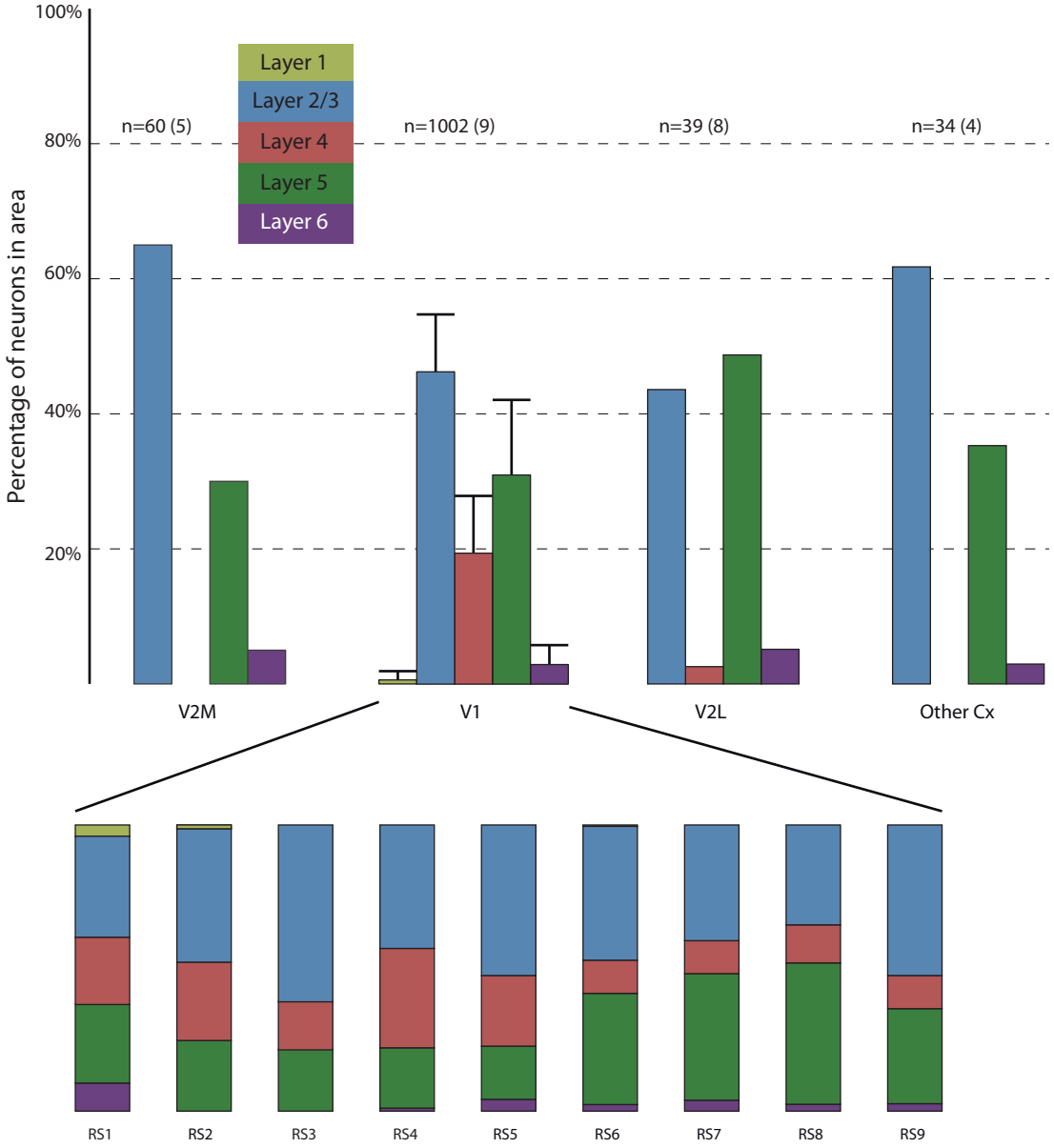

Figure 4.4: Laminar Distribution of Presynaptic Inputs

Above: Laminar distribution of presynaptic neurons in medial secondary visual areas ('V2M'), primary visual cortex ('V1'), lateral secondary visual areas ('V2M') and all other ipsilateral cortical areas ('Other Cx'). For areas other than V1, neurons have first been pooled across experiments owing to the small numbers of neurons in these. For V1, percentages have been calculated individually for each experiment, and then averaged; error bars indicate SD. The total number of neurons in each cortical area is shown above the plot, with the number of experiments with any neurons given in brackets.

Below: Individual experiment laminar distributions of presynaptic neurons, demonstrating significant variability.

along the AP axis, which was significantly greater than either ML or DV for both cell types (Wilcoxon rank-sum test). However, ML and DV distributions did not differ significantly in either cell type. Whether this indicates that AP connectivity specifically differs from the other dimensions is unclear, as V1 is elongated in this direction (Dräger, 1975; Mangini and Pearlman, 1980; Paxinos and Franklin, 2008), and so it is possible that 'stretched' connectivity along the AP axis merely preserves some kind of uniform local connectivity rule.

This analysis was limited to intra-V1 connections. However, when all neurons outside V1 were examined for molecular identity, in no case was an eGFP-positive cell found.

These pooled distances do, however, mask individual differences in the shapes of the local cloud of presynaptic connectivity (fig. 4.6). AP spread was the most consistent across experiments, with density being roughly equal in both the anterior and posterior dimension, and inhibitory density being narrower in most cases (with the exception of RS4).

In contrast, the distribution of connectivity with depth differed greatly across experiments, with some neurons (RS1, RS3) receiving excitatory inputs from across the cortical depth, and others (RS4,RS5) being far narrower in this parameter (fig. 4.6, left). In all cases, the peak of the presynaptic excitatory density was centred around L4. However, inhibitory density was more variable, being centred in L2/3 for RS3 and RS9, in L4 for RS4 and RS5, and near the L2/3/L4 border for RS1. Again, inhibitory spread was in general more restricted than excitatory, although not in all cases. In RS4, two presynaptic inhibitory neurons were observed in L6, near the dorsal border with L5. Martinotti in L6 cells are known to project widely throughout the cortical depth (Markram et al., 2004; Wang et al., 2004), although translaminar inhibition by a subgroup of fast-spiking parvalbumin positive neurons has also been described recently (Bortone et al., 2014).

ML connectivity was more mixed. In general, excitatory connectivity was slightly left (medial) skewed, with inhibitory connectivity being narrower and more evently spread. Inihibitory density was quite variable in this dimension, although excitatory density was comparatively consistent.

Overall, these data show that the presynaptic density of local inhibitory connectivity is, in general, more confined than that of excitatory connectivity; that this is somewhat variable between individual neurons, and that presynaptic connectivity densities vary with depth in quite a different fashion for individual neurons.

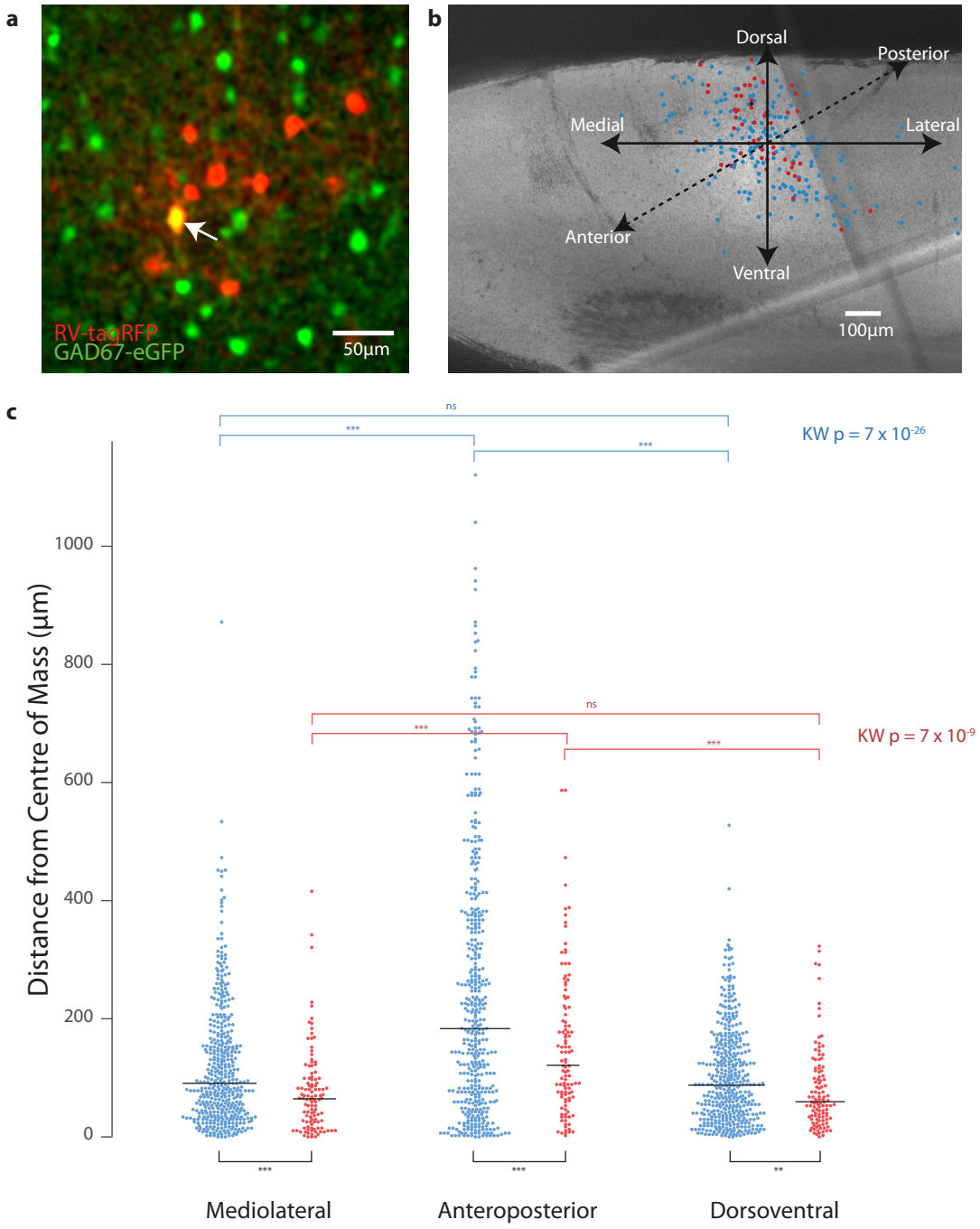

Figure 4.5: Location of GABAergic and non-GABAergic Presynaptic Cells in V1

(a) Single image from an unmixed STPT stack, showing several labelled presynaptic excitatory neurons labelled with RV-tagRFP (red), and many non-labelled inhibitory interneurons (green). One inhibitory neuron is also labelled with RV-tagRFP (yellow, indicated by the arrow).

(b) Maximum intensity projection showing all neurons identified as putative excitatory (blue) or inhibitory (red) and their location within V1. The image has been rotated, and cardinal directions are indicated.

(c) Distance of inhibitory (red) and putative excitatory (blue) neurons from the centre of mass. Individual significance was calculated using Wilcoxon Rank-Sum (with Holm-Bonferroni correction in the case of the post-hoc tests, above). Horizontal bars indicate median values.

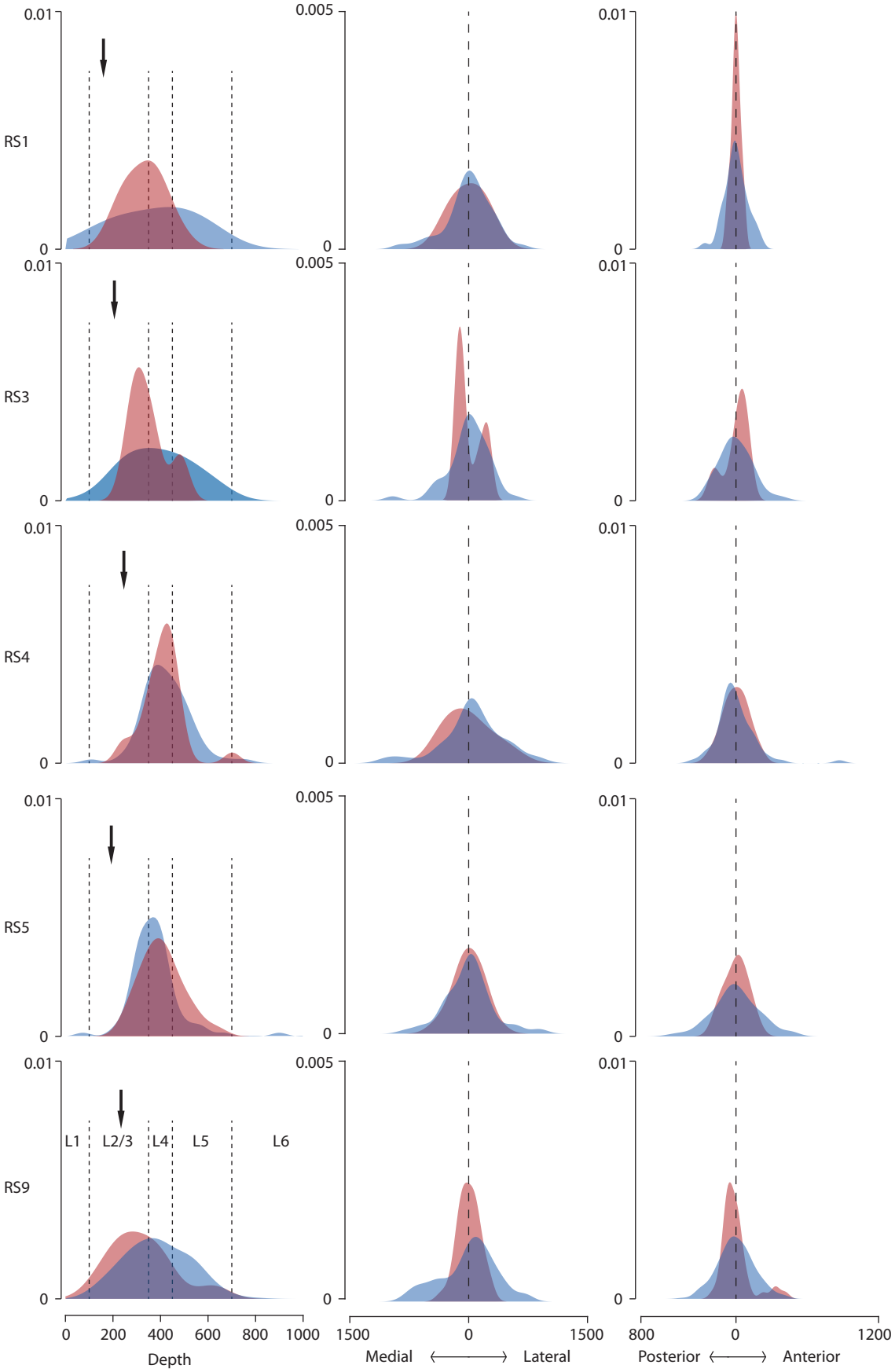

Figure 4.6: Connectivity density plots for all 5 individual experiments that comprise the pooled data of fig. 4.5. Densities are estimated using a kernel density estimate algorithm, separately for excitatory (blue) and inhibitory (red) neurons. Left: DV. The approximate borders of the cortical layers are indicated by dotted lines; the estimated depth of the recorded host neuron is indicated by the arrow. Middle: ML, with the centre of mass indicated by a dotted line; right: AP. Y-axis: inferred CDF.

4.3 Discussion

4.3.1 Limitations of RVCM

The experiments described here were obtained from a larger dataset of around 60 experiments in which tracing was attempted. This therefore translates to a success rate of approximately 1 in 6. However, this excludes experiments in which tracing could not be attempted, such as, for example, when a recording is unintentionally terminated prematurely. In such cases, since it is not known at the time of recording whether the neuron has survived, tracing can not be attempted in another neuron in the same animal without the possibility that the presynaptic connectivity revealed may include neurons presynaptic to more than one host cell. Therefore, including all such exclusion criteria pushes the success rate of the technique, at this stage, in L2/3 in my hands to approximately 1 in 10, perhaps even fewer. This rate of success, should make experiments of the kind described here and in (Wertz et al., 2015) possible, revealing for the first time the connectivity of individual neurons. However, it makes it very difficult to obtain large enough numbers of experiments to make quantitative statements about the variability of presynaptic connectivity, or the anatomical correlates of neuronal function, one of the original aims of my project (see fig. A.1 for orientation tuning of individual neurons alongside a summary of their areal distribution of presynaptic neurons). It remains to be seen whether, and how, the technique can be honed to bring this ratio to a more favourable level.

Another concern for these data is the low numbers of neurons labelled by the rabies virus. The dendrites of pyramidal neurons in L2/3 are known to contain thousands of denritic spines (Spruston, 2008), with estimates for L2/3 neurons in the rat numbering around 4,000-10,000 (Schüz and Palm, 1989; Larkman, 1991; Defelipe and Fariñas, 1992). Whilst pyramidal neurons make synapses on to dendritic spines, interneurons may also synapse on to various locations including the axon initial segment, the soma, and the dendritic shaft; therefore there are many more synapses than spines. Although it is likely that neurons may make more than one synaptic contact on to another (Feldmeyer et al., 2002; Bock et al., 2011) a conservative estimate of the average number of distinct presynaptic neurons of a particular L2/3 would be somewhere in the region of 800-1500 (Marshel et al., 2010).

The numbers reported here are certainly lower than the true number of presynaptic neurons, but are in the mid range of reported numbers of presynaptic neurons labelled by single-cell rabies-virus circuit mapping. Marshel et al. (2010), using electroporation

to transfect, report numbers ranging from 36-97 neurons per host. Wertz et al. (2015) report 417 ± 74 cells (range 70-846) in immunostained slices. Whilst immunostaining was carried out on a subset on the experiments described in this thesis, it did not significantly increase the number of labelled neurons.

The low numbers of neurons reported here present two distinct but related problems. The first is one of limited sampling. Rare connections may be missed if only a small subset (in the region of around 10% by these estimates) are labelled. This may explain why some authors report 100% of L2/3 V1 hosts as having dLGN input (Wertz et al., 2015). It is also plausible that the subset of labelled neurons is not a fully representative sample. There is currently no data on whether or not this may be the case. It should be noted that neurons were commonly labelled in extrastriate and even subcortical locations including dLGN. This would seem to argue against the possibility that the glycoprotein only reaches very proximal regions of the dendrite. However, the possibility of a more subtle gradient in labelling efficiency can not be ruled out. Therefore, great caution must be applied when comparing the numbers of presynaptic neurons of different classes or in different locations. Ongoing efforts by other groups (Osakada et al., 2011; Ghanem and Conzelmann, 2015) to improve the efficiency of transmission and labelling may settle some of these issues in the near future.

4.3.2 Presynaptic Connectivity of Layer 2/3 Neurons

Despite these limitations, the data presented in this chapter provide a number of conclusions about the connectivity of layer 2/3 regular spiking neurons. Firstly, connectivity on to these neurons is predominantly intra-areal, with the overwhelming majority of connections (around 90%) from other neurons within V1. This finding is roughly consistent with the finding of Marshel et al. (2010), who report that 81% of presynaptic neurons are located within 200µm of the host cell, with the discrepancy likely being explained by the more stringent criterion used by Marshel et al. to define 'local' connectivity.

Within V1, the peak density of both excitatory and inhibitory presynaptic connectivity was typically found to be in layer 4, or deep in layer 3 (fig. 4.6). However, the plurality of presynaptic neurons was observed in layer 2/3 (fig. 4.4); this apparently contradictory finding is explained simply by the smaller absolute thickness of layer 4 leading to a lower *number* of neurons, despite a higher density. Whilst the rabies-virus labelling does not provide information on the strength of the functional connection, this finding reinforces previous reports that the L2/3→L2/3 recurrent connection is particularly strong

(Binzegger et al., 2004), and that features such as orientation selectivity may be explained satisfactorily by biased excitatory input from other L2/3 excitatory neurons alone (Ko et al., 2011; Cossell et al., 2015). This is not to ignore the role of feedforward connectivity. Clearly, visual input must arrive in to the circuit at some point, either directly from the thalamus or via layer 4, in order for visually-evoked responses to occur. However, it is clear that the notion of a simple feedforward chain of connectivity must be replaced by a model in which recurrent connectivity plays a central role, perhaps being modulated by feedforward inputs that are just-enough/just-in-time (Douglas and Martin, 2007) in order to drive responses in V1.

One outstanding question with regard to local connectivity is the spread of excitatory and inhibitory connections - and whether these may differ. Inhibitory interneurons have been found to form 'hot spots' in layers 2 and 5A (Meyer et al., 2011), as well as to cluster non-randomly in L2/3 (Ebina et al., 2014). However, the distribution of excitatory and inhibitory neurons presynaptic to a single cell has not yet been described. The data presented in figs. 4.5 and 4.6 demonstrate that the somata of inhibitory presynaptic neurons are significantly closer to the postsynaptic neuron than excitatory inputs. Whilst rodent V1 is arranged in a salt-and-pepper topography, with no functional columns as regards orientation (Ohki et al., 2005), ocular dominance (Hofer et al., 2006), or precise retinotopic location (Smith and Häusser, 2010), this finding would further argue against a possible role for lateral inhibition, since the inhibitory input on to a given regular-spiking neuron is more narrowly confined than the excitatory input. It is also notable that presynaptic GABAergic (GAD67+) neurons were *never* detected outside of V1.

In addition to intra-areal connectivity, a smaller number of connections were typically found in other cortical areas, most prominently medial and lateral secondary visual cortices, as well as associative and retrosplenial cortex. Direct investigation of the functional relevance of such connections is only beginning to be explored in the mouse. Many models of feedback connectivity from 'higher' to 'lower' visual areas focus on modulatory processes such as spatial attention-related gain control (Gilbert and Li, 2013). However, the finding that neurons in mouse V1 may directly encode features such as sensorimotor mismatch (Keller et al., 2012) or reward (Poort et al., 2015) implies that the V1 circuit must have access to higher-order information, perhaps subserved in part by the connections described in this chapter. For example, it has recently been shown that retrosplenial input on to layer 2/3 neurons is increased, as compared to layer 4 input, during learning (Makino and Komiyama, 2015). Further experiments will be needed in order to investigate the

functional roles of these, and other feedback connections.

Subcortical presynaptic neurons were also detected in a number of experiments. The majority (6/9) of RS neurons had at least one presynaptic neuron in the dLGN, indicating that direct feedforward input on to L2/3 neurons is a feature of visual cortex. In addition to the classical inputs on to layer 4 and layer 6 neurons, direct thalamic inputs have been reported in layer 5 in the somatosensory cortex (Constantinople and Bruno, 2013), however these experiments did not demonstrate direct feedforward input on to layer 2/3 neurons. This may reflect an anatomical difference between the sensory cortices, or perhaps weaker Thal→L2/3 inputs being missed by the spike-triggered averaging used. Using rabies-virus tracing, Wertz et al. (2015) report 100% of V1 L2/3 neurons as having at least one presynaptic input from dLGN. The finding here that 3/9 neurons do not have any thalamic input can not be explained as a function of smaller total numbers of presynaptic neurons, as Wertz et al. report total numbers as low as 70 still as including at least one dLGN input. The possibility remains, therefore, that thalamic input may be an important, but not universal, feature of L2/3 RS neurons.

Whilst it is clear that patterns of presynaptic connectivity do vary between individual neurons (figs. 4.2, 4.4 and 4.6), the relatively low numbers of experiments described in this chapter unfortunately preclude a quantitative assessment of variability in patterns of connectivity, and investigation of any potential correlation between such variability and functional response properties (see appendix, fig. A.1). Further refinement of the RV tracing system may, hopefully, allow for more precise quantitation of the nature, and possible effect, of such variability in V1, and in cortical circuits more generally.

Chapter 5

Responses to Drifting Grating Stimuli

5.1 Introduction

As outlined in the general introduction, (table 1.1), the responses of neurons in the primary visual cortex (V1) of the rodent to classic drifting grating stimuli have been characterised in numerous studies. Many of these were carried out using extracellular recording techniques, either of single units (Dräger, 1975; Gao et al., 2010; Van den Bergh et al., 2010), or utilising multisite electrodes to record many units simultaneously (Niell and Stryker, 2008). The invention of two-photon microscopy (Denk et al., 1990) and its use to image deep in to living brain tissue (Theer et al., 2003; Helmchen and Denk, 2005), in conjunction with the use of bulk-loaded synthetic calcium indicators (Stosiek et al., 2003; Ohki et al., 2005) revealed that responses of individual neurons in rodent V1 may be well tuned for orientation, just as in the cat (Ohki et al., 2005). Two-photon calcium imaging has fostered a proliferation of studies of the responses of groups of individual neurons to visual stimuli, particularly in the mouse (Stosiek et al., 2003; Sohya et al., 2007; Kerlin et al., 2010; Bonin et al., 2011; Ko et al., 2011; Marshel et al., 2011; Rochefort et al., 2011; Roth et al., 2012; Ko et al., 2014). The use of genetically-encoded (Tian et al., 2009; Zariwala et al., 2011; Chen et al., 2012, 2013) calcium indicators has expanded the capabilities of imaging based studies, enhancing signal-to-noise whilst providing stable expression over days to weeks, and the ability to target molecularly identified neuronal subtypes.

Response properties in the rodent visual cortex, recorded using whole-cell patch clamp *in vivo* have been reported by a more limited number of papers (Jia et al., 2010; Liu

et al., 2011; Medini, 2011a; Tan et al., 2011; Smith et al., 2013; Vélez-Fort et al., 2014; Cossell et al., 2015). To date, none of these provide a detailed description of the synaptic depolarisation and spiking properties of a large number of layer II/III (L2/3) neurons to visual stimuli.

Medini (2011a) describes neuronal morphology in the rat in some detail, along with a number of evoked and biophysical properties. However, this characterisation is patchy in parts, with a limited discussion of population distributions, and discussion of neuronal processing focuses on the mean differences between L2/3 and layer IV (L4) neurons (for example, the finding that peak evoked depolarisations are of similar magnitude in both cell types, but that peak evoked firing rate is higher in L4). Tan et al. (2011) provide a more complete description of the manner in which the mean membrane potential depolarisation OSI (OSI_{Vm0}) and resting membrane potential (RMP) (or, at least p, a parameter which probably derives in large part from RMP) combine to set mean firing rate OSI (OSI_{F0}). However, this discussion is limited to orientation selectivity, the cells are recorded in L2/3 and L4 in both cats and mice, and the authors do not investigate directly the origin of their key exponent variable p. Whole-cell patch clamp has been used to investigate dendritic processing of visually evoked synaptic inputs (Jia et al., 2010; Smith et al., 2013), as well as to demonstrate the effect of broad inhibition on orientation selectivity (Liu et al. (2011); see also Tan et al. (2011)) . However, these studies were all performed in small numbers of cells in order to investigate specific hypotheses regarding neuronal processing. A larger-scale investigation of neuronal processing has recently been published by colleagues in our laboratory (Vélez-Fort et al., 2014), investigating the intrinsic and visually-evoked properties of two classes of layer VI (L6) excitatory neurons, as well as characterising their presynaptic connectivity. However, similar studies have not been undertaken in L2/3.

Intracellular recording of the responses of a large number of neurons to visual stimuli is of value for two principal reasons. Firstly, it may provide estimates of population properties less prone to selection bias, since neurons with very low spontaneous or evoked firing rates may not be detected with the same probability as more active units by extracellular recording methods. Whilst calcium imaging techniques can, in principle, reveal silent or sparsely active neurons, modern genetically encoded indicators such as GCaMP6s have very low baseline fluorescence levels (Chen et al., 2013), making unambiguous detection of neurons difficult in the absence of spiking activity. Furthermore, the reconstruction of the underlying action potential train from continuous changes in fluorescence levels remains

challenging under potentially noisy conditions *in vivo* , although various statistical techniques have been developed to this end (Grewe et al., 2010; Vogelstein et al., 2010). The long decay time of calcium indicators poses an additional problem in studying temporal frequency dependent changes, as well as spiking modulation ratio (F1/F0). These potential limitations may introduce uncertainty in to estimates of the population distribution of tuning parameters. For example, the distribution of F1/F0 in the mouse, as well as the laminar distribution of this parameter, remain mostly unknown. Using single unit recordings, (Van den Bergh et al., 2010) report that the large majority of L2/3 neurons in the mouse have complex-type responses (with F1/F0 < 1). Similarly, (Gao et al., 2010) found that the overwhelming majority (94%) of neurons in mouse V1 are complex, and whilst they state that all recorded simple cells were located in L2/3 and L4, they do not break down further the fraction of simple and complex responses by layer. In contrast, Niell and Stryker (2008) report that the majority of L2/3 neurons are simple cells (F1/F0 > 1), using multisite silicon electrodes. These basic uncertainties over the distribution of commonly-used metrics in mouse V1 present a challenge to the field.

Secondly, whole-cell patch clamp recordings provide information on the intrinsic biophysical properties and evoked synaptic activity of neurons that can allow for investigation of information processing within the neuron (Chadderton et al., 2014). Intracellular recordings have been used to study the excitatory and inhibitory components of sensory-evoked inputs on to V1 neurons (Ferster, 1986; Borg-Graham et al., 1996), as well as integration of these components (Ferster and Jagadeesh, 1992; Hirsch et al., 1998); the effect of contrast and orientation on input conductance and gain control (Anderson et al., 2000); the role of threshold in sharpening spiking orientation tuning (Carandini and Ferster, 2000), and defining F1/F0 (Priebe et al., 2004). However, these studies were all carried out in the cat; similar data for neurons in mouse V1 remains scarce. Furthermore, most either do not specify the laminar location of the recorded neurons (Priebe et al., 2004) or pool recordings from multiple layers (Tan et al., 2011). Neurons located in different layers of the cortex vary in terms of their presynaptic connectivity (Douglas and Martin, 1991; Kätzel et al., 2011), morphology (Medini, 2011a; Oberlaender et al., 2012) and biophysical properties (McCormick et al., 1985; Medini, 2011a). Whilst the general rules of information processing may be addressed by examining a mixed population, the effect of *variation* in biophysical properties and synaptic input is best studied in an otherwise homogenous population.

Therefore, I sought firstly to characterise classical tuning properties (preferred spatial

and temporal frequency, orientation selectivity, frequency-dependent modulation) systematically for evoked spiking and membrane potential (V_m) responses in mouse L2/3 regular spiking (RS) neurons. Secondly, I undertook a statistical analysis of the correlates of the most diverse of these parameters - orientation tuning - in order to try to understand the mechanisms by which a heterogenous spiking distribution may be created by an apparently homogenous group of neurons. Recording from a large number (>100) of neurons provided unprecedented statistical power for a study of this kind.

The orientation tuning of the spiking output of regular spiking / pyramidal neurons in L2/3 is known to be extremely variable (Niell and Stryker, 2008; Zariwala et al., 2011; Hofer et al., 2011), with responses in some neurons being highly sensitive to the orientation of the stimulus, whilst in others responses are practically equal to drifting gratings of all orientations. The distribution of spiking orientation selectivities, as measured by the Orientation Selectivity Index (OSI), is quite flat, with no obvious 'tuned' or 'untuned' subgroups (Zariwala et al., 2011; Ko et al., 2014). The mechanisms by which the orientation tuning of a neuron is generated have been investigated in the mouse and the cat by (Tan et al., 2011), with a focus on the interaction of the orientation tuning of the mean evoked synaptic depolarisation (Vm0) and variation in the threshold nonlinearity. However, their findings may be driven, in part, by laminar and species difference. Furthermore, they do not investigate the possible effects of other intrinsic biophysical parameters, such as input resistance or rheobase, or of the *modulation* of the membrane potential. This parameter has been investigated in the context of the spiking F1/F0, both theoretically (Mechler and Ringach, 2002) and experimentally (Priebe et al., 2004); however its role in defining the mean spike rate of a neuron in response to visual stimulation remains largely unexplored.

5.2 Results

5.2.1 Tuning Properties of L2/3 Neurons

Once the resting membrane potential and spontaneous activity had recovered to a stable level (section 2.4), and responses to ballistic stimuli were recorded (see section 6.2.2.2), membrane potential responses to drifting grating stimuli were recorded in the current clamp mode (fig. 5.1).

Orientation tuning properties, and the factors which may contribute to their definition, are described in detail later in this chaper (sections 5.2.2 to 5.2.4). Before discussing these, I first outline other tuning properties of L2/3 neurons.

5.2.1.1 Spatial and Temporal Frequency Tuning

Following recording of responses to gratings of different orientation and direction, an online analysis was made to determine the preferred direction of the mean spike rate (F0) response to drifting gratings. Gratings of different spatial and temporal frequencies were then used to investigate the spatiotemporal tuning properties of neurons, at the cell's preferred direction.

Recordings were made in 72 neurons using 5 temporal frequencies and 6 spatial frequencies, presented in all combinations ('ST frequency pairs') in a pseudorandom order. Whilst variable, neurons typically responded to all frequencies with at least some membrane potential activity (fig. 5.2). Spiking responses to stimuli were more sparse (fig. 5.3), however most neurons did spike to the majority of ST frequency pairs.

The synaptic and spiking preferred ST frequency pair of individual neurons was determined as the condition which evoked the maximum mean depolarising (Vm0) or spiking (F0) response respectively (fig. 5.4). Responses maps were typically smooth and convex, with a single global maximum, although this was not always the case. Responses did not appear to be obviously speed tuned, although this was not quantified rigorously.

The modal preferred spatial frequency for both Vm0 and F0 was 0.0283 cycles/degree (fig. 5.5a), the exact same frequency used in orientation tuning experiments. For temporal frequency, the modal preferred frequency was 2.83Hz (fig. 5.5b), slightly higher than that used in orienation tuning experiments (2Hz).

The effect of varying spatial and temporal frequency alone was investigated by taking responses to all spatial frequencies at the neuron's preferred temporal frequency, and vice versa, separately for Vm0 and F0. (fig. 5.4, dotted lines). Responses were then averaged

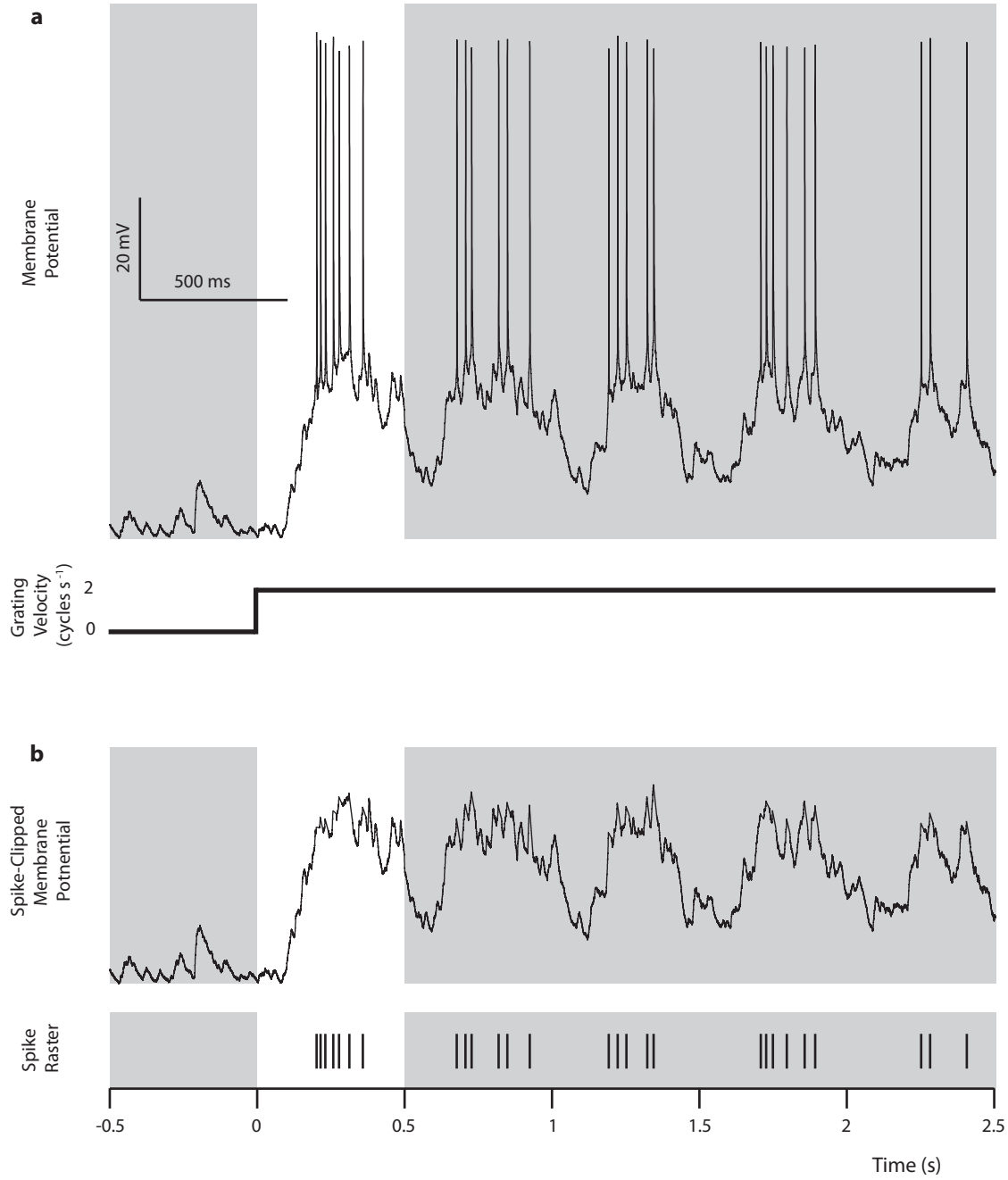

Figure 5.1: Example response of a neuron to a single trial at the preferred orientation and direction, before and after spike detection and clipping.
(a) Raw current-clamp recording, showing membrane potential and spiking responses to drift onset. The epochs used to define baseline activity and stimulus-evoked activity are outlined by the first and second gray boxes respectively. The first 500ms of drift were excluded from analysis of specific stimulus-evoked activity.
(b) Spike-clipped membrane potential (above) and spike raster (below) of the same trial.

across neurons to give a population mean response to stimuli of varying frequency. These population mean responses (figs. 5.5c and 5.5d) were generally similar to the distributions of preferred frequency, but more broadly spread. For spatial frequency (fig. 5.5c) the peak firing response was observed at the same frequency as the modal preferred (0.0283 cpd). However, the peak mean depolarisation (blue) was slightly lower, at 0.02cpd. For temporal frequency, both the population mean Vm0 and F0 peak were at the same value as the modal preferred, 2.83Hz (fig. 5.5d). For both spatial and temporal frequency changes the bandwidth of spiking responses was slightly lower than that for mean depolarisations.

These experiments therefore should provide some reassurance that the spatial and temporal frequencies used in orientation tuning experiments following were appropriate for this population. They also are in broad agreement with tuning properties calculated for mouse V1 using extracellular methods by (Niell and Stryker, 2008; Gao et al., 2010).

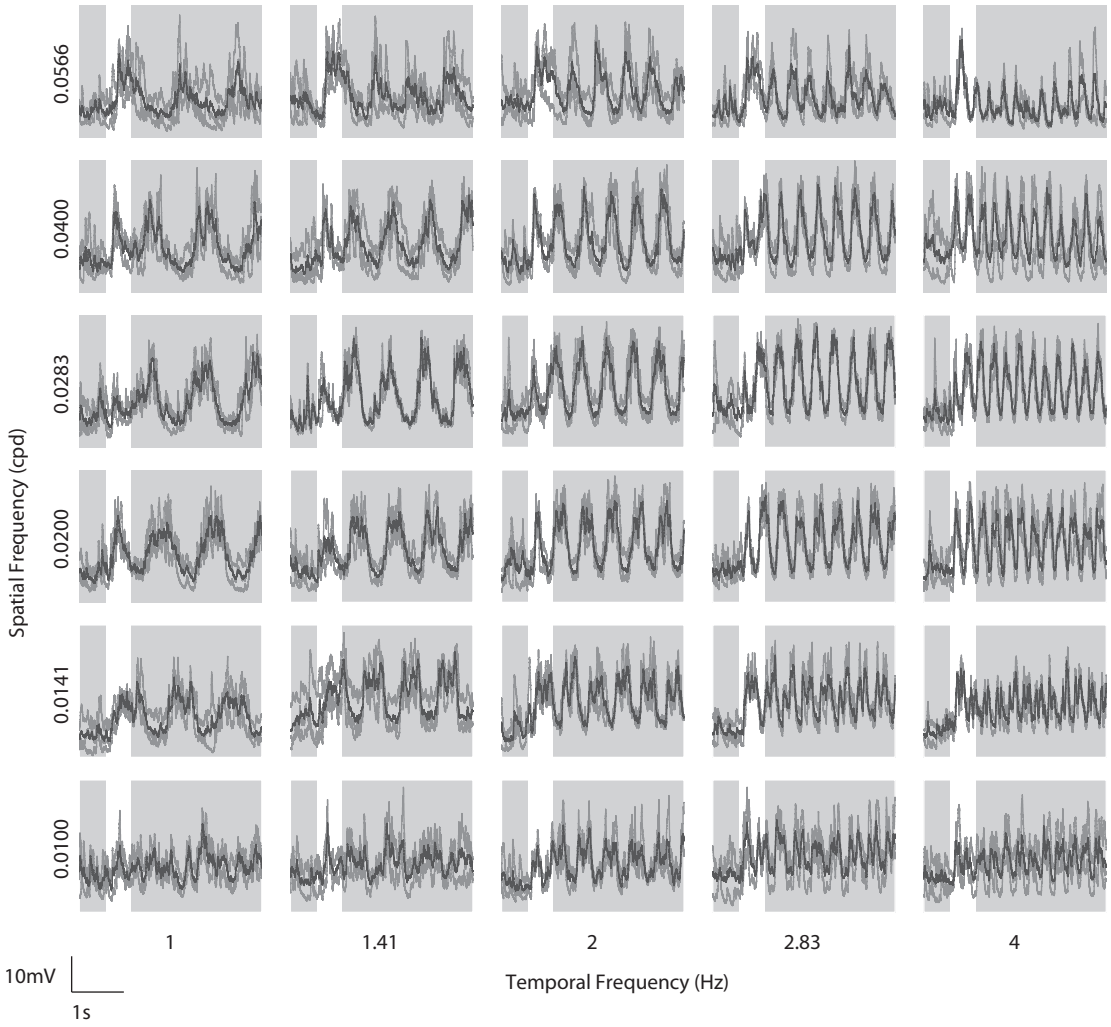

Figure 5.2: Membrane Potential Responses (spike-clipped) of an example neuron to varying spatial and temporal stimulus frequency.
All three individual trials are shown overlaid in gray, with the exception of one frequency pair (TF 2.83Hz, SF 0.0283cpd) in which one recording had to be excluded due to stimulus presentation jitter.
Mean responses are shown overlaid in black. Baseline and drifting grating analysis epochs are denoted by gray boxes; drift onset began at the end of the baseline epoch.

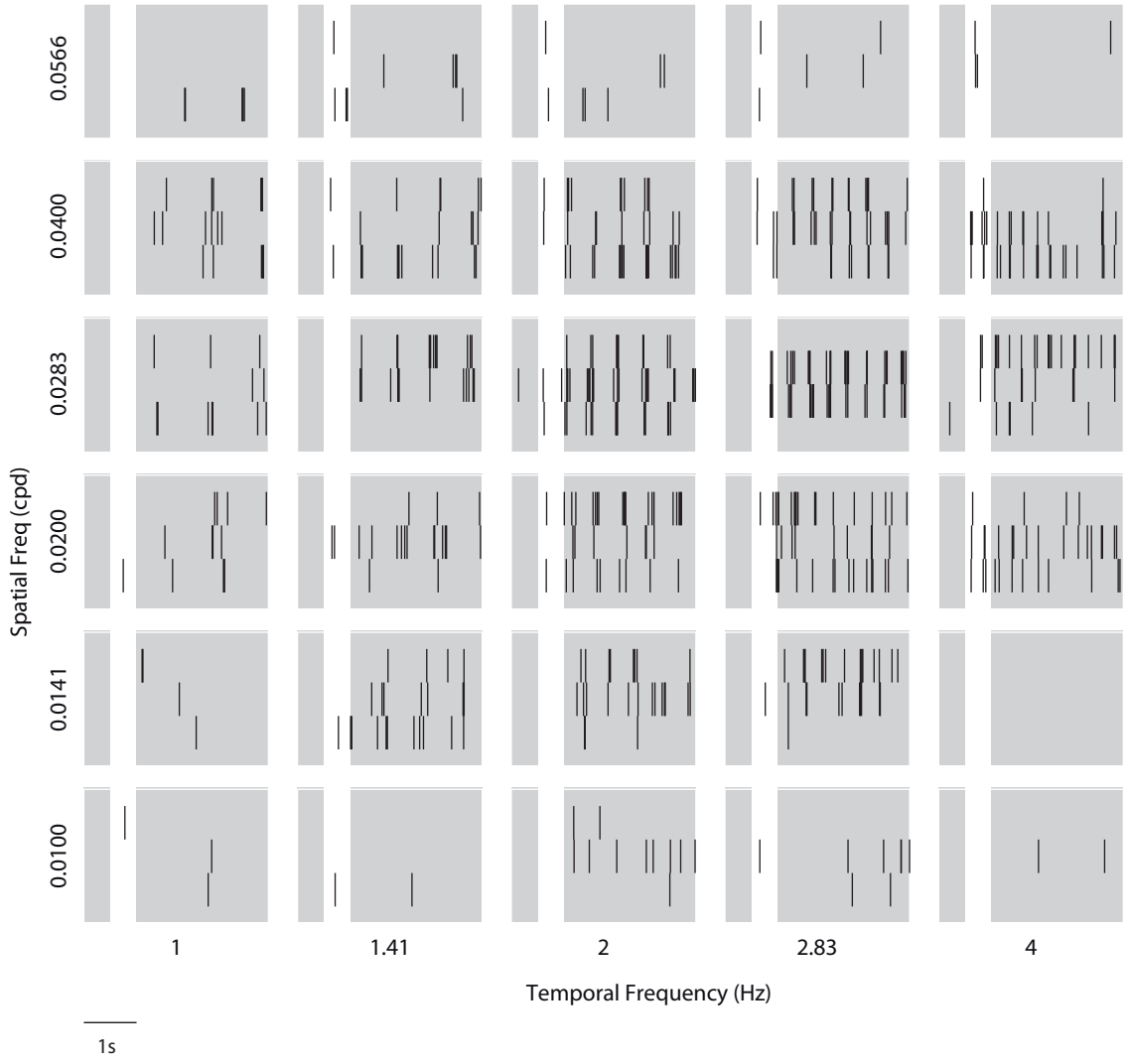

Figure 5.3: Spike raster, showing responses of the same neuron as in fig. 5.2 to individual trials of varying spatial and temporal stimulus frequency. Baseline and drifting grating epochs are denoted by gray boxes; drift onset began at the end of the baseline epoch.

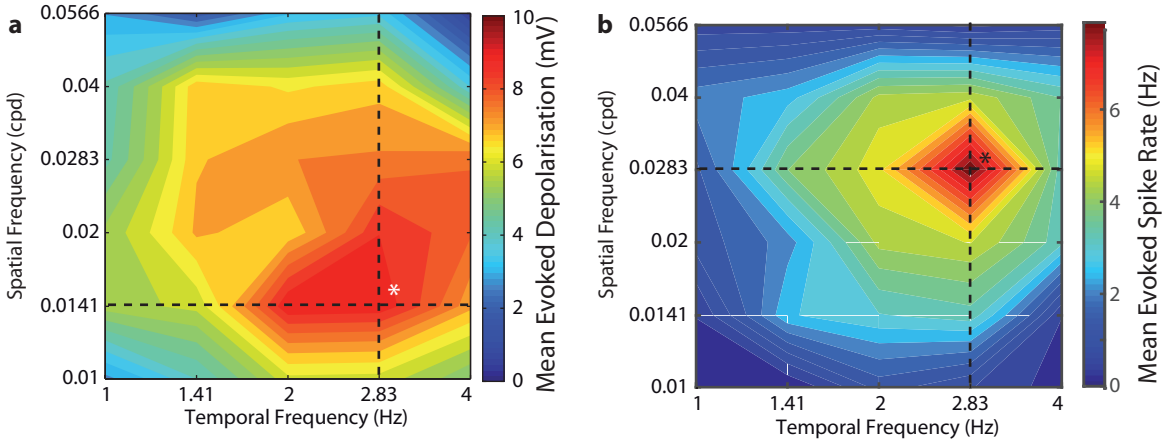

Figure 5.4: Frequency tuning response profile for the same neuron as in figs. 5.2 and 5.3
(a) Mean evoked depolarisation (Vm0) response. Peak response is denoted with an asterisk; dotted lines indicate the conditions used to calculate response to varying either spatial or temporal frequency alone (fig. 5.5c)
(b) Mean evoked spike rate (F0) response. In this particular case, the preferred temporal frequency of the F0 response is identical to that of the Vm0 response. However, the preferred spatial frequency of the F0 is higher than the preferred spatial frequency of the Vm0.

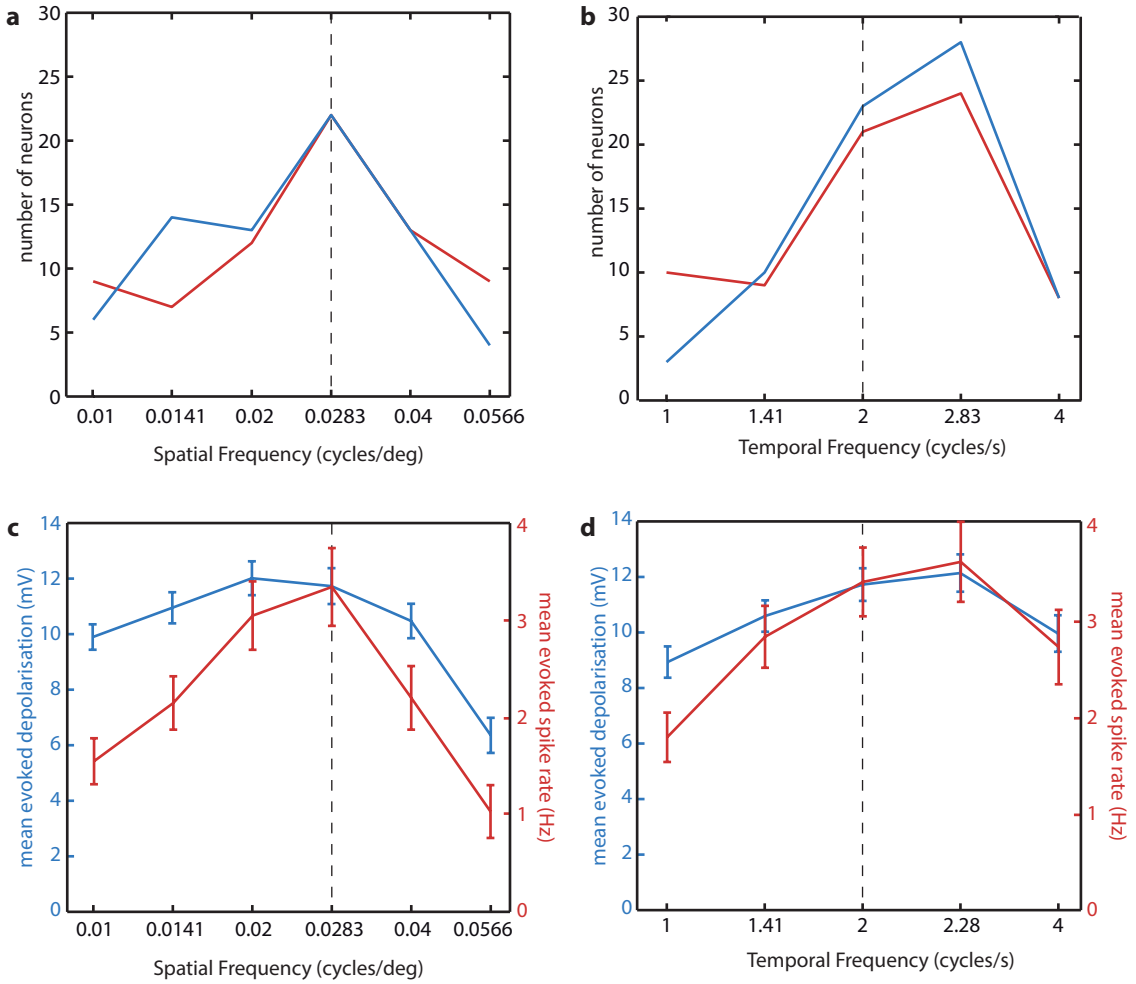

Figure 5.5: Spatial and Temporal Tuning of L2/3 neurons

(a) Preferred spatial frequency of Vm0 (blue) and F0 (red) responses in all neurons in which frequency tuning recordings were obtained (n=72). The dashed line indicates the spatial frequency used in orientation tuning experiments.

(b) Preferred temporal frequency ofVm0 (blue) and F0 responses in all neurons. The dashed line indicates the temporal frequency used in orientation tuning experiments.

(c) Response profile, averaged across all neurons, for responses to varying spatial frequency at the particular neuron's preferred temporal frequency. Error bars indicate standard deviation.

(d) Response profile, averaged across all neurons, for responses to varying temporal frequency at the particular neuron's preferred spatial frequency.

5.2.1.2 F1/F0

As described in the introduction to this chapter, the distribution of F1/F0 values in L2/3 of the mouse has been investigated in few studies (Niell and Stryker, 2008; Van den Bergh et al., 2010), with mixed results. In order to investigate the ratio of simple:complex cells, spiking F1/F0 was quantified at the preferred direction for all neurons responsive to oriented drifting grating stimuli at a spatial frequency of 0.0283cpd, and a temporal frequency of 2Hz (n=112). Of these 112 neurons, 9 neurons fired so sparsely that spiking firing rate modulation at the stimulus fundamental frequency (F1) could not be defined.

Although the number of cells with F1/F0 values <1 (complex responses according to this standard criterion) was low, the F1/F0 distribution did appear to be bimodally distributed (fig. 5.6). When formally tested for bimodality, this effect was determined to be significant (Hartigan's Dip test, p=0.026*), supporting the classical finding of an apparent dichotomy between simple and complex responses (Skottun et al. (1991), although see also Mechler and Ringach (2002); Priebe et al. (2004)). Taking a critical value of 1, 17/103 cells would be considered complex (16.5%), and 86 simple (83.5%). It would appear, therefore, that complex responses make up only a small minority of regular spiking neurons in L2/3 of mouse V1.

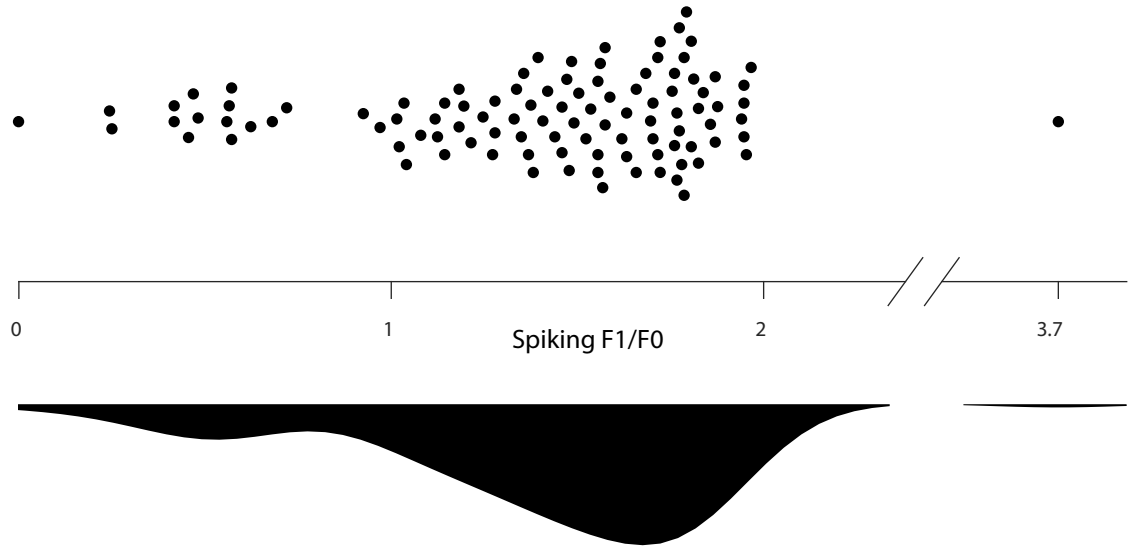

Figure 5.6: Distribution of F1/F0 values for L2/3 neurons
Above: Individual F1/F0 values of responses to stimuli of the preferred direction, at 0.0283cpd, 2Hz, plotted for all responsive cells with a definable F1/F0 (n=103).
Below: Kernel Smoothing Density estimate of the same data, showing a peak at around 1.7 and a second, smaller peak at around 0.5, indicative of a dichotomy between simple- and complex-type responses.

As demonstrated in fig. 5.5, neurons in L2/3 of mouse V1 display a range of preferred spatial and temporal frequencies. It is therefore questionable whether the F1/F0 mea-

sure made at the standard spatial and temporal frequencies used in orientation tuning experiments (0.0283cpd, 2Hz) is appropriate for all neurons.

Therefore, the F1/F0 defined from the orientation tuning dataset (the measure used in fig. 5.6) was compared to the F1/F0 measure obtained at the preferred direction, spatial and temporal frequency of the neuron. The preferred ST frequency pair was defined as that which evoked the greatest mean spike rate (as in fig. 5.4). F1/F0 values measured at standard (0.0283cpd, 2Hz) and preferred conditions were compared in 61 neurons, and were found to be highly linearly correlated (Pearson's r 0.609, p=1.88x10^{-7}, fig. 5.7), indicating that F1/F0 measured at a single spatial and temporal frequency is a good proxy for F1/F0 at the individual neuron's preferred spatial and temporal frequency. However, F1/F0 values recorded at the neuron's preferred ST frequency pair were systematically lower than those at standard conditions (0.0283cpd, 2Hz), with the slope of the relation having a gradient of 0.51 (95% confidence interval 0.337-0.639). This indicates that whilst the two measures are well related, they can not be said to be identical, since this confidence interval excludes the possibility that the true gradient of the slope is unity. Even the additional (possibly artificial) constraint of fixing the y-intercept at 0 did not yield a slope with a 95% confidence interval including 1 (0.789-0.905 using this method).

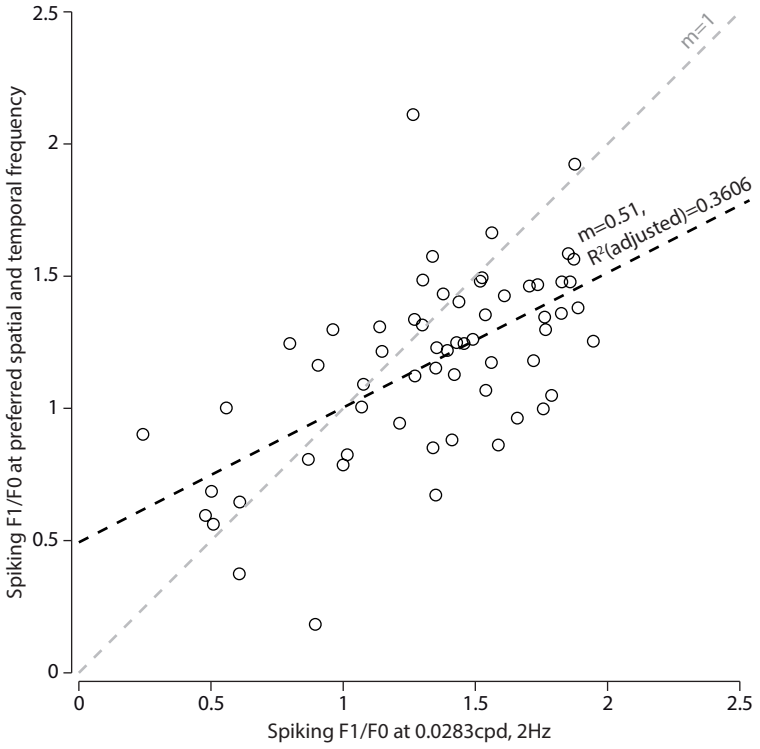

Figure 5.7: Comparison of spiking F1/F0 at standard and preferred spatiotemporal conditions. Spiking response modulation (F1/F0), at the preferred orientation condition but standard spatial and temporal frequency (0.0283cpd, 2Hz) is compared to the F1/F0 at the preferred ST frequency pair, for neurons in which frequency tuning experiments were carried out. The preferred frequency conditions were defined as the ST pair which evoked the greatest mean spike rate (F0).
The line of best fit is shown in black, with a line of unity shown in gray for comparison.

5.2.1.3 Temporal Frequency Dependence of F1/F0

As established in the previous section, F1/F0 is not an invariant property of neuronal responses, but rather can vary with stimulus conditions. This should be expected under all models of V1 function for changes in orientation, however it is not clear that changing spatial and temporal frequency should affect F1/F0. Whilst almost no neurons showed anything resembling a flat F1/F0 response to varying spatial and temporal frequencies, analysing the significance of such changes is difficult, since F1 is calculated on pooled responses to multiple trials. The frequency tuning experiments described previously (section 5.2.1.1) consisted only of 3 repeats of each ST frequency pair, in order to complete the recording in a reasonable length of time.

Therefore, we decided to test whether, in fact, varying temporal frequency did affect the measured F1/F0. By restricting the experiment to temporal frequency alone, a larger number of trials could be conducted to each stimulus condition. The effect of spatial frequency on F1/F0 was not examined (see discussion).

Responses to changing temporal frequency alone (fig. 5.8) were measured in 8 neurons. In all cases, at least 5 repeats of the stimulus were made, up to 15 for some neurons. Of these, 5 responded with a significant F0 to at least 4/5 stimuli (of the same temporal frequencies as used in the frequency tuning experiments - 1, 1.41, 2, 2.83 and 4 Hz) and were included in subsequent analysis.

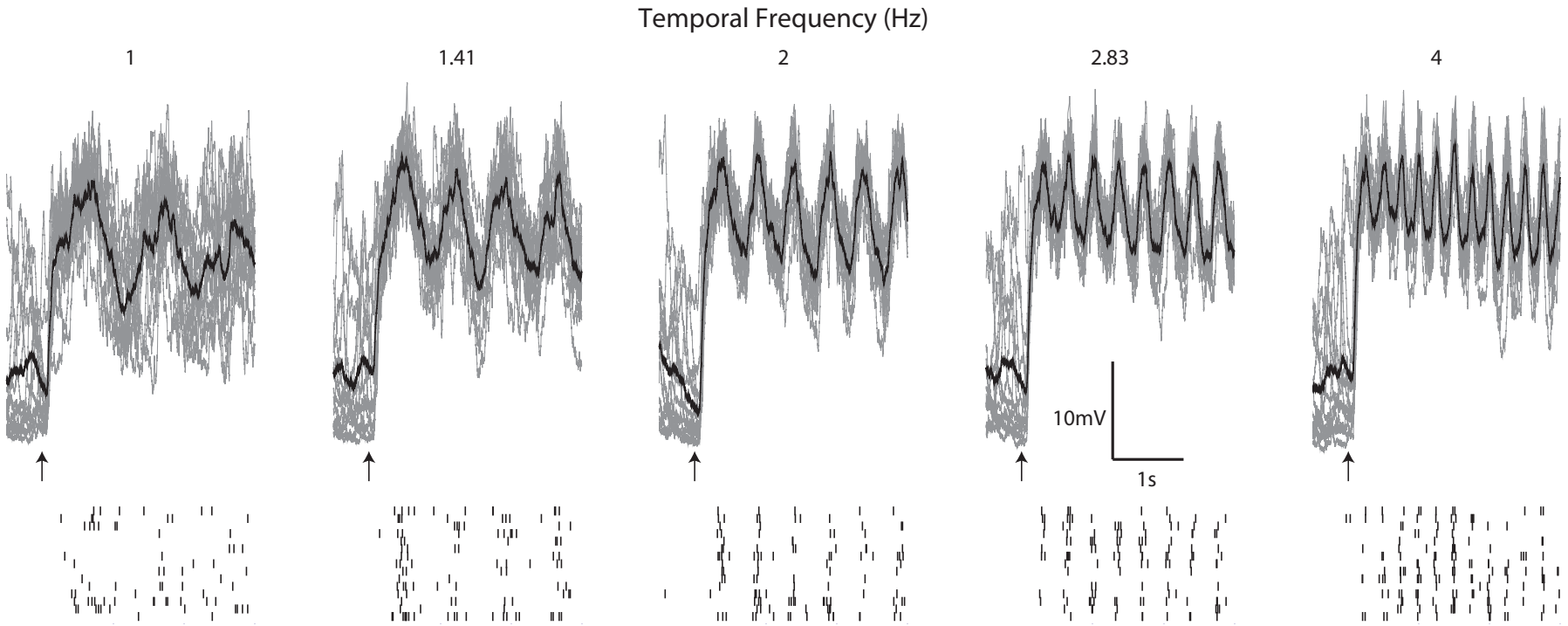

Figure 5.8: Membrane potential and spiking response to changing temporal frequency.
Above: Spike-clipped membrane potential responses (gray) to 15 repeats of stimuli at varying temporal frequency for a single neuron, with mean response overlaid in black. Drift onset is indicated by the arrows.
Below: Spike raster for this same cell

In order to assess the variability of F1/F0 to a particular temporal frequency stimulus, a bootstrap analysis was performed. For each condition, 100 repeats were carried out sampling from all trials for that condition chosen randomly (with replacement). The F1/F0 of each of the 100 ensembles of responses was then calculated, allowing for a Kruskal-Wallis analysis in order to test the hypothesis that F1/F0 changed significantly with varying temporal frequency (fig. 5.9).

In all 5 neurons examined, the variation of F1/F0 with temporal frequency (fig. 5.10) was highly significant ($p<10^{-10}$ in all cases). When the same Kruskal-Wallis test was performed on bootstrapped samples of responses that were first shuffled across stimulus conditions it was not significant in any case ($p > 0.1$ in all 5 cases). Therefore, this analysis shows a specific effect of temporal frequency on F1/F0.

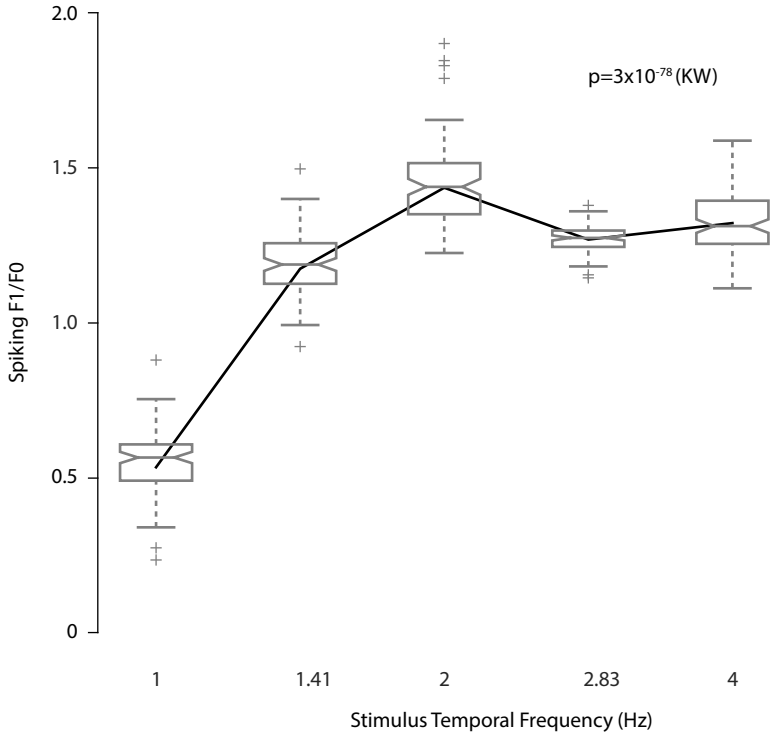

Figure 5.9: Example Analysis of Bootstrapped F1/F0 Estimates

100 bootstrapped estimates of F1/F0 were made at each stimulus condition. These bootstrapped F1/F0 estimates are plotted as box-and whisker plots in gray. Outliers (values more extreme than 150% of the interquartile range from the 25th and 75th percentiles) are plotted as crosses.

For comparison, the F1/F0 calculated on the pooled (non-bootstrapped) responses is plotted in black, agreeing very closely with the median values of the bootstrapped samples (gray lines in the centre of each box plot).

Significance of the changes was determined by a Kruskal-Wallis test ($p < 10^{-10}$ in this neuron, as well as all 4 other neurons tested).

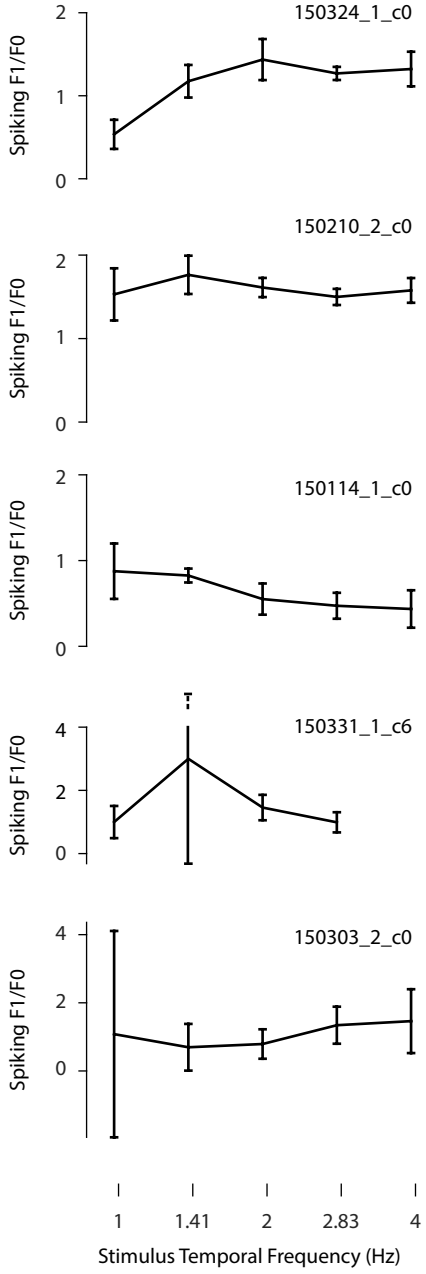

Figure 5.10: Temporal-Frequency Dependence of F1/F0

The effect of varying temporal frequency on F1/F0 is plotted for all 5 neurons which responded with a significant F0 to at least 4/5 temporal frequencies.

For each neuron, the F1/F0 calculated by pooling all trials to a given stimulus is plotted against temporal frequency. Error bars are derived from a bootstrap analysis (see text), and indicate 150% interquartile range.

Whilst all neurons showed a statistically significant variation in F1/F0 according to temporal frequency ($p<10^{-10}$ in all cases, Kruskal-Wallis test), no overall trend could be discerned, with some neurons (150324_1_c0, top) exhibiting a clear rise in F1/F0 with increasing temporal frequency, and others (150114_1_c0, middle) a clear decrease in F1/F0 with increasing temporal frequency.

5.2.2 Orientation Tuning

As established in fig. 5.6, a large majority of neurons in L2/3 are 'simple' cells. However, the population distribution of orientation tuning (defined by the OSI measure) of pyramidal/regular-spiking cells in this layer is known to be highly heterogenous (Niell and Stryker, 2008; Hofer et al., 2011; Roth et al., 2012), making this property an attractive target in the study of if, and how, diverse outputs can be produced by a seemingly homogenous neuronal population.

The data and analyses that follow in this section were all taken from drifting grating stimuli presented at 2Hz temporal frequency and 0.0283 cycles/deg spatial frequency. Responses to oriented gratings (fig. 5.11) were recorded in 128 neurons, with at least 3 repeats of the stimulus in 12 directions in all cases, and at least 5 repeats in the large majority. Typically, neurons spiked infrequently during the baseline period before visual stimulation. The onset of grating drift evoked a depolarisation in most neurons to all directions, although in a few neurons some stimuli evoked very little depolarisation or even a small hyperpolarisation, most commonly at orientations orthogonal to the preferred.

In agreement with published data, OSI_{F0} values covered the entire range of possible values and were quite broadly distributed within this range, (fig. 5.12a) with a median value of 0.41 and an interquartile range of 0.39.

In addition, OSI_{Vm0} and membrane potential modulation OSI (OSI_{Vm1}) values were calculated for all recorded neurons. OSI_{Vm0} values were similar to the more limited reports for this parameter in the mouse (Tan et al., 2011), tending to be quite low with values ranging between 0.0055 to 0.33 (fig. 5.12b). The distribution was highly right-skewed, with a median value of 0.068 and an interquartile range of just 0.072. OSI_{Vm1} values were more broadly distributed (fig. 5.12c), although not quite to the same extent as OSI_{F0} (fig. 5.12a). Median OSI_{Vm1} was 0.20, and the IQR was 0.16.

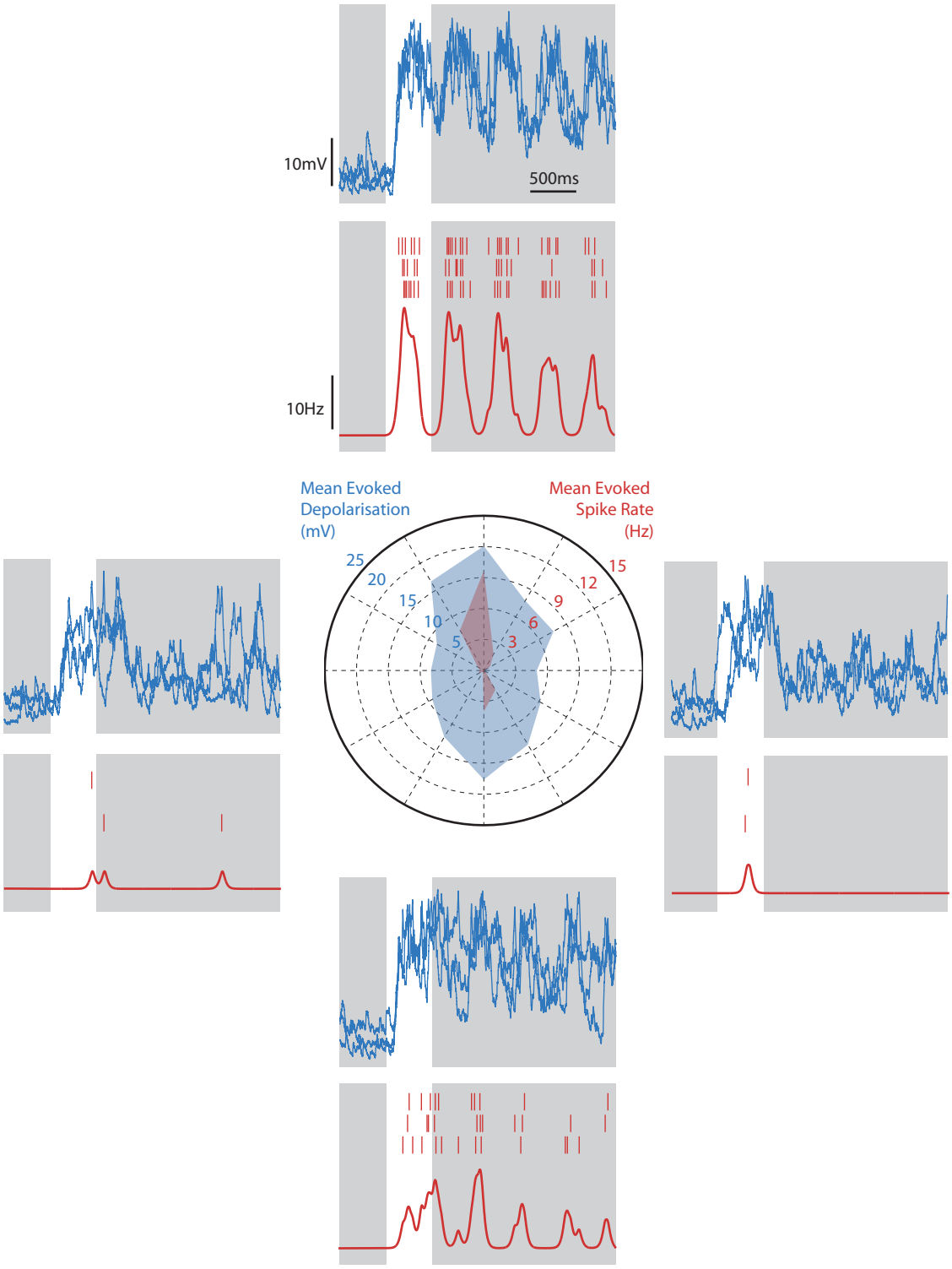

Figure 5.11: Orientation Tuning of a single L2/3 neuron.
Three repeats of spike-clipped membrane potential responses (blue) and spike rasters (red) are shown for the same neuron as in fig. 5.1, for each of the cardinal directions. Firing rate estimates, obtained using a causal α filter with $1/\alpha$=50ms are shown below each raster.
Centre: Polar plot showing Vm0 (blue) and F0 (red) responses to all 12 directions, averaged across trials.

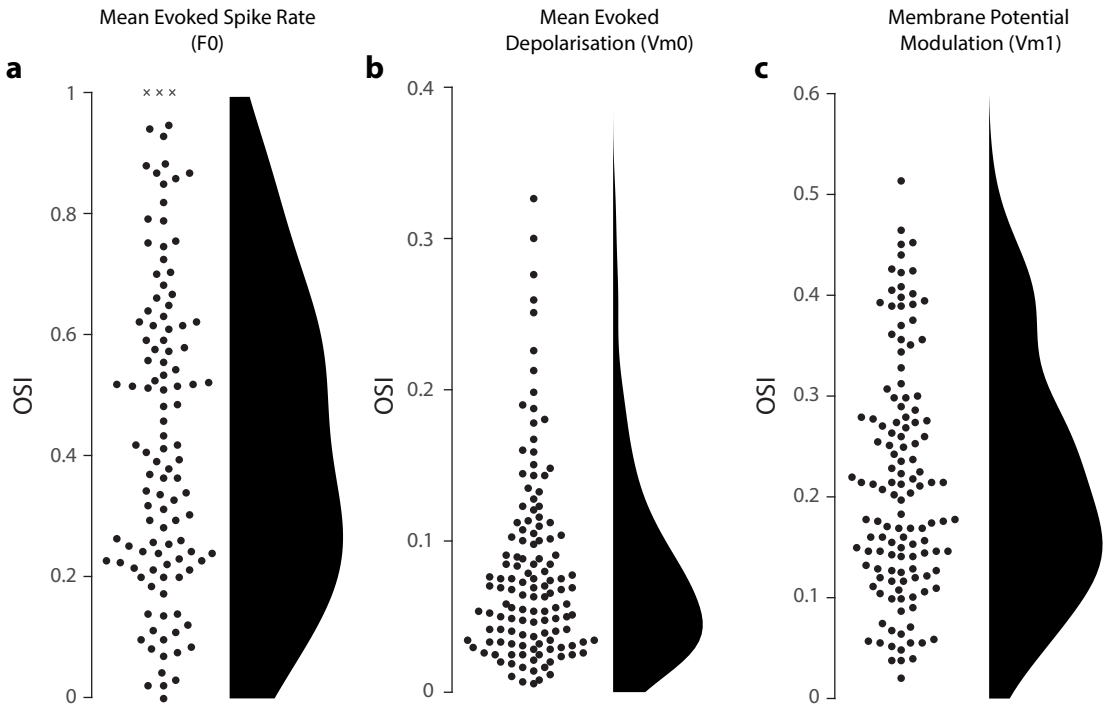

Figure 5.12: Population Distributions of OSI determined from F0, Vm0 and membrane potential modulation at the stimulus fundamental frequency (Vm1) responses
(a) Distribution of OSI_{F0} values for neurons whose spiking activity was significantly altered by drifting grating stimuli (n=112). Values are displayed as a dot plot showing individual data points, alongisde a kernel smoothing density estimate. Three neurons had a $\mathrm{OSI}_{F0} > 1$, these are displayed as crosses, truncated to a value of 1 here.
(b) Distribution of OSI_{Vm0} values for all recorded neurons (n=128).
(c) Distribution of OSI_{Vm1} for all recorded neurons (n=128).

5.2.2.1 Correlates of Mean Spike Rate OSI

In order to investigate the origins of this diversity in spiking orientation tuning, correlation measures were made using a non-parametric approach (Spearman rank correlation). Potential correlations were investigated between OSI_{F0} and all quantified intrinsic properties (as determined from the current injection experiments, table 3.1), as well as OSI_{Vm0} and OSI_{Vm1}.

OSI_{Vm0} has already been reported to be well correlated with OSI_{F0} (Tan et al., 2011), an intuitive finding. In my data, this correlation was also found to be highly significant (fig. 5.13a, ρ 0.323, p=0.00054***, n=112).

The relationship between OSI_{Vm1} and OSI_{F0} was found to be similar to that between OSI_{Vm0} and OSI_{F0} (fig. 5.13b, ρ 0.340, p=0.00026***, n=112). This result demonstrates that it is not just the mean depolarisation that is crucial in setting the output tuning of a neuron, but also the tuning of the modulation of the membrane potential. Importantly, OSI_{Vm0} and OSI_{Vm1} were *not* correlated (Spearman's ρ 0.104, p=0.27), implying that these variables are at least somewhat independently related to OSI_{F0}.

It is clear from these results that, whilst significantly correlated, neither measure alone nor both in concert can explain the observed variation in mean spike rate OSI. Diversity in neuronal processing has been implicated in setting orientation tuning properties (Tan et al., 2011). However, none of the intrinsic parameters derived from IV recordings correlated with OSI_{F0} (RMP ρ -0.102, p=0.30; input resistance ρ 0.125, p=0.20; rheobase ρ -0.026, p=0.79 all n=102).

However, the correlation of baseline membrane potential relative to spike threshold ($Vm_{dist-thresh}$) (a measure of intrinsic neuronal excitability, see section 2.4), measured during the visual stimulation recording, with spiking OSI_{F0} was the strongest of all tested (fig. 5.13c, ρ 0.449, p=8.9x10^{-7}, n=112). Whilst numerically higher than the correlation between OSI_{Vm0} and OSI_{F0} (ρ 0.323 and 0.340 respectively), the difference in correlation strength was not significant (Fisher's transformation p=0.27). $Vm_{dist-thresh}$ therefore can be said only to be at least no less important in setting output tuning width than either mean depolarisation or membrane potential modulation tuning. However, this finding alone is thought-provoking.

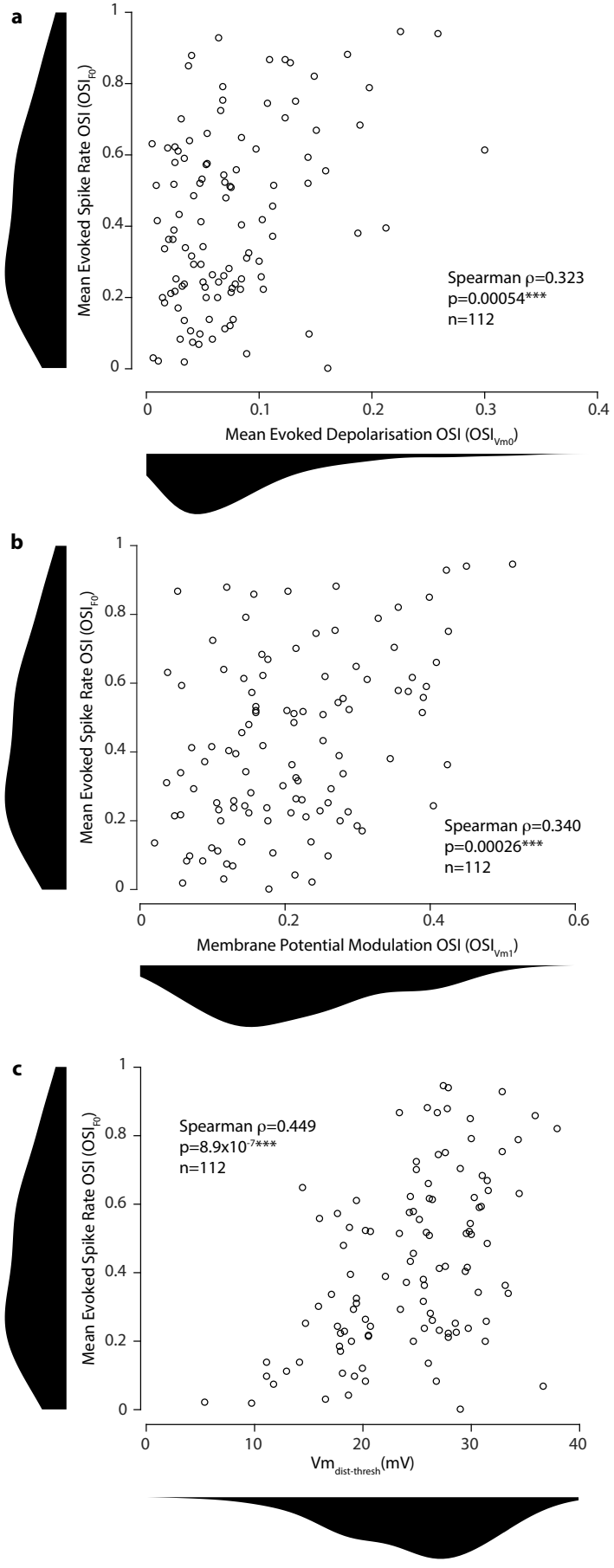

Figure 5.13: The relationship of OSI_{F0} to input tuning and intrinsic excitability. OSI_{F0} for neurons responsive to drifting grating stimuli (n=112) is plotted against OSI_{Vm0} **(a)**, OSI_{Vm1} **(b)**, and $Vm_{dist-thresh}$ **(c)**.

Marginal plots show kernel density estimates as in fig. 5.12

5.2.2.2 Reliability of Orientation Tuning

Whilst the orientation selectivity of the mean responses (OSI_{F0}, but also OSI_{Vm0}) to drifting gratings is probably the most commonly used parameter by which orientation tuning is quantified, this singular measure obscures the trial-to-trial variability underlying. In order to investigate the reliability of tuning, a reproducibility score was calculated by comparing the similarity of the preferred orientation (PO) of each individual set of responses to the 12 stimulus directions (section 2.7.4.2). By comparing this measure to a computationally generated random distribution, the preferred orientation reproducibility probability ($p(R_{PO})$) of a set of responses can be quantified (Grabska-Barwiska et al., 2012) and tested for statistical significance.

All visually responsive neurons with a significant change in firing rate in response to drift onset and at least 5 complete repetitions of the stimulus set were included in the analysis of PO reliability. Of these, 69/102 were reliably tuned in terms of their spiking PO (fig. 5.14, points above the horizontal dotted line). However, only 22/102 neurons had a significantly reliable Vm0 PO (fig. 5.14, points to the right of the vertical dotted line).

When compared directly, the reliability of the spiking PO was higher than the Vm0 PO reliability in 74/102 neurons. Therefore, it can be said that the preferred orientation of the spiking output of an individual neuron is much more reliable, on average, than the mean evoked synaptic drive recorded at the soma in that same neuron ($p=5.9\text{x}10^{-6}$, binomial test). Moreover, there was absolutely no correlation between input reliability and output reliability (Spearman's ρ 0.008, p=0.939); neurons with a reliably tuned Vm0 were no more likely to have a reliably tuned F0.

The preferred orientation of the Vm1 can be defined in the same way as Vm0. Since Vm1 tuning appears to have a significant effect upon OSI_{F0} (fig. 5.13b), it makes sense to ask how trial-to-trial variability in Vm1 preferred orientation affects the reliability of the preferred orientation of the spiking output. The results of this comparison differed quite dramatically from the results comparing F0 and Vm0 reliability. Firstly, a majority of neurons had a reliable Vm1 PO (58/102, fig. 5.15, points to the right of the horizontal line). This is almost triple the number of neurons with a reliable Vm0 PO (22/102). Secondly, Vm1 reliability was well correlated with F0 PO reliability (ρ 0.523, $p=1.7\text{x}10^{-8}$, Spearman's rank correlation). This finding provides further evidence that membrane potential modulation plays an important role in defining the tuning of the spiking output of L2/3 neurons.

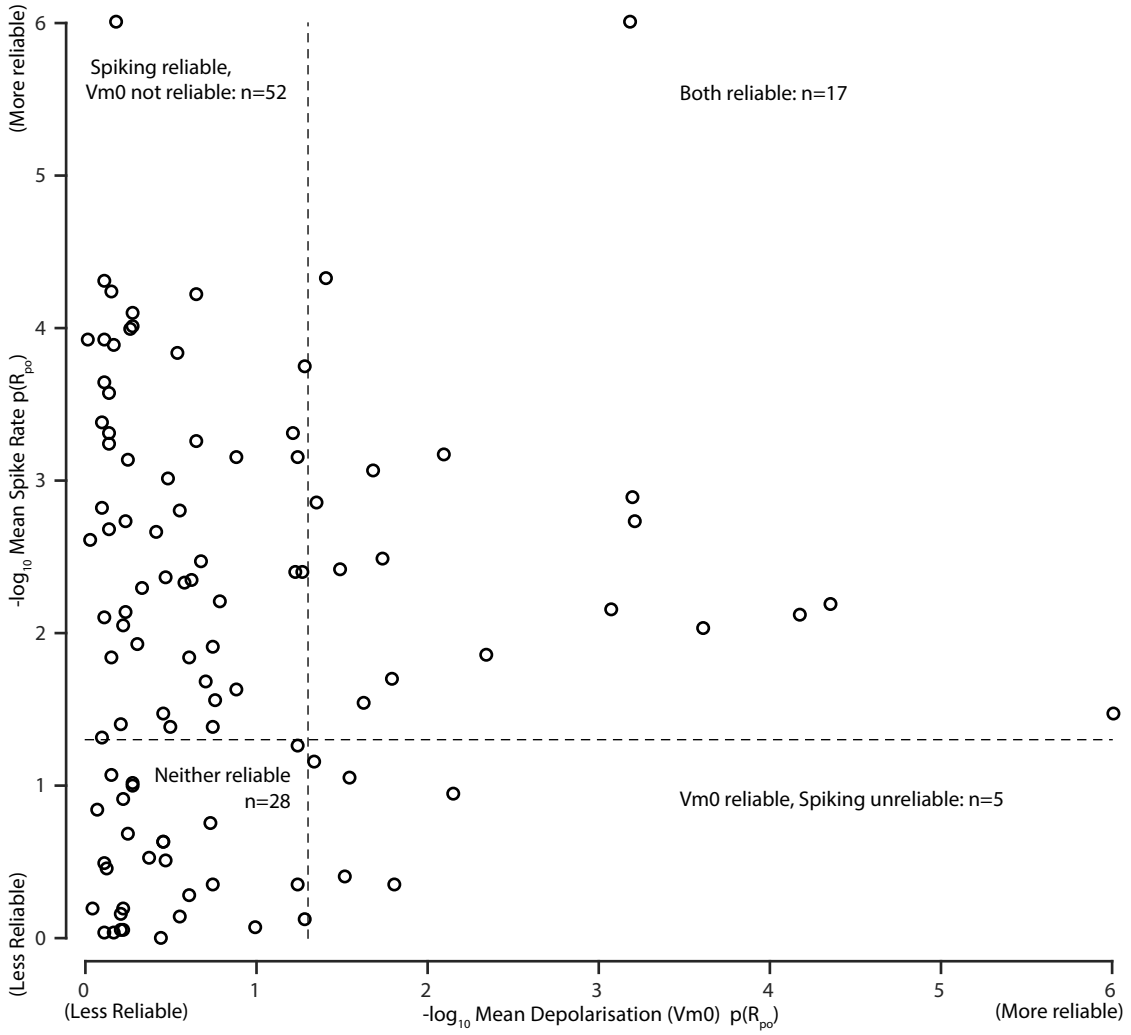

Figure 5.14: Reliability of mean evoked depolarisation Vm0 and spike rate F0 preferred orientations

The probability that an observed reliability measure has occurred by chance - p(Rpo) - is plotted for Vm0 against F0 reliability on a negative log scale, such that higher numbers correspond to more reliably tuned cells. Dotted lines indicate the p=0.05 criterion, above or to the right of the reliability of the F0 and Vm0 PO respectively are considered to be significant.

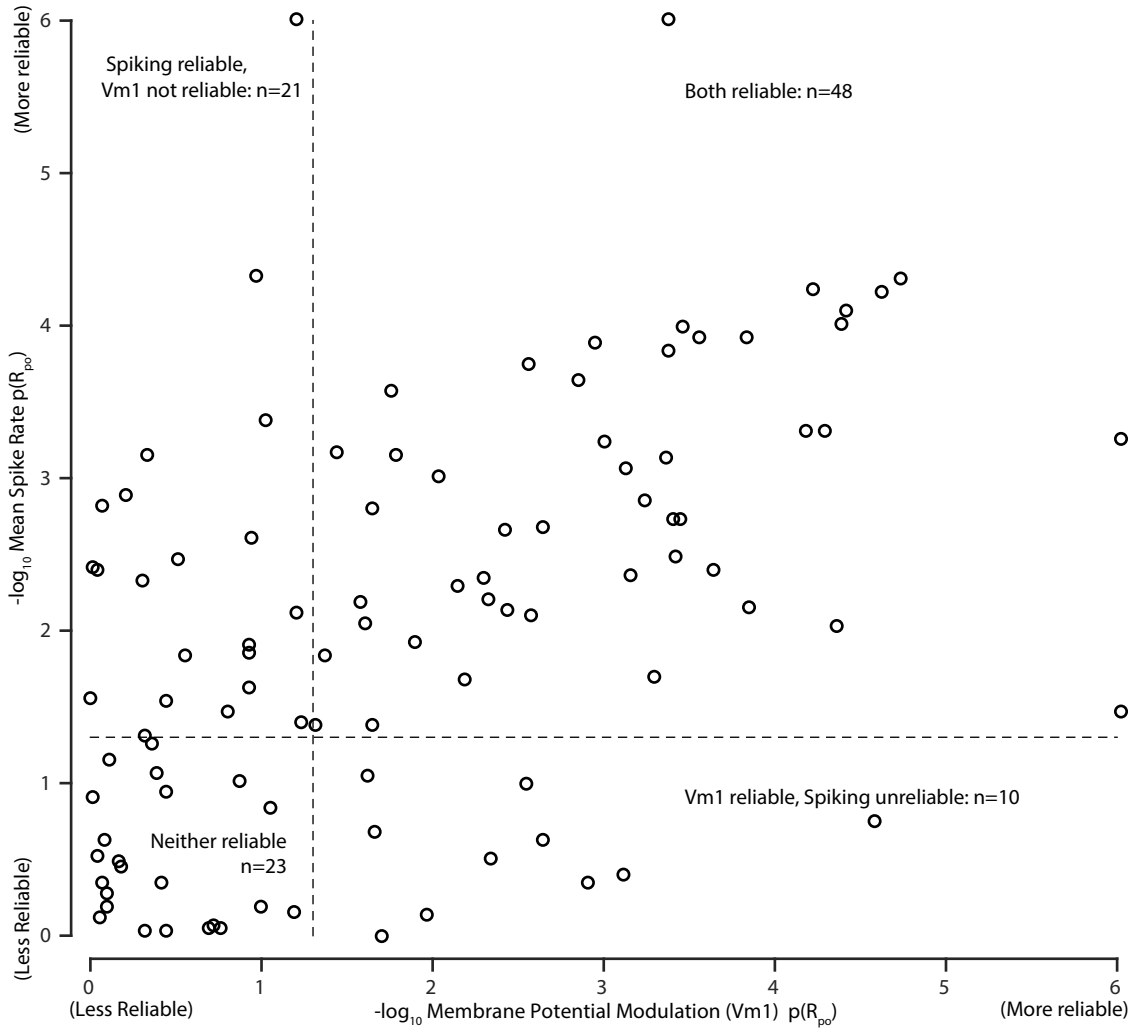

Figure 5.15: Reliability of membrane potential modulation (Vm1) and mean evoked spike rate F0 preferred orientations

5.2.2.3 Correlation of Vm0 and Vm1 with F0 during individual trials

It is intuitive that there may be some correlation between abstracted properties of membrane potential tuning and spiking tuning, such as OSI or preferred orientation reliability. However these correlations, where they exist, derive from a more fundamental relationship between membrane potential changes in the soma, near the axon initial segment, and generation of action potentials. The neuron in isolation does not know anything about the orientation of the stimulus. Rather, in a complex series of computations, excitatory and inhibitory inputs are integrated to produce a somatic membrane potential change (Silver (2010); see also section 1.2.3). This, in turn, sets the probability that a spike will be generated at a given time point.

Therefore, rather than simply measure correlations between membrane potential tuning properties and their spiking equivalents, the relationship between Vm0, Vm1 and F0 were examined directly, pooling responses to all trials to all orientations in each neuron.

The aim of this analysis was to determine which of Vm0 or Vm1 variation is most well related to changes in F0. Spearman rank coefficients were determined for Vm0 against F0, and Vm1 against F0 separately (fig. 5.16). These coefficients (ρ_{Vm0-F0} and ρ_{Vm1-F0}) were then compared across all 102 responsive neurons with at least five complete sets of stimuli (giving at least 60 data points from which to construct each correlation coefficient). However, one neuron was excluded from this analysis as its evoked F0 did not vary sufficiently to give a correlation coefficient.

When compared directly, Vm1 was a better predictor than Vm0 of F0 in 71/101 cases (fig. 5.17, points above the line of unity). This fraction was highly significant ($p=5.5x10^{-5}$, binomial test), demonstrating that the F0 response to visual stimulation may be more dependent upon variation in membrane potential modulation than variation in the mean evoked depolarisation.

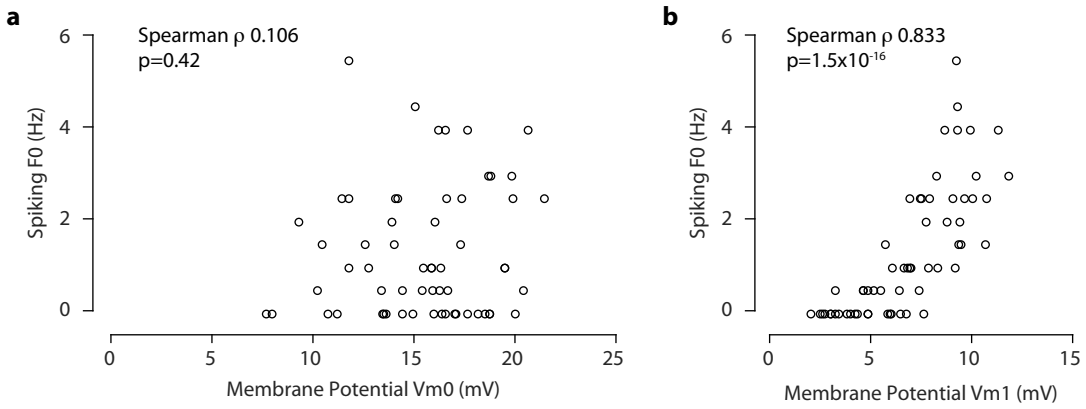

Figure 5.16: Example comparison of Vm0-F0 and Vm1-F0 correlation in a single neuron
(a) Correlation between Vm0 and F0 in one neuron. All trials to all orientations have been pooled together (n=60). In this example, there was no significant correlation between mean membrane depolarisation and mean spike rate.
(b) Correlation between Vm1 and F0 in this same neuron. The correlation, in this case, was highly significant, despite the smaller range of Vm1 values as compared to Vm0 (x-axis scaling identical for both figures).

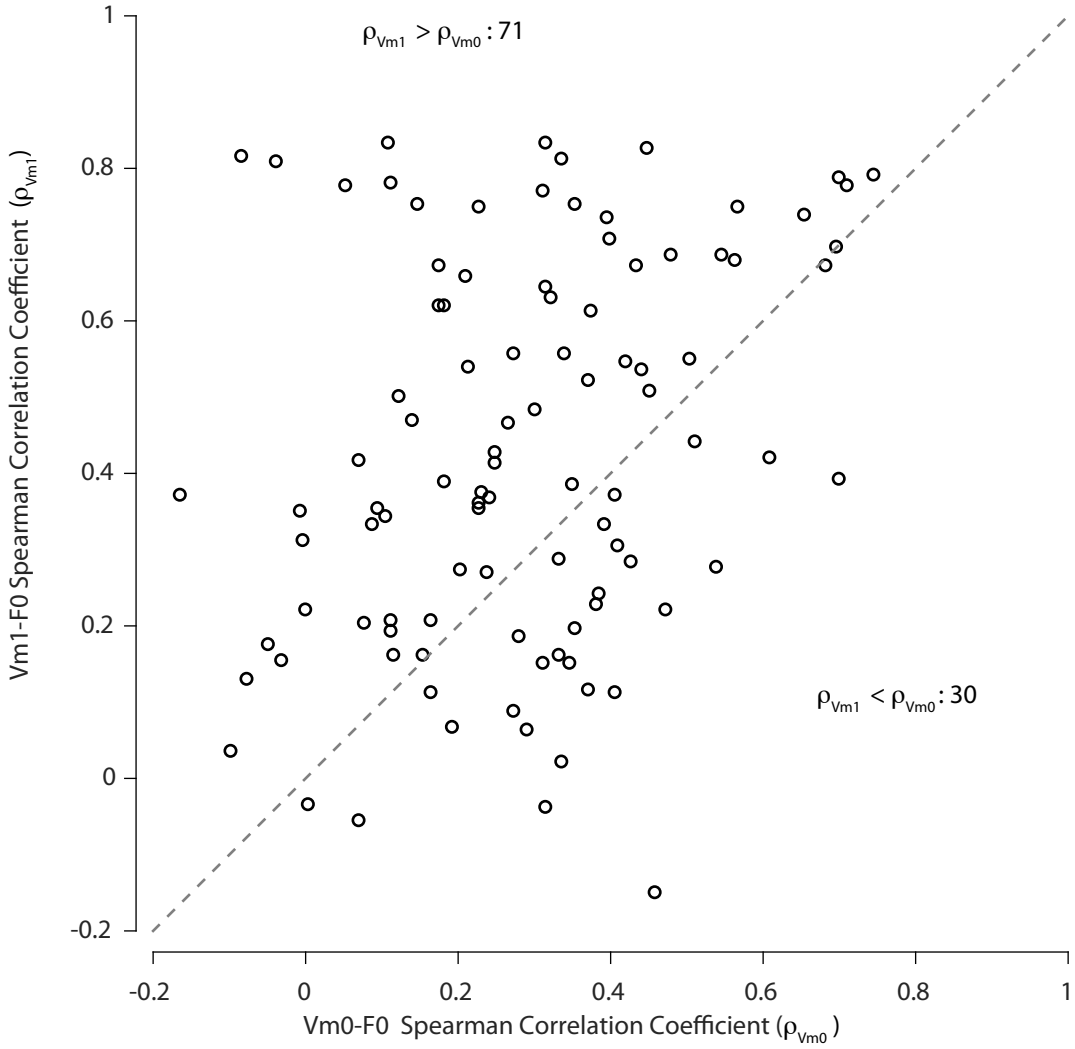

Figure 5.17: Comparison of Vm0-F0 and Vm1-F0 correlation coefficients. ρ_{Vm0-F0} is plotted agains ρ_{Vm1-F0} for all neurons responsive to grating drift with at least 5 complete sets of 12 orientations (black circles). The line of unity is marked in gray. In 71/101 cases Vm1 was a better predictor than Vm0 of F0.

5.2.3 Effect of $Vm_{dist-thresh}$ on synaptic and spike tuning

Unlike Vm0 and Vm1, the distance from baseline membrane potential to spike threshold ($Vm_{dist-thresh}$) is a property of the neuron which, by definition does not vary by stimulus condition (as it is not related in any way to activity during the stimulus itself). Furthermore, although defined for the entire recording as the *average* distance between mean baseline membrane potential and spike threshold, when calculated for individual baseline conditions prior to each stimulus, the standard error of the mean was less than 1mV in all cells (mean $Vm_{dist-thresh}$ SEM 0.40mV).

Therefore, it is not meaningful to ask how $Vm_{dist-thresh}$ affects responses to individual stimuli. Whilst the correlation between in $Vm_{dist-thresh}$ and OSI_{F0} across neurons was higher than that for either OSI_{Vm0} or OSI_{Vm1}, this was not significant by Fisher's transformation method. Other methods, therefore, are needed in order to investigate the potential importance of the distance to AP threshold in setting the output tuning of the neuron.

To investigate this, $Vm_{dist-thresh}$ was varied by applying a constant holding current in order to moderately depolarise or hyperpolarise the cell. This experiment was carried out primarily in order to investigate whether variation in $Vm_{dist-thresh}$ does, in fact, *cause* changes in OSI_{F0}, or merely correlates with it. 34 recordings were obtained from 14 neurons in which a current injection was used to alter $Vm_{dist-thresh}$, and compared to the passive recording in order to obtain the relative changes in OSI_{F0} and $Vm_{dist-thresh}$. After excluding 5 recordings in which evoked spiking was reduced to minimal levels at which spiking OSI could not reliably be defined, we find that distance to threshold has a profound effect on OSI_{F0} (fig. 5.18a ρ 0.693 p=5.0x10^{-5}, n=29 Spearman's rank correlation).

It is possible that this effect could be due in part to changes in voltage-dependent processing of synaptic inputs. However, in contrast to the effect on OSI_{F0}, altered $Vm_{dist-thresh}$ did not significantly increase OSI_{Vm0} or (fig. 5.18b, ρ -0.003 p=0.988, n=34) or OSI_{Vm1} (fig. 5.18c, ρ -0.303 p=0.082, n=34), implying that the small changes in baseline membrane potential in this experiment did not systematically alter the input tuning of the neuron.

It is difficult to relate these data directly to the analysis of the relative importance of Vm0 and Vm1 in setting neuronal orientation tuning. However, in order to obtain a measure of how much a neuron's $Vm_{dist-thresh}$ needs to change in order to have a meaningful impact on the cell's tuning, the changes in OSI_{F0} were analysed by counting

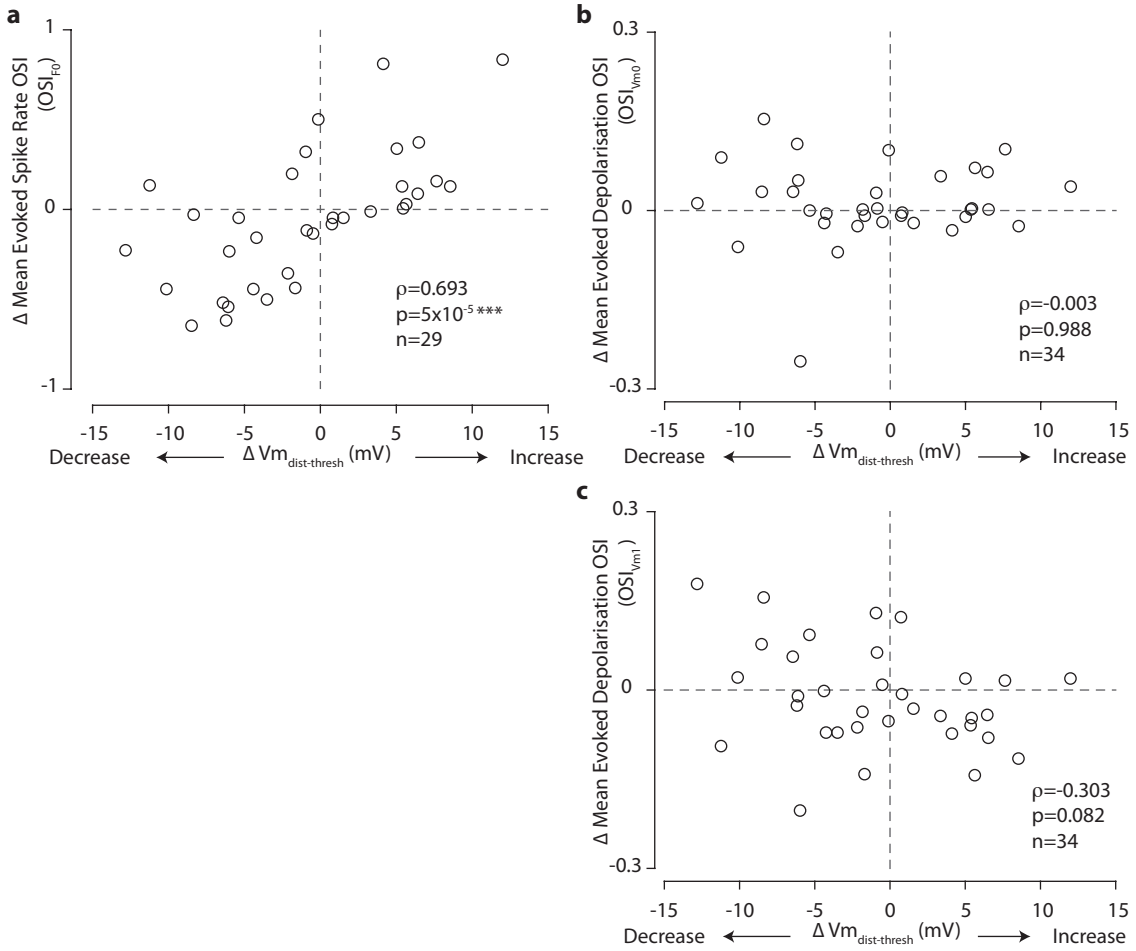

Figure 5.18: The Effect of $Vm_{dist-thresh}$ on OSI.
(a) The effect of moderate depolarisation (left) or hyperpolarisation (right) on OSI_{F0}. Values are plotted relative to the zero-current passive recording, with zero $Vm_{dist-thresh}$ and OSI_{F0} change indicated by gray dotted lines.
(b) The effect of current injection on OSI_{Vm0}.
(c) The effect of current injection on OSI_{Vm1}

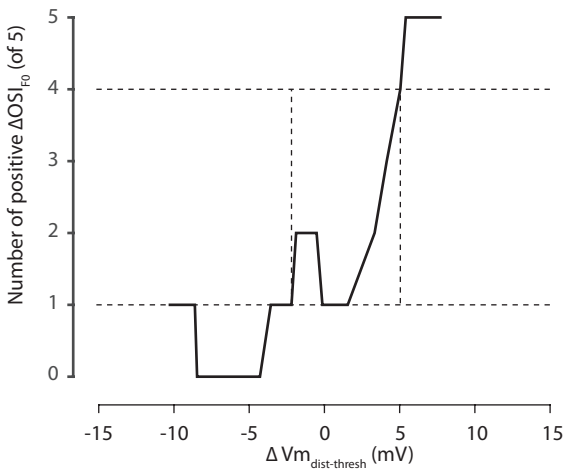

Figure 5.19: Critical Value Analysis of the effect of altered $Vm_{dist-thresh}$ on OSI_{F0}. Data from fig. 5.18a were analysed by counting the number of positive $\Delta\mathrm{OSI}_{F0}$ within a 5-element sliding window. Horizontal dashed lines indicate the critical values defined as indicating a reliable increase in OSI_{F0} (4/5 positive $\Delta\mathrm{OSI}_{F0}$, top) and a reliable decrease in OSI_{F0} (1/5 positive $\Delta\mathrm{OSI}_{F0}$, bottom). Vertical dashed lines highlight the critical values at which a change in $Vm_{dist-thresh}$ caused a reliable change in OSI_{F0}.

the number of points with a positive $\Delta\mathrm{OSI}_{F0}$ within a 5-element sliding window. This allowed a determination to be made of the depolarisation needed for a neuron to become reliably less tuned (a decrease in OSI_{F0} in 4/5 points), and the hyperpolarisation needed to cause the neuron to become reliably more tuned (an increase in OSI_{F0} in 4/5 points). These values may be of some assistance in interpreting the relative effect of Vm0, Vm1 and $Vm_{dist-thresh}$ on OSI_{F0}. A depolarisation of around 3mV was found to be sufficient to reduce the OSI_{F0} of a neuron (fig. 5.19), whilst a hyperpolarisation of around 5mV was necessary to significantly sharpen the OSI_{F0}.

5.2.4 Cell-to-cell variation in $Vm_{dist-thresh}$

Since $Vm_{dist-thresh}$ variation of only a few millivolts can significantly alter the OSI_{F0} of a neuron, and $Vm_{dist-thresh}$ varies widely between neurons within L2/3 (10.1mV interquartile range, overall range 5.4-37.9mV, fig. 5.13c), the origin of this variation may be relevant in understanding how the observed broad OSI_{F0} distribution is produced. One recent finding in whisker somatosensory cortex (Elstrott et al., 2014) described a seemingly paradoxical inverse relationship between the activation threshold of L2/3 neurons to electrical stimulation in L4, and the $Vm_{dist-thresh}$ of the same neurons. The authors of this study suggest a possible homeostatic mechanism whereby intrinsic excitability is regulated in order to compensate for variability in feedforward input strength or mean evoked spike rate.

To test whether $Vm_{dist-thresh}$ may be inversely related to the strength of the synaptic input received by a particular neuron, the total mean evoked depolarisation (Σ_{Vm0}) was calculated as the area of the Vm0 response polar plot (see section 2.7.4.3). This measure varied widely across the population, although the distribution was distinctly right-skewed ($333 \pm 258 mV^2$, mean $\pm$ standard deviation; range 16-1230mV^2, fig. 5.20).

A homeostatic mechanism regulating intrinsic excitability would be predicted to increase the $Vm_{dist-thresh}$ in neurons with larger Σ_{Vm0}. Therefore, a one-tailed Spearman's rank test was used (fig. 5.21). This was highly significant (ρ 0.519, p=2.8x10^{-10}, n=127), indicating that neurons which experienced large mean evoked depolarisations across all visual stimuli *were* less intrinsically excitable (as determined by $Vm_{dist-thresh}$).

One possible explanation of this finding is that spike threshold could effectively saturate the Vm0 in neurons whose baseline membrane potential was close to spike threshold; in contrast, more hyperpolarised neurons, whose baseline membrane potential was further from spike threshold can experience a greater Vm0, generating a spurious correlation. This possibility seems unlikely, as Σ_{Vm0} values were far below the theoretical maximum (the Σ_{Vm0} that would be obtained by a neuron experiencing an evoked depolarisation equal to 100% of the $Vm_{dist-thresh}$ to all stimuli), or even 75% of this value, in all cases (fig. 5.21).

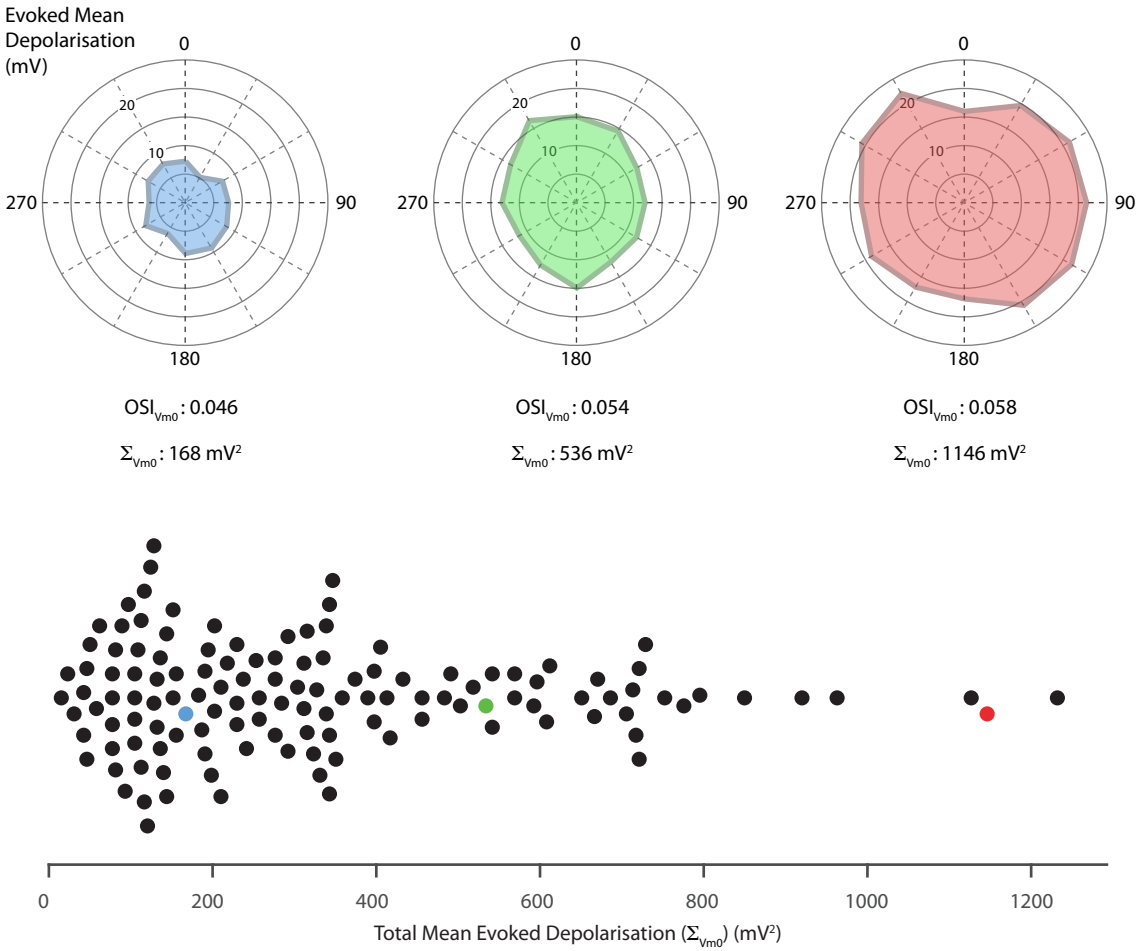

Figure 5.20: Total Mean Evoked Depolarisation in V1 neurons.
Above: Polar plots of Vm0 responses for a neuron with a low total mean evoked depolarisation(Σ_{Vm0}) (left, 168mV^2), a neuron with a moderate Σ_{Vm0} (middle, 536mV^2), and a neuron with a high Σ_{Vm0} (right, 1146mV^2)
The OSI$_{Vm0}$ of all three of these neurons was roughly similar, close to the population median.
Below: Σ_{Vm0} values for all neurons (n=128). Values for the example neurons shown above are highlighted.

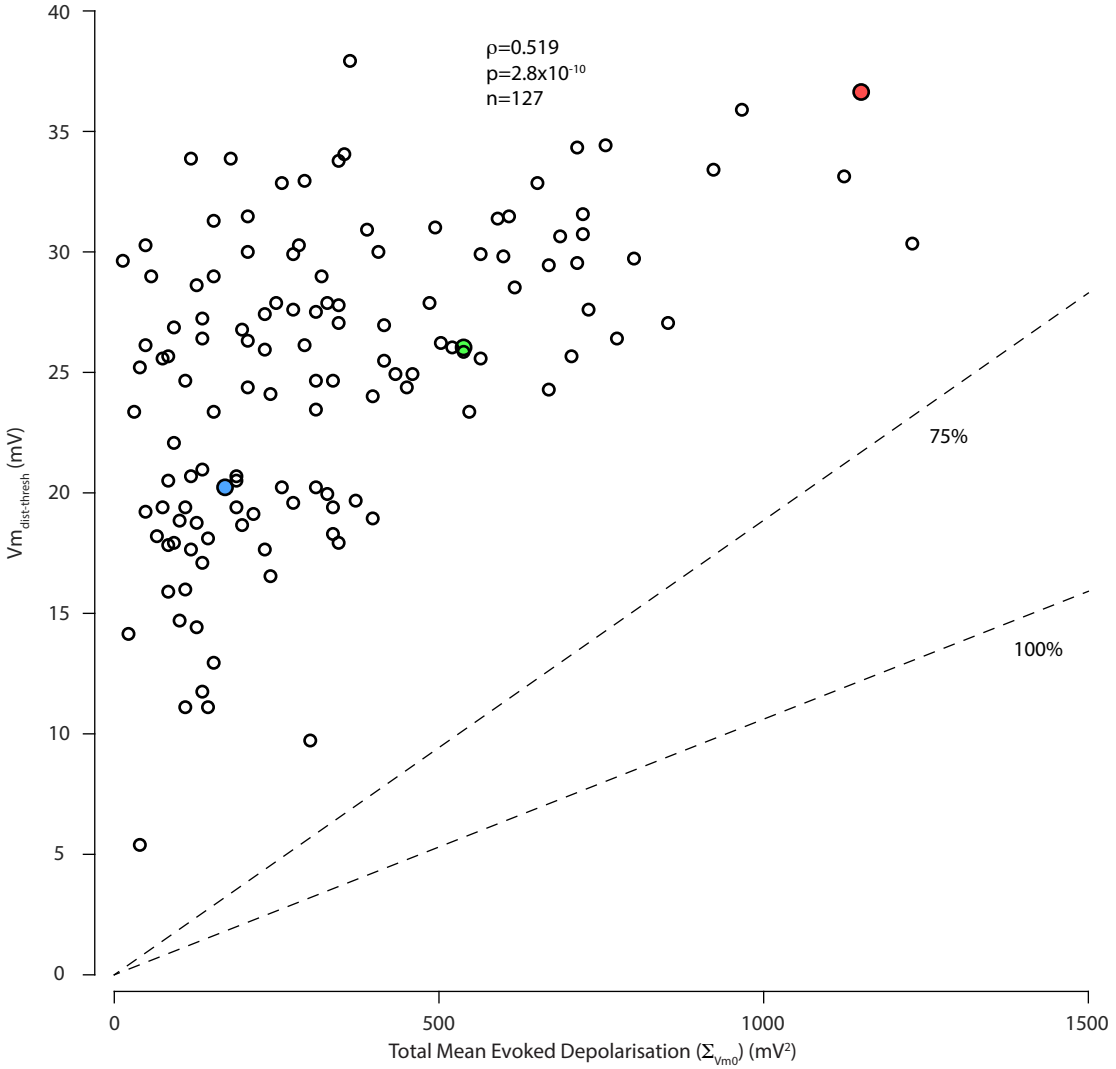

Figure 5.21: Total Mean Evoked Depolarisation (Σ_{Vm0}) correlates with Baseline Distance to Threshold ($Vm_{dist-thresh}$).
Σ_{Vm0} was plotted agains $Vm_{dist-thresh}$ for all 127 neurons with a defined $Vm_{dist-thresh}$ (one neuron did not fire any action potentials whatsoever during drifting grating stimulation, and so this value could not be calculated for this neuron). The relationship was highly significant (one-tailed Spearman rank correlation p=2.8x10^{-10}). The three examples illustrated in fig. 5.20 are highlighted.
For comparison, dotted lines indicate the theoretical Σ_{Vm0} of responses at 100% and 75% $Vm_{dist-thresh}$ to all stimuli, indicating that this effect can not be explained as resulting from saturating Vm0 in neurons whose baseline was close to spike threshold.

To test directly for the effect of input saturation, Σ_{Vm0} was measured again in a subset of neurons in which a hyperpolarising current injection was used in order to increase $Vm_{dist-thresh}$ to a level at which action potential frequency was minimal (increase in $Vm_{dist-thresh}$ 18.7 ± 11.8 mV, mean ± standard deviation; mean evoked firing rate during drifting grating stimuli 0.0229Hz, n=16 neurons). If the observed relationship between $Vm_{dist-thresh}$ and total mean evoked depolarisation (Σ_{Vm0}) were, in fact caused by input saturation, hyperpolarisation should increase total mean evoked depolarisation specifically in neurons with a low $Vm_{dist-thresh}$.

However, total mean evoked depolarisation during hyperpolarised recordings was well-related to the same measure during passive recordings, with no evidence of any increase (Pearson's coefficient 0.918, $p<10^{-10}$, fig. 5.22a). This finding confirms that the observed relation between $Vm_{dist-thresh}$ and Σ_{Vm0} can not be explained by input saturation. In fact, hyperpolarisation *reduced* the total mean evoked depolarisation (Wilcoxon sign-rank test, p=0.002**). In 5 neurons, no action potentials whatsoever were recorded during stimulation. As a result, in these neurons, the change in $Vm_{dist-thresh}$ could not be calculated. In the remaining 11 neurons, the observed decrease in total mean evoked depolarisation was related to the magnitude of the increase in $Vm_{dist-thresh}$ (p=0.031*, Spearman's rank correlation, fig. 5.22b). Input tuning, as measured by OSI_{Vm0}, was not affected by hyperpolarisation (fig. 5.22c, p=0.56, n=16, Wilcoxon sign-rank test), consistent with the results of more modest perturbation of $Vm_{dist-thresh}$ (fig. 5.18b).

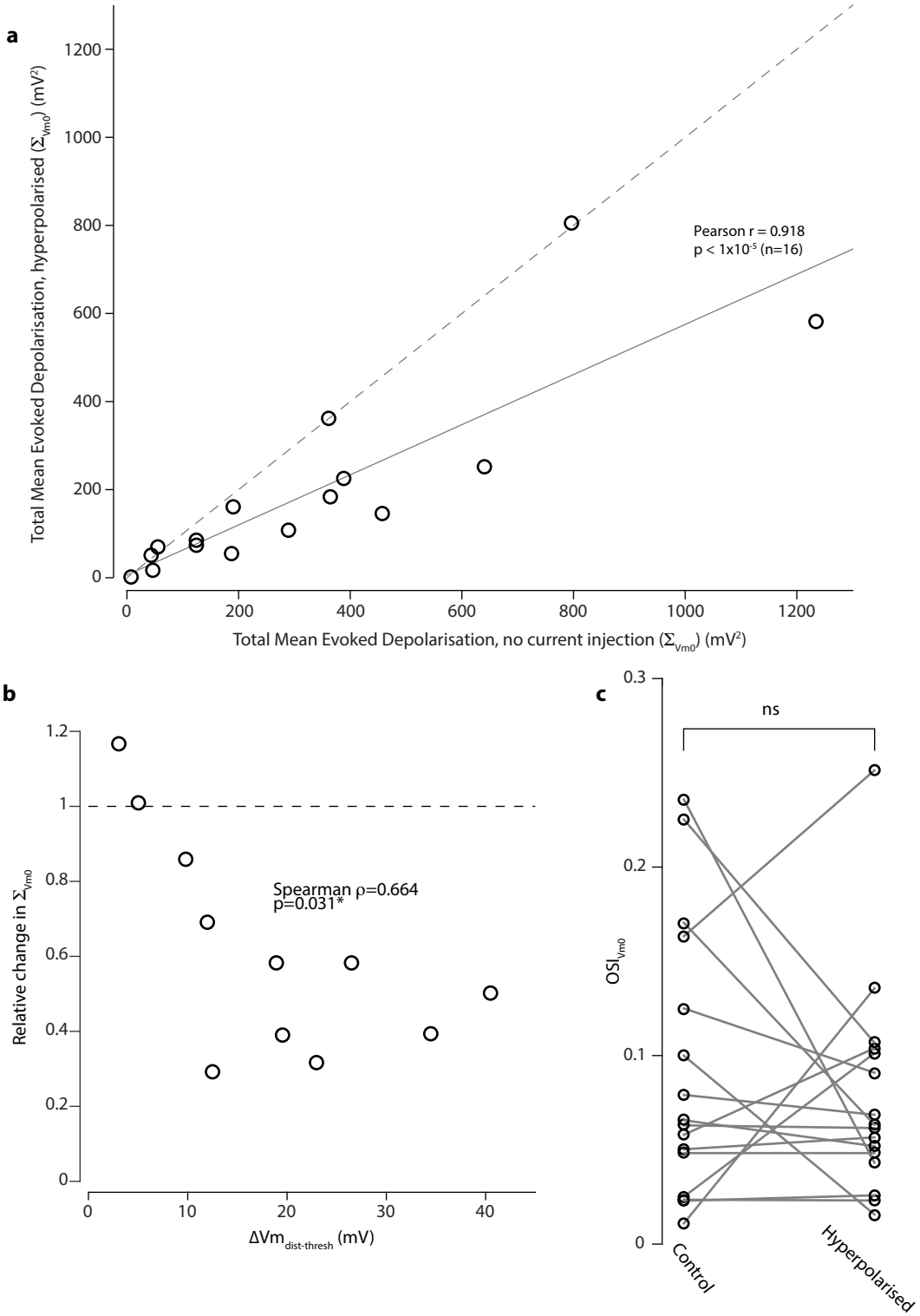

Figure 5.22: The Effect of Hyperpolarisation on total mean evoked depolarisation and OSI_{Vm0}
(a) Plot showing Total Mean Evoked Depolarisation (Σ_{Vm0}) during visual stimulation in neurons hyperpolarised to eliminate the possible effect of Vm0 saturation in 16 neurons in which a constant hyperpolarising current was used to reduce action potential frequency to minimal levels, plotted against Σ_{Vm0} recorded with no current injection. The dotted line indicates unity; the solid line indicates the fitted line (gradient 0.57). In contrast to a possible effect of input saturation, hyperpolarisation significantly *reduced* the Σ_{Vm0}.
(b) Plot showing the effect of the magnitude of the hyperpolarisation on the total evoked depolarisation. Greater hyperpolarisation resulted in a greater reduction of Σ_{Vm0} (n=11).
(c) Plot showing no significant effect of hyperpolarisation upon the tuning of Vm0 (n=16).

5.3 Discussion

5.3.1 Spatial and Temporal Frequency Tuning

In this chapter, I have explored the spatial and temporal frequency, and orientation tuning properties of L2/3 RS neurons, as well as the spiking modulation ratio (F1/F0) using blind whole cell recordings *in vivo* . The preferred spatial and temporal frequency of neurons in L2/3 was found to be quite consistent with previous reports of these parameters. Estimates of preferred spatial frequency generally report peaks at around 0.04cpd (Niell and Stryker, 2008; Zariwala et al., 2011; Kerlin et al., 2010; Roth et al., 2012) in L2/3, slightly higher than the observed peak at 0.0283cpd described here. However, this difference is a matter of only one stimulus condition, and so should be treated cautiously. The preferred temporal frequency of L2/3 neurons was reported in the mouse by (Niell and Stryker, 2008) to be around 1.6Hz, using multisite silicon electrodes. In contrast, (Marshel et al., 2011; Roth et al., 2012) report a mean value of 0.69Hz, and median value of 0.25Hz respectively, using two-photon calcium imaging. This finding is not supported by my data, in which I find the population modal response to be at around 2.83Hz. Although I did not test frequencies lower than 1Hz, few neurons responded preferentially to stimulation even at this temporal frequency. This discrepancy may arise, in part, due to the slow kinetics of calcium-sensitive indicators, and it highlights the need for robust quantification of neuronal properties using a variety of experimental approaches. The finding that the modal preferred spatial and temporal frequencies were close to those used in the orientation tuning experiments should reassure the reader that the findings in the remainder of the chapter were obtained using appropriate stimuli. Neurons in my dataset showed no sign of speed tuning (Priebe et al., 2006; Roth et al., 2012), although the relatively crude sampling (6 spatial frequencies, 5 temporal frequencies) necessitated by the time limits imposed by the whole-cell patch clamp technique may be insufficient to detect a more subtle speed tuning effect.

5.3.2 F1/F0

Whilst F1/F0 was initially proposed as a robust measure revealing the a bimodal distribution of responses (Skottun et al., 1991) supportive of the notion of distinct classes of cell within visual cortical areas (Hubel and Wiesel, 1962), theoretical (Mechler and Ringach, 2002) and experimental (Priebe et al., 2004) studies have questioned the validity of this simple classification. Nevertheless, F1/F0 remains an important measure of neuronal function in studies of V1 physiology (Bardy et al., 2006), extrastriate areas (Romo

et al., 2011), and comparative studies of visual cortical function (Ibbotson et al., 2005).

In mouse L2/3, I find the overwhelming majority of L2/3 neurons to be simple cells, with a F1/F0 > 1, although enough complex responses were apparent to create a statistically bimodal distribution (fig. 5.6). Measuring F1/F0 at the preferred spatial and temporal frequency of the neuron systematically lowered this measure, but in a manner which preserved a good correlation to the measurement at a single spatiotemporal stimulus frequency close to the modal population preferred values (0.0283cpd, 2Hz). However, since preferred frequency was defined as that which evoked the greatest mean evoked spike rate - F0, it may be inevitable that this measure would have a systematic tendency to be lower. Repeating the analysis, but defining preferred frequency condition as that which causes the greatest F1 was not possible, as it is difficult to compare F1 of conditions with greatly different numbers of action potentials in a meaningful way. Defining preferred frequency by F1/F0 and then measuring F1/F0 at that frequency is least appealing of all. If the 'preferred' spatiotemporal frequency were to be defined as that at which the F1/F0 was maximal, it is inevitable that this measure would be equal to or greater than the F1/F0 at standard conditions. Furthermore, as the F1/F0 is highly sensitive to the value of the denominator, maximal F1/F0 would be likely to be produced during very weak F0 responses, a fact which would not, intuitively, fit in with the definition of a condition being the preferred.

However, these data do demonstrate F1/F0 may not be an invariate, immutable property of the neuron. Changing the temporal frequency of the input across realistic ranges altered F1/F0 in 5/5 neurons tested. The maximum temporal frequency used was 4Hz - a 250ms cycle time. It seems difficult to argue that this duration even approaches the integration windows of transduction and synaptic transmission along the visual pathway, and within V1. It therefore is likely that this observed change can not be explained away as a result of the input to the visual system being blurred by excessive speed. Rather, it may point to the role of nonlinearities in temporal processing in cells in the visual cortex - even in simple cells, often described as linear integrators of synaptic input.

The effect of spatial frequency on F1/F0 was not examined, since differences in F1/F0 with varying spatial frequency can be explained simply. Assuming a simple receptive field of fixed spatial frequency, as the grating size increases the spatial frequency resonance will vary, varying F1/F0. Therefore, the potential finding that F1/F0 varies with spatial frequency should be expected. For temporal frequency, however, this is not the case. The stimulus is precisely the same, but is presented at different velocities. Linear (or even

linear-nonlinear-Poisson) models of neuronal processing should predict that varying the temporal frequency of the stimulus should not affect the linearity of the response (for stimuli that do not vary so greatly in velocity so as to exceed the integration window of the system).

5.3.3 Orientation Tuning

The large majority of neurons were found to be responsive to oriented grating stimuli, in terms of a statistically significant effect upon evoked spike rate (112/128, 88%). This is far higher than previous reports of around 50% using unit recordings (Gao et al., 2010) or using two-photon imaging of OGB1-AM (Rochefort et al., 2011). Whilst newer calcium indicators report a greater fraction of responsive neurons (around 60% using GCaMP6s, Chen et al. (2013)), this still fall short of the fraction described here.

In contrast to spatial and temporal frequency tuning, and F1/F0 distribution, the orientation tuning of the mean evoked spike rate (OSI_{F0}) was found to be extremely heterogenous in L2/3 (fig. 5.12a), confirming previous reports (Niell and Stryker, 2008; Zariwala et al., 2011; Hofer et al., 2011). OSI_{F0} therefore made for a tempting target to investigate the interplay of intrinsic properties and sensory-evoked input in creating diverse neuronal responses in a neuronal population.

5.3.3.1 Intrinsic determinants of orientation tuning

Of the 'intrinsic' properties tested, only the baseline membrane potential relative to spike threshold ($Vm_{dist-thresh}$) played a role in setting OSI_{F0}. This effect was comparable in magnitude to that of the tuning of the mean evoked depolarisations (Vm0). Pyramidal neurons in sensory cortex show considerable variation in both their baseline membrane potential and spike threshold (Elstrott et al., 2014). In concert, these two parameters can set the excitability of the neuron, by defining the distance from spike threshold at which it rests. More hyperpolarised neurons should tend to have a more narrowly tuned spiking output for the same membrane potential input, due to the 'iceberg' effect (Carandini and Ferster, 2000; Liu et al., 2011; Priebe and Ferster, 2012). It is, however, possible that for small changes in $Vm_{dist-thresh}$, within physiological ranges, compensatory mechanisms may adapt the tuning of the neuron in order to preserve a certain orientation tuning. However, this was found not to be the case; rather, physiological variation in the $Vm_{dist-thresh}$ of a single cell has a deterministic effect upon OSI_{F0} (fig. 5.18).

Variation in $Vm_{dist-thresh}$ has been proposed as a homeostatic mechanism by which

neuronal excitability may be reduced in neurons with large evoked depolarisations or spike rates, and increased in more sparsely active neurons (Yassin et al., 2010; Elstrott et al., 2014). This may be desirable in creating a more egalitarian distribution of firing rates, in conjunction with a number of other mechanisms (Turrigiano and Nelson, 2000), as well as in preventing positive feedback loops which may generate epileptiform discharge patterns. In the data presented here, the total evoked mean depolarisation was found to correlate with the $Vm_{dist-thresh}$ (fig. 5.21), supporting this hypothesis.

5.3.3.2 The role of membrane potential modulation in orientation tuning

As well as OSI_{Vm0} and $Vm_{dist-thresh}$, the tuning of the Vm1 response was also found to covary with OSI_{F0}. The evidence presented here would seem to imply further that Vm1 is, in fact, *more* critical in setting OSI_{F0} than Vm0 (figs. 5.14, 5.15 and 5.17 . Vm1 variation has been studied for its effect on F1/F0 in concert with spike threshold variation (Priebe et al., 2004) but although the phenomenon of orientation-dependent variation of Vm1 has been reported previously (Lien and Scanziani, 2013; Cossell et al., 2015) the idea that it plays a key role in orientation tuning is, to my knowledge, novel. Highly modulated membrane potential responses imply that, for the same mean depolarisation, there will be phases during which the maximal depolarisation will be much greater than that reached during less modulated responses. Since spike rate depends partly upon instantaneous membrane potential, it seems likely that modulation tuning should play a role in setting spiking orientation tuning. Furthermore, the probability of spike generation has been shown to depend not only upon instantaneous membrane potential, but also upon the $\text{d}V_m/\text{dT}$ (Azouz and Gray, 2000) in visual cortical neurons *in vivo* , owing to the gating kinetics of voltage-dependent sodium and potassium channels (Hodgkin and Huxley, 1952; Noble and Stein, 1966), further enhancing the role of membrane potential modulation in the setting of the mean evoked firing rate.

5.3.4 Other forms of orientation tuning

The effect of Vm0, Vm1 and $Vm_{dist-thresh}$ was studied only on spiking F0 OSI. It may seem profitable to broaden this study, and to investigate the effect of intrinsic properties and evoked depolarisations on F1 OSI. However, this would be difficult to realise. Firstly, many neurons fire very sparsely, if at all, to orthogonal directions. Analysing the F1 of sparse responses is fraught with difficulty, as defining the F1 of fewer than around 10 events over a stimulus cycle does not produce a reliable estimate. Furthemore, OSI_{F0} is

one of the most commonly used measures in the wider literature, being used as a measure of neuronal function in V1 when examining the nature thalamic input to the cortex (Lien and Scanziani, 2013), the role of specific interneuron subtypes on cortical processing (Cottam et al., 2013; Runyan and Sur, 2013), the organisation of inputs along dendrites (Jia et al., 2010) or comparing the properties of cells in 'higher' visual areas to cells in V1 (Andermann et al., 2011; Roth et al., 2012). Greater understanding of the origins of OSI_{F0} is therefore an important goal in deducing what, precisely, an experimental effect on this parameter may mean.

Chapter 6

The Effect of Altered Visual Experience on Intrinsic Properties and Sensory-Evoked Responses of L2/3 Neurons

6.1 Introduction

Intrinsic properties and functional connectivity of neurons within mature sensory circuits may be determined by genetically encoded developmental processes honed over evolutionary time, but also by the effect of sensory stimulation during development. Whilst some sensory systems, particularly those of invertebrates, develop in a highly stereotyped manner, cortical sensory areas are known to be affected dramatically by loss (Wiesel and Hubel, 1963a; Borges and Berry, 1978; Fagiolini et al., 1994; Lendvai et al., 2000; Trachtenberg et al., 2002; Medini, 2011b; Margolis et al., 2012) or alteration (Sengpiel et al., 1999; Kreile et al., 2011) of sensory input, especially at particular developmental time points (Blakemore and Van Sluyters, 1974; Berardi et al., 2000)

The developmental of synaptic plasticity has been studied using a variety of experimental paradigms. In the visual cortex, monocular deprivation - either by enucleation or lid-suturing - is perhaps the most commonly studied and most extreme form of perturbation of the developing visual system. This latter is particularly useful, as it can be reversed in order to stimulate the deprived eye. In a seminal series of papers, David Hubel and Torsten Wiesel demonstrated that neurons in primary visual cortex (V1) of visually naive

kittens were broadly similar to those of adult cats (Hubel and Wiesel, 1963), but that suturing the lid of one eye caused marked anatomical 'atrophy' in the dorsolateral geniculate nucleus of the thalamus (dLGN) (Wiesel and Hubel, 1963a), along with a marked shift in ocular dominance of cells in V1 (Wiesel and Hubel, 1963b). Ocular dominance plasticity has since become an important experimental paradigm in the study of plasticity in the visual system (Hofer et al., 2006).

The effects of other forms of altered visual experience have also been studied extensively. Stripe rearing, in which kittens are reared in an cages surrounded by oriented bars of a single, uniform orientation, or with cylindrical lenses over the eyes has been shown to alter the distribution of orientation maps in the cat (Sengpiel et al., 1999). However, whilst significant, this effect was by no means absolute, with large regions of the cortex remaining responsive to orientations that were presumably never experienced by the animal. This effect has also been observed in the mouse, using two-photon calcium imaging (Kreile et al., 2011). Since there are no orientation columns in the rodent, orientation tuning must be studied on the level of the individual neuron. Kreile et al. (2011) suggest that the effect is best explained by instructive changes in orientation preference, rather than by a responsiveness mechanism, in which neuronal tuning remains fixed, but neurons tuned to orientations not encountered during development become preferentially silenced. A related method, drum-rearing, involves surrounding the animals with a rotating drum for several hours per day. This has been shown to have a significant effect on the directional sensitivity of neurons in cat V1 (Daw and Wyatt, 1976).

Varying forms of anatomical and physiological plasticity, including monocular-deprivation evoked ocular dominance plasticity, orientation and directional plasticity are all easiest to evoke during an early period of development, the 'critical period' (Berardi et al., 2000) . In the cat, this stage lasts for several months (Daw, 1994), with a peak at around 4-5 weeks. The transition from an early period of heightened plasticity to a less plastic 'adult' brain is mediated by a variety of signalling cascades (Sur et al., 2013) , with Brain-Derived Neurotrophic Factor (BDNF) thought to play a key role (Berardi et al., 2000; Gianfranceschi et al., 2003). The critical period is not a singular, discrete epoch, but rather represents a discretisation of a continuous period from early childhood through to adolescence during which various forms of plasticity are heightened. Plasticity endures long after the end of the classical critical period; observable ocular dominance plasticity has been reported to be evoked in cats aged one year (Daw et al., 1992), although this requires a longer period of monocular deprivation. Furthermore, different paradigms of plasticity have been

shown to follow different timecourses of criticality. It is in the context of plasticity in which the majority of studies involving dark-rearing have been carried out. Dark-rearing has been found to delay the end of the critical period for ocular dominance plasticity (Mower, 1991). The end of the critical period is associated with increased GABAergic signalling in layer II/III (L2/3), a process found to be dependent upon sensory experience (Morales et al., 2002). Later studies have focussed upon the role of perisomatic inhibition by parvalbumin-positive basket and chandelier cells (Hensch, 2005; Kuhlman et al., 2013).

Some studies report a reduction in the normal developmental refinement of visual acuity (Frégnac and Imbert, 1978) and a reduction in the proportion of neurons classified as orientation tuned (Fagiolini et al., 1994) as a result of dark rearing. However, more recent studies (Rochefort et al., 2011; Ko et al., 2014) have reported an unchanged distribution of Orientation Selectivity Index (OSI) in L2/3 neurons of mice dark reared from eye-opening, with normal refinement of orientation selectivity being unaffected by visual deprivation. Some aspect of this discrepancy may be ascribed to recording methodology, although species differences may also have an effect. Even granting that visual deprivation does not affect orientation tuning distributions in mouse V1, the possibility remains that a reduction in sensory input affects more nuanced aspects of tuning, or that *input* tuning to neurons does differ, but neuronal processing of this input is altered in order to produce a certain distribution of orientation tuning properties. To date, to my knowledge, there have been no studies of the effect of visual deprivation on the visually evoked synaptic activity and intrinsic properties of L2/3 neurons in V1 recorded *in vivo* , although in the acute slice widespread changes in synaptic properties in A1 have been reported following 7 days of visual deprivation, accompanied by more limited changes in V1 (Petrus et al., 2015).

The results described in the previous chapter demonstrate that the orientation tuning of an individual neuron is determined, in large part, by the baseline membrane potential relative to spike threshold ($Vm_{dist-thresh}$) of that neuron (fig. 5.13c). This parameter was investigated by Elstrott et al. (2014), who showed that, in the barrel cortex, $Vm_{dist-thresh}$ is correlated with the strength of feedforward connectivity from layer IV (L4). The suggestion is that $Vm_{dist-thresh}$ acts as a homeostatic mechanism, by which the gain of a neuron can be tuned to account for the strength of input it receives. My data support this notion in visual cortex, in which I find a correlation between total input across all orientations, and $Vm_{dist-thresh}$ (fig. 5.21). I therefore hypothesised that by depriving a group of animals of visual input, the total input on to L2/3 cortical neurons would be

reduced, and therefore the $Vm_{dist-thresh}$ might be systematically reduced, as homeostatic mechanisms effectively compensate by increasing the intrinsic gain control. This was the primary motivation for conducting the visual deprivation paradigm described in this chapter. In conducting these experiments, I was further able to test for a number of potential changes in intrinsic and sensory-evoked properties in animals deprived of visual input.

6.2 Results

6.2.1 Altered Intrinsic Properties of V1 Neurons in Visually Deprived Animals

In order to assess the effect of visual deprivation on properties of RS neurons, groups of mice were housed in groups in blackened-out cages from weaning (P19) for at least two weeks (see section 2.6). Visual deprivation therefore began several days following eye opening, which typically occurs at P13-15 in the mouse (Rochefort et al., 2009; Ko et al., 2014). Experiments in these animals were not interdigitated with animals kept in standard housing, although the intracellular solution used was from the same batch. For comparison, results from visually deprived animals were compared with the dataset obtained from the experiments described in the previous chapters, hereafter referred to as the 'control' dataset. Current injection experiments were first performed in the same manner as described in section 3.2.3, in order to characterise biophysical differences (table 6.1 and fig. 6.1). Neurons in visually deprived (VD) animals were found to have a significantly more depolarised resting membrane potential (RMP) at breakin in comparison to control neurons (fig. 6.1a, mean -71.8mV compared to -75.6mV, p=0.0018**, MW test). However, this was accompanied by a similar rise in the membrane voltage threshold of the first spike elicited at rheobase (fig. 6.1b), such that overall there was no difference in the distance from RMP to spike threshold during the current injection experiment (p=0.64, MW test). Rheobase was, however, significantly lower in neurons in visually deprived animals than in controls (fig. 6.1c mean 240pA vs. 285pA, p=0.008**).

Input resistance measured at the first hyperpolarising step was not affected by visual deprivation (p=0.71, fig. 6.1d). However, examining the entire IV curve averaged across neurons grouped by experimental group (fig. 6.2) revealed a clear increase in input resistance to depolarising steps in visually deprived animals, but no change in input resistance to hyperpolarising steps. The general difference between control and visually deprived was highly significant when tested using a two-way ANOVA (effect of visual deprivation

p=0.0002***). This effect appeared to increase with increasing steps of positive current injection / depolarisation, however post-hoc testing (t-tests with Holm-Bonferroni correction for multiple comparisons) did not reveal a specific set point for this difference.

Spiking activity at 150% rheobase was also affected by visual deprivation. Mean firing rate was reduced in VD neurons (fig. 6.1e, mean 14.9Hz vs. 19.3Hz in control, p=0.0015**), as was maximal firing rate (fig. 6.1f, mean 37.4Hz vs. 50.4Hz, p=0.003**). However, neither early nor late accommodation were affected by visual deprivation (p=0.33 and 0.20 respectively).

After-hyperpolarisation (AHP) amplitude and spike full width at half-maximum (FWHM) were not analysed for these data, as these parameters were used to classify neurons as regular spiking or otherwise.

In summary, these results demonstrate that visual deprivation affects the resting membrane potential of L2/3 neurons as well as causing a steeper current-voltage relation for depolarising, but not hyperpolarising current injections.

Property	Control (n=150)	VD (n=40)	P
Resting Membrane Potential (RMP) (mV)	-75.6 ± 7.6	-71.8 ± 6.9	0.0018 **
First Spike Threshold (mV)	-27.4 ± 6.9	-22.4 ± 6.2	0.00015***
Rheobase (pA)	285 ± 111	240 ± 75	0.008 **
Hyperpolarising input resistance (R_i) (MΩ)	57.6 ± 28	57.9 ± 23	0.71
Mean Firing Rate (Hz)	19.3 ± 7.6	14.9 ± 7.5	0.0015 **
Max. Firing Rate (Hz)	50.4 ± 23	37.4 ± 17	0.003 **
Early Accommodation (%)	48.6 ± 17	44.5 ± 19	0.33
Late Accommodation (%)	51.1 ± 49	42.1 ± 46	0.20

Table 6.1: Intrinsic Spiking Properties of Neurons in Visually-Deprived and Control Animals
Two VD and sixteen control neurons were not sufficiently depolarised for analysis of spike rate and accommodation properties properties at 150% rheobase; measures based upon this reduced dataset are shown in the bottom half of the table. All values given as mean ± standard deviation; control values are as in table 3.1.

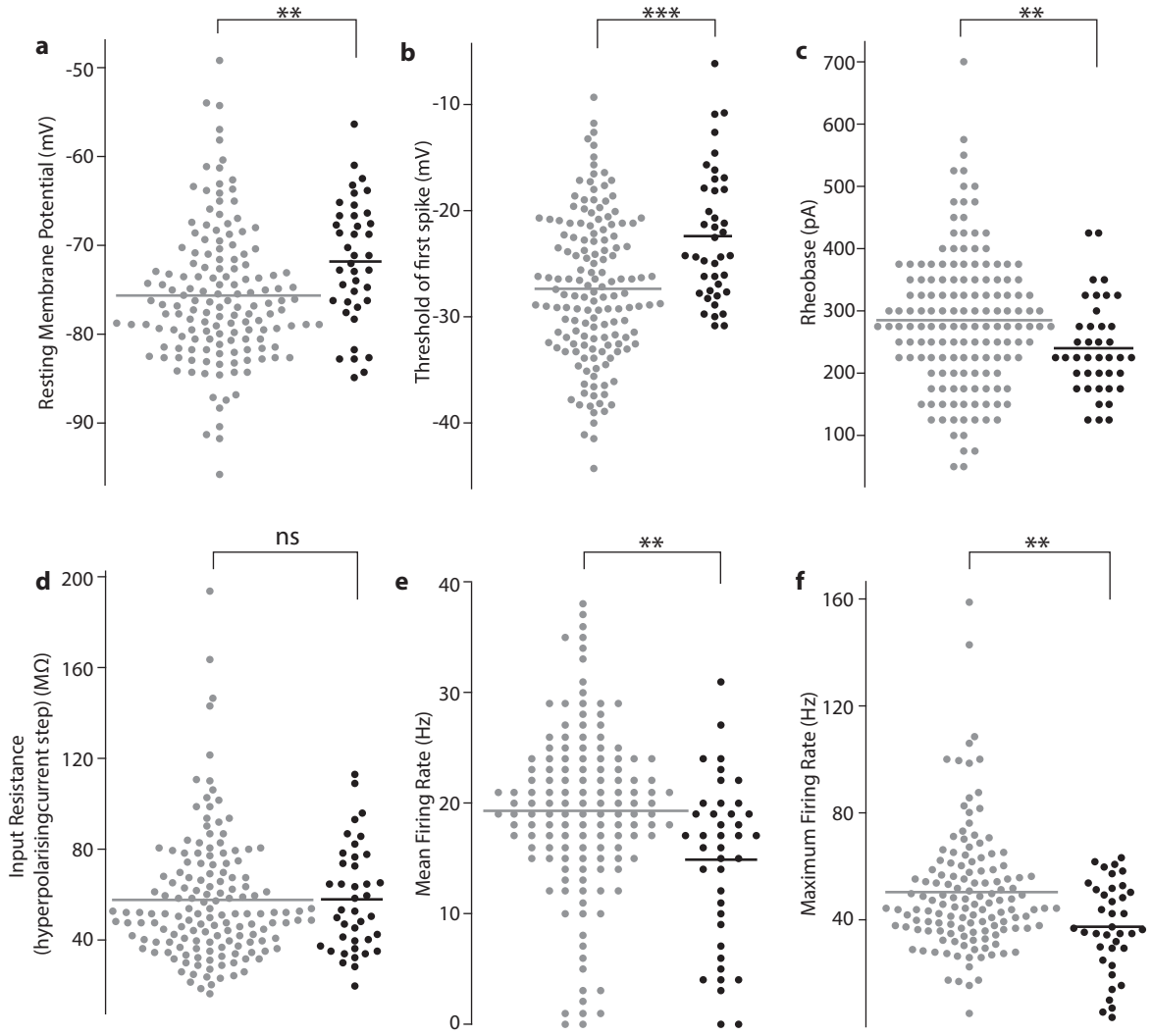

Figure 6.1: Intrinsic Properties of Neurons in Visually Deprived and Control Animals

(a) Plot showing the resting membrane potential (steady-state membrane potential (Vm_{ss}) at 0pA current injection) of all control (gray, n=150) and VD (black, n=40) neurons.

(b) Plot showing the distributions of the threshold of the first spike elicited at rheobase for all control and VD neurons.

(c) Plot showing the minimal current injection required to elicit at least one action potential for all control and VD neurons.

(d) Plot of the input resistance, measured at the maximal hyperpolarising current injection step (-400pA) for all control and VD neurons.

(e) Plot of the mean firing rate at 150% rheobase for control (n=134) and VD (n=38) neurons depolarised to 150% rheobase.

(f) Maximum instantaneous firing rate at 150% rheobase of the same subset of neurons as in **(e)**.

In each panel, gray and black dots indicate the value of single control and visually deprived regular spiking neurons respectively; horizontal bars indicate sample mean. Significance levels are determined by a Mann-Whitney test.

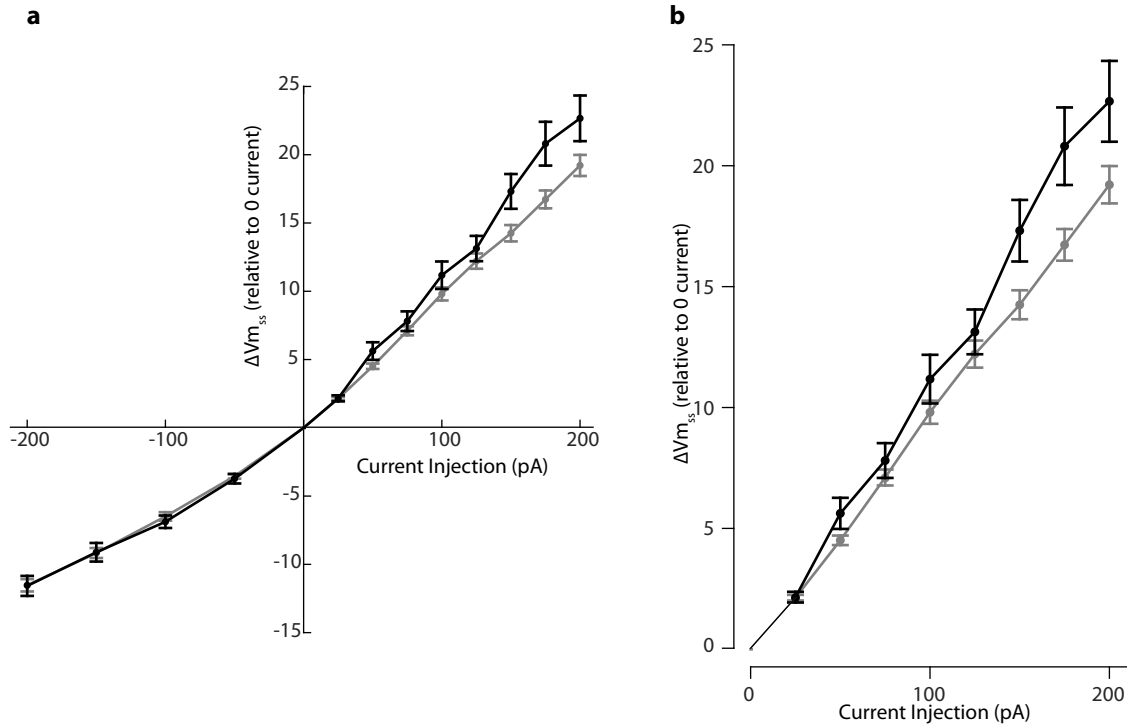

Figure 6.2: Mean IV response of neurons in control and visually deprived amials.
(a) Voltage responses to current injections were aligned to the Vm_{ss} at 0pA injection (resting membrane potential). Voltage responses in control animals are displayed in gray, visually deprived in black. Error bars standard error of the mean. Only current steps below rheobase for each particular neuron were included in this analysis.
(b) Enlarged view of the voltage responses to depolarising current only in neurons in control (gray) and visually deprived (black) animals.

6.2.2 Responses to Ballistic Stimuli

As a first pass, in order to assess the impact of visual deprivation on visual and non-visual sensory processing in L2/3 of V1 in general, two forms of simple 'ballistic' stimuli were used. These consisted of a full field flicker ('flip') visual stimulus and a series of brief auditory white noise stimuli.

The majority of neurons in both control and visually deprived animals fired at least one spike during presentation of the flicker stimulus (excluding the first presentation, control 95/150 [63%], VD 23/40 [58%]). However, a variety of spiking responses were observed in response to flip stimulation (fig. 6.3) in both control and VD animals.

Dividing neurons in to four classes - (i) non-spikers, (ii) those which responded to down only, (iii) up only, or (iv) both ('mixed') did not reveal a significant difference in proportions between control and visually deprived animals. Firstly, the effect of visual deprivation was examined by means of a two-by-two contingency table, comparing the fraction of cells in each experimental group that were totally silent (as opposed to those which fired any spikes at all during the recording, groups ii-iv). This was not significantly different (p=0.50 ns, χ^2 test). A Cochran-Armitage test for trend in up/down fraction was performed in order to assess whether visual deprivation shifted the response of neurons which did spike. This, too, was not significant(Down vs. Mixed vs. Up 0=0.14 ns, Cochran-Armitage test). Lastly, a Mann Whitney test of the ungrouped up/down ratio values for all neurons which did spike was not significant (p=0.062). Overall, therefore, there is no evidence in my data to support the notion that visual deprivation alters the fraction of neurons which spike in response to full-field flicker. Furthermore, there is no evidence that visual deprivation affects the distribution of up/down transition responses, at a population level.

Pooling data within experimental groups did, however, reveal a clear population-level difference in spiking time course over the duration of the response. Whilst neurons in control animals fired a similar number of action potentials to both up and dark transitions (population total 608 vs. 571, p=0.15 ns, binomial test), the response to up transitions had a shorter latency, and was more sharply-peaked (fig. 6.4; median spike time 155ms compared to 251ms for an off transition, p=1.2x10^{-35}, responses pooled from 95 neurons). In contrast, VD neurons fired preferentially to down transitions (101 vs. 246, p=2.1x10^{-15}, responses pooled from 23 neurons). This difference was extremely significant when the total number of spikes follow up versus down transitions, across all neurons, was directly

compared between experimental groups (p=1.7x10^{-13}, χ^2 test).

It should be noted that in control animals, responses to up and down flicker stimuli were not independent. Neurons were more likely to fire either to both up and down stimuli, or to neither, than to up or down alone ('mixed') (Fisher's exact test, p=0.0008***, fig. 6.5).

6.2.2.1 Membrane Potential Response to Full-Field Flicker

Analysis of the underlying membrane potential (fig. 6.6) may provide an insight in to the mechanisms that underlie this apparent change in spiking behaviour. In control animals, a larger (median integral 3.12mVs vs. 2.32 mVs, Wilcoxon rank sum test p=3.9x10^{-5}, n=150, fig. 6.7a), more rapid (median time-to-peak 137ms vs. 206ms, p=2.3x10^{-12}***, fig. 6.7b) depolarisation was observed in response to an up transition than to a down transition. The shapes of these depolarisations qualitatively matched closely the kinetics of the control spike PSTH (fig. 6.4, top).

In visually deprived animals, the membrane potential response to up transitions was not altered greatly, with no significant change in integral (p=0.32) and a modest change in time-to-peak (121ms in VD vs. 137ms in control, p=0.006**, both n=40 VD, 150 control). However, responses to down transitions were more greatly altered, particularly the integral (median 3.57mVs in VD, compared to 2.32mVs in control animals, Wilcoxon rank sum test p=4.4x10^{-5}***).

Taken together, these results demonstrate that L2/3 neurons in visually deprived mice process ballistic visual stimuli slightly differently, being more responsive to light offset than neurons in control animals.

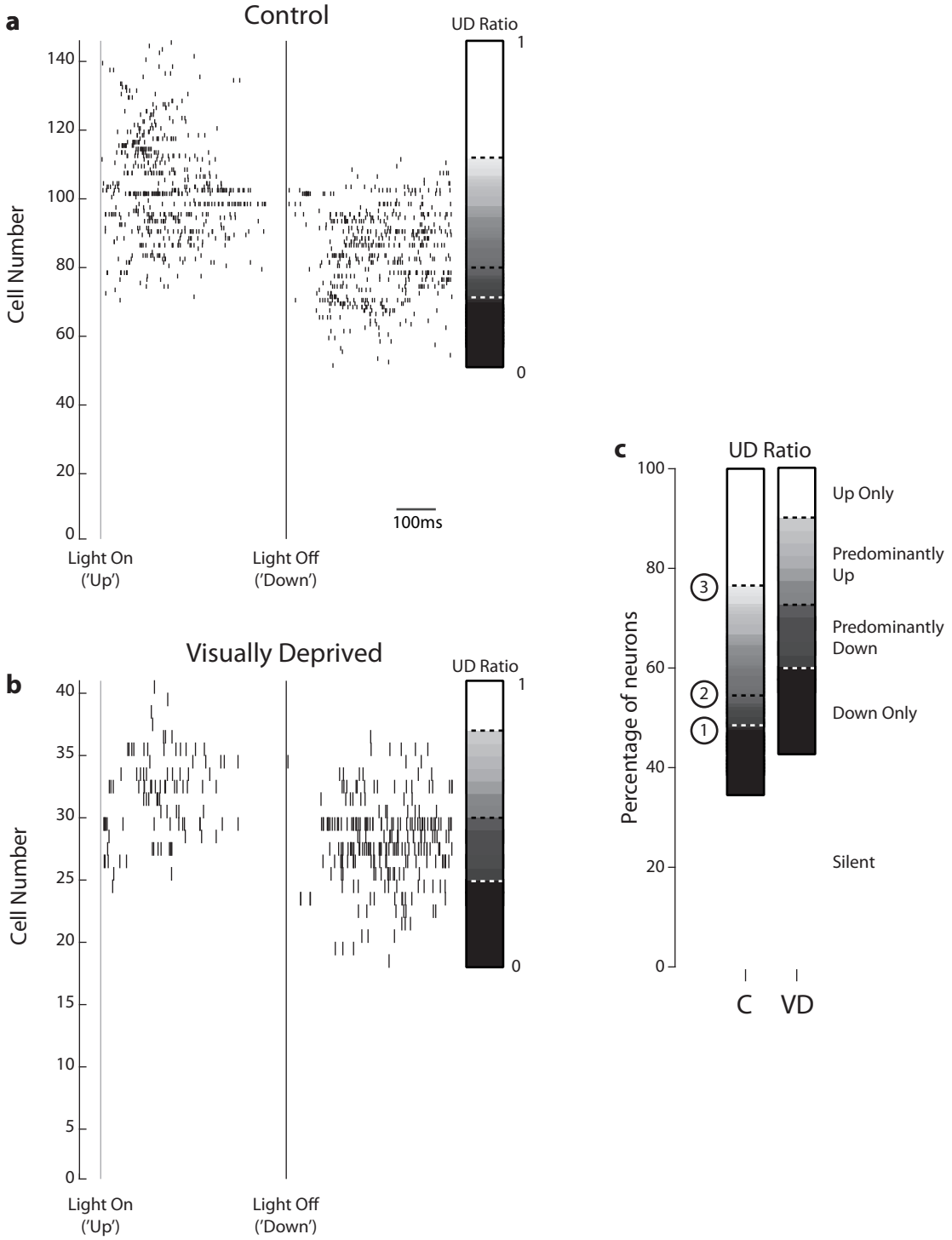

Figure 6.3: Population spiking responses to full-field flicker stimuli.
(a) Spike raster of neuronal responses to full-field flicker stimulus in control animals. Neurons are sorted first by their up/down ratio, and then by the number of recorded spikes. Note that spikes are shown superimposed for all 9 analysed repetitions. Transitions are denoted by solid vertical lines: gray for 'up' (dark-to-light) and black for 'down' (light-to-dark). For neurons which fired at least one action potential, the up-to-down (UD) ratio was defined as outlined in section 2.7.3 . This ratio is displayed to the right. **(b)** Spike raster and UD ratio of neuronal responses to full-field flicker in VD animals. **(c)** Comparison of Up/Down ratio distributions in control and visually deprived animals. Dashed lines indicate (1) the boundary between down only and mixed responses, (2) equal UD ratio, and (3) between mixed and up only responses. C, Control; VD, visually deprived.

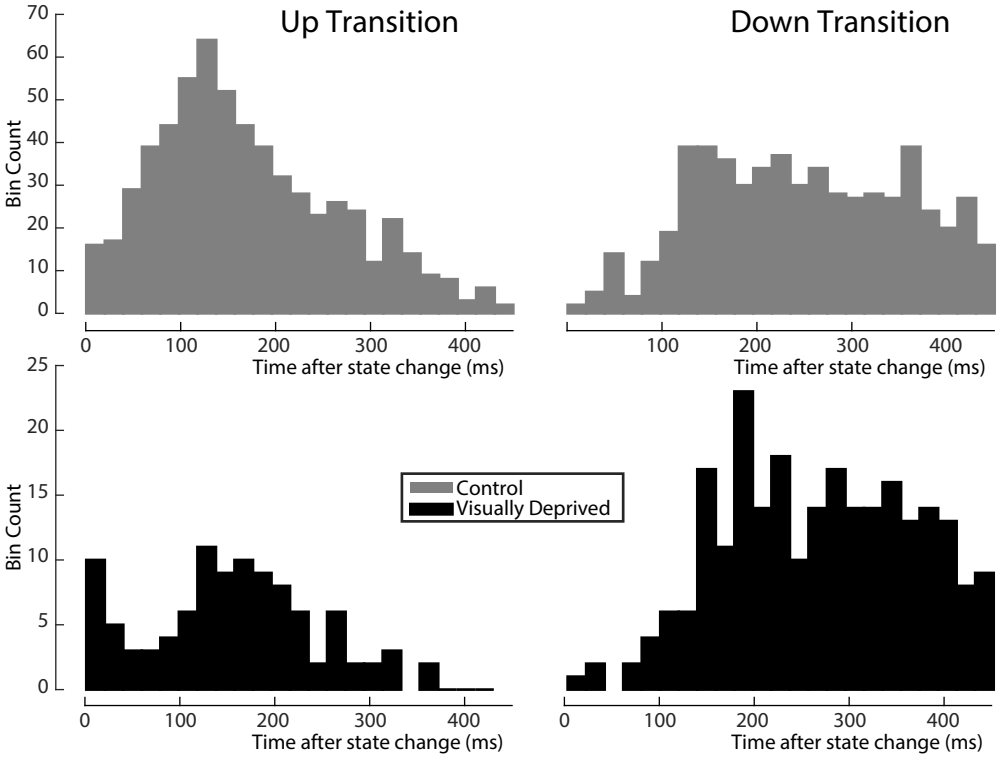

Figure 6.4: Population PSTH of spiking responses in Control (gray) and Visually Deprived (black) animals to flip stimuli. Responses to up (dark-to-light) transitions are shown on the left, with the transition time marked with open arrows; to down transitions on the right, with the transition time marked with filled arrows. Responses are pooled for all repetitions analysed. Bin size 20ms.

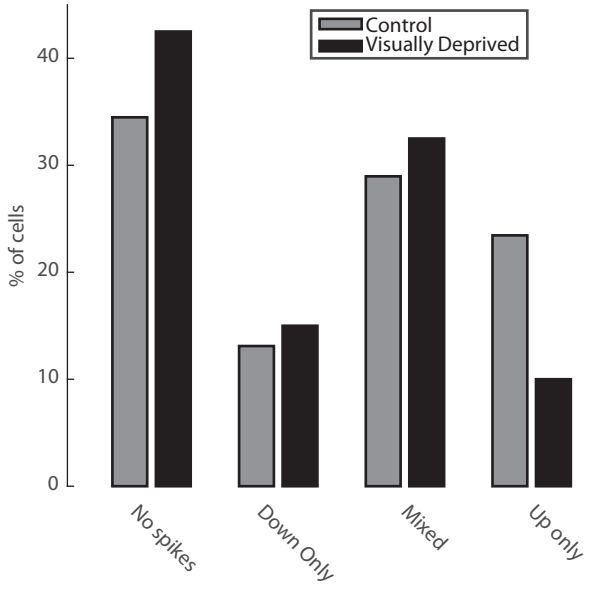

Figure 6.5: Percentage of Cells According to Spiking Response Class to Flicker Stimuli

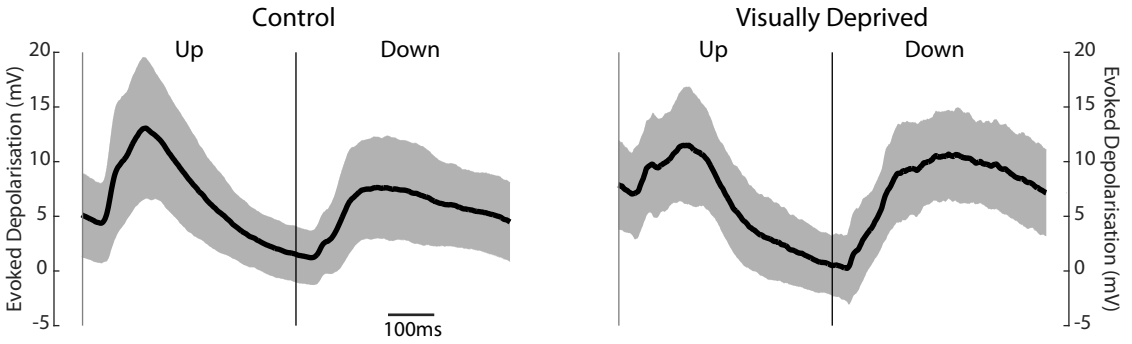

Figure 6.6: Membrane Potential changes following Up and Down transitions in control (left) and visually deprived (right) animals.
Average membrane potential depolarisation, relative to baseline Vm, for all repetitions, across all neurons, is shown in black, with standard deviation bounds shown in gray. Gray vertical lines indicate the timing of Up transition; black lines indicate the timing of Down transition.

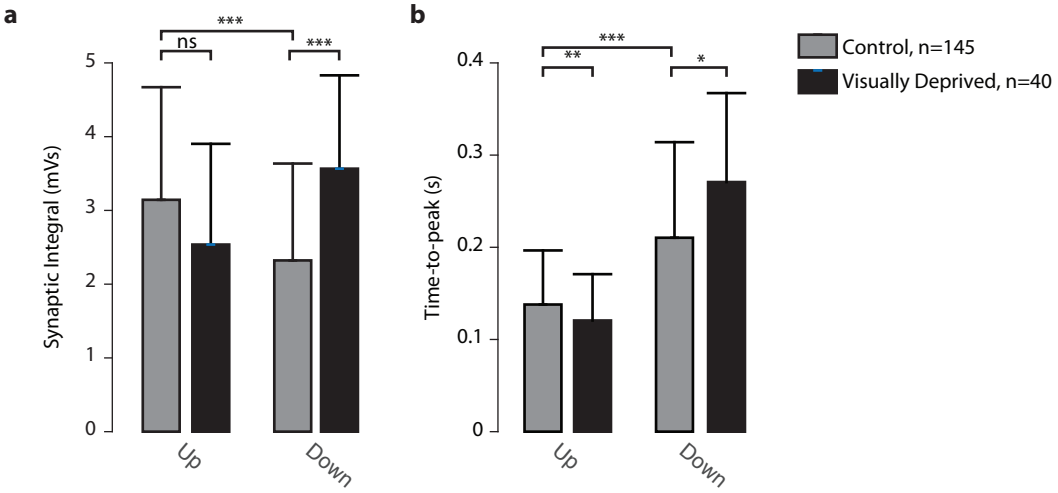

Figure 6.7: The Effect of Visual Deprivation on Flip-Evoked Depolarisations
(a) In cells recorded in control animals (n=145, gray bars), the integral of the evoked depolarisation was significantly smaller for down (light-to-dark) transitions than up transitions (dark-to-light). This pattern was reversed by visual deprivation (black bars), which did not cause a significant change in the synaptic integral in response to up transitions, but a large, significant increase in the integral in response to down transitions.
(b) The time-to-peak of the evoked depolarisation was also affected by visuall deprivation. For control animals, the evoked depolarisation to up transitions was significantly quicker than to down transitions. Deprivation enhanced this effect, significantly reducing the time-to-peak for up transitions, but increasing the time-to-peak for down transitions In both panels, bars display the median value. Error bars indicate standard deviation.

6.2.2.2 Membrane Potential and Spiking Responses to Auditory White Noise stimulus

The possibility of a more general change in cortical sensory processing was investigated by recording neuronal responses to auditory white noise stimuli, immediately after the flip stimulus. This provided a convenient measure of cross-modal input in to primary visual cortex (Olcese et al., 2013).

These recordings consisted of a baseline period of 2000ms, followed by a 100ms burst of white noise, then a post-stimulus recording period of 2000ms. Trials were separated by 5s to ensure that any evoked activity returned to baseline levels. In general, most L2/3 neurons displayed large, slow spontaneous depolarisations at rest (fig. 6.8a-c). These spontaneous depolarisations qualitatively resembled cortical up and down states as described previously (Steriade et al., 1993; Crochet and Petersen, 2006; Poulet and Petersen, 2008; Saleem et al., 2010). In the majority of neurons, white noise stimuli appeared to reset the phase of these depolarising events, with events following the stimulus being of a similar magnitude to spontaneous events, but aligned trial-to-trial. However, some neurons did show evoked depolarisations in the absence of spontaneous activity (fig. 6.8d).

As a result of this alignment effect, when averaged across trials (fig. 6.9a), a membrane potential rise was observed, beginning shortly after the stimulus onset and peaking around 250ms later. This peak was followed by a small trough, reaching 3mV below the average prestimulus membrane potential, 700ms following stimulus onset.

Population responses to white noise stimuli in visually deprived animals did not differ to those of controls in terms of the integral (fig. 6.11a, n=77 control, 38 visually deprived, p=0.90 ns, Wilcoxon rank-sum test) or the time-to-peak (fig. 6.11b, p=0.99 ns) of the mean membrane potential change following stimulus onset. This lack of an effect of VD on auditory-evoked responses may indicate that the effect of visual deprivation is specific to visual input, rather than altering sensory processing either in V1, or more generally.

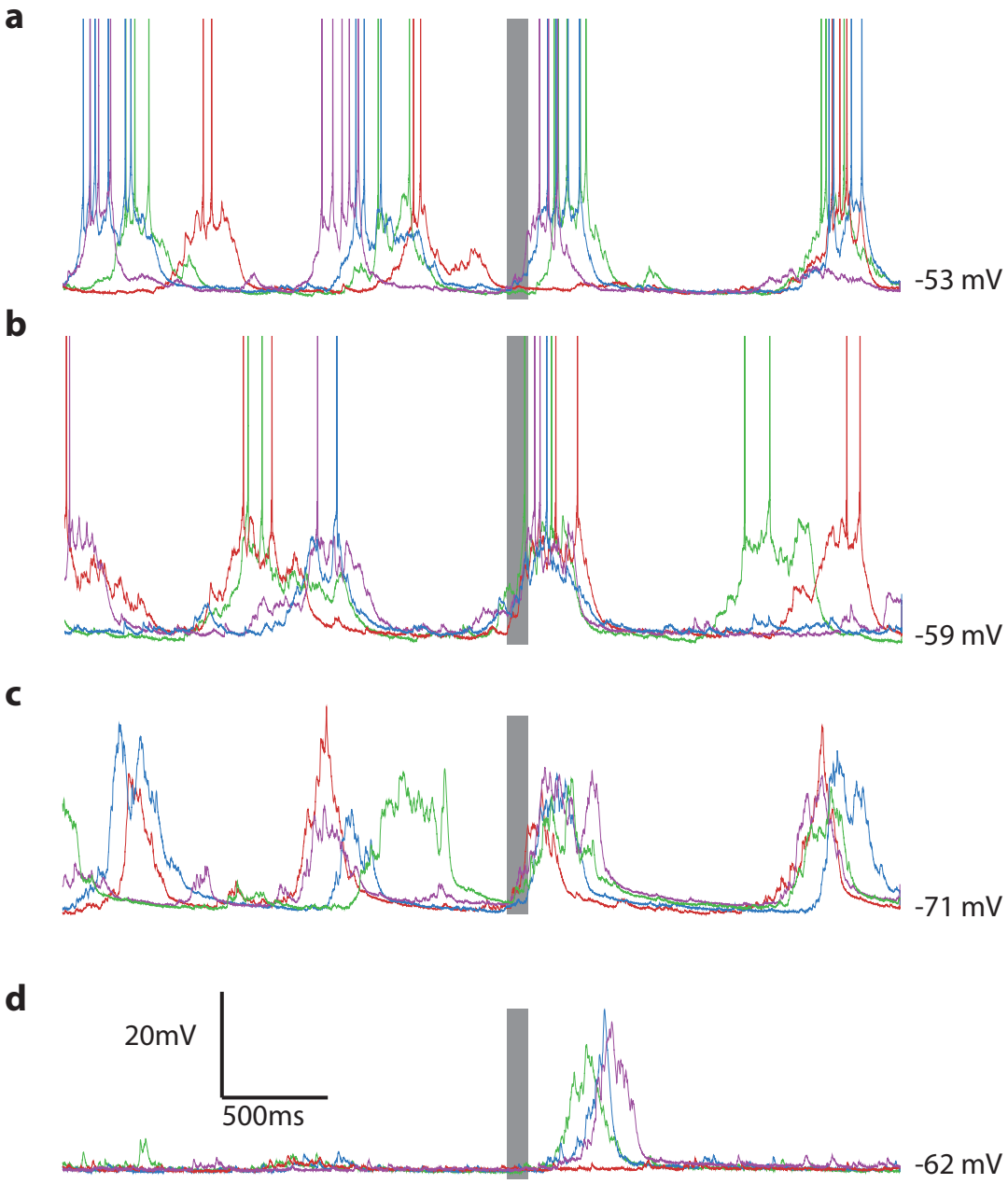

Figure 6.8: Example White Noise recordings from four neurons in control animals. Spikes have been clipped at 0mV; resting (minimum) membrane potential (V_m) values are given to the right of each trace.
(a,b) Two example traces showing typical responses in spiking neurons. Four individual repetitions are shown for each neuron, with the 100ms white noise stimulus denoted by the gray box. Spontaneous depolarising events and action potentials are seen before stimulus onset, with aligned events following the stimulus.
(c) Example responses in a non-spiking neuron, showing a similar pattern of alignment.
(d) Example responses in a neuron which did not display any spontaneous depolarisations. Events following the stimulus are still apparent.

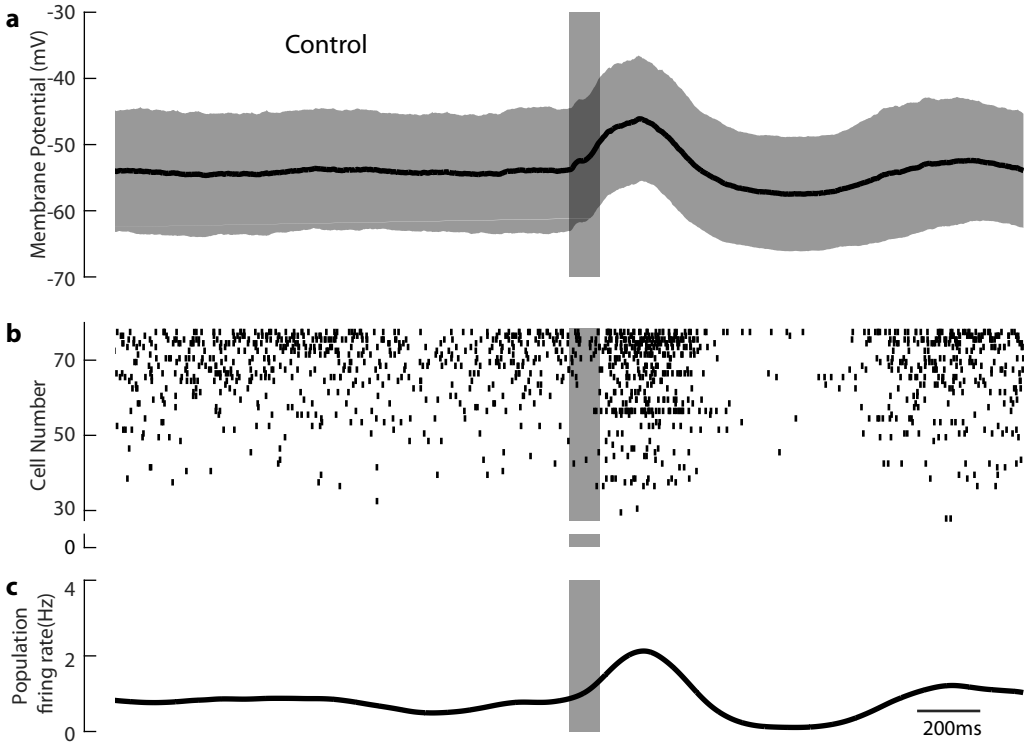

Figure 6.9: Population response to white noise stimuli in control animals
(a) Average membrane potential (black) ± standard deviation (gray) for all repeats of the stimulus, across all neurons.
(b) Spike raster, sorted by baseline firing rate. Spikes are shown superimposed from all 7 trials
(c) Trial-wise population spike rate, determined using a causal α-filter ($1/\alpha = 50ms$)

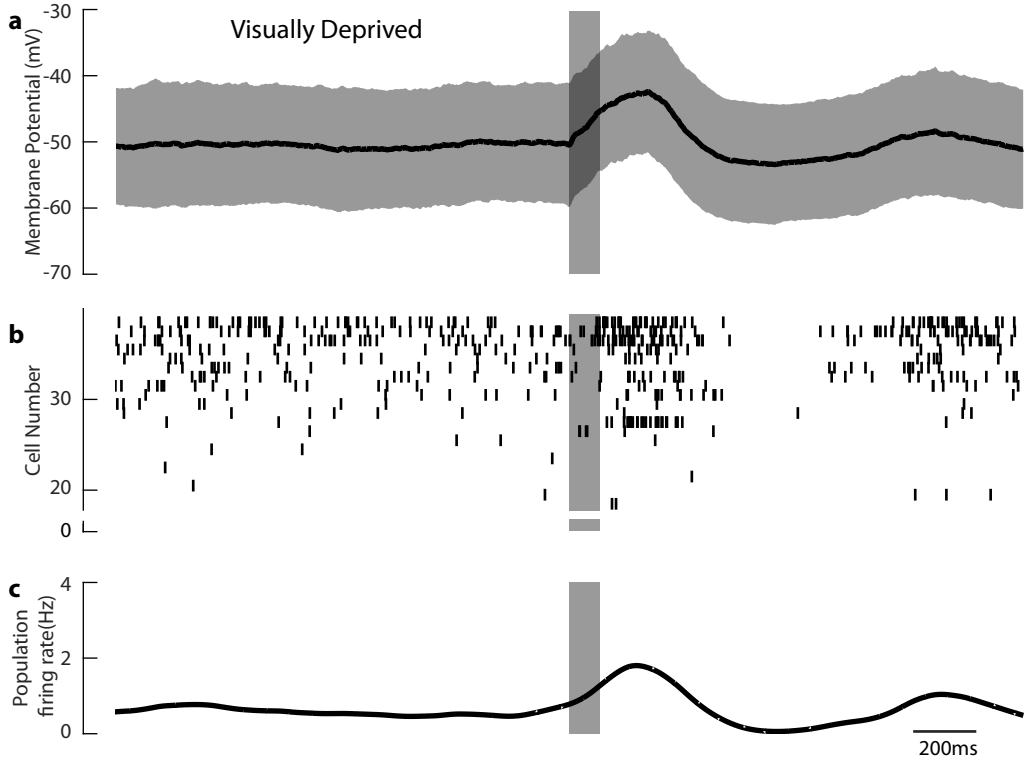

Figure 6.10: Population response to white noise stimuli in visually deprived animals. **(a-c)** as for fig. 6.9

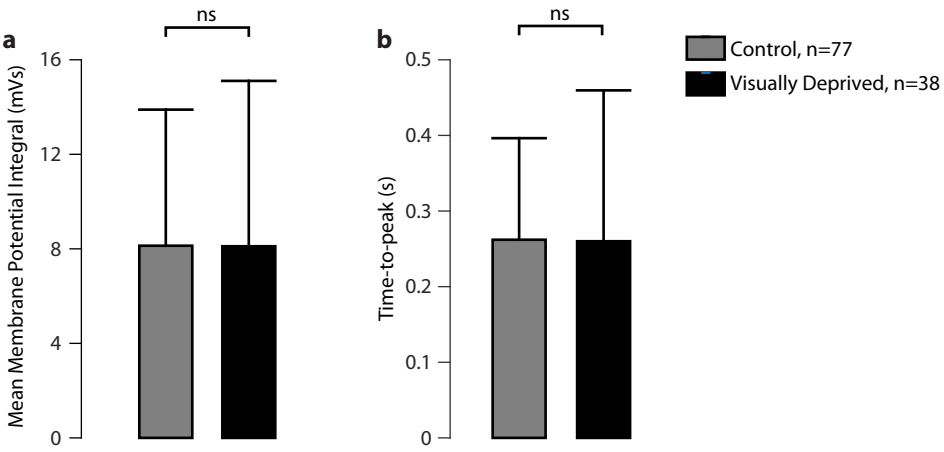

Figure 6.11: Visual Deprivation does not affect responses to auditory stimuli in V1. Neither **(a)** the integral nor **(b)** the time-to-peak of the mean membrane potential changes following white noise stimulation were significantly altered in visually deprived animals (black bars n=38), as compared to control animals (gray bars n=77). Bars display median values; error bars indicate standard deviation.

6.2.3 Orientation Tuning of V1 Neurons in VD Animals

6.2.3.1 Orientation Selectivity

Following the characterisation of intrinsic properties and responses to ballistic stimuli, membrane potential and spiking responses to drifting gratings were characterised in visually deprived animals. Data were recorded and analysed in the same manner as in control animals (section 6.2.1), beginning immediately after recording responses to ballistic stimuli.

In agreement with previous studies (Rochefort et al., 2011; Ko et al., 2014), the distributions of mean firing rate OSI (OSI_{F0}) for cells statistically responsive to drifting gratings was not found to be affected by visual deprivation (fig. 6.12a, p=0.71 ns, Mann-Whitney test, n = 112 control, 26 visually deprived (VD)) . Further to this, however, the distribution of mean V_m OSI in all cells in which responses to drifting gratings were recorded was also found not to be significantly altered by deprivation (fig. 6.12b, p=0.16 ns, n = 128 control, 35 VD). Membrane potential modulation OSI (OSI_{Vm1}) in these cells was also unaffected by visual deprivation (fig. 6.12c, p=0.40 ns).

These additional findings would seem to imply that both the visual input to a L2/3 neuron, as well as its spiking output, are unaffected by visual deprivation. However, the findings of the current injection experiments imply that V1 neuronal properties are affecting by VD. It is puzzling as to how intrinsic properties governing the impact of sensory integration of information could change, and yet the same input produce the same output. Furthermore, if neuronal responses to ballistic visual stimuli are altered in VD animals, this would seem to imply that, either the visual input to V1 is affected, or that changes occur in feedback or recurrent processing within the visual system.

It is possible that, whilst population input and output OSI distributions remain unchanged, the interaction between the two is altered in individual cells. To test this, the correlation between mean membrane potential depolarisation OSI (OSI_{Vm0}) and OSI_{F0} for VD neurons responsive to drifting gratings was tested in the same way as for control animals (fig. 5.13). The correlation was not found to be significant (Spearman's ρ 0.309, p=0.125), but the low numbers of responsive neurons limited the power of this test somewhat. Furthermore, altered statistical significance in a treatment group is not sufficent grounds for determining treatment effect (Nieuwenhuis et al., 2011), but rather a direct comparison needs to be made between the control and the visually deprived. This was therefore carried out using a method developed by Fisher (Fisher, 1921), which trans-

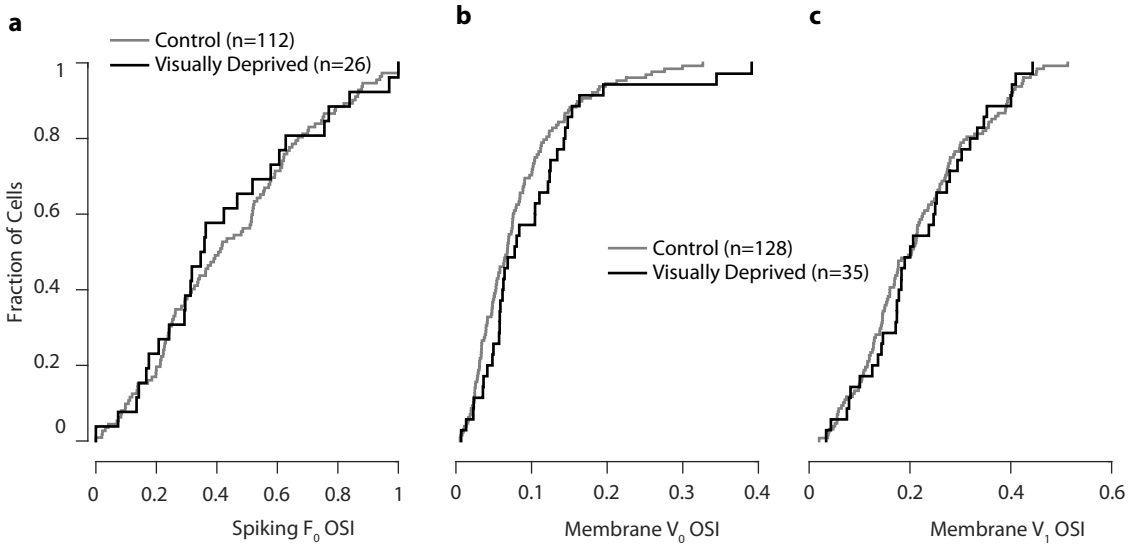

Figure 6.12: Distribution of Spiking and Membrane Potential OSI in Control and Visually Deprived Neurons
(a) Plot of the empirical cumulative probability density of mean spike rate OSI in neurons whose firing rate was significantly modified by drifting grating stimuli
(b) Plot of the empirical cumulative probability density of mean membrane potential OSI in all neurons
(c) Plot of the empirical cumulative probability density of membrane potential modulation OSI in all neurons

forms the difference between two correlation coefficients in to a z-score. According to this method, the correlation coefficient between OSI_{Vm0} and OSI_{F0} was not altered (control ρ 0.323, VD ρ 0.309, z 0.068, p=0.95 2 tailed). Therefore, there is no evidence that the relation between input and output OSI is altered. When this analysis was also carried out for the correlation between OSI_{Vm1} and OSI_{F0}, the correlation coefficient between the tuning of the membrane potential modulation and the mean evoked spike rate was found to be 0.448 in VD animals, as compared to 0.340 in control animals. However, this difference was again not found to be significant (p=0.58 ns, Fisher's Transformation n=26 VD, 112 control). Based on these comprehensive analyses, it is clear that visual deprivation has no effect on either the input or output tuning of evoked responses to drifting gratings.

The question reamins, therefore, of how similar OSI_{Vm0} input be associated with similar OSI_{F0} output in neurons with altered intrinsic properties and different responses to at least some visual stimuli. Firstly, it is possible that these observed changes in responses to ballistic visual stimuli have no functional effect relevant to more complex visual stimuli, or at least to drifting grating stimuli. Secondly, it is possible that aspects of processing not captured by OSI are overlooked by this singular, simple measure. The remaining results in this chapter examine these possibilities.

6.2.3.2 Responsiveness to Drifting Grating Stimuli

Whilst orientation selectivity in often used as a proxy measure for visual responsiveness, these parameters need not necessarily covary. For example, a neuron may be quite unselective in terms of the orientations to which it fires action potentials, as a result of being highly responsive to all presented orientations. A change in the numbers of silent or unresponsive cells may indicate a change in spiking properties of neurons not captured by OSI alone. Therefore, in order to assess the effect of visual deprivation on neuronal responsiveness in V1, neurons in control and VD animals were classified in to one of three groups. The first group, termed 'responsive' neurons showed a statistically significant change in mean firing rates in response to grating drift (see section 2.7.4.1) . The second group, 'unresponsive' neurons, did not have a statistically significant change in firing rate in response to drift, but did fire at least some action potentials. The final group, 'silent' neurons, did not fire any action potentials during the entire presentation of the drifting grating stimuli.

Numbers of neurons in these three classes are given in table 6.2, and differed significantly between control and VD animals ($p=8.5x10^{-4}$, Cochran-Armitage test). Notably, silent cells were rare in control animals, with only one neuron out of 128 not firing any action potentials during stimulation, whereas 20% of neurons recorded in VD animals were silent. This indicates that deprivation decreases the fractional responsiveness of the population to drifting grating stimuli.

	Responsive	Unresponsive	Silent
Control	112 (87.5%)	15 (11.7%)	1 (0.8%)
VD	26 (74.3%)	2 (5.7%)	7 (20.0%)

Table 6.2: Neuronal Responsiveness to Drifting Grating Stimuli in Control and Visually Deprived Animals.
Cells were classified as responsive or unresponsive based upon the significance of their absolute change in mean firing rate to drifting gratings (see section 2.7.4.1). Silent cells were defined as neurons which did not fire any action potentials during drifting grating stimulation

6.2.4 Spontaneous Activity

Another possible difference that could mask changes in neuronal processing of visual information is altered spontaneous activity. In the absence of visual input it is possible that spontaneous activity is altered by homeostatic network mechanisms in L2/3 circuits control by visual information.

Spontaneous activity was assessed by analysing the membrane potential and spike frequency during the baseline period before the flicker stimulus. This period was chosen as it occurred after network recovery following breakin, but before the network was exposed to any sensory stimulation which could 'reset' the network if any putative homeostatic mechanism were sufficiently rapidly acting. The frequency and magnitude of spontaneous synaptic events was estimated as the standard deviation of the spike-clipped membrane potential, a crude but simple measure. Whilst membrane potential standard deviation (fig. 6.13a) was slightly higher in VD animals than in control (4.69±3.1mV compared to 3.93±2.6mV, median ± IQR), this difference was not statistically significant(p=0.088, Mann-Whitney test).

The distribution of spontaneous AP frequency was very similar (p=0.71, MW test) in VD animals to control animals (fig. 6.13b). Futhermore, there was no difference in the proportion of neurons which did not fire any spontaneous action potentials whatsoever (control:83/145, 57%, VD:22/40, 55%, p=0.80, Pearson's χ^2 test), nor any difference in spontaneous firing rate between control and VD animals when silent cells were excluded (p=0.67, MW test).

In summary, neither spontaneous synaptic activity nor spontaneous firing rate were significantly altered by visual deprivation. However, membrane potential standard deviation, a measure of spontaneous synaptic activity, did show a trend toward a significant increase in visually deprived animals. Therefore, the observed preservation of orientation selectivity occurs on a background of roughly similar spontaneous activity.

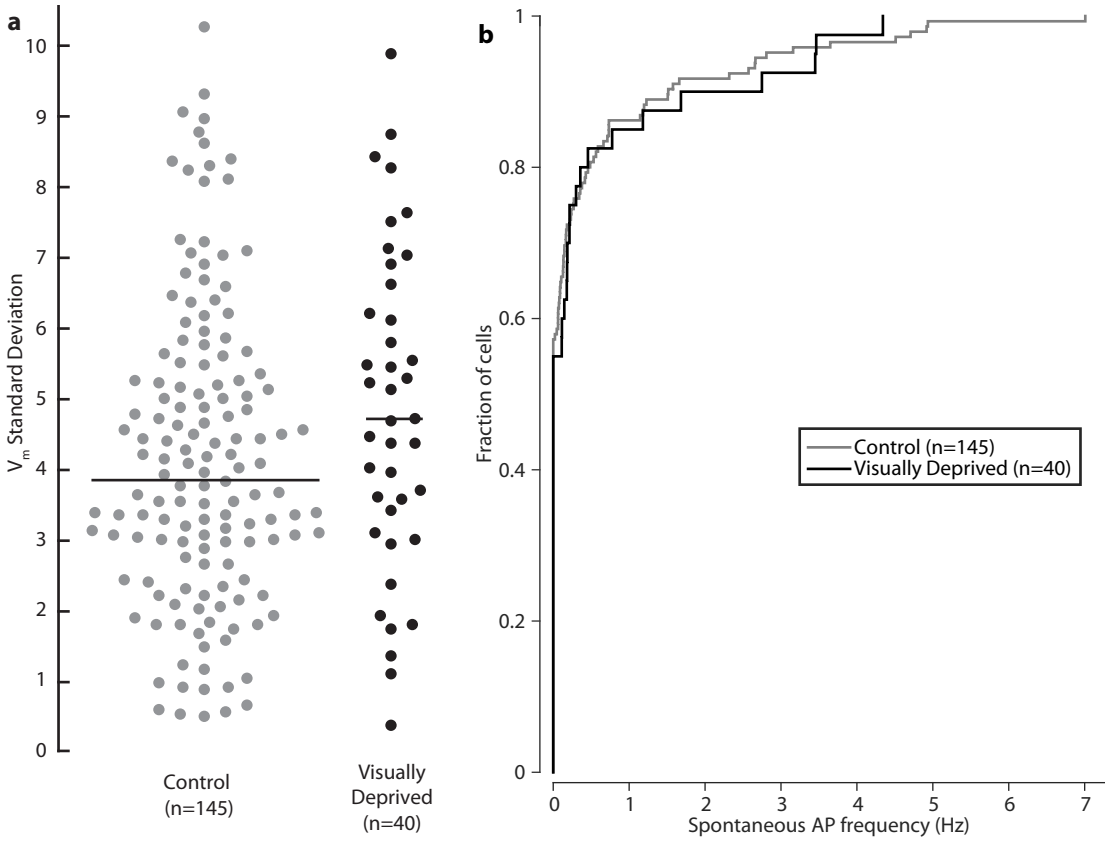

Figure 6.13: Spontaneous Activity in Control and Visually Deprived Animals
(a) Spontaneous synaptic activity, assessed as the standard deviation of the spike-clipped membrane potential. Horizontal bars indicate median values.
(b) Spontaneous AP frequency, plotted as an empirical cumulative density function

6.2.5 $Vm_{dist-thresh}$ in Visually Deprived Animals

As described in section 5.2.2, the difference between mean V_m during baseline and spike threshold ($Vm_{dist-thresh}$) provides a measure of neuronal excitability that is roughly as well correlated to OSI_{F0} as is OSI_{Vm0}. In turn, $Vm_{dist-thresh}$ was found to be correlated to total mean evoked depolarisation (Σ_{Vm0}), implying a potential homeostatic mechanism regulating excitability. In principle, if visual deprivation were to reduce the total input onto a L2/3 neuron, such a homeostatic mechanism could be expected to decrease the $Vm_{dist-thresh}$. Therefore $Vm_{dist-thresh}$ was measured for VD neurons during drifting grating stimuli and compared to control neurons. This parameter was calculated for all responsive and unresponsive cells, but not silent cells (since a relative V_m at rest could not be calculated in cases where there were no action potentials from which threshold could be determined).

The mean $Vm_{dist-thresh}$ of neurons in VD animals was virtually identical to that of controls (fig. 6.14, mean 24.82 ± 6.3 mV vs. 24.75 ± 4.3 mV, p=0.96 ns, unpaired t-test). However, variation in $Vm_{dist-thresh}$ was significantly reduced in neurons in VD animals (Levene test, p=0.0229*). This could indicate that homeostatic mechanisms do play a role in setting neuronal excitability, determined by visual experience, but that this occurs around a population average that is unchanged by visual deprivation.

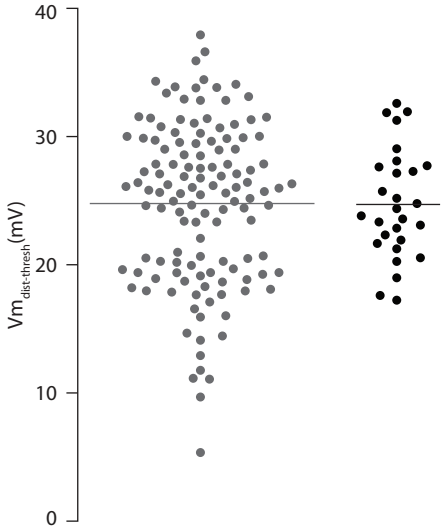

Figure 6.14: Distributions of $Vm_{dist-thresh}$ in control (gray) and VD animals (black). Horizontal bars indicate sample means.

Unlike in control animals (ρ 0.449, p=8.9x10^{-7}, n=112), $Vm_{dist-thresh}$ was not correlated with spiking OSI (ρ -0.110, p=0.61, n=26, fig. 6.15). When this correlation coefficient was compared to that of neurons in control animals, the difference was found to be signif-

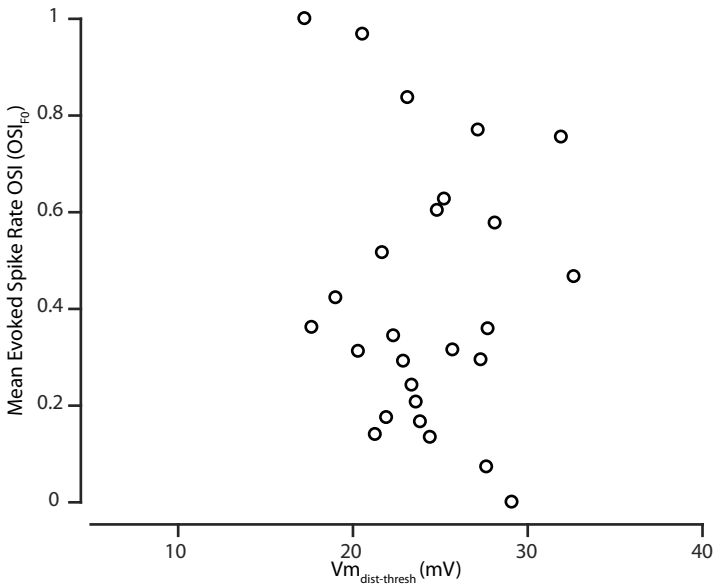

Figure 6.15: Spiking OSI-$Vm_{dist-thresh}$ Correlation in Visually Deprived Neurons.
Baseline membrane potential relative to spike threshold ($Vm_{dist-thresh}$) is plotted against OSI_{F0}. Only responsive neurons (n=26) are included in the comparison. Spearman's ρ -0.110, p=0.61, significantly less than in cells in control animals (Levene's test p=0.0229*) Scale is identical to that of fig. 5.13c.

icant (control ρ 0.449, Fisher's z 2.59, p=0.0096** 2-tailed). Therefore it can be said that spiking OSI in VD animals is significantly less coupled to $Vm_{dist-thresh}$ than in control animals.

6.2.6 Other Measures of Membrane Potential Response

Whilst orientation selectivity is a commonly used method of summarising responses to oriented drifting gratings, this singular measure may overlook more nuanced differences in the underlying activity. For example, if responses are linearly transformed equally to all stimuli, the orientation selectivity of the responses will remain equal, but underlying activity may be quite obviously different when measured in an alternative manner.

To investigate this possibility, responses to all directions in the first five trials were pooled to give 60 trials for each neuron. The magnitude of Vm0, membrane potential modulation at the stimulus fundamental frequency (Vm1) and F0 were then ranked independently. Deciles corresponding to the minimum, 10%, 20%, ... 90% and maximum were then taken from each ranking, and plotted grouped by experimental condition.

Picking an appropriate statistical test on these data was difficult, since they were quite far from being normally distributed, precluding the use of 2 way ANOVA. Therefore, individual Mann-Whitney tests were performed at each decile, followed by Holm-Bonferroni

correction for multiple comparisons. Mean membrane potential distributions were entirely unchanged by visual deprivation (fig. 6.16a), with no decile being significantly altered by VD even *before* multiple comparison correction. In contrast, Vm1 distributions were significantly affected by deprivation. Both before and after Holm-Bonferroni correction, every single decile was significantly lower in neurons in VD animals than in control neurons. This shows that while mean stimulus-evoked depolarisations are not affected by deprivation, membrane potential modulation is significantly reduced.

Applying this same analysis to mean spike rate (fig. 6.17) yielded a less clear result. Before Holm-Bonferroni correction, the population median F0 responses were lower in the VD cells for values at the 40th percentile and above (fig. 6.17). However, following correction, no individual difference was found to be significant. It is therefore difficult to state conclusively whether population F0 responses were reduced by visual deprivation or not, although an increase can be ruled out.

Therefore, it appears that membrane potential modulations in response to drifting grating stimuli are significantly reduced in VD animals, compared to controls. This difference is quite large: the median (across neurons) maximum (across all trials) modulation was 6.59mV for control neurons but only 4.87mV in neurons in visually deprived animals, a reduction of 26%. In contrast, mean depolarisations were not significantly altered, and evoked spike rate may be altered in deprived animals, although the results of this analysis were equivocal. This may suggest that visually evoked input to L2/3 neurons is *not* unaffected by visual deprivation, and that enhanced neuronal excitability can somehow compensate for the reduced input modulation to preserve a similar population spiking OSI distribution.

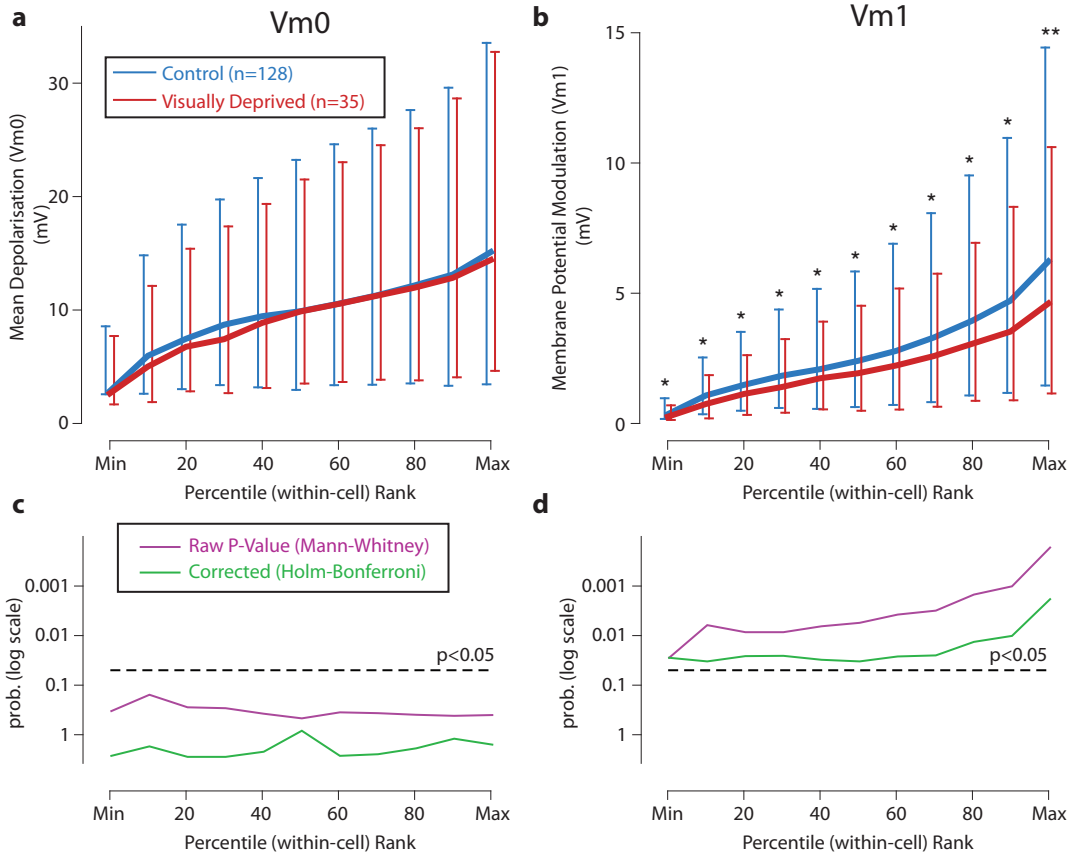

Figure 6.16: Effect of Visual Deprivation on Input Distributions

(a) Mean membrane potential response deciles for control (blue) and visually deprived (red) neurons. The joined lines indicate population median values at each decile; error bars indicate IQR. No statistically significant difference (MW two-tailed test) was detected at any decile, neither before nor after Holm-Bonferroni correction. Error bars have been offset slightly to enhance readability.

(b) Membrane potential modulation (Vm1) response deciles. Vm1 was significantly reduced at all deciles (MW two-tailed test, followed by Holm-Bonferroni correction). Asterisks denote significance following correction.

(c) Raw (purple) and Holm-Bonferroni corrected (green) p-values for the Mann-Whitney tests in **(a)**.

(d) Raw and corrected p-values for the Mann-Whitney tests in **(b)**.

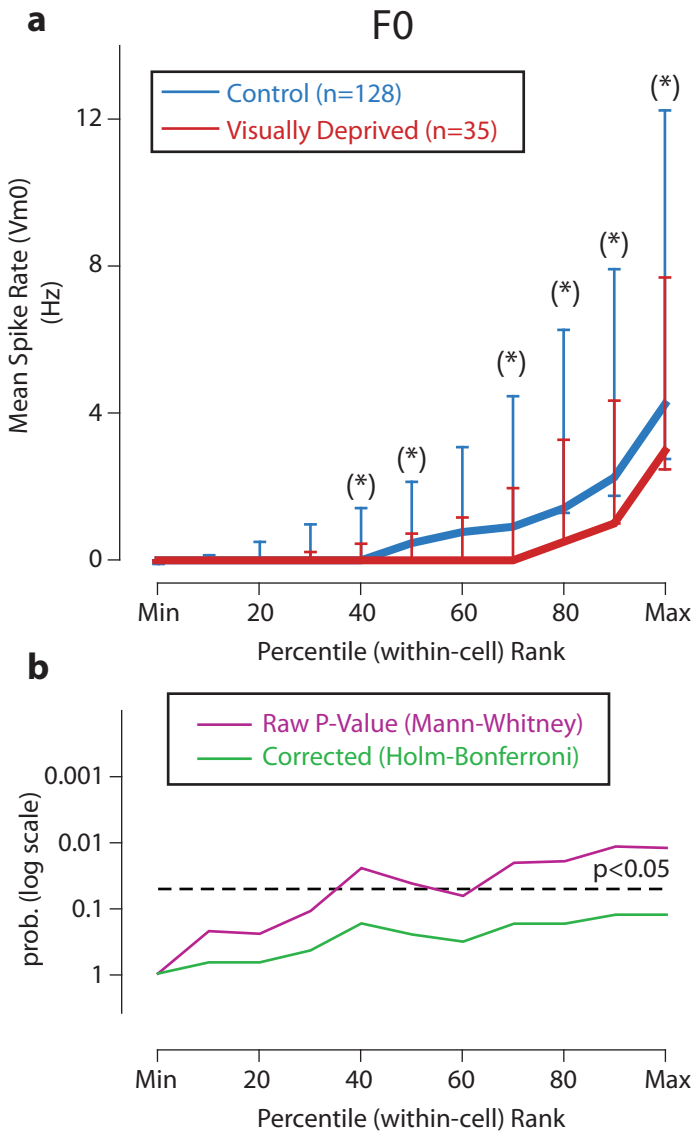

Figure 6.17: Effect of Visual Deprivation on Spiking Output Distribution

(a) Mean Evoked Spike Rate (F0) distributions of control (blue) and and visually deprived (red) neurons. Deciles were taken in the same manner as in fig. 6.16. No differences between decile medians of control and visually deprived animals were significant following Holm-Bonferroni correction, although several were significant before the correction. Significance levels preceding correction are indicated by asterisks in parentheses.

(b) Raw (purple) and Holm-Bonferroni corrected (green) p-values for the Mann-Whitney tests used in **(a)**

6.2.7 Modelling of Spiking Response to Mean Depolarisation and Vm Modulation

The results in the previous sections, taken together, suggest an intriguing possibility: that visual deprivation reduces stimulus-evoked membrane potential modulation, but that enhanced neuronal excitability compensates for this effect such that no discernible difference is apparent in spiking output tuning. To test this hypothesis, I use a model-fitting approach to examine how individual neurons process membrane potential changes in to a mean spiking output.

Each neuron was fitted with a double power-law model (see section 2.7.5), of the form

$$F0 = k_0[Vm0]_+^{p0} + k_1[Vm1]_+^{p1} \tag{6.1}$$

Interpretation of the four fitted parameters in isolation is difficult and non-intuitive, providing little information about the response of the model to an arbitrary combination of Vm0 and Vm1 (within physiological limits). Therefore, a direct analysis of the impact of visual deprivation on each parameter in isolation was not carried out.

A more intuitive method of inspection is to take a grid of points, within the limits of Vm0 and V1 for the particular cell, and pass these points through the model to generate a surface of predicted responses. Two example results of this modelling are shown in fig. 6.18. Consistent with the results in section 5.2.2.3, qualitative inspection of the fitted models revealed that spiking responses were more strongly governed by variation in membrane potential modulation than mean depolarisation in the majority of neurons (see fig. 6.18a for an example). This was typical of the majority of neurons, although some did appear to be more sensitive to increasing Vm0 than to Vm1 (fig. 6.18b).

By comparing modelled responses from each experimental group, the effect of visual deprivation upon population distribution of spiking responses to arbitrary combinations of Vm0 and Vm1 can be examined. However, it is obviously important to use realistic values of these parameters - in other words, to interpolate rather than extrapolate to non-physiological levels. For example, it is not meaningful to ask what the predicted spiking response of a neuron is to a 100mV mean depolarisation with a 50mV modulation.

Median decile values were taken from the control input distributions (fig. 6.16, blue) in order to define a realistic input parameter space. These values were passed through all models fitted from responses in control and VD animals, and the median spike rate across all neurons within an experimental group was plotted at each input pair (fig. 6.19). This

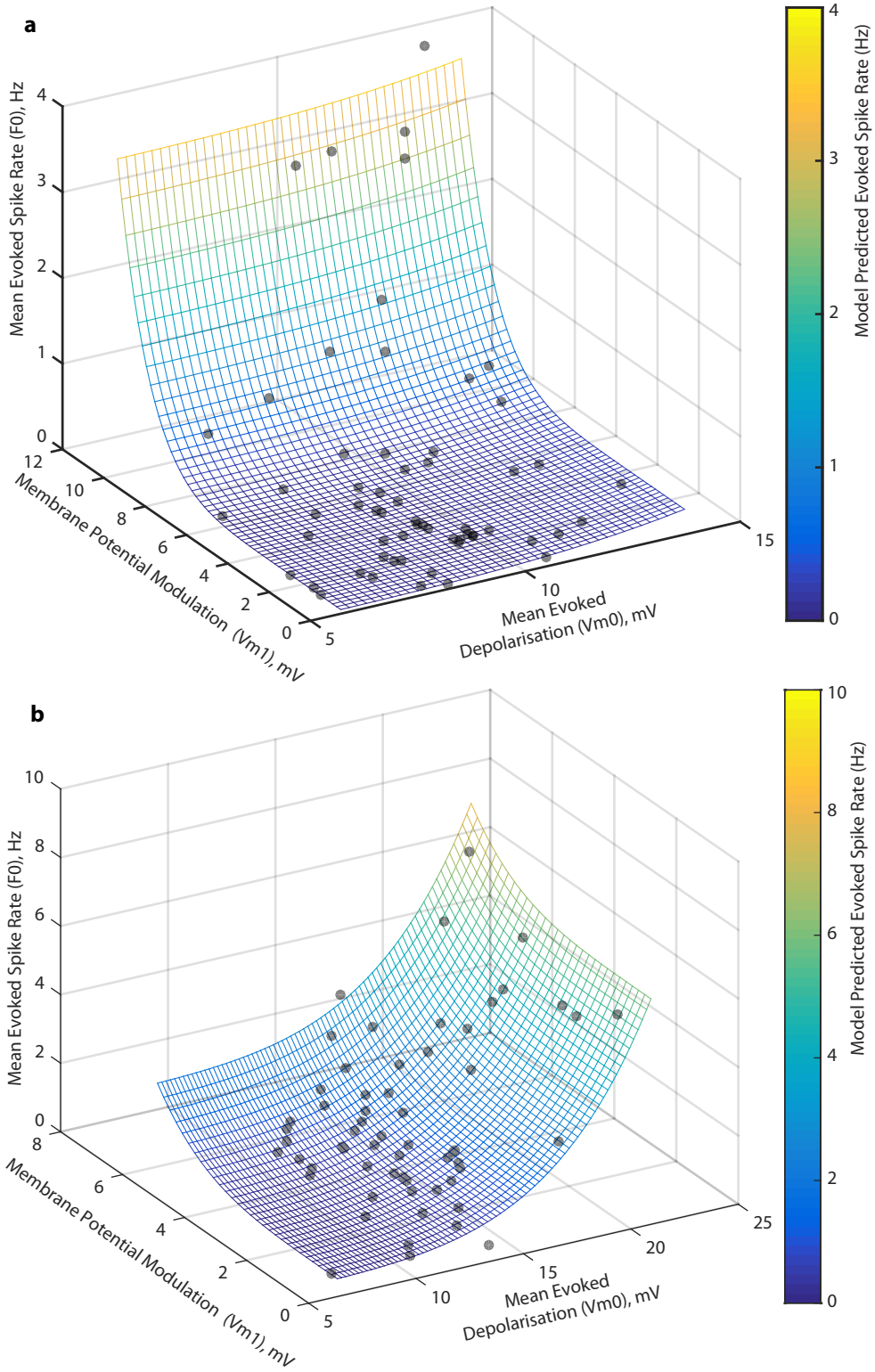

Figure 6.18: Two examples of fitting a power law spike rate model (section 2.7.5) to individual neuronal responses. Individual trials are shown as gray spheres. Responses predicted by the model using parameters calculated for using these trials are shown as a mesh surface, coloured by precicted evoked spike rate.
(a) An example neuron whose model predicts response being sensitive to increasing membrane potential modulation, but almost totally insensitive to increasing mean depolarisation
(b) An example neurons whose model predicts that responses will be more sensitive to increasing mean depolarisation, although still somewhat sensitive to increasing modulation. Both neurons were recorded in control animals.

analysis showed, as expected, that populations of neurons in both control (fig. 6.19a) and VD animals (fig. 6.19b) responded more acutely to increasing modulation decile than to increasing mean depolarisation decile. However, the VD neuronal population responded, on average, more sharply to increasing V1 than did control neurons.

As described in fig. 6.16, Vm0 distributions were similar for control and deprived animals (fig. 6.16a); however Vm1 values were significantly reduced in VD animals (fig. 6.16b). Therefore, predicted responses of VD neurons were re-calculated using the empirical distributions of Vm0 and Vm1 for VD neurons. In this simulation, population median predicted spiking responses were far more similar to those of control neurons (fig. 6.19d). Overall, the root mean squared error when comparing the responses across all deciles to control predictions was reduced from 0.43 when using control deciles to 0.22 using VD deciles, a reduction of 49%. This result indicates that neurons in L2/3 of V1 in visually deprived animals experience a less modulated input as a result of visual stimulation, but responding more sharply to this input results increases the similarity of the spiking response to that of control animals.

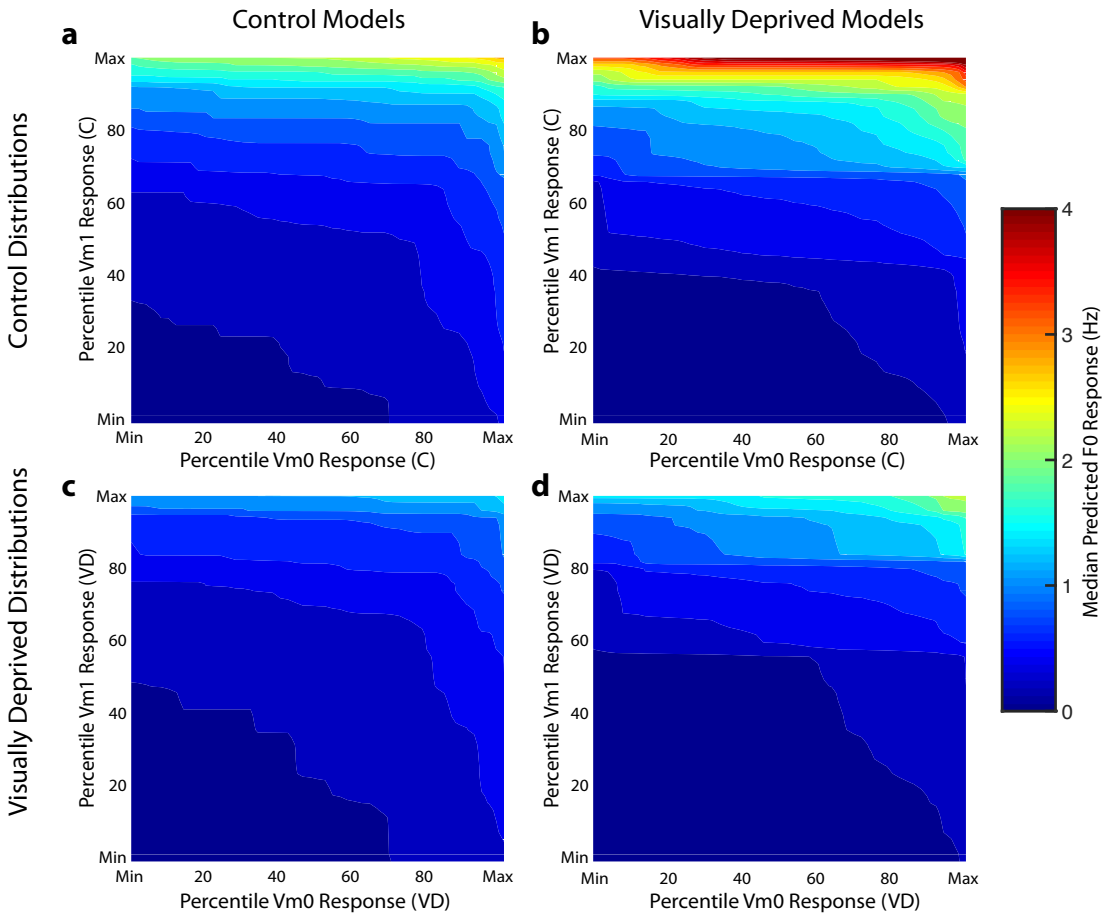

Figure 6.19: Predicted responses to mean depolarisation and membrane potential modulation for control and VD neurons

(a) Median predicted response of control neurons to Vm0 and Vm1 response distributions. Image contours represent the median predicted spiking F0 response of all models fitted to responses of control neurons, in response to increasing evoked Vm0 (horizontal) and Vm1 (vertical). The values of Vm0 and Vm1 used were the population median decile responses for control neurons, as shown in fig. 6.16a.

(b) Median predicted response of VD neurons to the same input values (deciles measured from the control population) as in **(a)**. Note the sharper increase in predicted spike rate to increasing membrane potential modulation, to higher maximal firing rates.

(c) Median predicted response of control neurons to stimulus evoked synaptic response distributions measured in the *visually deprived* population.

(d) Median predicted response of visually deprived neurons to visually deprived stimulus evoked synaptic response distributions.

6.3 Discussion

The results presented in this chapter demonstrate that visual deprivation does affect the intrinsic properties and synaptic responses of L2/3 neurons to oriented drifting grating stimuli, although spiking output distributions may be broadly preserved.

6.3.1 Visual Deprivation Alters Intrinsic Properties of Neurons

Several intrinsic properties were found to be significantly different in L2/3 neurons of visually deprived animals. Neurons in VD animals had a more depolarised resting membrane potential, lower rheobase and lower mean and maximal firing rates at 150% rheobase, as compared to neurons in control animals. Accommodation and hyperpolarising input resistance were unaffected.

It is difficult to state for certain that these changes in intrinsic properties each represents a distinct change caused by visual deprivation, or whether a smaller number of underlying molecular changes are responsible. It is likely, for example, that maximal and mean firing rates are not wholly orthogonal. It is possible that the slightly higher RMP has an effect on input resistance, given its dependance on membrane potential. However, the lack of a change in input resistance observed at hyperpolarising steps would argue against this possibility.

One of the major motivations for carrying out the visual deprivation experiments was to investigate the possible effect of sensory deprivation on neuronal processing, most particularly $Vm_{dist-thresh}$. The mean value of this measure was found, in VD animals, to be almost precisely the same as in control animals (fig. 6.14), although the variability was significantly decreased (see below section 6.3.3). The lack of a change in the mean $Vm_{dist-thresh}$ was reflected in a matched increase in the RMP (fig. 6.1a) and spike threshold (fig. 6.1b) of cells in VD animals, as measured during current injection experiments (figs. 6.1a and 6.1b). Naively, one might conclude from these data that neuronal excitability is unchanged by visual deprivation, since the distance from rest to spike threshold remains constant. However, it is possible that the absolute shift in resting membrane potential will have an effect on the driving force of synaptically-evoked conductances, with resultant changes in the amplitude and kinetics of both EPSPs and IPSPs. Whilst possible, this effect is likely to be small, given the difference of less than 5mV.

Most interestingly, in comparison to control neurons, VD neurons showed a significant increase in input resistance to depolarising, but not hyperpolarising, current steps. This

phenomenon may represent a homeostatic mechanism that increases the excitability of neurons to depolarising input in the context of reduced sensory stimulation. It is impossible to determine from these experiments alone the mechanism of this effect. It may arise from a change in the density of ion channels, alteration of the balance of different forms of ion channel, or of channel subunits (Burnashev et al., 1992; Bochet et al., 1994; Hille, 2001).

6.3.2 Altered Responses to Flip But Not Auditory Stimuli in VD Animals

The ballistic stimuli experiments were designed to test whether visual deprivation affected visual and multimodal input to V1 in general. Orientation tuning within visual cortex is a complex, dynamic process (Priebe and Ferster, 2012). It therefore it seems prudent to investigate whether any differences in simpler, perhaps more fundamental and feedforward-driven stimuli, are apparent.

Clear differences were apparent in both the membrane potential and spiking responses to full-field contrast reversal ('flip') stimuli in visually deprived animals, as compared to control animals. Overall VD neurons responded with a larger, slower depolarisation to down (light-to-dark) transitions than did neurons in control animals. Changes in responses to up (dark-to-light) transitions were more modest, with no significant change in the integral, and a small reduction in time-to-peak. At a population level, the mean spike rate following transitions was altered from being roughly equal to up and down transitions in control animals to being more than double following down transitions in VD animals. This may reflect a difference in adaptation to natural scene statistics, with adaption occurring at potentially any point along the visual pathway: transduction in the retina, processing within the retina, dLGN or V1, or even from 'higher' visual areas. It is also possible that visual deprivation affects cortical processing more generally, perhaps by perturbing sleep/wake cycles or stress hormone levels.

A recently published study on the effect of 7 days of visual deprivation on synaptic transmission in both V1 and primary auditory cortex (A1) has recently been published(Petrus et al., 2015). The authors measured changes in the amplitude of mEPSCs and mIPSPs, between and within L2/3 and L4 neurons in both areas, as well as feedforward excitatory input from the thalamus. In A1, excitatory feedforward synapses from the thalamus to L4 and L4→L2/3, as well as increased recurrent excitation within L4 and feedback inhibition from L4→L2/3 were all found to be potentiated. It is clear, therefore, that dark exposure *does* affect auditory responses, at least within A1. However, the

functional effect of these changes *in vivo* was not reported.

In my experiments, however, compound responses to auditory white-noise stimuli appeared to be entirely unaffected by visual deprivation, in terms of the integral and the time-to-peak of the mean membrane potential depolarisation. This would seem to imply that auditory information reaching primary visual cortex is unaffected by visual deprivation, and therefore that the observed changes in response to visual stimuli may be modally specific, at least within V1.

Petrus et al. (2015) did report increased lateral intracortical input, most probably representing recurrent excitatory inputs from nearby L2/3 in V1, but found no difference in the dLGN→L4, L4→L4 or L4→L2/3 pathways. It is possible that functional differences in response to flip stimuli may arise, in part, from this increased recurrent connectivity. However, differences may well be present at earlier stages (transduction, retinal processing, RGC− >dLGN) that were not tested by this approach. It should also be noted that the experimental paradigm used by Petrus et al. (2015) (7 day deprivation at P90) is not identical that as that used here (18-34 days deprivation, at P19).

Lastly, it is interesting that the results reported here with regard to responses of neurons in V1 to auditory stimuli differ from a previous report which described small hyperpolarisations in L2/3 V1 neurons following 50ms bursts of white noise (Iurilli et al., 2011). The authors of this study used a similar design to that used here; their findings were robust to changes in sound volumes and anaesthesia. The only explanation that I can offer is perhaps that the placement of the speaker has an effect; in the experiments described here the speaker was located near the visual stimulus, contralateral to the recording. The authors of (Iurilli et al., 2011) do not state precisely where they placed the speaker.

6.3.2.1 Spontaneous activity

The spontaneous activity (fig. 6.8a-c) described in this chapter was typically present during most recordings before stimulation began. This activity consisted of large depolarising events, typically lasting around for several hundreds of milliseconds, at a frequency of around 0.5-1Hz, resembling descriptions of cortical up and down states (Steriade et al., 2001; Poulet and Petersen, 2008; Saleem et al., 2010). Up and down states are thought to arise from the correlated activity of populations of neurons during slow-wave sleep, under some forms of anaesthesia and quiet wakefulness (Crochet and Petersen, 2006), although this may also be dependent upon brain region - for example, up states have been found to be rare in auditory cortex of awake rats (Hromádka et al., 2013). Up and down states

are not well defined in the literature, with some authors using the term to describe any observation of large amplitude, slow depolarising events, whereas others require evidence of membrane bistability thought to underpin the phenomenon (Harris and Thiele, 2011). However, the frequency and amplitude of the events observed in the experiments described here match well the described nature of up and down states and, in most cases, the spike-clipped membrane potential showed a broadly bimodal distribution characteristic of this pattern of activity (Saleem et al., 2010). However, a small number of neurons (fig. 6.8d) were recorded in which no obvious up states were observed.

Notably, these events seemed to either be masked by, or perhaps abolished by, visual grating stimulation (chapter 5). However, during white noise stimulation the major effect of the stimulus seemed to be to reset the phase of the spontaneous events, rather than to evoked new, additional depolarisations. I make this suggestion based upon the following observations. Firstly, events that followed the white noise stimulus were very similar in amplitude and duration to those which preceded it. Secondly, there was a reliable absence of activity immediately following the stimulus-evoked event, with the next depolarisation occurring typically 1-2s after the first. Thirdly, when the white noise stimulus was delivered during a spontaneous event, this seemed to prevent the stimulus-evoked event from occurring. In the experiments described here, stimulus timing was independent of the phase of the spontaneous activity, and further experiments in which the phase of the auditory stimulus is systematically varied could be performed in order to test this idea. Taken together, these findings indicate that the effect of the white noise was to reset the phase of up and down states.

6.3.3 Reduced Variability of $Vm_{dist-thresh}$

The primary motivation for the visual deprivation experiments was to investigate the effect of reduced visual input on intrinsic, sensory-evoked synaptic, and functional properties of L2/3 neurons, most especially on neuronal excitability in the light of the findings by Elstrott et al. (2014) in the whisker somatosensory cortex. In the previous chapter, I show how this measure is of a similar importance in setting the tuning width of neurons as is the tuning of the synaptic input.

One idea was that a reduction of visual input would decrease the $Vm_{dist-thresh}$, as neurons compensated for reduced sensory input by increasing their gain. However, the findings presented here do not support this. Mean $Vm_{dist-thresh}$ was almost precisely identical in VD animals as in controls. However, the variance in VD animals was sig-

nificantly reduced. This could indicate that the population set point for $Vm_{dist-thresh}$ remains unchanged. However, in the absence of visual input to the network, spontaneous or non-visual activity dominates, and is far less variable (cell-to-cell) than visual input. Therefore, the variability of the $Vm_{dist-thresh}$ decreases, but the overall population average remains similar.

An intriguing possibility is that the excess of silent neurons in VD animals is, in part, a result of the loss of $Vm_{dist-thresh}$ variation. In control animals, in which visual input presumably dominates in V1, neurons with weak synaptic responses to visual stimuli may adjust their excitability in order to respond more vigorously to evoked synaptic input. However, in the case of VD neurons this tuning does not occur. Neurons may well be adjusting their excitability to some other type of signal (such as spontaneous activity, multimodal input), rather than to visual input.

6.3.4 Correlation Loss in VD Animals

In the previous chapter, I demonstrated that a modest perturbation of a particular neuron's $Vm_{dist-thresh}$ has a large effect on OSI. It should therefore follow that any but the smallest variation in this parameter should be accompanied by a concomitant variation in tuning.

However, this is not the case. In the data presented here, the OSI_{F0} of neurons in VD animals is uncorrelated with $Vm_{dist-thresh}$. This correlation loss was significant when tested with standard hypothesis tests for difference in correlation coefficients (Fisher's Transformation). Furthermore, comparing bootstrapped correlation coefficients in the VD data set to bootstrapped CCs in the control animals (subsets with the same size as the VD dataset) gave a near identical result to the analytical method. Loss of correlation is not the result of undersampling in the VD population.

The most straightforward explanation for this correlation loss is the reduction in variation. A feature may be well correlated with a measured output, but if it does not vary this correlation becomes insignificant, since correlation is simply the observation of how variation in one variable tends to accompany variation in another. The significantly reduced variation in $Vm_{dist-thresh}$ may therefore explain this finding.

6.3.5 Preservation of OSI Despite Visual Deprivation

6.3.5.1 Correlation Loss: Should cells be more moderately tuned than in control animals?

The most intriguing aspect of the findings presented in this chapter is how output OSI_{F0} distributions remain unchanged by visual deprivation, despite the reduction of $Vm_{dist-thresh}$ variation that is a significant cause of a particular neuron's orientation selectivity in control animals. One might expect that OSI_{F0} values would tend towards central values, as one source of variation was removed.

In the control dataset, whilst the correlation was strong, $Vm_{dist-thresh}$ only accounted for around 20% of the variation in OSI_{F0}. Towards the extreme ends of the distribution, cells with a large $Vm_{dist-thresh}$ did tend to be more well tuned, but some were more moderately tuned. Neurons close to spike threshold cells tended to be less well tuned, but again, not exclusively - 5/31 neurons with a $Vm_{dist-thresh} < 20\mathrm{mV}$ had an $\mathrm{OSI}_{F0} > 0.5$ (fig. 5.13c). In the central zone of the distribution, OSI_{F0} values varied substantially across the entire range. Therefore, the reduction in variation in $Vm_{dist-thresh}$ observed in VD animals should not be expected to remove only very tuned or wholly untuned responses from the dataset. It is certainly possible that a sufficiently large sample could detect subtle differences in output tuning, but this sample size is likely to be unfeasible.

6.3.5.2 Increased Response to Reduced Vm Modulation

As also established in the previous chapter, F0 responses to drifting grating stimuli are dependent upon the modulation of the membrane potential (Vm1) to a greater degree than the mean depolarisation (Vm0). The finding that this modulation is reduced in visually deprived animals may reflect a subtle loss of normal developmental refinement of cortical connectivity, although intrinsic mechanisms can not be ruled out. The enhanced spiking response of VD neurons to Vm1 would seem, however, to compensate for this reduction. The mechanism for this may be related to the observed differential rectification (increased R_i to depolarising current injections only) in these neurons.

However, it is possible that this difference is unrelated. The differential rectification implies that the an evoked synaptic conductance may cause an enhanced somatic depolarisation, although drawing a direct inference from responses to somatic current injection to the physiological processing of synaptic input is not straight forward. The measured increased sensitivity to Vm1 in VD neurons can be thought of as acting at a later stage

in the integrative process, during which changes in V_m are converted in to trains of action potentials - so-called EPSP-spike ('E-S') coupling (Daoudal et al., 2002; Ferguson and Stone, 2010; Malik and Chattarji, 2012). It is therefore possible that the increased coupling between Vm1 and F0 therefore represents another homeostatic adaptation to visual deprivation, in which neurons compensate for the reduced temporal modulation of synaptic input by increasing their responsiveness to dV/dt, so as to maintain neuronal output within certain bounds.

6.3.5.3 Alternative Response Models

The model used in fitting F0 responses to Vm0 and Vm1 input was a linear combination of the classical half-wave rectified power law model (Carandini and Ferster, 2000). Other models were used, including models in which an additional term was added for the interaction between these two parameters. However, these changes did not improve the fits of the models dramatically enough to justify the addition of the two extra parameters needed. It may well be that Vm0 and Vm1 do interact in some way to create a non-linear response to a combination of these parameters, but this is not clear from these data alone.

Taken in combination, it is clear from the findings presented in this chapter that, whilst the distributions of orientation selectivity tuning parameters are not experience dependent (as reported for spiking data by Rochefort et al., 2011; Ko et al., 2011), this apparent lack of an effect of visual experience in fact masks a multitude of changes occuring in both the synaptic input and biophysical properties.

Chapter 7

General Discussion

The work of this thesis focusses on the intrinsic properties, input connectivity, and evoked synaptic and spiking properties of layer II/III (L2/3) neurons in mouse primary visual cortex. The major findings, are as follows:

1. Presynaptic connectivity is overwhelmingly intrareal, with the largest number of inputs being from other L2/3 neurons in primary visual cortex (V1) (although the density of presynaptic neurons did, in some cases, peak in layer 4, fig. 4.6)

2. Presynaptic local excitatory neurons are significantly more widely spread than presynaptic local inhibitory neurons (fig. 4.5)

3. The overwhelming majority are simple cells, as defined by spiking modulation ratio (F1/F0)

4. Preferred spatial frequency matches well the previously described values in the literature. Preferred temporal frequency broadly matches values described using extracellular electrical recordings, but are considerably higher than estimates made using imaging-based techniques.

5. The orientation tuning of the mean spike rate (F0) is correlated well to mean depolarisation (Vm0), membrane potential modulation at the stimulus fundamental frequency (Vm1), and baseline membrane potential relative to spike threshold ($Vm_{dist-thresh}$). However, grating-evoked F0 is better predicted by the Vm1 than the Vm0.

6. Visual deprivation causes a number of changes in intrinsic and synaptic properties. These include an increased voltage response to depolarising current injection, altered

functional response to contrast reversal, and a reduced variation in $Vm_{dist-thresh}$ which, in turn, breaks the correlation between this intrinsic parameter and spiking orientation tuning.

7. Whilst visual deprivation does not alter the tuning of the Vm0 or Vm1 synaptic response, nor the tuning of the mean firing rate OSI (OSI_{F0}) output, the *magnitude* of the Vm1 response is significantly reduced. However, the coupling between membrane potential modulation and mean spike rate is enhanced in visually deprived neurons, mitigating the functional effect of this change.

In addition, several other tentative findings are suggested by these data, but require greater investigation:

i. An absence of chattering and intrinsically bursting phenotypes in mouse L2/3.

ii. In addition to the regular-spiking and fast-spiking waveforms described classically, two further distinct spike waveforms that may be generated by parvalbumin negative inhibitory interneurons.

iii. F1/F0 is dependent upon the temporal frequency of the stimulus

iv. There may exist fast-spiking neurons, with a very strong feedforward input from the lateral geniculate nucleus, in layer 2/3.

I now proceed to discuss these specific findings, their limitations, and possible future directions for this work.

7.1 Intrinsic Properties of L2/3 Neurons

7.1.1 Classification of L2/3 Neurons by After-Hyperpolarisation

In chapter 3, I outline the intrinsic properties of 3 classes of recorded neurons, defined by spike waveform alone (the amplitude, and time-to-peak of the after-hyperpolarisation), as well as the possible existence of a fourth class of response, with a dual fast and a slow after-hyperpolarisation.

In accordance with published literature, L2/3 neurons with a large, fast after-hyperpolarisation were found to have a narrow spike half width, and considerably higher spike rate to depolarising current injections above rheobase (Gentet et al., 2010; Gentet, 2012). A second group of three neurons I have termed broad after-hyperpolarisation (BAH) displayed a

prominent after-hyperpolarisation, but with a considerably slower time-to-peak. These BAH neurons qualitatively matched the properties of non-fast spiking (NFS) neurons described in (Gentet et al., 2010), defined as neurons known to be GABAergic (based upon visualisation of eGFP expression in the GAD67-GFP mouse), but whose spike waveform does not match that of a fast-spiking interneuron. Like descriptions of NFS, BAH neurons have an action potential half-width close to that of an excitatory neuron, but a considerably higher input resistance, and a depolarised membrane potential. Their AP frequency is far lower than that of a fast-spiking neuron, being close to that of a regular-spiking pyramidal neuron.

These observations point to the probable interpretation that BAH neurons are, in fact, NFS interneurons. However, since these neurons were recorded blind, with no visualisation either during the experiment, or post-hoc, I can not state conclusively that this is the case. It may be profitable to perform targeted patch-clamp recordings in acute slices of GAD67-GFP animals, in order to validate a classification procedure that can distinguish NFS neurons from regular spiking (RS) neurons without direct visualisation. This would be greatly advantageous, allowing for the identification of NFS neurons recorded *in vivo* , without direct visualisation, which may be impossible in non-transgenic animals, or with recordings in deep cortical layers, beyond the reach of two photon microscopy.

One last, tantalising possibility, is that the single neuron recorded with a double-AHP may be a somatostatin-positive interneuron, a subclass of the NFS group, as these neurons are known to have a double-AHP waveform similar to that described here (Gentet, 2012). Again, this suggested interpretation is offered as potential avenue for investigation, rather than as a conclusive fact. It should, however, be noted that direct visualisation and targeting *in vivo* (Margrie et al., 2003) may remain the best option for recording from a sparse neuronal subclass, as few recordings from these would be expected by chance alone.

7.1.2 Lack of chattering and intrinsically bursting responses

No neuron recorded in the experiments reported here even approached the criteria for classification as a chattering or intrinsically bursting neuron, with the very high instantaneous spike rate typically reported for these (Nowak et al. (2003); Cardin et al. (2005)). Both of these classes of neurons have been reported in supragranular layers of the cat and ferret. To my knowledge, there have been no reports of the chattering / fast rhythmic bursting spiking phenotype in the mouse, and intrinsically bursting responses have been reported only in layers 4-5 (Chagnac-Amitai and Connors, 1989). The absence of IB and

CH responses may be interpreted as species difference, however the differences in anaesthesia and preparation may have a profound effect on bursting behaviour (Steriade et al., 2001).

7.2 Insight into single cell connectivity

The data presented in chapter 4 provide one of the first characterisations of the brain-wide presynaptic connectivity of individual cortical neurons. As previously described (Marshel et al., 2010; Rancz et al., 2011; Wertz et al., 2015), one of the most prominent features is that this connectivity is overwhelmingly intra-areal, with the vast majority of inputs to a L2/3 neuron arising from within V1 itself. Unlike the predictions of a simple laminar model of information flow, the majority of presynaptic neurons were located in L2/3. The precise nature of this recurrent connectivity, and its functional importance, is only beginning to be investigated (Song et al., 2005; Ko et al., 2011; Cossell et al., 2015).

Whilst connectivity was found to exhibit some degree of variability (figs. 4.2, 4.4 and 4.6), both the number of successful tracing experiments, and the numbers of labelled presynaptic neurons in these, prevented a quantitative analysis of the degree to which functional properties of the neuron correlate with variations in the presynaptic network. For example, it could be hypothesised that neurons with a more prominent Vm1 receive a stronger input from layer IV (L4) or even more direct inputs from the dorsolateral geniculate nucleus of the thalamus (dLGN). There could be variation in the relative numbers of feedback inputs from higher visual cortical areas, which may then be reflected in variation in parameters such as sensorimotor mismatch signalling in V1 (Keller et al., 2012). Technical developments in enhancing the success rate of whole-cell transfection with rabies-virus tracing, may make such experiments more feasible.

Perhaps the most tantalising result in the rabies tracing experiments is the connectivity of a single fast spiking neuron, in which the fraction of presynaptic neurons located in dLGN was ten times the average for regular spiking neurons. This chance finding was the only occasion on which tracing was carried out on a fast-spiking neuron. It is therefore not possible to state whether this represents a hitherto unreported feedforward connection from thalamus to fast-spiking interneurons, or whether this single result is not representative of the fast-spiking population. One feature that challenges the possibility that this connectivity may be typical is the tightly tuned orientation selectivity of this neuron. Parvalbumin-positive neurons, in general, display a substantially reduce orientation se-

lectivity, as compared to adjacent cortical neurons (Hofer et al., 2011). Therefore, it is possible that this neuron represents the extreme end of a distribution, receiving an unusual number of thalamocortical synapses, and, in turn, being unusually well tuned. It is also possible that this neuron was not, in fact, a parvalbumin-positive chandelier or basket neuron, as is the case for the overwhelming majority of fast-spiking neurons (Kawaguchi et al., 1987; Kawaguchi and Kubota, 1997). In order to test the possibility that parvalbumin-positive neurons, or a subset of this group, may receive a strong feedforward input from the thalamus, we have begun to compare the synaptic connectivity of parvalbumin neurons with that of GABAergic and pyramidal neurons, using Cre-dependent population rabies virus tracing. These experiments are currently at a preliminary stage.

The identity of presynaptic neurons, alone, provides only limited insight in to information flow. Characterisation of the functional responses of presynaptic neurons (Wertz et al., 2015), as well as the strength of the connection (Cossell et al., 2015), and features such as the short term plasticity of the synapse are not revealed by rabies virus tracing alone. Furthermore, complex dendritic processing may preclude simple predictions about how synaptic inputs are integrated. Clearly, a combinatorial approach is needed, in which the first step is to establish the general rules of cortical connectivity. Following this, single-cell techniques will allow for the variation in connectivity to be quantified (see fig. A.1). Lastly, a range of electrophysiological, optical, and other techniques may be employed in order to test the functional relevance of a particular projection, either on the responses of neurons themselves, or using behavioural paradigms.

7.3 Tuning Properties

One of the major goals of this project was to define intrinsic, synaptic and connectivity differences, if any, between neurons with a visually-evoked firing pattern that could be classified as simple, according to the F1/F0 ratio (Skottun et al., 1991), and those classified as complex, within L2/3. There has been some dispute over the distribution of this property in the mouse, with some authors (Niell and Stryker, 2008) reporting the large majority of neurons to be simple, whereas others (Van den Bergh et al., 2010) report that most cells to be complex, as is the case in the cat and the macaque, using the F1/F0 measure in both cases.

We find that the vast majority (84%) of neurons within L2/3 to be simple cells. Furthermore, this classification, made at a single spatial and temporal frequency (0.0283cpd,

2Hz), correlated well with a measure of F1/F0 made at the individual neuron's preferred spatial and temporal frequency. This would seem to be at odds with the finding that, in all 5 neurons in which temporal frequency dependence of F1/F0 was directly tested, this effect was found to be significant (fig. 5.10). However, for a considerable number of neurons (20/72), the preferred temporal frequency *was* that used in the orientation tuning recordings (2Hz), and so no difference between these two measures is to be expected. A further 31 neurons had a preferred temporal frequency within 0.5 octaves of this value, and again, in these neurons, no great difference is to be expected.

This finding, that temporal frequency does affect F1/F0, would benefit from a larger number of experimental observations. Drawing a rigorous conclusion from the responses of 5 neurons is fraught with danger, and quantification of this effect is simply not possible. To the extent that F1/F0 is a useful measure of neuronal function in visual cortex, a greater exposition of the factors which may contribute to its variation would be beneficial.

It is, of course, true that F1/F0 has become a more unfashionable measure in recent years, most particularly following the demonstration that membrane potential modulation ratio (Vm1/Vm0) does not follow a bimodal distribution in the same manner as F1/F0 (Priebe et al., 2004), suggesting that no true bimodal simple / complex connectivity pattern may exist. However, it is still a widely used metric, and rightly so: the fact that it may not demonstrate a true biological class difference does not detract from the finding that some neurons appear to encode precisely the phase of a grating stimulus, whereas others respond more tonically to motion.

However, it should be borne in mind that, per Hubel & Wiesel, F1/F0 is not the only definition of what makes a simple cell simple. In the cat, some neurons in L2/3 may display a modulated response, but lack segregated ON/OFF subfields in a push-pull arrangement, as is typical for a layer 4 simple cell (Martinez et al., 2005). Therefore, the possibility remains that mouse L2/3 neurons are not true simple cells, by all definitions.

7.4 Orientation Selectivity

Orientation selectivity is the hallmark of V1. It has inspired the development of models of function in visual cortex (Hubel and Wiesel, 1962), cortex more generally (Douglas and Martin, 1991), and even biologically inspired artificial systems. Despite over fifty years of research, the question of precisely how orientation tuning is created in cortical neurons is still hotly debated, and the finding of orientation tuned responses in LGN in the

rodent (Scholl et al., 2013) and marmoset (Cheong et al., 2013) challenges even the basic assumption that orientation tuning is a feature that emerges at the LGN→L4 projection, although this feature may be species-specific (Scholl et al., 2013).

Whatever the stage at which orientation tuning emerges in the visual system, it is clear that a broad synaptic tuning distribution is sharpened by the iceberg effect of spike threshold (Carandini and Ferster, 2000), and possibly by lateral inhibition (Carandini and Heeger, 2012), although this is disputed (Priebe and Ferster, 2012). For the first time, the data reported here address directly the question of which property of the evoked synaptic response - mean depolarisation, or membrane potential modulation - has the greater effect upon the mean evoked spike rate, in the context of orientation tuned responses. The considerably sharper tuning of Vm1, as compared to that of Vm0, has been reported qualitatively (Carandini and Ferster, 2000; Longordo et al., 2013; Cossell et al., 2015). Despite this, the membrane potential modulation is more usually regarded as the substrate upon which F1/F0 is built, in conjunction with the spike threshold (Priebe et al., 2004) with F0 usually being considered to result mainly from Vm0 (Tan et al., 2011; Smith et al., 2013). However, this assumption is challenged by the findings presented here, most clearly by the fact that mean spike rate correlates best with Vm1, rather than Vm0, in the majority of neurons (fig. 5.17.

To further extend this finding, controlled test stimuli could be used in order to probe individual neurons. Rather than simply injecting a square wave current step, as carried out in the IV recordings described here, waveforms consisting of varying combinations of mean and sine wave components could be used to finely characterise the responses of neurons to each of Vm0 and Vm1. This may more conveniently be done in acute brain slices, in which spontaneous activity is greatly reduced. However, individual neurons were found to receive greatly varying ranges of both Vm0 and Vm1 (fig. 6.16). Therefore, using one particular range of Vm0 and Vm1 values may be inappropriate. These current injections may then be carried out *in vivo* , following visual stimulation and an online characterisation of the particular distribution of the individual Vm0 and Vm1 distributions of the neuron.

One feature of the dataset upon which these conclusions are based is that it is gathered from one cortical neuronal class, in one layer of one species under one anaesthetic regimen. This should make possible rigorous conclusions about the relative contribution of a set of factors to particular outcomes in L2/3 neurons. However, the downside of this approach is that it makes generalisation difficult. Based upon these data alone, I have no basis on which to speculate whether Vm1 is better correlated to F0 than Vm0 in other cortical layers,

much less in other species. Similar recordings to those made for L2/3, from other cortical layers, would allow for direct comparisons to be made, revealing whether the relative contributions of Vm0, Vm1 and $Vm_{dist-thresh}$ differ between neurons in different cortical layers. Interspecies comparisons are far more fraught with difficulty, since experimental preparations vary considerably (Van Hooser, 2007). Whilst it might, therefore, seem to be desirable to repeat this analysis in the cat or primate, this is unlikely to be feasible using single-cell intracellular recordings, requiring the use of too many animals to be practically achievable or ethically justifiable.

The relative functional importance of Vm0 and Vm1 in setting the mean spike rate of a neuron in response to drifting grating stimuli may be tested directly by a number of measures such as reliability (figs. 5.14 and 5.15) or direct correlation with mean spike rate (fig. 5.17). The question of whether a diverse spiking population arises from diversity in synaptic input or intrinsic biophysical properties has remained more difficult to address. Unlike synaptic responses, which vary with each stimulus, biophysical properties such as $Vm_{dist-thresh}$ are singular values that remain relatively stable across a recording, making comparisons only possible between cells, rather than within the responses of a single cell. However, cell-to-cell variation in $Vm_{dist-thresh}$ was well correlated to OSI_{F0}, with a correlation coefficient higher than either mean membrane potential depolarisation OSI (OSI_{Vm0}) or membrane potential modulation OSI (OSI_{Vm1}), although this difference was not statistically significant. It is therefore not possible to state categorically, from these data alone, that intrinsic variability plays a greater role in the setting of OSI_{F0} than synaptic tuning, either OSI_{Vm0} or OSI_{Vm1}. However, the findings presented here do demonstrate that heterogenous responses in L2/3 arise from a mixture of both intrinsic biophysical and synaptic diversity.

7.5 Altered Processing of Visual Input in Visually Deprived Animals

The suggestion that $Vm_{dist-thresh}$ may arise, in part, as a homeostatic mechanism (Elstrott et al., 2014) in response to varying feedforward input strength, suggested that a perturbation of the input received by the visual system may reveal an altered distribution of this parameter. The most convenient approach to reducing visually-evoked feedforward input, as used here, is a simple visual deprivation paradigm.

The results of these experiments present several clear findings. Firstly, the altered

responses of neurons to ballistic visual, but not auditory, stimuli, imply that deprivation has a specific effect on the visual system.

Secondly, assuming $Vm_{dist-thresh}$ to be set by or reflective of a homeostatic mechanism that preserves the population spike rate within a certain range, one possible result of visual deprivation is that the mean distance to threshold is reduced in order to increase the excitability of the neuron. This was not found to be the case. However, the reduction in population $Vm_{dist-thresh}$ variability may imply an alternative: that, under conditions of visual deprivation, activity in V1 is dominated by non-visual input, either multi-modal or spontaneous. This activity may be far less variable than the visual feedforward drive, and so variation in $Vm_{dist-thresh}$ is reduced. One difficulty with speculations of this sort is that there is no data on precisely what form of activity dominates in the rodent visual cortex under conditions of absolute darkness. It is entirely possible that the population average spiking activity is considerably reduced. It is equally possible that compensatory processes amplify the effects of spontaneous or multimodal inputs in order to try to preserve the average spike rate. Therefore, population activity in visually deprived animals could be monitored over the course of a few days, in order to address this question.

In the context of investigating homeostatic regulation of $Vm_{dist-thresh}$, a more elegant approach would be to replace the relatively crude total visual deprivation paradigm with a more refined experimental approach. Expression of a channelrhodopsin could be used to alter the activity levels of neurons in freely moving animals, by the implantation of an optical fibre. By expressing the channel only in a small subset of neurons, the effect on the network as a whole would be limited. Following a period of stimulation (between a day to a week), the transfected neurons could be patched in an acute slice preparation, and their $Vm_{dist-thresh}$ compared to that of neighbouring non-transfected neurons, as well as neurons in control animals transfected with eGFP. Further experiments, using halorhodopsins, could reduce the activity levels of transfected neurons. This approach, whilst technically challenging, could provide stronger evidence of the precise manner in which activity levels may alter intrinsic parameters.

Visual deprivation affected a number of intrinsic parameters in addition $Vm_{dist-thresh}$, including the resting membrane potential and spike threshold, rheobase, and input resistance to depolarising (but not hyperpolarising) current injections. However, the tuning of Vm0, Vm1, as well as F0 was preserved in visually deprived animals. These findings may seem contradictory - that neurons which receive similarly tuned synaptic inputs produce similarly tuned spiking outputs despite having altered biophysical properties. It is possi-

ble that either the observed differences in intrinsic properties are functionally irrelevant, at least as regards responses to drifting gratings, or that additional intrinsic properties not assessed in these experiments negate any effects of those described. The use of a biophysically plausible mean spike rate model (section 2.7.5) allows for the investigation of the input-output transformation of individual neurons *in toto*, rather than attempting to account for, and simulate the effect of, every individual change in biophysical properties caused by visual deprivation. The results of the modelling presented in fig. 6.19 suggest that, in fact, neurons in animals deprived of visual stimulation do produce a greater mean evoked spike rate for the same levels of membrane potential modulation. Taken with the finding that Vm1 magnitudes are reduced in visually deprived animals (fig. 6.16), it would seem that intrinsic and synaptic changes caused by visual deprivation may be matched, in order to preserve spiking output.

7.6 Future Directions

The data presented in this thesis challenge an implicit assumption behind much of neural circuit analysis: that systems may be understood by dissection of circuits in to component neuronal classes, and that by studying intrinsic, connectomic and functional differences of the 'average' neuron of a particular class, the roles of individual, idealised components may be understood. Whilst certainly an important starting point, this approach overlooks the tremendous variability inherent within a single neuronal class, in this case the layer 2/3 regular-spiking neuron, as well as their dependence upon sensory experiencee. By studying the properties of individual neurons, both within and between classes, a greater understanding may be built of how visual information is processed within a real cortical circuit, and whether neuronal variability arises from stochastic processes or is a biologically desirable feature of the cortex. Only when the emerging field of connectomics is united with traditional experimental paradigms will the cortical thicket begin to give up its fruit.

Appendices

Appendix A

Connectivity Profiles of Individual, Functionally Characterised Layer 2/3 RS Neurons

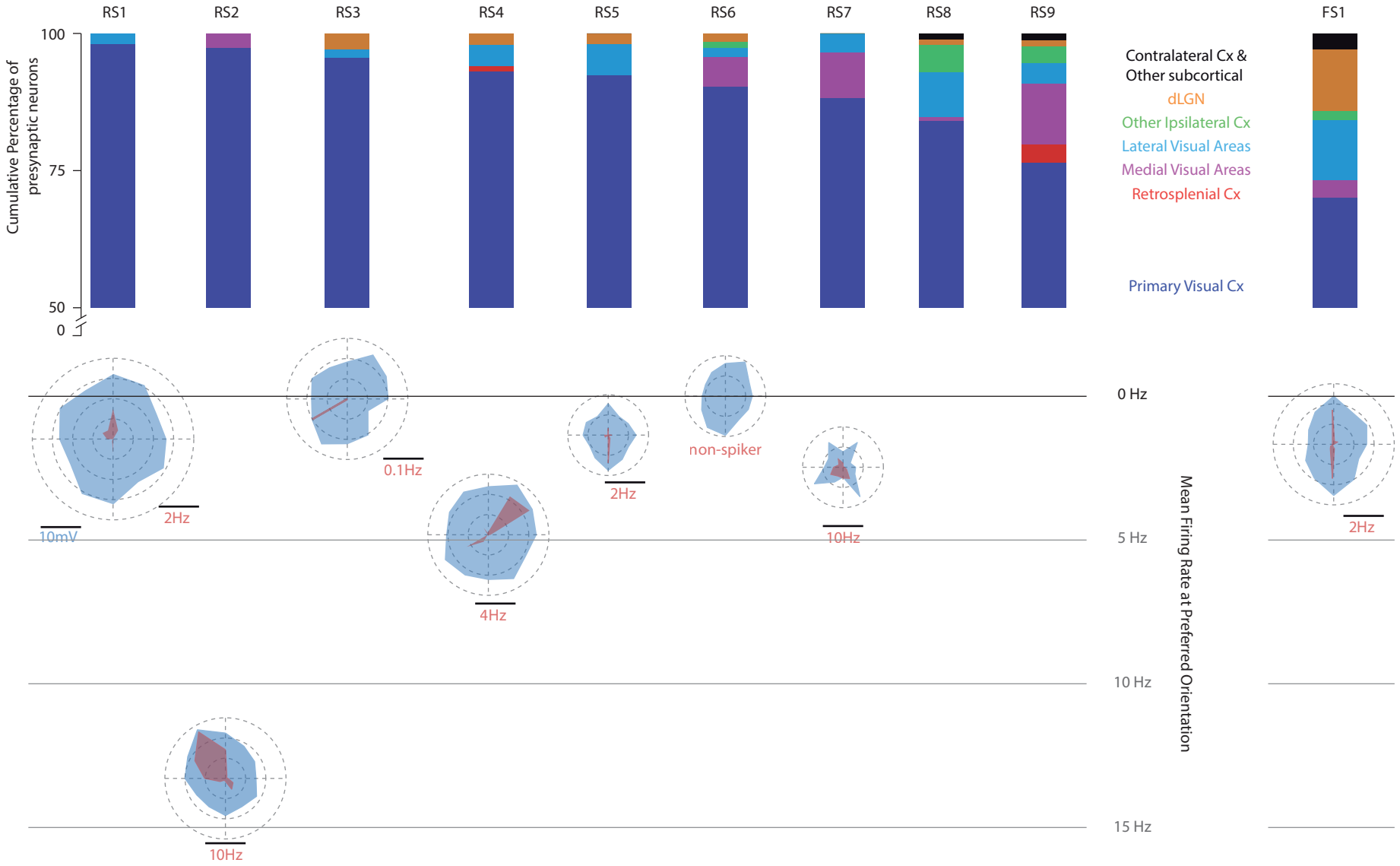

Figure A.1: (Caption on the following page)

Figure A.1: (Previous page.) Orientation Tuning and Presynaptic Cell Area Distribution of Individual Neurons

Areal distributions of presynaptic neurons for 10 neurons (9 regular-spiking, 1 fast-spiking) are shown as in fig. 4.2, with orientation tuning responses displayed below. Orientation tuning responses are shown as polar plots, displaying mean evoked depolarisation (Vm0) responses in blue and mean evoked spike rate (F0) responses in red. All Vm0 responses are displayed on the same scale, however since spiking response peak magnitude varied by more than 100-fold, individual neurons have been plotted with different scales shown alongside. The plots have been aligned vertically by their maximal mean evoked spike frequency in order to aid visualisation of this factor. Note that polar plots for two neurons, RS8 and RS9, are not shown, as recordings in these were not of good quality.

Appendix B

Abbreviations

R_i input resistance

$Vm_{dist-thresh}$ baseline membrane potential relative to spike threshold

Σ_{Vm0} total mean evoked depolarisation

τ membrane decay constant

ADP after-depolarisation

AHP after-hyperpolarisation

AP anter-posterior

AP action potential

BAH broad after-hyperpolarisation

CCK cholecystokinin

CH chattering

ChAT choline acetyltransferase

CR calretinin

CV Circular Variance

DAPI 4',6-diamidino-2-phenylindole

dLGN dorsolateral geniculate nucleus of the thalamus

DV dorso-ventral / depth

f-I frequency-current slope

F1 firing rate modulation at the stimulus fundamental frequency

F1/F0 spiking modulation ratio

FRB fast-rhythmic bursting

FS fast spiking

FWHM full width at half-maximum

GABA $\gamma-$aminobutyrate

IB intrinsically bursting

IpsiCx other ipsilateral cortical areas

L1 layer 1

L2/3 layer II/III

L4 layer IV

L5 layer V

L6 layer VI

LPMR lateral posterior nucleus, mediorostral part

MEFR mean evoked firing rate

ML medio-lateral

NFS non-fast spiking

NPY neuropeptide Y

OI Orientation Index

OSI Orientation Selectivity Index

OSI$_{F0}$ mean firing rate OSI

OSI$_{Vm0}$ mean membrane potential depolarisation OSI

OSI$_{Vm1}$ membrane potential modulation OSI

$\boldsymbol{OSI_{pt}}$ orientation selectivity, peak-trough method

other other brain areas

PFA paraformaldehyde

PO preferred orientation

$\boldsymbol{p(R_{PO})}$ preferred orientation reproducibility probability

PV parvalbumin

RMP resting membrane potential

$\boldsymbol{R_{PO}}$ preferred orientation reproducibility

RS regular spiking

RSP retrosplenial cortex

RVCM Rabies Virus assisted Circuit Mapping

SST somatostatin

STPT Serial Two Photon Tomography

V1 primary visual cortex

V2L lateral secondary visual areas

V2M medial secondary visual areas

VD visually deprived

VIP vasoactive intestinal peptide

vLGN ventral geniculate nucleus of the thalamus

$\boldsymbol{V}_m$ membrane potential

Vm1 membrane potential modulation at the stimulus fundamental frequency

Vm1/Vm0 membrane potential modulation ratio

Vm$_{ss}$ steady-state membrane potential

Bibliography

Abbott, L. F. and Chance, F. S. (2005). Drivers and modulators from push-pull and balanced synaptic input. *Progress in Brain Research*, 149:147–155.

Abbott, L. F., Varela, J. A., Sen, K., and Nelson, S. B. (1997). Synaptic Depression and Cortical Gain Control. *Science*, 275:220–224.

Agmon, A. and Connors, B. W. (1992). Correlation between intrinsic firing patterns and thalamocortical synaptic responses of neurons in mouse barrel cortex. *Journal of Neuroscience*, 12(1):319–329.

Ahmed, B., Anderson, J. C., Martin, K. A. C., and Nelson, J. C. (1997). Map of the synapses onto layer 4 basket cells of the primary visual cortex of the cat. *Journal of Comparative Neurology*, 380(2):230–242.

Alonso, J. M., Yeh, C. I., Weng, C., and Stoelzel, C. (2006). Retinogeniculate connections: a balancing act between connection specificity and receptive field diversity. *Progress in Brain Research*, 154:3–13.

Amatrudo, J. M., Weaver, C. M., Crimins, J. L., Hof, P. R., Rosene, D. L., and Luebke, J. I. (2012). Influence of highly distinctive structural properties on the excitability of pyramidal neurons in monkey visual and prefrontal cortices. *Journal of Neuroscience*, 32(40):13644–60.

Andermann, M. L., Kerlin, A. M., Roumis, D. K., Glickfeld, L. L., and Reid, R. C. (2011). Functional Specialization of Mouse Higher Visual Cortical Areas. *Neuron*, 72(6):1025–1039.

Anderson, J. S., Carandini, M., and Ferster, D. (2000). Orientation tuning of input conductance, excitation, and inhibition in cat primary visual cortex. *Journal of Neurophysiology*, 84(2):909–26.

Angelo, K., Rancz, E. a., Pimentel, D., Hundahl, C., Hannibal, J., Fleischmann, A., Pichler, B., and Margrie, T. W. (2012). A biophysical signature of network affiliation and sensory processing in mitral cells. *Nature*, 488(7411):375–8.

Aston-Jones, G. and Card, J. P. (2000). Use of pseudorabies virus to delineate multisynaptic circuits in brain: Opportunities and limitations. *Journal of Neuroscience Methods*, 103(1):51–61.

Atallah, B. V., Bruns, W., Carandini, M., and Scanziani, M. (2012). Parvalbumin-expressing interneurons linearly transform cortical responses to visual stimuli. *Neuron*, 73(1):159–70.

Azouz, R. and Gray, C. M. (2000). Dynamic spike threshold reveals a mechanism for synaptic coincidence detection in cortical neurons in vivo. *Proceedings of the National Academy of Sciences of the United States of America*, 97(14):8110–8115.

Bardy, C., Huang, J. Y., Wang, C., FitzGibbon, T., and Dreher, B. (2006). 'Simplification' of responses of complex cells in cat striate cortex: suppressive surrounds and 'feedback' inactivation. *Journal of Physiology*, 574(Pt 3):731–50.

Bastos, A. M., Usrey, W. M., Adams, R. a., Mangun, G. R., Fries, P., and Friston, K. J. (2012). Canonical microcircuits for predictive coding. *Neuron*, 76(4):695–711.

Bates, P., Young, J. A., and Varmus, H. E. (1993). A receptor for subgroup A Rous sarcoma virus is related to the low density lipoprotein receptor. *Cell*, 74(6):1043–1051.

Beier, T., Saunders, A., Oldenburg, I. A., Miya, K., Akhtar, N., Luo, L., and Whelan, S. P. J. (2012). Anterograde or retrograde transsynaptic labeling of CNS neurons with vesicular stomatitis virus vectors. *Proceedings of the National Academy of Sciences of the United States of America*, 109(23):9219–9219.

Benucci, A., Frazor, R. a., and Carandini, M. (2007). Standing waves and traveling waves distinguish two circuits in visual cortex. *Neuron*, 55(1):103–17.

Berardi, N., Pizzorusso, T., and Maffei, L. (2000). Critical periods during sensory development. *Current Opinion in Neurobiology*, 10(1):138–145.

Berson, D. M. (2003). Strange vision: Ganglion cells as circadian photoreceptors. *Trends in Neurosciences*, 26(6):314–320.

Binzegger, T., Douglas, R. J., and Martin, K. A. C. (2004). A quantitative map of the circuit of cat primary visual cortex. *Journal of Neuroscience*, 24(39):8441–8453.

Blakemore, C. and Van Sluyters, R. C. (1974). Reversal of the physiological effects of monocular deprivation in kittens: further evidence for a sensitive period. *Journal of Physiology*, 237(1):195–216.

Blanton, M. G., Lo Turco, J. J., and Kriegstein, a. R. (1989). Whole cell recording from neurons in slices of reptilian and mammalian cerebral cortex. *Journal of Neuroscience Methods*, 30(3):203–210.

Blasdel, G. G. and Fitzpatrick, D. (1984). Physiological organization of layer 4 in macaque striate cortex. *Journal of Neuroscience*, 4(3):880–895.

Bochet, P., Audinat, E., Lambolez, B., Crépel, F., Rossier, J., Iino, M., Tsuzuki, K., and Ozawa, S. (1994). Subunit composition at the single-cell level explains functional properties of a glutamate-gated channel. *Neuron*, 12(2):383–388.

Bock, D. D., Lee, W.-C. A., Kerlin, A. M., Andermann, M. L., Hood, G., Wetzel, A. W., Yurgenson, S., Soucy, E. R., Kim, H. S., and Reid, R. (2011). Network anatomy and in vivo physiology of visual cortical neurons. *Nature*, 471(7337):177–82.

Bonhoeffer, T. and Grinvald, a. (1991). Iso-orientation domains in cat visual cortex are arranged in pinwheel-like patterns. *Nature*, 353(6343):429–431.

Bonin, V., Histed, M., Yurgenson, S., and Reid, R. (2011). Local Diversity and Fine-Scale Organization of Receptive Fields in Mouse Visual Cortex. *Journal of Neuroscience*, 31(50):18506–18521.

Borg-Graham, L., Monier, C., and Frégnac, Y. (1996). Voltage-clamp measurement of visually-evoked conductances with whole-cell patch recordings in primary visual cortex. *Journal of Physiology (Paris)*, 90(3-4):185–188.

Borges, S. and Berry, M. (1978). The effects of dark rearing on the development of the visual cortex of the rat. *Journal of Comparative Neurology*, 180(2):277–300.

Bortone, D. S., Olsen, S. R., and Scanziani, M. (2014). Translaminar inhibitory cells recruited by layer 6 corticothalamic neurons suppress visual cortex. *Neuron*, 82(2):474–485.

Bosking, W. H., Zhang, Y., Schofield, B., and Fitzpatrick, D. (1997). Orientation selectivity and the arrangement of horizontal connections in tree shrew striate cortex. *Journal of Neuroscience*, 17(6):2112–2127.

Botcherby, E. J., Smith, C. W., Kohl, M. M., Débarre, D., Booth, M. J., Juskaits, R., Paulsen, O., and Wilson, T. (2011). Aberration-free three-dimensional multiphoton imaging of neuronal activity at kHz rates. *Proceedings of the National Academy of Sciences of the United States of America*.

Bradley, J., Luo, R., Otis, T. S., and DiGregorio, D. A. (2009). Submillisecond optical reporting of membrane potential in situ using a neuronal tracer dye. *Journal of Neuroscience*, 29(29):9197–209.

Braitenberg, V. and Schuz, A. (1998). *Cortex: Statistics and Geometry of Neuronal Connectivity*. Springer.

Branco, T., Clark, B. A., and Hausser, M. (2010). Dendritic Discrimination of Temporal Input Sequences in Cortical Neurons. *Science*, 329(5999):1671–1675.

Branco, T. and Häusser, M. (2011). Synaptic Integration Gradients in Single Cortical Pyramidal Cell Dendrites. *Neuron*, 69(5):885–892.

Briggman, K. L., Helmstaedter, M., and Denk, W. (2011). Wiring specificity in the direction-selectivity circuit of the retina. *Nature*, 471(7337):183–8.

Brodmann, K. (1909). Vergleichende Lokalisationslehre der Groshirnrinde. *Leipzig: Barth*.

Bullier, J. and Henry, G. H. (1979). Laminar distribution of first-order neurons and afferent terminals in cat striate cortex. *Journal of Neurophysiology*, 42(5):1271–1281.

Bullmore, E. and Sporns, O. (2012). The economy of brain network organization. *Nature Reviews Neuroscience*, 13:336–349.

Burnashev, N., Monyer, H., Seeburg, P. H., and Sakmann, B. (1992). Divalent ion permeability of AMPA receptor channels is dominated by the edited form of a single subunit. *Neuron*, 8(1):189–198.

Buser, P. and Albe-Fessard, P. (1953). Premiers résultats d'une analyse de l'activité électrique du cortex cérébral du chat par microelectrodes intracellulaires. *C.R. Acad. Sci, Paris*, 236:1197–1199.

Callaway, E. M. (2005). Structure and function of parallel pathways in the primate early visual system. *Journal of Physiology*, 566(1):13–19.

Campbel, F. W., Cooper, G. F., and Enroth-Cugell, C. (1969). THE SPATIAL SELECTIVITY OF THE VISUAL CELLS OF THE CAT. *Journal of Physiology*, 203:223–235.

Campbell, F. W., Cleland, B. G., Cooper, G. F., and Enroth-Cugell, C. (1968). The angular selectivity of visual cortical cells to moving gratings. *Journal of Physiology*, 198(1):237–250.

Carandini, M., Demb, J. B., Mante, V., Tolhurst, D. J., Dan, Y., Olshausen, B. a., Gallant, J. L., and Rust, N. C. (2005). Do we know what the early visual system does? *Journal of Neuroscience*, 25(46):10577–97.

Carandini, M. and Ferster, D. (2000). Membrane potential and firing rate in cat primary visual cortex. *Journal of Neuroscience*, 20(1):470–84.

Carandini, M. and Heeger, D. J. (2012). Normalization as a canonical neural computation. *Nature Reviews Neuroscience*, 13:51–62.

Carandini, M., Heeger, D. J., and Movshon, J. a. (1997). Linearity and normalization in simple cells of the macaque primary visual cortex. *Journal of Neuroscience*, 17(21):8621–8644.

Carandini, M., Heeger, D. J., and Senn, W. (2002). A synaptic explanation of suppression in visual cortex. *Journal of Neuroscience*, 22(22):10053–10065.

Cardin, J., Palmer, L. a., and Contreras, D. (2005). Stimulus-dependent gamma (30-50 Hz) oscillations in simple and complex fast rhythmic bursting cells in primary visual cortex. *Journal of Neuroscience*, 25(22):5339–50.

Cardin, J., Palmer, L. a., and Contreras, D. (2007). Stimulus feature selectivity in excitatory and inhibitory neurons in primary visual cortex. *Journal of Neuroscience*, 27(39):10333–10344.

Casagrande, V. A. (1994). A third parallel visual pathway to primate area V1. *Trends in Neurosciences*, 17(7):305–310.

Cauli, B., Audinat, E., Lambolez, B., Angulo, M. C., Ropert, N., Tsuzuki, K., Hestrin, S., and Rossier, J. (1997). Molecular and Physiological Diversity of Cortical Nonpyramidal Cells. *Journal of Neuroscience*, 17(10):3894–3906.

Cauli, B., Porter, J. T., Tsuzuki, K., Lambolez, B., Rossier, J., Quenet, B., and Audinat, E. (2000). Classification of fusiform neocortical interneurons based on unsupervised clustering. *Proceedings of the National Academy of Sciences of the United States of America*, 97(11):6144–6149.

Cavanaugh, J. R., Bair, W., and Movshon, J. A. (2002a). Nature and interaction of signals from the receptive field center and surround in macaque V1 neurons. *Journal of Neurophysiology*, 88(5):2530–2546.

Cavanaugh, J. R., Bair, W., and Movshon, J. A. (2002b). Selectivity and spatial distribution of signals from the receptive field surround in macaque V1 neurons. *Journal of Neurophysiology*, 88(5):2547–2556.

Caviness, V. S. (1975). Architectonic map of neocortex of the normal mouse. *The Journal of Comparative Neurology*, 164(2):247–63.

Chadderton, P., Schaefer, A. T., Williams, S. R., and Margrie, T. W. (2014). Sensory-evoked synaptic integration in cerebellar and cerebral cortical neurons. *Nature Reviews Neuroscience*, 15(2):71–83.

Chagnac-Amitai, Y. and Connors, B. W. (1989). Synchronized excitation and inhibition driven by intrinsically bursting neurons in neocortex. *Journal of Neurophysiology*, 62(5):1149–1162.

Chamberlin, N. L., Du, B., De Lacalle, S., and Saper, C. B. (1998). Recombinant adeno-associated virus vector: Use for transgene expression and anterograde tract tracing in the CNS. *Brain Research*, 793:169–175.

Chance, F. S., Abbott, L. F., and Reyes, A. D. (2002). Gain modulation from background synaptic input. *Neuron*, 35(4):773–782.

Chapman, B., Stryker, M. P., and Bonhoeffer, T. (1996). Development of orientation preference maps in ferret primary visual cortex. *Journal of Neuroscience*, 16(20):6443–6453.

Chen, Q., Cichon, J., Wang, W., Qiu, L., Lee, S.-J. R., Campbell, N. R., Destefino, N., Goard, M. J., Fu, Z., Yasuda, R., Looger, L. L., Arenkiel, B. R., Gan, W.-B., and Feng, G. (2012). Imaging Neural Activity Using Thy1-GCaMP Transgenic Mice. *Neuron*, 76(2):297–308.

Chen, T.-W., Wardill, T. J., Sun, Y., Pulver, S. R., Renninger, S. L., Baohan, A., Schreiter, E. R., Kerr, R. a., Orger, M. B., Jayaraman, V., Looger, L. L., Svoboda, K., and Kim, D. S. (2013). Ultrasensitive fluorescent proteins for imaging neuronal activity. *Nature*, 499(7458):295–300.

Cheong, S. K., Tailby, C., Solomon, S. G., and Martin, P. R. (2013). Cortical-like receptive fields in the lateral geniculate nucleus of marmoset monkeys. *Journal of Neuroscience*, 33(16):6864–76.

Churchland, M. M., Yu, B. M., Cunningham, J. P., Sugrue, L. P., Cohen, M. R., Corrado, G. S., Newsome, W. T., Clark, A. M., Scott, B. B., Bradley, D. C., Smith, M. A., Kohn, A., Movshon, J. A., Armstrong, K. M., Moore, T., Chang, S. W., Snyder, L. H., Lisberger, S. G., Priebe, N. J., Finn, I. M., Ferster, D., Ryu, S. I., Santhanam, G., Sahani, M., and Shenoy, K. V. (2010). Stimulus onset quenches neural variability: a widespread cortical phenomenon. *Nature Neuroscience*, 13(3):369–378.

Connors, B. W. and Gutnick, M. J. (1990). Intrinsic firing patterns of diverse neocortical neurons. *Trends in Neurosciences*, 13(3):99–104.

Connors, B. W., Gutnick, M. J., and Prince, D. a. (1982). Electrophysiological properties of neocortical neurons in vitro. *Journal of Neurophysiology*, 48(6):1302–1320.

Constantinople, C. M. and Bruno, R. M. (2013). Deep Cortical Layers Are Activated Directly by Thalamus. *Science*, 340(6140):1591–1594.

Contreras, D. (2004). Electrophysiological classes of neocortical neurons. *Neural Networks*, 17(5-6):633–46.

Conzelmann, K. K., Cox, J. H., Schneider, L. G., and Thiel, H. J. (1990). Molecular cloning and complete nucleotide sequence of the attenuated rabies virus SAD B19. *Virology*, 175(2):485–499.

Coppola, D. M., White, L. E., Fitzpatrick, D., and Purves, D. (1998). Unequal representation of cardinal and oblique contours in ferret visual cortex. *Proceedings of the National Academy of Sciences of the United States of America*, 95(5):2621–2623.

Cossell, L., Iacaruso, M. F., Muir, D. R., Houlton, R., Sader, E. N., Ko, H., Hofer, S. B., and Mrsic-Flogel, T. D. (2015). Functional organization of excitatory synaptic strength in primary visual cortex. *Nature*, 518(7539):399–403.

Cottam, J. C. H., Smith, S. L., and Häusser, M. (2013). Target-specific effects of somatostatin-expressing interneurons on neocortical visual processing. *Journal of Neuroscience*, 33(50):19567–78.

Creutzfeldt, O. and Ito, M. (1968). Functional synaptic organization of primary visual cortex neurones in the cat. *Experimental Brain Research*, 6(4):324–352.

Crochet, S. and Petersen, C. C. H. (2006). Correlating whisker behavior with membrane potential in barrel cortex of awake mice. *Nature Neuroscience*, 9(5):608–610.

Cruz-Martín, A., El-Danaf, R. N., Osakada, F., Sriram, B., Dhande, O. S., Nguyen, P. L., Callaway, E. M., Ghosh, A., and Huberman, A. D. (2014). A dedicated circuit links direction-selective retinal ganglion cells to the primary visual cortex. *Nature*, 4(7492):358–61.

Curcio, C. A., Sloan, K. R., Kalina, R. E., and Hendrickson, A. E. (1990). Human photoreceptor topography. *Journal of Comparative Neurology*, 292(4):497–523.

Dacey, D. M. and Lee, B. B. (1994). The 'blue-on' opponent pathway in primate retina originiates from a distinct bistratified ganglion cell type. *Nature*, 367:731–735.

Dacey, D. M. and Packer, O. S. (2003). Colour coding in the primate retina: Diverse cell types and cone-specific circuitry. *Current Opinion in Neurobiology*, 13(4):421–427.

Dana, H., Chen, T.-W., Hu, A., Shields, B. C., Guo, C., Looger, L. L., Kim, D. S., and Svoboda, K. (2014). Thy1-GCaMP6 Transgenic Mice for Neuronal Population Imaging In Vivo. *PLoS ONE*, 9(9):e108697.

Daoudal, G., Hanada, Y., and Debanne, D. (2002). Bidirectional plasticity of excitatory postsynaptic potential (EPSP)-spike coupling in CA1 hippocampal pyramidal neurons. *Proceedings of the National Academy of Sciences of the United States of America*, 99(22):14512–14517.

Daw, N. W. (1994). Mechanisms of plasticity in the visual cortex. *Investigative Opthamology and Visual Science*, 35(13):4168–4178.

Daw, N. W., Fox, K., Sato, H., and Czepita, D. (1992). Critical period for monocular deprivation in the cat visual cortex. *Journal of Neurophysiology*, 67(1):197–202.

Daw, N. W. and Wyatt, H. J. (1976). Kittens reared in a unidirectional environment: evidence for a critical period. *Journal of Neurophysiology*, 237:155–170.

De Valois, R. L., Albrecht, D. G., and Thorell, L. G. (1982). SPATIAL FREQUENCY SELECTIVITY OF CELLS IN MACAQUE VISUAL CORTEX. *Vision Research*.

DeAngelis, G. C., Robson, J. G., Ohzawa, I., and Freeman, R. D. (1992). Organization of suppression in receptive fields of neurons in cat visual cortex. *Journal of Neurophysiology*, 68(1):144–163.

Defelipe, J. (2011). The evolution of the brain, the human nature of cortical circuits, and intellectual creativity. *Frontiers in Neuroanatomy*, 5(May):29.

DeFelipe, J., Alonso-Nanclares, L., and Arellano, J. (2002). Microstructure of the neocortex : Comparative aspects. *Journal of Neurocytology*, 31:299–316.

Defelipe, J. and Fariñas, I. (1992). The Pyramidal Neuron of the Cerebral Cortex: Morphological and Chemical Characteristics of the Synaptic Inputs. *Progress in Neurobiology*, 39:563–607.

DeFelipe, J., Hendry, S. H. C., and Jones, E. G. (1989). Visualization of chandelier cell axons by parvalbumin immunoreactivity in monkey cerebral cortex (interneurons/inhibition). *Proceedings of the National Academy of Sciences of the United States of America*, 86:2093–2097.

DeFelipe, J., López-Cruz, P. L., Benavides-Piccione, R., Bielza, C., Larrañaga, P., Anderson, S., Burkhalter, A., Cauli, B., Fairén, A., Feldmeyer, D., Fishell, G., Fitzpatrick, D., Freund, T. F., González-Burgos, G., Hestrin, S., Hill, S., Hof, P. R., Huang, J., Jones, E. G., Kawaguchi, Y., Kisvárday, Z., Kubota, Y., Lewis, D. a., Marín, O., Markram, H., McBain, C. J., Meyer, H. S., Monyer, H., Nelson, S. B., Rockland, K., Rossier, J., Rubenstein, J. L. R., Rudy, B., Scanziani, M., Shepherd, G. M., Sherwood, C. C., Staiger, J. F., Tamás, G., Thomson, A., Wang, Y., Yuste, R., and Ascoli, G. a. (2013). New insights into the classification and nomenclature of cortical GABAergic interneurons. *Nature Reviews Neuroscience*, 14(3):202–16.

Denk, W., Strickler, J., and Webb, W. W. (1990). Two-photon laser scanning fluorescence microscopy. *Science*, 248(4951):73–76.

Dickinson, M. E., Bearman, G., Tille, S., Lansford, R., and Fraser, S. E. (2001). Multi-Spectral Imaging and Linear Unmixing Add a Whole New Dimension to Laser Scanning Fluorescence Microscopy. *BioImaging*, 31(6):1272–1278.

Djurisic, M., Antic, S., Chen, W. R., and Zecevic, D. (2004). Voltage imaging from dendrites of mitral cells: EPSP attenuation and spike trigger zones. *Journal of Neuroscience*, 24(30):6703–14.

Dombeck, D. a., Khabbaz, A. N., Collman, F., Adelman, T. L., and Tank, D. W. (2007). Imaging large-scale neural activity with cellular resolution in awake, mobile mice. *Neuron*, 56(1):43–57.

Douglas, R. J., Koch, C., Mahowald, M., Martin, K. A. C., and Suarez, H. H. (1995). Recurrent excitation in neocortical circuits. *Science*, 269(5226):981–5.

Douglas, R. J. and Martin, K. A. C. (1991). A Functional Microcircuit for Cat Visual Cortex. *Journal of Physiology*, 440:735–769.

Douglas, R. J. and Martin, K. A. C. (2004). Neuronal circuits of the neocortex. *Annual Review of Neuroscience*, 27:419–51.

Douglas, R. J. and Martin, K. A. C. (2007). Mapping the matrix: the ways of neocortex. *Neuron*, 56(2):226–38.

Douglas, R. J., Martin, K. A. C., and Whitteridge, D. (1988). Selective responses of visual cortical cells do not depend on shunting inhibition.

Dräger, U. C. (1975). Receptive fields of single cells and topography in mouse visual cortex. *The Journal of Comparative Neurology*, 160(3):269–90.

Draper, M. H. and Weidmann, S. (1951). Cardiac resting and action potentials recorded with an intracellular electrode. *Journal of Physiology*, 115:74–94.

Dreher, B. Y. B., Fukada, Y., and Rodieck, R. W. (1976). Identification, classification and anatomical segregation of cells with X-like and Y-like properties in the lateral geniculate nucleus of old-world primates. *Journal of Physiology*, 258:433–452.

Ebina, T., Sohya, K., Imayoshi, I., Yin, S.-T., Kimura, R., Yanagawa, Y., Kameda, H., Hioki, H., Kaneko, T., and Tsumoto, T. (2014). 3D Clustering of GABAergic Neurons Enhances Inhibitory Actions on Excitatory Neurons in the Mouse Visual Cortex. *Cell Reports*, 9(5):1896–1907.

Ecker, J. L., Dumitrescu, O. N., Wong, K. Y., Alam, N. M., Chen, S. K., LeGates, T., Renna, J. M., Prusky, G. T., Berson, D. M., and Hattar, S. (2010). Melanopsin-

expressing retinal ganglion-cell photoreceptors: Cellular diversity and role in pattern vision. *Neuron*, 67(1):49–60.

Einevoll, G., Franke, F., Hagen, E., Pouzat, C., and Harris, K. (2011). Towards reliable spike-train recordings from thousands of neurons with multielectrodes. *Current Opinion in Neurobiology*, 22(1):11–17.

Elstrott, J., Clancy, K. B., Jafri, H., Akimenko, I., and Feldman, D. E. (2014). Cellular mechanisms for response heterogeneity among L2/3 pyramidal cells in whisker somatosensory cortex. *Journal of Neurophysiology*, 112(2):233–48.

Emerson, R. C., Citron, M. C., Vaughn, W. J., and Klein, S. a. (1987). Nonlinear directionally selective subunits in complex cells of cat striate cortex. *Journal of Neurophysiology*, 58(1):33–65.

Enroth-Cugell, C. and Robson, J. G. (1966). The contrast sensitivity of retinal ganglion cells of the cat. *Journal of Physiology*, 187(3):517–552.

Etessami, R., Conzelmann, K. K., Fadai-Ghotbi, B., Natelson, B., Tsiang, H., and Ceccaldi, P. E. (2000). Spread and pathogenic characteristics of a G-deficient rabies virus recombinant: An in vitro and in vivo study. *Journal of General Virology*, 81(9):2147–2153.

Euler, T., Detwiler, P. B., and Denk, W. (2002). Directionally selective calcium signals in dendrites of starburst amacrine cells. *Nature*, 418(6900):845–852.

Fagiolini, M., Pizzorusso, T., Berardi, N., Domenici, L., and Maffei, L. (1994). Functional postnatal development of the rat primary visual cortex and the role of visual experience: Dark rearing and monocular deprivation. *Vision Research*, 34(6):709–720.

Famiglietti, E. V. and Kolb, H. (1976). Structural basis for ON and OFF center responses in retinal ganglion cells. *Science*, 194(4261):193–195.

Federspiel, M. J., Bates, P., Young, J. a., Varmus, H. E., and Hughes, S. H. (1994). A system for tissue-specific gene targeting: transgenic mice susceptible to subgroup A avian leukosis virus-based retroviral vectors. *Proceedings of the National Academy of Sciences of the United States of America*, 91(23):11241–11245.

Feldman, M. L. (1984). Morphology of the neocortical pyramidal neuron. In Jones, E. G.

and Peters, A., editors, *Cellular Components of the Cerebral Cortex*, pages 123–200. Plenum Press, New York.

Feldmeyer, D., Lübke, J., Silver, R. A., and Sakmann, B. (2002). Synaptic connections between layer 4 spiny neurone-layer 2/3 pyramidal cell pairs in juvenile rat barrel cortex: physiology and anatomy of interlaminar signalling within a cortical column. *Journal of Physiology*, 538(3):803–822.

Felleman, D. J. and Van Essen, D. C. (1991). Distributed hierarchical processing in the primate cerebral cortex. *Cerebral Cortex*, 1(1):1–47.

Ferguson, A. L. and Stone, T. W. (2010). Glutamate-induced depression of EPSP-spike coupling in rat hippocampal CA1 neurons and modulation by adenosine receptors. *European Journal of Neuroscience*, 31(7):1208–1218.

Ferster, D. (1986). Orientation selectivity of synaptic potentials in neurons of cat primary visual cortex. *Journal of Neuroscience*, 6(5):1284–301.

Ferster, D. and Jagadeesh, B. (1992). EPSP-IPSP interactions in cat visual cortex studied with in vivo whole-cell patch recording. *Journal of Neuroscience*, 12(4):1262–74.

Ferster, D. and Lindström, S. (1983). An intracellular analysis of geniculo-cortical connectivity in area 17 of the cat. *Journal of Physiology*, 342:181–215.

Figueres-Onate, M., Gutierrez, Y., and Lopez-Mascaraque, L. (2014). Unraveling Cajal's view of the olfactory system. *Frontiers in Neuroanatomy*, 8:55.

Fino, E. and Yuste, R. (2011). Dense inhibitory connectivity in neocortex. *Neuron*, 69(6):1188–203.

Fisher, R. A. (1921). On the probable error of a coefficient of correlation deduced from a small sample. *Metron*, 1:3–32.

Fitzpatrick, D. (1996). The functional organization of local circuits in visual cortex: insights from the study of tree shrew striate cortex. *Cerebral Cortex*, 6:329–341.

Foster, K. H., Gaska, J. P., Nagler, M., and Pollen, D. a. (1985). Spatial and temporal frequency selectivity of neurones in visual cortical areas V1 and V2 of the macaque monkey. *Journal of Physiology*, 365:331–63.

Freeman, T. C. B., Durand, S., Kiper, D. C., and Carandini, M. (2002). Suppression without inhibition in visual cortex. *Neuron*, 35(4):759–771.

Frégnac, Y. and Imbert, M. (1978). Early development of visual cortical cells in normal and dark-reared kittens: relationship between orientation selectivity and ocular dominance. *Journal of Physiology*, 278:27–44.

Freund, T. F. (2002). Changes in the views of neuronal connectivity and communication after Cajal: Examples from the hippocampus. *Progress in Brain Research*, 136:203–213.

Gandhi, N. J. and Katnani, H. A. (2011). Motor Functions of the Superior Colliculus. *Annual Review of Neuroscience*, 34:205–231.

Gao, E., DeAngelis, G. C., and Burkhalter, A. (2010). Parallel input channels to mouse primary visual cortex. *Journal of Neuroscience*, 30(17):5912–26.

Garaschuk, O., Milos, R.-I., and Konnerth, A. (2006). Targeted bulk-loading of fluorescent indicators for two-photon brain imaging in vivo. *Nature Protocols*, 1(1):380–6.

Garini, Y., Young, I. T., and Mcnamara, G. (2006). Spectral Imaging : Principles and Applications. *Cytometry A*, 69(8):735–747.

Garrett, M. E., Nauhaus, I., Marshel, J. H., and Callaway, X. E. M. (2014). Topography and Areal Organization of Mouse Visual Cortex. *Journal of Neuroscience*, 34(37):12587–12600.

Gasparini, S., Migliore, M., and Magee, J. C. (2004). On the initiation and propagation of dendritic spikes in CA1 pyramidal neurons. *Journal of Neuroscience*, 24(49):11046–11056.

Gaudin, Y., Ruigrok, R. W., Tuffereau, C., Knossow, M., and Flamand, a. (1992). Rabies virus glycoprotein is a trimer. *Virology*, 187(2):627–632.

Gennari, F. (1782). *De peculiari structura cerebri*. Parma.

Gentet, L. J. (2012). Functional diversity of supragranular GABAergic neurons in the barrel cortex. *Frontiers in neural circuits*, 6:52.

Gentet, L. J., Avermann, M., Matyas, F., Staiger, J. F., and Petersen, C. C. H. (2010). Membrane potential dynamics of GABAergic neurons in the barrel cortex of behaving mice. *Neuron*, 65(3):422–35.

Ghanem, A. and Conzelmann, K.-K. (2015). G gene-deficient single-round rabies viruses for neuronal circuit analysis. *Virus Research*.

Gianfranceschi, L., Siciliano, R., Walls, J., Morales, B., Kirkwood, A., Huang, Z. J., Tonegawa, S., and Maffei, L. (2003). Visual cortex is rescued from the effects of dark rearing by overexpression of BDNF. *Proceedings of the National Academy of Sciences of the United States of America*, 100(21):12486–91.

Gilbert, C. D. (1977). Laminar differences in receptive field properties of cells in cat primary visual cortex. *Journal of Physiology*, 268(2):391–421.

Gilbert, C. D. (1983). Microcircuitry of the Visual Cortex. *Annual Review of Neuroscience*, 6:217–247.

Gilbert, C. D. and Li, W. (2013). Top-down influences on visual processing. *Nature Reviews Neuroscience*, 14:350–363.

Gilbert, C. D. and Wiesel, T. (1990). The influence of contextual stimuli on the orientation selectivity of cells in primary visual cortex of the cat. *Vision research*, 30(11):1689–701.

Gilbert, C. D. and Wiesel, T. N. (1989). Columnar specificity of intrinsic horizontal and corticocortical connections in cat visual cortex. *Journal of Neuroscience*, 9(7):2432–2442.

Girman, S. V., Sauvé, Y., and Lund, R. D. (1999). Receptive field properties of single neurons in rat primary visual cortex. *Journal of Neurophysiology*, 82(1):301–311.

Glees, P. (1946). Terminal Degeneration Within The Central Nervous System As Studied By A New Silver Method. *Journal of Neuropathology and Experimental Neurology*, 5:54–59.

Glezer, V. D., Tsherbach, T. A., Gauselman, V. E., and Bondarko, V. M. (1982). Spatio-Temporal Organization of Receptive Fields of the Cat Striate Cortex. *Biological Cybernetics*, 454:447–454.

Glover, J. C., Petursdottir, G., and Jansen, J. K. (1986). Fluorescent dextran-amines used as axonal tracers in the nervous system of the chicken embryo. *Journal of neuroscience methods*, 18(3):243–254.

Goense, J. B. M. and Logothetis, N. K. (2006). Laminar specificity in monkey V1 using high-resolution SE-fMRI. *Magnetic Resonance Imaging*, 24(4):381–92.

Golding, N. L. and Spruston, N. (1998). Dendritic sodium spikes are variable triggers of axonal action potentials in hippocampal CA1 pyramidal neurons. *Neuron*, 21(5):1189–1200.

Gonatas, N. K., Harper, C., Mizutani, T., and Gontas, J. O. (1979). Superior Sensitivity of Conjugates of Horseradish Peroxidase with Wheat Germ Agglutinin for Studies of Retrograde Axonal Transport. *The Journal of Histochemistry and Cytochemistry*, 27(3):728–734.

Gonchar, Y., Wang, Q., and Burkhalter, A. (2007). Multiple distinct subtypes of GABAergic neurons in mouse visual cortex identified by triple immunostaining. *Frontiers in Neuroanatomy*, 1:3.

Goodale, M. and Milner, A. (1992). Separate visual pathways for perception and action. *Trends in Neurosciences*, 15(I):20–5.

Grabska-Barwiska, A., Ng, B. S. W., and Jancke, D. (2012). Orientation selective or not? - Measuring significance of tuning to a circular parameter. *Journal of Neuroscience Methods*, 203(1):1–9.

Gray, C. M., Konig, P., Engel, A. K., and Singer, W. (1989). Oscillatory responses in cat visual cortex exhibit inter-columnar synchronisation which reflects globel stimulus properties. *Nature*, 338:334–337.

Gray, C. M. and McCormick, D. (1996). Chattering cells: superficial pyramidal neurons contributing to the generation of synchronous oscillations in the visual cortex. *Science*, 274(5284):109–13.

Gray, E. G. (1959). Axo-somatic and axo-dendritic synapses of the cerebral cortex. *Journal of Anatomy*, 93(4):420–433.

Greenberg, D. S. and Kerr, J. N. D. (2009). Automated correction of fast motion artifacts for two-photon imaging of awake animals. *Journal of Neuroscience Methods*, 176(1):1–15.

Grewe, B. F., Langer, D., Kasper, H., Kampa, B. M., and Helmchen, F. (2010). High-speed in vivo calcium imaging reveals neuronal network activity with near-millisecond precision. *Nature Methods*, 7(5):399–405.

Grieve, K. L., Acuña, C., and Cudeiro, J. (2000). The primate pulvinar nuclei: Vision and action. *Trends in Neurosciences*, 23(1):35–39.

Grinevich, V., Brecht, M., and Osten, P. (2005). Monosynaptic pathway from rat vibrissa motor cortex to facial motor neurons revealed by lentivirus-based axonal tracing. *Journal of Neuroscience*, 25(36):8250–8258.

Grinvald, A., Lieke, E., Frostig, R. D., Gilbert, C. D., and Wiesel, T. N. (1986). Functional architecture of cortex revealed by optical imaging of intrinsic signals. *Nature*, 324(6095):361–364.

Grynkiewicz, G., Poenie, M., and Tsien, R. Y. (1985). A new generation of Ca2+ indicators with greatly improved fluorescence properties. *The Journal of Biological Chemistry*, 260(6):3440–50.

Guido, W. (2008). Refinement of the retinogeniculate pathway. *Journal of Physiology*, 586(18):4357–4362.

Haas, K., Sin, W. C., Javaherian, A., Li, Z., and Cline, H. T. (2001). Single-cell electroporation for gene transfer in vivo. *Neuron*, 29(3):583–91.

Hammill, O. P., Marty, A., Neher, E., Sakmann, B., and Sigworth, F. J. (1981). Improved Patch-Clamp Techniques for High-Resolution Current Recording from Cells and Cell-Free Membrane Patches. *Pflügers Archiv: European Journal of Physiology*, 391:85–100.

Hamos, J. E., Van Horn, S. C., Raczkowski, D., and Sherman, S. M. (1987). Synaptic circuits involving an individual retinogeniculate axon in the cat. *Journal of Comparative Neurology*, 259(2):165–192.

Hardy, S., Kitamura, M., Harris-Stansil, T., Dai, Y., and Phipps, M. L. (1997). Construction of adenovirus vectors through Cre-lox recombination. *Journal of Virology*, 71(3):1842–1849.

Harris, J. a., Wook Oh, S., and Zeng, H. (2012). Adeno-associated viral vectors for anterograde axonal tracing with fluorescent proteins in nontransgenic and Cre driver mice. *Current Protocols in Neuroscience*, 1(SUPPL.59):1–18.

Harris, K. D. and Mrsic-Flogel, T. D. (2013). Cortical connectivity and sensory coding. *Nature*, 503:51–58.

Harris, K. D. and Shepherd, G. M. G. (2015). The neocortical circuit: themes and variations. *Nature Neuroscience*, 18(2):170–181.

Harris, K. D. and Thiele, A. (2011). Cortical state and attention. *Nature Reviews Neuroscience*, 12(9):509–523.

Hartline, H. (1938). The Response of Single Optic Nerve Fibres of the Vertebrate Eye to Illumination of the Retina. *American Journal of Physiology*, 121(2):400–415.

Heeger, D. J. (1992). Normalization of cell responses in cat striate cortex. *Visual Neuroscience*, 9(2):181–97.

Helm, J., Akgul, G., and Wollmuth, L. P. (2013). Subgroups of parvalbumin-expressing interneurons in layers 2/3 of the visual cortex. *Journal of Neurophysiology*, 109(6):1600–13.

Helmchen, F. and Denk, W. (2005). Deep tissue two-photon microscopy. *Nature Methods*, 2(12):932–940.

Hendry, S. H. and Yoshioka, T. (1994). A neurochemically distinct third channel in the macaque dorsal lateral geniculate nucleus. *Science*, 264(5158):575–577.

Hendry, S. H. C. and Reid, R. C. (2000). The Koniocellular Pathway in Primate Vision. *Annual Review of Neuroscience*, 23:127–153.

Hensch, T. K. (2005). Critical period plasticity in local cortical circuits. *Nature Reviews Neuroscience*, 6(11):877–888.

Hill, D. N., Varga, Z., Jia, H., Sakmann, B., and Konnerth, A. (2013). Multibranch activity in basal and tuft dendrites during firing of layer 5 cortical neurons in vivo. *Proceedings of the National Academy of Sciences of the United States of America*, 110(33):13618–13623.

Hille, B. (2001). *Ion Channels of Excitable Membranes, Third Edition*. Sinauer Associates.

Hirsch, J. A., Alonso, J. M., Reid, R. C., and Martinez, L. M. (1998). Synaptic integration in striate cortical simple cells. *Journal of Neuroscience*, 18(22):9517–28.

Hodgkin, A. L. and Huxley, A. F. (1939). Action Potentials Recorded from Inside a Nerve Fibre. *Nature*, 144:710–711.

Hodgkin, A. L. and Huxley, A. F. (1952). A Quantitative description of membrane current and its application to conduction and excitation in nerve. *Journal of Physiology*, 117:500–544.

Hofer, S. B., Ko, H., Pichler, B., Vogelstein, J. T., Ros, H., Zeng, H., Lein, E., Lesica, N. a., and Mrsic-Flogel, T. D. (2011). Differential connectivity and response dynamics of excitatory and inhibitory neurons in visual cortex. *Nature Neuroscience*, 14(8).

Hofer, S. B., Mrsic-Flogel, T. D., Bonhoeffer, T., and Hübener, M. (2006). Lifelong learning: ocular dominance plasticity in mouse visual cortex. *Current Opinion in Neurobiology*, 16(4):451–9.

Holt, G. R. and Koch, C. (1997). Shunting inhibition does not have a divisive effect on firing rates. *Neural computation*, 9(5):1001–13.

Honig, M. G. and Hume, R. I. (1986). Fluorescent carbocyanine dyes allow living neurons of identified origin to be studied in long-term cultures. *Journal of Cell Biology*, 103(1):171–187.

Horikawa, K. and Armstrong, W. E. (1988). A versatile means of intracellular labeling: injection of biocytin and its detection with avidin conjugates. *Journal of neuroscience methods*, 25(1):1–11.

Horton, J. C. and Adams, D. L. (2005). The cortical column: a structure without a function. *Philosophical Transactions of the Royal Society B*, 360(1456):837–62.

Hromádka, T., Zador, A. M., and DeWeese, M. R. (2013). Up states are rare in awake auditory cortex. *Journal of Neurophysiology*, 109(8):1989–95.

Hubel, D. H. and Wiesel, T. N. (1959). Receptive Fields of Single Neurones in the Cat's Striate Cortex. *Journal of Physiology*, 148:574–591.

Hubel, D. H. and Wiesel, T. N. (1962). Receptive fields, binocular interaction and functional architecture in the cat's visual cortex. *Journal of Physiology*, 160:106–154.

Hubel, D. H. and Wiesel, T. N. (1963). Receptive Fields of Cells in Striate Cortex of Very Young, Visually Inexperienced Kittens. *Journal of Neurophysiology*, 26:994–1002.

Hubel, D. H. and Wiesel, T. N. (1974a). Sequence regularity and geometry of orientation columns in the monkey striate cortex. *Journal of Comparative Neurology*, 158(3):267–293.

Hubel, D. H. and Wiesel, T. N. (1974b). Uniformity of monkey striate cortex: a parallel relationship between field size, scatter, and magnification factor. *Journal of Comparative Neurology*, 158(3):295–305.

Hubel, D. H. and Wiesel, T. N. (1977). Ferrier Lecture: Functional architecture of macaque monkey visual cortex. *Proceedings of the Royal Society of London B: Biological Sciences*, 198:1–59.

Hubel, D. H., Wiesel, T. N., and Levay, S. (1977). Plasticity of ocular dominance columns in monkey striate cortex. *Philosophical transactions of the Royal Society of London. Series B, Biological sciences*, 278(961):377–409.

Hubel, D. H., Wiesel, T. N., and Stryker, M. P. (1978). Anatomical demonstration of orientation columns in macaque monkey. *Journal of Comparative Neurology*, 177(3):361–380.

Hübener, M. (2003). Mouse visual cortex. *Current Opinion in Neurobiology*, 13(4):413–420.

Huberman, A. D. and Niell, C. M. (2011). What can mice tell us about how vision works? *Trends in Neurosciences*, 34(9):464–473.

Ibbotson, M. R., Price, N. S. C., and Crowder, N. a. (2005). On the division of cortical cells into simple and complex types: a comparative viewpoint. *Journal of Neurophysiology*, 93(6):3699–702.

Isaacson, J. and Scanziani, M. (2011). How Inhibition Shapes Cortical Activity. *Neuron*, 72(2):231–243.

Iurilli, G., Ghezzi, D., Olcese, U., Lassi, G., Nazzaro, C., Tonini, R., Tucci, V., Benfenati, F., and Medini, P. (2011). Article Sound-Driven Synaptic Inhibition in Primary Visual Cortex. *Neuron*, 73(4):814–828.

Jeon, C.-j., Strettoi, E., and Masland, R. H. (1998). The Major Cell Populations of the Mouse Retina. *Journal of Neuroscience*, 18(21):8936–8946.

Jia, H., Rochefort, N. L., Chen, X., and Konnerth, A. (2010). Dendritic organization of sensory input to cortical neurons in vivo. *Nature*, 464:1307–1312.

Johnston, D. and Narayanan, R. (2008). Active dendrites: colorful wings of the mysterious butterflies. *Trends in Neurosciences*, 31(6):309–316.

Jones, E. G. (2007). *The Thalamus*. Cambridge University Press, 2 edition.

Jones, J. P. and Palmer, L. a. (1987). An evaluation of the two-dimensional Gabor filter model of simple receptive fields in cat striate cortex. *Journal of Neurophysiology*, 58(6):1233–1258.

Kalatsky, V. A. and Stryker, M. P. (2003). New paradigm for optical imaging: temporally encoded maps of intrinsic signal. *Neuron*, 38(4):529–45.

Kanwisher, N., McDermott, J., and Chun, M. M. (1997). The fusiform face area: a module in human extrastriate cortex specialized for face perception. *Journal of Neuroscience*, 17(11):4302–4311.

Kaplan, E. (2012). The M, P, and K Pathways of the Primate Visual System revisited. In Werner, J. and Chalupa, L., editors, *The New Visual Neuroscience*, pages 481–493. MIT Press.

Kaschube, M. (2014). Neural maps versus salt-and-pepper organization in visual cortex. *Current Opinion in Neurobiology*, 24(1):95–102.

Katz, L. C., Burkhalter, a., and Dreyer, W. J. (1984). Fluorescent latex microspheres as a retrograde neuronal marker for in vivo and in vitro studies of visual cortex. *Nature*, 310(5977):498–500.

Kätzel, D., Zemelman, B. V., Buetfering, C., Wölfel, M., and Miesenböck, G. (2011). The columnar and laminar organization of inhibitory connections to neocortical excitatory cells. *Nature Neuroscience*, 14(1):100–7.

Katzner, S., Nauhaus, I., Benucci, A., Bonin, V., Ringach, D. L., and Carandini, M. (2009). Local origin of field potentials in visual cortex. *Neuron*, 61(1):35–41.

Kawaguchi, Y., Katsumaru, H., Kosaka, T., Heizmann, C. W., and Hama, K. (1987). Fast spiking cells in rat hippocampus (CA1 region) contain the calcium-binding protein parvalbumin. *Brain Research*, 416(2):369–374.

Kawaguchi, Y. and Kubota, Y. (1997). GABAergic cell subtypes and their synaptic connections in rat frontal cortex. *Cerebral Cortex*, 7(6):476–86.

Keller, G. B., Bonhoeffer, T., Hübener, M., and Hu, M. (2012). Sensorimotor Mismatch Signals in Primary Visual Cortex of the Behaving Mouse. *Neuron*, 74(5):809–815.

Kelly, R. M. and Strick, P. L. (2000). Rabies as a transneuronal tracer of circuits in the central nervous system. *Journal of Neuroscience Methods*, 103(1):63–71.

Kerlin, A. M., Andermann, M. L., Berezovskii, V. K., and Reid, R. C. (2010). Broadly tuned response properties of diverse inhibitory neuron subtypes in mouse visual cortex. *Neuron*, 67(5):858–71.

Kerr, J. N. D., Greenberg, D., and Helmchen, F. (2005). Imaging input and output of neocortical networks in vivo. *Proceedings of the National Academy of Sciences of the United States of America*, 102(39):14063–8.

Kimura, R., Safari, M.-S., Mirnajafi-Zadeh, J., Ebina, T., Yanagawa, Y., Sohya, K., and Tsumoto, T. (2014). Curtailing Effect of Awakening on Visual Responses of Cortical Neurons by Cholinergic Activation of Inhibitory Circuits. *Journal of Neuroscience*, 34(30):10122–10133.

Kirkby, P. A., Srinivas, N. K. M. N., and Silver, R. A. (2010). A compact acousto-optic lens for 2D and 3D femtosecond based 2-photon microscopy. *Optics Express*, 18(13):13721.

Kitamura, K., Judkewitz, B., Kano, M., Denk, W., and Ha, M. (2008). Targeted patch-clamp recordings and single-cell electroporation of unlabeled neurons in vivo. 5(1):61–67.

Knipe, D. and Howley, P. (2007). *Fields virology*. Lippincott Williams & Wilkins, Philadelphia, 5 edition.

Ko, H., Hofer, S. B., Pichler, B., Buchanan, K. A., Sjöström, P. J., and Mrsic-Flogel, T. D. (2011). Functional specificity of local synaptic connections in neocortical networks. *Nature*, 473(7345):87–91.

Ko, H., Mrsic-Flogel, T. D., and Hofer, S. B. (2014). Emergence of Feature-Specific Connectivity in Cortical Microcircuits in the Absence of Visual Experience. *Journal of Neuroscience*, 34(29):9812–9816.

Komai, S., Denk, W., Osten, P., Brecht, M., and Margrie, T. W. (2006). Two-photon targeted patching (TPTP) in vivo. *Nature Protocols*, 1(2):647–52.

Koulakov, A. and Chklovskii, D. B. (2001). Orientation Preference Patterns in Mammalian Visual Cortex: A Wire Length Minimization Approach. *Neuron*, 29(2):519–527.

Kreile, A. K., Bonhoeffer, T., and Hubener, M. (2011). Altered Visual Experience Induces Instructive Changes of Orientation Preference in Mouse Visual Cortex. *Journal of Neuroscience*, 31(39):13911–13920.

Kristensson, K. and Olsson, Y. (1971). Retrograde axonal transport of protein. *Brain Research*, 29:363–365.

Kuffler, S. (1953). Discharge patterns and functional organization of mammalian retina. *Journal of Neurophysiology*, 16(1):37–68.

Kuhlman, S. J., Olivas, N. D., Tring, E., Ikrar, T., Xu, X., and Trachtenberg, J. T. (2013). A disinhibitory microcircuit initiates critical-period plasticity in the visual cortex. *Nature*, 501(7468):543–546.

Kuypers, H. G. and Maisky, V. a. (1975). Retrograde axonal transport of horseradish peroxidase from spinal cord to brain stem cell groups in the cat. *Neuroscience Letters*, 1(1):9–14.

Lafon, M. (2005). Rabies virus receptors. *Journal of NeuroVirology*, 11:82–87.

Larkman, A. U. (1991). Dendritic morphology of pyramidal neurones of the visual cortex of the rat: III. Spine distributions. *Journal of Comparative Neurology*, 306(2):332–43.

Larkum, M. (2012). A cellular mechanism for cortical associations: an organizing principle for the cerebral cortex. *Trends in Neurosciences*, pages 1–11.

Larkum, M. E., Waters, J., Sakmann, B., and Helmchen, F. (2007). Dendritic spikes in apical dendrites of neocortical layer 2/3 pyramidal neurons. *Journal of Neuroscience*, 27(34):8999–9008.

Larkum, M. E., Zhu, J. J., and Sakmann, B. (1999). A new cellular mechanism for coupling inputs arriving at different cortical layers. *Nature*, 398(6725):338–341.

Lendvai, B., Stern, E. A., Chen, B., and Svoboda, K. (2000). Experience-dependent plasticity of dendritic spines in the developing rat barrel cortex in vivo. *Nature*, 404(6780):876–81.

Li, W.-C., Soffe, S. R., and Roberts, A. (2004). A direct comparison of whole cell patch and sharp electrodes by simultaneous recording from single spinal neurons in frog tadpoles. *Journal of Neurophysiology*, 92(1):380–386.

Li, Y., Lu, H., Cheng, P.-l., Ge, S., Xu, H., Shi, S.-h., and Dan, Y. (2012a). Clonally related visual cortical neurons show similar stimulus feature selectivity. *Nature*, 486:118–121.

Li, Y.-T., Ma, W.-P., Pan, C.-J., Zhang, L. I., and Tao, H. W. (2012b). Broadening of Cortical Inhibition Mediates Developmental Sharpening of Orientation Selectivity. *Journal of Neuroscience*, 32(12):3981–3991.

Lien, A. D. and Scanziani, M. (2013). Tuned thalamic excitation is amplified by visual cortical circuits. *Nature Neuroscience*, 16(9):1315–23.

Linden, D. J. (1999). The Return of the Spike: Postsynaptic Action Potentials and the Induction of LTP and LTD. *Neuron*, 22(4):661–666.

Ling, G. and Gerard, R. (1949). The normal membrane potential of frog sartorius fibers. *Journal of Cellular and Comparative Physiology*, 34(3):383–396.

Liu, B.-h., Li, P., Li, Y.-t., Sun, Y. J., Yanagawa, Y., Obata, K., Zhang, L. I., and Tao, H. W. (2009). Visual receptive field structure of cortical inhibitory neurons revealed by two-photon imaging guided recording. *Journal of Neuroscience*, 29(34):10520–32.

Liu, B.-H., Li, Y.-T., Ma, W.-P., Pan, C.-J., Zhang, L. I., and Tao, H. W. (2011). Broad inhibition sharpens orientation selectivity by expanding input dynamic range in mouse simple cells. *Neuron*, 71(3):542–54.

Livet, J., Weissman, T. a., Kang, H., Draft, R. W., Lu, J., Bennis, R. a., Sanes, J. R., and Lichtman, J. W. (2007). Transgenic strategies for combinatorial expression of fluorescent proteins in the nervous system. *Nature*, 450(7166):56–62.

Llinas, R. and Nicholson, C. (1971). Electrophysiological properties of dendrites and somata in alligator Purkinje cells. *Journal of Neurophysiology*, 34(4):532–551.

Llinás, R. R. (1988). The intrinsic electrophysiological properties of mammalian neurons: insights into central nervous system function. *Science*, 242(4886):1654–64.

London, M., Hausser, M., and Häusser, M. (2005). Dendritic computation. *Annual Review of Neuroscience*, 28:503–532.

Longordo, F., To, M.-S., Ikeda, K., and Stuart, G. J. (2013). Sublinear integration underlies binocular processing in primary visual cortex. *Nature Neuroscience*, 16(6):714–23.

Looger, L. and Griesbeck, O. (2012). Genetically encoded neural activity indicators. *Current Opinion in Neurobiology*, 22(1):18–23.

Löwel, S., Freeman, B., and Singer, W. (1987). Topographic organization of the orientation column system in large flat-mounts of the cat visual cortex: a 2-deoxyglucose study. *Journal of Comparative Neurology*, 255(3):401–415.

Luo, L., Callaway, E. M., and Svoboda, K. (2008). Genetic dissection of neural circuits. *Neuron*, 57(5):634–60.

Magee, J. C. and Carruth, M. (1999). Dendritic voltage-gated ion channels regulate the action potential firing mode of hippocampal CA1 pyramidal neurons. *Journal of Neurophysiology*, 82(4):1895–1901.

Magee, J. C. and Johnston, D. (1997). A synaptically controlled, associative signal for Hebbian plasticity in hippocampal neurons. *Science*, 275(5297):209–213.

Major, G., Larkum, M. E., and Schiller, J. (2013). Active properties of neocortical pyramidal neuron dendrites. *Annual Review of Neuroscience*, 36:1–24.

Makino, H. and Komiyama, T. (2015). Learning enhances the relative impact of top-down processing in the visual cortex. *Nature Neuroscience*, 2015(July).

Malik, R. and Chattarji, S. (2012). Enhanced intrinsic excitability and EPSP-spike coupling accompany enriched environment-induced facilitation of LTP in hippocampal CA1 pyramidal neurons. *Journal of Neurophysiology*, 107(5):1366–1378.

Mangini, N. J. and Pearlman, A. L. (1980). Laminar distribution of receptive field properties in the primary visual cortex of the mouse. *The Journal of Comparative Neurology*, 193(1):203–22.

Marblestone, A. H., Zamft, B. M., Maguire, Y. G., Shapiro, M. G., Cybulski, T. R., Glaser, J. I., Amodei, D., Stranges, P. B., Kalhor, R., Dalrymple, D. a., Seo, D., Alon, E., Maharbiz, M. M., Carmena, J. M., Rabaey, J. M., Boyden, E. S., Church, G. M., and Kording, K. P. (2013). Physical principles for scalable neural recording. *Frontiers in Computational Neuroscience*, 7:137.

Marcelja, S. (1980). Mathematical description of the responses of simple cortical cells. *Journal of the Optical Society of America*, 70(11):1297–1300.

Marder, E. and Taylor, A. L. (2011). Multiple models to capture the variability in biological neurons and networks. *Nature Neuroscience*, 14(2):133–138.

Margolis, D. J., Lütcke, H., Schulz, K., Haiss, F., Weber, B., Kügler, S., Hasan, M. T., and Helmchen, F. (2012). Reorganization of cortical population activity imaged throughout long-term sensory deprivation. *Nature Neuroscience*, 15(11):1539–46.

Margrie, T. W., Brecht, M., and Sakmann, B. (2002). In vivo, low-resistance, whole-cell recordings from neurons in the anaesthetized and awake mammalian brain. *Pflügers Archiv: European Journal of Physiology*, 444(4):491–8.

Margrie, T. W., Meyer, A. H., Caputi, A., Monyer, H., Hasan, M. T., Schaefer, A. T., Denk, W., and Brecht, M. (2003). Targeted whole-cell recordings in the mammalian brain in vivo. *Neuron*, 39(6):911–8.

Markram, H., Toledo-Rodriguez, M., Wang, Y., Gupta, A., Silberberg, G., and Wu, C. (2004). Interneurons of the neocortical inhibitory system. *Nature Reviews Neuroscience*, 5(10):793–807.

Marshel, J. H., Garrett, M. E., Nauhaus, I., and Callaway, E. M. (2011). Functional Specialization of Seven Mouse Visual Cortical Areas. *Neuron*, 72(6):1040–1054.

Marshel, J. H., Kaye, A. P., Nauhaus, I., and Callaway, E. M. (2012). Anterior-Posterior Direction Opponency in the Superficial Mouse Lateral Geniculate Nucleus. *Neuron*, 76(4):713–720.

Marshel, J. H., Mori, T., Nielsen, K. J., and Callaway, E. M. (2010). Targeting single neuronal networks for gene expression and cell labeling in vivo. *Neuron*, 67(4):562–74.

Martinez, L. M. and Alonso, J.-M. (2003). Complex Receptive Fields in Primary Visual Cortex. *The Neuroscientist*, 9(5):317–331.

Martinez, L. M., Wang, Q., Reid, R. C., Pillai, C., Alonso, J.-M. J.-M., Sommer, F. T. F., and Hirsch, J. J. a. (2005). Receptive field structure varies with layer in the primary visual cortex. *Nature Neuroscience*, 8(3):372–379.

Marx, M. and Feldmeyer, D. (2013). Morphology and physiology of excitatory neurons in layer 6b of the somatosensory rat barrel cortex. *Cerebral Cortex*, 23(12):2803–17.

Marx, M., Günter, R. H., Hucko, W., Radnikow, G., and Feldmeyer, D. (2012). Improved biocytin labeling and neuronal 3D reconstruction. *Nature Protocols*, 7(2):394–407.

Masland, R. H. (2012). The Neuronal Organization of the Retina. *Neuron*, 76(2):266–280.

Masland, R. H. and Martin, P. R. (2007). The unsolved mystery of vision. *Current Biology*, 17(15):577–582.

Matz, M. V., Fradkov, a. F., Labas, Y. a., Savitsky, a. P., Zaraisky, a. G., Markelov, M. L., and Lukyanov, S. a. (1999). Fluorescent proteins from nonbioluminescent Anthozoa species. *Nature Biotechnology*, 17(10):969–973.

Mazurek, M., Kager, M., and Van Hooser, S. D. (2014). Robust quantification of orientation selectivity and direction selectivity. *Frontiers in Neural Circuits*, 8:1–17.

McCormick, D., Connors, B. W., Lighthall, J. W., and Prince, D. a. (1985). Comparative electrophysiology of pyramidal and sparsely spiny stellate neurons of the neocortex. *Journal of Neurophysiology*, 54(4):782–806.

Mebatsion, T., Konig, M., and Conzelmann, K. K. (1996). Budding of rabies virus particles in the absence of the spike glycoprotein. *Cell*, 84(6):941–951.

Mebatsion, T., Weiland, F., and Conzelmann, K. K. (1999). Matrix protein of rabies virus is responsible for the assembly and budding of bullet-shaped particles and interacts with the transmembrane spike glycoprotein G. *Journal of Virology*, 73(1):242–250.

Mechler, F. and Ringach, D. L. (2002). On the classification of simple and complex cells. *Vision Research*, 42(8):1017–33.

Medini, P. (2011a). Cell-type-specific sub- and suprathreshold receptive fields of layer 4 and layer 2/3 pyramids in rat primary visual cortex. *Neuroscience*, 190:112–26.

Medini, P. (2011b). Layer- and Cell-Type-Specific Subthreshold and Suprathreshold Effects of Long-Term Monocular Deprivation in Rat Visual Cortex. *Journal of Neuroscience*, 31(47):17134–17148.

Meyer, H. S., Schwarz, D., Wimmer, V. C., Schmitt, A. C., Kerr, J. N. D., Sakmann, B., and Helmstaedter, M. (2011). Inhibitory interneurons in a cortical column form hot zones of inhibition in layers 2 and 5A. *Proceedings of the National Academy of Sciences of the United States of America*, 108(40):16807–12.

Migliore, M. and Shepherd, G. M. (2002). Emerging rules for the distributions of active dendritic conductances. *Nature Reviews Neuroscience*, 3(5):362–370.

Mittmann, W., Wallace, D. J., Czubayko, U., Herb, J. T., Schaefer, A. T., Looger, L. L., Denk, W., and Kerr, J. N. D. (2011). Two-photon calcium imaging of evoked activity from L5 somatosensory neurons in vivo. *Nature Neuroscience*, 14(8):1089–1093.

Mitzdorf, U. (1985). Current source-density method and application in cat cerebral cortex: investigation of evoked potentials and EEG phenomena. *Physiological Reviews*, 65(1):37–100.

Miyamichi, K., Shlomai-Fuchs, Y., Shu, M., Weissbourd, B. C., Luo, L., and Mizrahi, A. (2013). Article Dissecting Local Circuits : Parvalbumin Interneurons Underlie Broad Feedback Control of Olfactory Bulb Output. *Neuron*, 80(5):1232–45.

Mohanty, D., Scholl, B., and Priebe, N. J. (2012). The accuracy of membrane potential reconstruction based on spiking receptive fields. *Journal of Neurophysiology*, 107:2143–2153.

Monier, C., Chavane, F., Baudot, P., Graham, L. J., and Frégnac, Y. (2003). Orientation and direction selectivity of synaptic inputs in visual cortical neurons: A diversity of combinations produces spike tuning. *Neuron*, 37(4):663–680.

Moore, R. Y. (2013). The suprachiasmatic nucleus and the circadian timing system. *Progress in Molecular Biology and Translational Science*, 119:1–28.

Morales, B., Choi, S.-Y., and Kirkwood, A. (2002). Dark rearing alters the development of GABAergic transmission in visual cortex. *Journal of Neuroscience*, 22(18):8084–8090.

Morrone, M. C., Burr, D. C., and Maffei, L. (1982). Functional implications of cross-orientation inhibition of cortical visual cells. I. Neurophysiological evidence. *Proceedings of the Royal Society of London B: Biological Sciences*, 216(1204):335–354.

Mountcastle, V. B. (1957). Modality and topographic properties of single neurons of cat's somatic sensory cortex. *Journal of Neurophysiology*, 20(4):408–434.

Mountcastle, V. B., Talbot, W. H., Sakata, H., and Hyvarinen, J. (1969). Cortical Studied Periodicity Neuronal Mechanisms in Flutter-Vibration Neuronal in Unanesthetized Monkeys . Discrimination. *Journal of Neurophysiology*, 32:452–484.

Movshon, J., Thompson, I. D., and Tolhurst, D. J. (1978a). Receptive Field Organization of Complex Cells in the Cat's Striate Cortex. *Journal of Physiology*, 283:79–99.

Movshon, J., Thompson, I. D., and Tolhurst, D. J. (1978b). Spatial summation in the receptive fields of simple cells in the cat's striate cortex. *Journal of Physiology*, 283:53–77.

Mower, G. D. (1991). The effect of dark rearing on the time course of the critical period in cat visual cortex. *Developmental Brain Research*, 58(2):151–158.

Nance, D. M. and Burns, J. (1990). Fluorescent dextrans as sensitive anterograde neuroanatomical tracers: Applications and pitfalls. *Brain Research Bulletin*, 25(1):139–145.

Nassi, J. J., Cepko, C. L., Born, R. T., and Beier, K. T. (2015). Neuroanatomy goes viral! *Frontiers in Neuroanatomy*, 9:1.

Nelson, R., Famiglietti, E. V., and Kolb, H. (1978). Intracellular staining reveals different levels of stratification for on- and off-center ganglion cells in cat retina. *Journal of Neurophysiology*, 41(2):472–483.

Niell, C. M. and Stryker, M. P. (2008). Highly selective receptive fields in mouse visual cortex. *Journal of Neuroscience*, 28(30):7520–36.

Nieuwenhuis, S., Forstmann, B. U., and Wagenmakers, E.-J. (2011). Erroneous analyses of interactions in neuroscience: a problem of significance. *Nature Neuroscience*, 14(9):1105–1107.

Noble, D. and Stein, R. B. (1966). The threshold conditions for initiation of action potentials by excitable cells. *Journal of Physiology*, 187(1):129–162.

Nowak, L. G., Azouz, R., Sanchez-Vives, M. V., Gray, C. M., and McCormick, D. (2003). Electrophysiological classes of cat primary visual cortical neurons in vivo as revealed by quantitative analyses. *Journal of Neurophysiology*, 89(3):1541–1566.

Nowak, L. G., Sanchez-Vives, M. V., and McCormick, D. (2008). Lack of orientation and direction selectivity in a subgroup of fast-spiking inhibitory interneurons: cellular and synaptic mechanisms and comparison with other electrophysiological cell types. *Cerebral Cortex*, 18(5):1058–78.

Oberlaender, M., de Kock, C. P. J., Bruno, R. M., Ramirez, A., Meyer, H. S., Dercksen, V. J., Helmstaedter, M., and Sakmann, B. (2012). Cell type-specific three-dimensional structure of thalamocortical circuits in a column of rat vibrissal cortex. *Cerebral Cortex*, 22(10):2375–91.

Oh, S. W., Harris, J. a., Ng, L., Winslow, B., Cain, N., Mihalas, S., Wang, Q., Lau, C., Kuan, L., Henry, A. M., Mortrud, M. T., Ouellette, B., Nguyen, T. N., Sorensen, S. a., Slaughterbeck, C. R., Wakeman, W., Li, Y., Feng, D., Ho, A., Nicholas, E., Hirokawa, K. E., Bohn, P., Joines, K. M., Peng, H., Hawrylycz, M. J., Phillips, J. W., Hohmann, J. G., Wohnoutka, P., Gerfen, C. R., Koch, C., Bernard, A., Dang, C., Jones, A. R., and Zeng, H. (2014). A mesoscale connectome of the mouse brain. *Nature*, 508(7495):207–14.

Ohki, K., Chung, S., Ch'ng, Y. H., Kara, P., and Reid, R. C. (2005). Functional imaging with cellular resolution reveals precise micro-architecture in visual cortex. *Nature*, 433(7026):597–603.

Ohtsuki, G., Nishiyama, M., Yoshida, T., Murakami, T., Histed, M., Lois, C., and Ohki, K. (2012). Similarity of visual selectivity among clonally related neurons in visual cortex. *Neuron*, 75(1):65–72.

Olcese, U., Iurilli, G., and Medini, P. (2013). Cellular and Synaptic Architecture of Multisensory Integration in the Mouse Neocortex. *Neuron*, 79(3):579–593.

Olshausen, B. a. and Field, D. J. (2005). How close are we to understanding V1? *Neural Computation*, 17(8):1665–99.

Oñativia, J., Schultz, S. R., and Dragotti, P. L. (2013). A finite rate of innovation algorithm for fast and accurate spike detection from two-photon calcium imaging. *Journal of Neural Engineering*, 10(4):046017.

Osakada, F., Mori, T., Cetin, A. H., Marshel, J. H., Virgen, B., and Callaway, E. M. (2011). New Rabies Virus Variants for Monitoring and Manipulating Activity and Gene Expression in Defined Neural Circuits. *Neuron*, 71(4):617–631.

Packer, A. M. and Yuste, R. (2011). Dense, Unspecific Connectivity of Neocortical Parvalbumin-Positive Interneurons: A Canonical Microcircuit for Inhibition? *Journal of Neuroscience*, 31(37):13260–13271.

Padmanabhan, K. and Urban, N. N. (2010). Intrinsic biophysical diversity decorrelates neuronal firing while increasing information content. *Nature Neuroscience*, 13(10):1276–1282.

Panda, S., Provencio, I., Tu, D. C., Pires, S. S., Rollag, M. D., Castrucci, A. M., Pletcher, M. T., Sato, T. K., Wiltshire, T., Andahazy, M., Kay, S. a., Gelder, R. N. V., and Ho-

genesch, J. B. (2003). Melanopsin Is Required for Non Image-Forming Photic Responses in Blind Mice. *Science*, 301:525–527.

Panda, S., Sato, T. K., Castrucci, A. M., Rollag, M. D., DeGrip, W. J., Hogenesch, J. B., Provencio, I., and Kay, S. a. (2002). Melanopsin (Opn4) requirement for normal light-induced circadian phase shifting. *Science*, 298(5601):2213–2216.

Paxinos, G. and Franklin, K. (2008). *The Mouse Brain in Stereotaxic Coordinates*. Academic Press, 3 edition.

Pei, X., Volgushev, M., Vidyasagar, T., and Creutzfeldt, O. D. (1991). Whole cell recording and conductance measurements in cat visual cortex in-vivo. *NeuroReport*, 2(8):485–488.

Petersen, C. C. H., Grinvald, A., and Sakmann, B. (2003). Spatiotemporal dynamics of sensory responses in layer 2/3 of rat barrel cortex measured in vivo by voltage-sensitive dye imaging combined with whole-cell voltage recordings and neuron reconstructions. *Journal of Neuroscience*, 23(4):1298–309.

Petrus, E., Rodriguez, G., Patterson, R., Connor, B., Kanold, P. O., and Lee, H.-K. (2015). Vision Loss Shifts the Balance of Feedforward and Intracortical Circuits in Opposite Directions in Mouse Primary Auditory and Visual Cortices. *Journal of Neuroscience*, 35(23):8790–8801.

Pi, H.-J., Hangya, B., Kvitsiani, D., Sanders, J. I., Huang, Z. J., and Kepecs, A. (2013). Cortical interneurons that specialize in disinhibitory control. *Nature*, 503(7477):521–4.

Piccinotti, S., Kirchhausen, T., and Whelan, S. P. J. (2013). Uptake of rabies virus into epithelial cells by clathrin-mediated endocytosis depends upon actin. *Journal of Virology*, 87(21):11637–47.

Piccolino, M. (1988). Cajal and the retina: a 100-year retrospective. *Trends in Neurosciences*, 11(12):521–525.

Pinto, L. and Dan, Y. (2015). Cell-Type-Specific Activity in Prefrontal Cortex during Goal-Directed Behavior. *Neuron*, 87:437–450.

Piscopo, D. M., El-Danaf, R. N., Huberman, a. D., and Niell, C. M. (2013). Diverse Visual Features Encoded in Mouse Lateral Geniculate Nucleus. *Journal of Neuroscience*, 33(11):4642–4656.

Poort, J., Khan, A., Pachitariu, M., Nemri, A., Orsolic, I., Krupic, J., Bauza, M., Sahani, M., Keller, G., Mrsic-Flogel, T., and Hofer, S. B. (2015). Learning Enhances Sensory and Multiple Non-sensory Representations in Primary Visual Cortex. *Neuron*, 86(6):1–13.

Poulet, J. F. a. and Petersen, C. C. H. (2008). Internal brain state regulates membrane potential synchrony in barrel cortex of behaving mice. *Nature*, 454(7206):881–885.

Priebe, N. J. and Ferster, D. (2012). Mechanisms of Neuronal Computation in Mammalian Visual Cortex. *Neuron*, 75(2):194–208.

Priebe, N. J., Lisberger, S. G., and Movshon, J. A. (2006). Tuning for spatiotemporal frequency and speed in directionally selective neurons of macaque striate cortex. *Journal of Neuroscience*, 26(11):2941–50.

Priebe, N. J., Mechler, F., Carandini, M., and Ferster, D. (2004). The contribution of spike threshold to the dichotomy of cortical simple and complex cells. *Nature Neuroscience*, 7(10):1113–22.

Prinz, A. a., Bucher, D., and Marder, E. (2004). Similar network activity from disparate circuit parameters. *Nature Neuroscience*, 7(12):1345–52.

Ragan, T., Kadiri, L. R., Venkataraju, K. U., Bahlmann, K., Sutin, J., Taranda, J., Arganda-Carreras, I., Kim, Y., Seung, H. S., and Osten, P. (2012). Serial two-photon tomography for automated ex vivo mouse brain imaging. *Nature Methods*, 9(3):255–8.

Rakic, P. (1988). Specification of Cerebral Cortical Areas. *Science*, 241:170–176.

Rall, W. (1964). Theoretical significance of dendritic trees for neuronal input-output relations. In Reiss, R., editor, *Neural Theory and Modelling*, pages 73–97. Stanford University Press, Stanford, CA.

Ramón Y Cajal, S. (1995). *Histology of the nervous system of man and vertebrates, Vol. 1.* Oxford University Press.

Rancz, E. A., Franks, K. M., Schwarz, M. K., Pichler, B., Schaefer, A. T., and Margrie, T. W. (2011). Transfection via whole-cell recording in vivo: bridging single-cell physiology, genetics and connectomics. *Nature Neuroscience*, 14(4):527–32.

Rapaport, D. H. and Stone, J. (1984). The area centralis of the retina in the cat and other mammals: Focal point for function and development of the visual system. *Neuroscience*, 11(2):289–301.

Reid, R. C. and Alonso, J. M. (1995). Specificity of monosynaptic connections from thalamus to visual cortex. *Nature*, 378(6554):281–284.

Ringach, D. L., Shapley, R. M., and Hawken, M. J. (2002). Orientation selectivity in macaque V1: diversity and laminar dependence. *Journal of Neuroscience*, 22(13):5639–51.

Rochefort, N. L., Garaschuk, O., Milos, R.-I., Narushima, M., Marandi, N., Pichler, B., Kovalchuk, Y., and Konnerth, A. (2009). Sparsification of neuronal activity in the visual cortex at eye-opening. *Proceedings of the National Academy of Sciences of the United States of America*, 106(35):15049–54.

Rochefort, N. L., Narushima, M., Grienberger, C., Marandi, N., Hill, D. N., and Konnerth, A. (2011). Development of direction selectivity in mouse cortical neurons. *Neuron*, 71(3):425–32.

Rockland, K. S. and Lund, J. (1982). Widespread Periodic Intrinsic Connections in the Tree Shrew Visual Cortex. *Science*, 215:1532–1534.

Romo, P. A., Wang, C., Zeater, N., Solomon, S. G., and Dreher, B. (2011). Phase-sensitivities, excitatory summation fields and silent suppressive receptive fields of single neurons in the parastriate cortex of the cat. *Journal of Neurophysiology*, 106(4):1688–1712.

Rosenblatt, F. (1958). The perceptron: a probabilistic model for information storage and organization in the brain. *Psychological Review*, 65(6):386–408.

Roth, M. M., Helmchen, F., and Kampa, B. M. (2012). Distinct functional properties of primary and posteromedial visual area of mouse neocortex. *Journal of Neuroscience*, 32(28):9716–26.

Ruby, N. F., Brennan, T. J., Xie, X., Cao, V., Franken, P., Heller, H. C., and Hara, B. F. O. (2002). Role of Melanopsin in Circadian Responses to Light. *Science*, 298:2211–2214.

Runyan, C. a. and Sur, M. (2013). Response selectivity is correlated to dendritic structure in parvalbumin-expressing inhibitory neurons in visual cortex. *Journal of Neuroscience*, 33(28):11724–33.

Saleem, A. B., Ayaz, A., Jeffery, K. J., Harris, K. D., and Carandini, M. (2013). Integration of visual motion and locomotion in mouse visual cortex. *Nature Neuroscience*, 16(12):1864–1869.

Saleem, A. B., Chadderton, P., Apergis-Schoute, J., Harris, K. D., and Schultz, S. R. (2010). Methods for predicting cortical UP and DOWN states from the phase of deep layer local field potentials. *Journal of Computational Neuroscience*, 29(1-2):49–62.

Schiller, J., Major, G., Koester, H. J., and Schiller, Y. (2000). NMDA spikes in basal dendrites of cortical pyramidal neurons. *Nature*, 404(6775):285–289.

Schneider, G. E. (1969). Two Visual Systems. *Science*, 163(3870):895–902.

Schnell, M. J., McGettigan, J. P., Wirblich, C., and Papaneri, A. (2010). The cell biology of rabies virus: using stealth to reach the brain. *Nature Reviews Microbiology*, 8(1):51–61.

Scholl, B., Pattadkal, J., Dilly, G., Priebe, N., and Zemelman, B. (2015). Local Integration Accounts for Weak Selectivity of Mouse Neocortical Parvalbumin Interneurons. *Neuron*, 87(2):424–436.

Scholl, B., Tan, a. Y. Y., Corey, J., and Priebe, N. J. (2013). Emergence of Orientation Selectivity in the Mammalian Visual Pathway. *Journal of Neuroscience*, 33(26):10616–10624.

Scholvinck, M. L., Saleem, a. B., Benucci, A., Harris, K. D., and Carandini, M. (2015). Cortical State Determines Global Variability and Correlations in Visual Cortex. *Journal of Neuroscience*, 35(1):170–178.

Schulz, D. J., Goaillard, J.-M., and Marder, E. E. (2007). Quantitative expression profiling of identified neurons reveals cell-specific constraints on highly variable levels of gene expression. *Proceedings of the National Academy of Sciences of the United States of America*, 104(32):13187–13191.

Schüz, A. and Palm, G. (1989). Density of neurons and synapses in the cerebral cortex of the mouse. *Journal of Comparative Neurology*, 286(4):442–455.

Sclar, G. and Freeman, R. D. (1982). Orientation selectivity in the cat's striate cortex is invariant with stimulus contrast. *Experimental Brain Research*, 46(3):457–461.

Sengpiel, F., Stawinski, P., and Bonhoeffer, T. (1999). Influence of experience on orientation maps in cat visual cortex. *Nature Neuroscience*, 2(8):727–732.

Shaner, N. C., Campbell, R. E., Steinbach, P. a., Giepmans, B. N. G., Palmer, A. E., and Tsien, R. Y. (2004). Improved monomeric red, orange and yellow fluorescent proteins derived from Discosoma sp. red fluorescent protein. *Nature Biotechnology*, 22(12):1567–1572.

Shapley, R., Kaplan, E., and Soodak, R. (1981). Spatial summation and contrast sensitivity of X and Y cells in the lateral geniculate nucleus of the macaque. *Nature*, 292:543–545.

Shepherd, G. M. G. and Svoboda, K. (2005). Laminar and columnar organization of ascending excitatory projections to layer 2/3 pyramidal neurons in rat barrel cortex. *Journal of Neuroscience*, 25(24):5670–9.

Sherman, S. M., Wilson, J. R., Kaas, J. H., and Webb, S. V. (1976). X- and Y-cells in the dorsal lateral geniculate nucleus of the owl monkey (Aotus trivirgatus). *Science*, 192(4238):475–477.

Shou, T. D. and Leventhal, A. G. (1989). Organized arrangement of orientation-sensitive relay cells in the cat's dorsal lateral geniculate nucleus. *Journal of Neuroscience*, 9(12):4287–4302.

Shuler, M. G. and Bear, M. F. (2006). Reward timing in the primary visual cortex. *Science*, 311(5767):1606–1609.

Silberberg, G., Gupta, A., and Markram, H. (2002). Stereotypy in neocortical microcircuits. *Trends in Neurosciences*, 25(5):227–230.

Sillito, A. M. (1975). The contribution of inhibitory mechanisms to the receptive field properties of neurones in the striate cortex of the cat. *Journal of Physiology*, 259:395–329.

Silver, R. A. (2010). Neuronal arithmetic. *Nature Reviews Neuroscience*, 11(7):474–89.

Simons, D. J. (1978). Response properties of vibrissa units in rat SI somatosensory neocortex. *Journal of Neurophysiology*, 41(3):798–820.

Singer, W. and Gray, C. M. (1995). Visual feature integration and the temporal correlation hypothesis. *Annual Review of Neuroscience*, 18:555–586.

Skottun, B., De Valois, R., Grosof, D., Movshon, J., Albrecht, D., and Bonds, A. (1991). Classifying Simple and Complex Cells on the Basis of Response Modulation. *Vision Research*, 31(7-8):1078–1086.

Skottun, B. C., Bradley, a., Sclar, G., Ohzawa, I., and Freeman, R. D. (1987). The effects of contrast on visual orientation and spatial frequency discrimination: a comparison of single cells and behavior. *Journal of Neurophysiology*, 57(3):773–786.

Smith, S. L. and Häusser, M. (2010). Parallel processing of visual space by neighboring neurons in mouse visual cortex. *Nature Neuroscience*, 13(9):1144–9.

Smith, S. L., Smith, I. T., Branco, T., and Hausser, M. (2013). Dendritic spikes enhance stimulus selectivity in cortical neurons in vivo. *Nature*, 503:115–122.

Sohya, K., Kameyama, K., Yanagawa, Y., Obata, K., and Tsumoto, T. (2007). GABAergic neurons are less selective to stimulus orientation than excitatory neurons in layer II/III of visual cortex, as revealed by in vivo functional Ca2+ imaging in transgenic mice. *Journal of Neuroscience*, 27(8):2145–9.

Solomon, S. G. (2002). Striate cortex in dichromatic and trichromatic marmosets: Neurochemical compartmentalization and geniculate input. *Journal of Comparative Neurology*, 450(4):366–381.

Solomon, S. G. and Rosa, M. G. P. (2014). A simpler primate brain: the visual system of the marmoset monkey. *Frontiers in Neural Circuits*, 8:96.

Somogyi, P., Freund, T. F., and Cowey, a. (1982). The axo-axonic interneuron in the cerebral cortex of the rat, cat and monkey. *Neuroscience*, 7(11):2577–2607.

Song, S., Sjöström, P. J., Reigl, M., Nelson, S., and Chklovskii, D. B. (2005). Highly nonrandom features of synaptic connectivity in local cortical circuits. *PLoS Biology*, 3(3):e68.

Sporns, O. (2011). The non-random brain: efficiency, economy, and complex dynamics. *Frontiers in Computational Neuroscience*, 5:5.

Spruston, N. (2008). Pyramidal neurons: dendritic structure and synaptic integration. *Nature Reviews Neuroscience*, 9(3):206–21.

Stafford, J. M., Jarrett, B. R., Miranda-Dominguez, O., Mills, B. D., Cain, N., Mihalas, S., Lahvis, G. P., Lattal, K. M., Mitchell, S. H., David, S. V., Fryer, J. D., Nigg, J. T.,

and Fair, D. a. (2014). Large-scale topology and the default mode network in the mouse connectome. *Proceedings of the National Academy of Sciences of the United States of America*, 111(52):201404346.

Staley, K. J., Otis, T. S., and Mody, I. (1992). Membrane properties of dentate gyrus granule cells: comparison of sharp microelectrode and whole-cell recordings. *Journal of Neurophysiology*, 67(5):1346–1358.

Steriade, M., Contreras, D., Curró Dossi, R., and Nuñez, A. (1993). The slow (¡ 1 Hz) oscillation in reticular thalamic and thalamocortical neurons: scenario of sleep rhythm generation in interacting thalamic and neocortical networks. *Journal of Neuroscience*, 13(8):3284–3299.

Steriade, M., Timofeev, I., Dürmüller, N., and Grenier, F. (1998). Dynamic properties of corticothalamic neurons and local cortical interneurons generating fast rhythmic (30-40 Hz) spike bursts. *Journal of Neurophysiology*, 79(1):483–490.

Steriade, M., Timofeev, I., and Grenier, F. (2001). Natural Waking and Sleep States : A View From Inside Neocortical Neurons. *Journal of Neurophysiology*, 85:1969–1985.

Sterling, P. and Demb, J. B. (2005). Retina. In Shepherd, G. M., editor, *Synaptic organization of the brain*, pages 217–269. Oxford University Press, New York.

Stevenson, I. H. and Kording, K. P. (2011). How advances in neural recording affect data analysis. *Nature Neuroscience*, 14(2):139–142.

Stirman, J. N., Smith, I. T., Kudenov, M. W., and Smith, S. L. (2014). Wide field-of-view, multi-region two-photon imaging of neuronal activity in vivo. *bioRxiv*.

Stoeckel, K., Schwab, M., and Thoenen, H. (1977). Role of gangliosides in the uptake and retrograde axonal transport of cholera and tetanus toxin as compared to nerve growth factor and wheat germ agglutinin. *Brain Research*, 132(2):273–285.

Stosiek, C., Garaschuk, O., Holthoff, K., and Konnerth, A. (2003). In vivo two-photon calcium imaging of neuronal networks. *Proceedings of the National Academy of Sciences of the United States of America*, 100(12):7319–24.

Stuart, G., Spruston, N., Sakmann, B., and Hausser, M. (1997). Action potential initiation and back propagation in neurons of the mammalian central nervous system. *Trends in Neurosciences*, 20(3):125–131.

Stuart, G. J., Dodt, H. U., and Sakmann, B. (1993). Patch-clamp recordings from the soma and dendrites of neurons in brain slices using infrared video microscopy. *Pflugers Archiv : European journal of physiology*, 423(5-6):511–518.

Stuart, G. J. and Palmer, L. M. (2006). Imaging membrane potential in dendrites and axons of single neurons. *Pflügers Archiv: European Journal of Physiology*, 453(3):403–10.

Stuart, G. J. and Sakmann, B. (1994). Active propagation of somatic action potentials into neocortical pyramidal cell dendrites. *Nature*, 367(6458):69–72.

Sun, Y., Nguyen, A. Q., Nguyen, J. P., Le, L., Saur, D., Choi, J., Callaway, E. M., and Xu, X. (2014). Cell-type-specific circuit connectivity of hippocampal CA1 revealed through Cre-dependent rabies tracing. *Cell reports*, 7(1):269–80.

Sur, M., Nagakura, I., Chen, N., and Sugihara, H. (2013). Mechanisms of plasticity in the developing and adult visual cortex. *Progress in Brain Research*, 207:243–254.

Svoboda, K. and Yasuda, R. (2006). Principles of two-photon excitation microscopy and its applications to neuroscience. *Neuron*, 50(6):823–39.

Swindale, N. V. (1998). Orientation tuning curves : empirical description and estimation of parameters. *Biological Cybernetics*, 56:45–56.

Szabadics, J., Varga, C., Molnar, G., Olah, S., Barzo, P., and Tamas, G. (2006). Excitatory Effect of GABAergic Axo-Axonic Cells in Cortical Microcircuits. *Science*, 311(January):233–235.

Szmajda, B. a., Grünert, U., and Martin, P. R. (2008). Retinal ganglion cell inputs to the koniocellular pathway. *Journal of Comparative Neurology*, 510(3):251–268.

Tamamaki, N., Yanagawa, Y., Tomioka, R., Miyazaki, J.-I., Obata, K., and Kaneko, T. (2003). Green fluorescent protein expression and colocalization with calretinin, parvalbumin, and somatostatin in the GAD67-GFP knock-in mouse. *The Journal of Comparative Neurology*, 467(1):60–79.

Tan, A. Y. Y., Brown, B. D., Scholl, B., Mohanty, D., and Priebe, N. J. (2011). Orientation Selectivity of Synaptic Input to Neurons in Mouse and Cat Primary Visual Cortex. *Journal of Neuroscience*, 31(34):12339–12350.

Tanaka, K. (1983). Cross-correlation analysis of geniculostriate neuronal relationships in cats. *Journal of Neurophysiology*, 49(6):1303–1318.

Tasaki, I., Polley, E. H., and Orrego, F. (1953). ACTION IN POTENTIALS FROM INDIVIDUAL CAT GENICULATE AND STRIATE CORTEX. *Journal of Neurophysiology*, 17:454–474.

Theer, P., Hasan, M. T., and Denk, W. (2003). Two-photon imaging to a depth of 1000 micrometers in living brains by use of a Ti:Al2O3 regenerative amplifier. *Optics Letters*, 28(12):1022–1024.

Thomson, A. M., Deuchars, J., and West, D. C. (1993). Large, deep layer pyramid-pyramid single axon EPSPs in slices of rat motor cortex display paired pulse and frequency-dependent depression, mediated presynaptically and self-facilitation, mediated postsynaptically. *Journal of Neurophysiology*, 70(6):2354–69.

Thomson, A. M. and Lamy, C. (2007). Functional maps of neocortical local circuitry. *Frontiers in Neuroscience*, 1(1):19–47.

Tian, L., Hires, S. A., Mao, T., Huber, D., Chiappe, M. E., Chalasani, S. H., Petreanu, L., Akerboom, J., McKinney, S. a., Schreiter, E. R., Bargmann, C. I., Jayaraman, V., Svoboda, K., and Looger, L. L. (2009). Imaging neural activity in worms, flies and mice with improved GCaMP calcium indicators. *Nature Methods*, 6(12):875–81.

Toth, L. J., Rao, S. C., Kim, D. S., Somers, D., and Sur, M. (1996). Subthreshold facilitation and suppression in primary visual cortex revealed by intrinsic signal imaging. *Proceedings of the National Academy of Sciences of the United States of America*, 93(18):9869–9874.

Trachtenberg, J. T., Chen, B. E., Knott, G. W., Feng, G., Sanes, J. R., Welker, E., and Svoboda, K. (2002). Long-term in vivo imaging of experience-dependent synaptic plasticity in adult cortex. *Nature*, 420(6917):788–94.

Tripathy, S. J., Padmanabhan, K., Gerkin, R. C., and Urban, N. N. (2013). Intermediate intrinsic diversity enhances neural population coding. *Proceedings of the National Academy of Sciences of the United States of America*, 110(20):8248–53.

Troyer, T. W., Krukowski, a. E., Priebe, N. J., and Miller, K. D. (1998). Contrast-invariant orientation tuning in cat visual cortex: thalamocortical input tuning and correlation-based intracortical connectivity. *Journal of Neuroscience*, 18(15):5908–5927.

Tsien, R. Y. (1998). The green fluorescent protein. *Annual Review of Biochemistry*, 67:509–544.

Turrigiano, G. G. and Nelson, S. B. (2000). Hebb and homeostasis in neuronal plasticity. *Current Opinion in Neurobiology*, 10(3):358–364.

Ugolini, G. (1995a). Specificity of rabies virus as a transneuronal tracer of motor networks: Transfer from hypoglossal motoneurons to connected second-order and higher order central nervous system cell groups. *Journal of Comparative Neurology*, 356(3):457–480.

Ugolini, G. (1995b). Transneuronal Tracing with Alpha-herpesviriises: A Review of the Methodology. In Kaplitt, M. and Loewy, A., editors, *Viral Vectors: Gene Therapy and Neuroscience Applications*, pages 293–317. Academic Press, San Diego, CA.

Ugolini, G. (2010). Advances in viral transneuronal tracing. *Journal of Neuroscience Methods*, 194(1):2–20.

Ugolini, G., Kuypers, H. G., and Simmons, a. (1987). Retrograde transneuronal transfer of herpes simplex virus type 1 (HSV 1) from motoneurones. *Brain Research*, 422(2):242–256.

Ungerleider, L. and Mishkin, M. (1982). Two cortical visual systems. In Ingle, D., Goodale, M., and Mansfield, R., editors, *Analysis of visual behavior*, pages 549–586. Massachusetts Institute of Technology, Cambridge, MA.

Ungerleider, L. G. and Haxby, J. V. (1994). 'What' and 'where' in the human brain. *Current Opinion in Neurobiology*, 4(2):157–165.

Urban, D. J. and Roth, B. L. (2015). DREADDs (Designer Receptors Exclusively Activated by Designer Drugs): Chemogenetic Tools with Therapeutic Utility. *Annual Review of Pharmacology and Toxicology*, 55(1):399–417.

Van den Bergh, G., Zhang, B., Arckens, L., and Chino, Y. M. (2010). Receptive-field properties of V1 and V2 neurons in mice and macaque monkeys. *The Journal of Comparative Neurology*, 518(11):2051–70.

Van Hooser, S. D. (2007). Similarity and diversity in visual cortex: is there a unifying theory of cortical computation? *The Neuroscientist*, 13(6):639–656.

Van Hooser, S. D., Heimel, J. A. F., Chung, S., Nelson, S. B., and Toth, L. J. (2005). Orientation selectivity without orientation maps in visual cortex of a highly visual mammal. *Journal of Neuroscience*, 25(1):19–28.

Vélez-Fort, M., Rousseau, C. V., Niedworok, C. J., Wickersham, I. R., Rancz, E. A., Brown, A. P., Strom, M., and Margrie, T. W. (2014). The Stimulus Selectivity and Connectivity of Layer Six Principal Cells Reveals Cortical Microcircuits Underlying Visual Processing. *Neuron*, 83(6):1431–1443.

Vogelstein, J. T., Packer, A. M., Machado, T. a., Sippy, T., Babadi, B., Yuste, R., and Paninski, L. (2010). Fast nonnegative deconvolution for spike train inference from population calcium imaging. *Journal of Neurophysiology*, 104(6):3691–704.

Waller, A. (1850). Experiments on the Section of the Glossopharyngeal and Hypoglossal Nerves of the Frog, and Observations of the Alterations Produced Thereby in the Structure of Their Primitive Fibres. *Philosophical Transactions of the Royal Society of London*, 140:423–429.

Wang, Q. and Burkhalter, A. (2007). Area map of mouse visual cortex. *The Journal of Comparative Neurology*, 502(3):339–357.

Wang, Q., Gao, E., and Burkhalter, A. (2007). In vivo transcranial imaging of connections in mouse visual cortex. *Journal of Neuroscience Methods*, 159(2):268–76.

Wang, Q., Gao, E., and Burkhalter, A. (2011). Gateways of ventral and dorsal streams in mouse visual cortex. *Journal of Neuroscience*, 31(5):1905–18.

Wang, Y., Toledo-Rodriguez, M., Gupta, A., Wu, C., Silberberg, G., Luo, J., and Markram, H. (2004). Anatomical, physiological and molecular properties of Martinotti cells in the somatosensory cortex of the juvenile rat. *Journal of Physiology*, 561(Pt 1):65–90.

Wässle, H. (2004). Parallel processing in the mammalian retina. *Nature Reviews Neuroscience*, 5(10):747–757.

Watabe-Uchida, M., Zhu, L., Ogawa, S. K., Vamanrao, A., and Uchida, N. (2012). Article Whole-Brain Mapping of Direct Inputs to Midbrain Dopamine Neurons. *Neuron*, 74(5):858–873.

Wertz, A., Trenholm, S., Yonehara, K., Hillier, D., Raics, Z., Leinweber, M., Szalay, G., Ghanem, A., Keller, G., Rózsa, B., Conzelmann, K.-k., and Roska, B. (2015). Single-cell initiated monosynaptic tracing reveals layer-specific cortical network modules. *Science*, 349(6243).

White, A. J., Solomon, S. G., and Martin, P. R. (2001a). Spatial properties of koniocellular cells in the lateral geniculate nucleus of the marmoset Callithrix jacchus. *Journal of Physiology*, 533(2):519–535.

White, L. E., Coppola, D. M., and Fitzpatrick, D. (2001b). The contribution of sensory experience to the maturation of orientation selectivity in ferret visual cortex. 330(2000):1049–1052.

Wickersham, I. R., Finke, S., Conzelmann, K.-K., and Callaway, E. M. (2007a). Retrograde neuronal tracing with a deletion-mutant rabies virus. *Nature methods*, 4(1):47–49.

Wickersham, I. R., Lyon, D. C., Barnard, R. J. O., Mori, T., Finke, S., Conzelmann, K.-K., Young, J. a. T., and Callaway, E. M. (2007b). Monosynaptic restriction of transsynaptic tracing from single, genetically targeted neurons. *Neuron*, 53(5):639–47.

Wiesel, T. N. and Hubel, D. H. (1963a). Effects of visual deprivation on morphology and physiology of cells in the cat's lateral geniculate body. *Journal of Neurophysiology*, 26:978–993.

Wiesel, T. N. and Hubel, D. H. (1963b). Single-Cell Responses in Striate Cortex of Kittens Deprived of Vision in One Eye. *Journal of Neurophysiology*, 26:1003–1017.

Williams, S. R. and Stuart, G. J. (1999). Mechanisms and consequences of action potential burst firing in rat neocortical pyramidal neurons. *Journal of Physiology*, 521 Pt 2:467–482.

Wilson, N. R., Runyan, C. A., Wang, F. L., and Sur, M. (2012). Division and subtraction by distinct cortical inhibitory networks in vivo. *Nature*, 488(7411):343–8.

Wu, G. K., Arbuckle, R., Liu, B. H., Tao, H. W., and Zhang, L. I. (2008). Lateral Sharpening of Cortical Frequency Tuning by Approximately Balanced Inhibition. *Neuron*, 58(1):132–143.

Xu, X., Ichida, J., Shostak, Y., Bonds, a. B., and Casagrande, V. a. (2002). Are primate

lateral geniculate nucleus (LGN) cells really sensitive to orientation or direction? *Visual Neuroscience*, 19(1):97–108.

Yassin, L., Benedetti, B. L., Jouhanneau, J.-S., Wen, J., Poulet, J. F. A., and Barth, A. L. (2010). An embedded subnetwork of highly active neurons in the neocortex. *Neuron*, 68(6):997–1003.

Yoshimura, Y., Dantzker, J. L. M., and Edward M. Callaway (2005). Excitatory cortical neurons form fine-scale functional networks. *Nature*, 433:868–872.

Young, J. A., Bates, P., and Varmus, H. E. (1993). Isolation of a chicken gene that confers susceptibility to infection by subgroup A avian leukosis and sarcoma viruses. *Journal of Virology*, 67(4):1811–1816.

Yu, Y.-C., He, S., Chen, S., Fu, Y., Brown, K. N., Yao, X.-H., Ma, J., Gao, K. P., Sosinsky, G. E., Huang, K., and Shi, S.-H. (2012). Preferential electrical coupling regulates neocortical lineage-dependent microcircuit assembly. *Nature*, 486:113–117.

Zariwala, H. A., Madisen, L., Ahrens, K. F., Bernard, A., Lein, E. S., Jones, A. R., and Zeng, H. (2011). Visual tuning properties of genetically identified layer 2/3 neuronal types in the primary visual cortex of cre-transgenic mice. *Frontiers in Systems Neuroscience*, 4:162.

Zhao, X., Liu, M., and Cang, J. (2013). Sublinear binocular integration preserves orientation selectivity in mouse visual cortex. *Nature communications*, 4(May):2088.

Zhao, Y., Araki, S., Wu, J., Teramoto, T., Chang, Y.-F., Nakano, M., Abdelfattah, A. S., Fujiwara, M., Ishihara, T., Nagai, T., and Campbell, R. E. (2011). An Expanded Palette of Genetically Encoded Ca2+ Indicators. *Science*, 1888.

Ziv, G., Connors, B. W., and Amitai, Y. (1999). Efficacy of thalamocortical and intracortical synaptic connections: Quanta, innervation, and reliability. *Neuron*, 23(2):385–397.